MCEER
EARTHQUAKE ENGINEERING TO EXTREME EVENTS

ISSN 1520-295X

Development of a Steel Plate Shear Wall Bridge Pier System Conceived from a Multi-Hazard Perspective

by
David Keller and Michel Bruneau

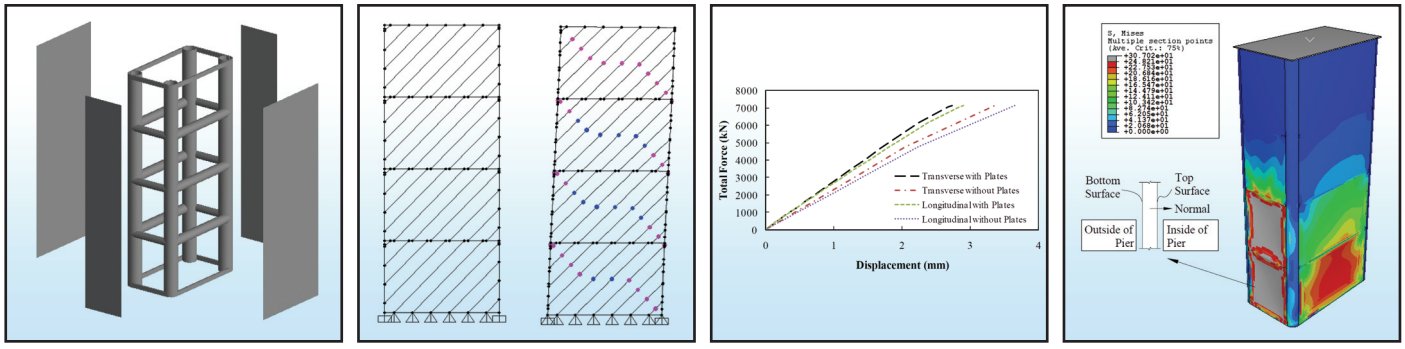

Technical Report MCEER-08-0030

December 19, 2008

This research was conducted at the University at Buffalo, State University of New York and was supported by the Federal Highway Administration under contract number DTFH61-07-C-00020.

NOTICE

This report was prepared by the University at Buffalo, State University of New York as a result of research sponsored by MCEER through a contract from the Federal Highway Administration. Neither MCEER, associates of MCEER, its sponsors, the University at Buffalo, State University of New York, nor any person acting on their behalf:

a. makes any warranty, express or implied, with respect to the use of any information, apparatus, method, or process disclosed in this report or that such use may not infringe upon privately owned rights; or

b. assumes any liabilities of whatsoever kind with respect to the use of, or the damage resulting from the use of, any information, apparatus, method, or process disclosed in this report.

Any opinions, findings, and conclusions or recommendations expressed in this publication are those of the author(s) and do not necessarily reflect the views of MCEER or the Federal Highway Administration.

Development of a Steel Plate Shear Wall Bridge Pier System Conceived from a Multi-Hazard Perspective

by

David Keller[1] and Michel Bruneau[2]

Publication Date: December 19, 2008
Submittal Date: May 14, 2008

Technical Report MCEER-08-0030

Task Number 020-3.4

FHWA Contract Number DTFH61-07-C-00020

1 Structural Engineer, Weidlinger Associates, Inc.; Former Graduate Student, Department of Civil, Structural and Environmental Engineering, University at Buffalo, State University of New York
2 Professor, Department of Civil, Structural and Environmental Engineering, University at Buffalo, State University of New York

MCEER
University at Buffalo, State University of New York
Red Jacket Quadrangle, Buffalo, NY 14261
Phone: (716) 645-3391; Fax (716) 645-3399
E-mail: *mceer@buffalo.edu*; WWW Site: *http://mceer.buffalo.edu*

Preface

MCEER is a national center of excellence dedicated to the discovery and development of new knowledge, tools and technologies that equip communities to become more disaster resilient in the face of earthquakes and other extreme events. MCEER accomplishes this through a system of multidisciplinary, multi-hazard research, in tandem with complimentary education and outreach initiatives.

Headquartered at the University at Buffalo, The State University of New York, MCEER was originally established by the National Science Foundation in 1986, as the first National Center for Earthquake Engineering Research (NCEER). In 1998, it became known as the Multidisciplinary Center for Earthquake Engineering Research (MCEER), from which the current name, MCEER, evolved.

Comprising a consortium of researchers and industry partners from numerous disciplines and institutions throughout the United States, MCEER's mission has expanded from its original focus on earthquake engineering to one which addresses the technical and socio-economic impacts of a variety of hazards, both natural and man-made, on critical infrastructure, facilities, and society.

The Center derives support from several Federal agencies, including the National Science Foundation, Federal Highway Administration (FHWA), and the Department of Homeland Security/Federal Emergency Management Agency, State of New York, other state governments, academic institutions, foreign governments and private industry.

The Center's Highway Project, primarily funded by the FHWA since 1992, focuses on the development of improved seismic design, evaluation, and retrofit methodologies and strategies for new and existing bridges and other highway structures. Over the years, MCEER has produced a new seismic retrofitting manual, consisting of two parts (bridges and other highway structures), as well as research products on the seismic retrofitting of truss bridges, seismic isolation manual and Risks from Earthquake Damage to Roadway System (REDARS).

In 2007, MCEER was awarded a new contract, "Innovative Technologies and Their Applications to Enhance the Seismic Performance of Highway Bridges." The major focus of the research program is on the development of detailed technology to apply accelerated bridge construction (ABC) in seismic regions, and the development of innovative seismic protection technologies that can enhance the seismic performances of precast reinforced concrete bridges with an emphasis on ABC.

This report introduces an innovative and integrative concept of a bridge box pier system that incorporates Steel Plate Shear Walls (SPSW) to resist multiple hazards including earthquakes, vehicle collisions, tsunamis (and indirectly storm surges), and blasts. The proposed bridge

pier concept simultaneously considers the constraints and demands for each hazard of interest. Simplified approaches for multi-hazard analyses and design are presented. Additionally, nonlinear finite element analyses are performed to better understand the system's behavior. It is found that the system has adequate ductility, redundancy and strength to resist each of the hazards. The system resists the seismic hazard through tension field action in the plates over the pier's height. For collision hazards, the steel plates mitigate global deformations of the piers by developing tension field action. It is also observed that the proposed SPSW pier system has significant capacity against tsunami demands, where the pier's plates are considered sacrificial and the columns remain essentially elastic. Barring local failure, the columns have the deformation capacity necessary to resist the deformations imposed by blast loads.

ABSTRACT

Bridges are built in a variety of locations, many of which are susceptible to multiple extreme hazards. New York City and South Carolina, for example, are regions susceptible to hurricanes and earthquakes, and bridges in all regions are susceptible to vehicle collisions and blasts. This exposure and vulnerability to multiple hazards underscores the need to develop an innovative design concept for bridges from a multi-hazard perspective, which is the objective of this research. Given that damage to bridge piers could lead to closure or, in extreme instances, to collapse of bridges, the focus of this research was on ductile and redundant pier systems. Accordingly, a bridge pier system incorporating the favorable qualities of steel plate shear walls (SPSWs) (e.g. ductility, redundancy, and ease of repair) capable of resisting multiple extreme hazards was sought.

This research considered four extreme hazards, namely, earthquakes, vehicle collisions, tsunamis (and indirectly storm surge), and blasts. A search for an integrative pier concept that simultaneously considered the constraints and demands germane to each hazard was conducted, resulting in a SPSW box pier concept. Through means of simplified analysis and design approaches, a detailed design of this concept was achieved, which was then analyzed for the demands of each hazard to investigate the system's anticipated global behavior and resistance to each hazard. For a better understanding of the system's behavior in resisting the hazards, nonlinear finite element analyses were conducted.

The proposed system was found to have adequate ductile performance and strength for each of the hazards. Investigation with finite element analyses demonstrated the system to behave as expected (based on simplified analysis) in resisting the seismic hazard. In resisting the collision hazard, the plates, which were conservatively neglected in the simplified analysis, were found to mitigate global deformation in the pier by developing tension field action. Moreover, the pier was observed to have significant capacity against the imposed tsunami demands, where the pier's plates were considered sacrificial, and where the pier's vertical boundary elements (VBEs) remained essentially elastic. Barring local failure, the VBEs were also observed to have significant deformation capacity for resisting the blast hazard, applied with statically distributed loads.

ACKNOWLEDGEMENTS

The authors thank Amjad Aref at the University at Buffalo, for his valuable advice regarding finite element modeling and analyses. This research was conducted at the University at Buffalo (The State University of New York) and was supported by the Federal Highway Administration under award number DTFH61-07-C-00020 to the Multidisciplinary Center for Earthquake Engineering Research. However, any opinions, findings, conclusions and recommendations presented in this report are those of the authors and do not necessarily reflect the views of the sponsors.

TABLE OF CONTENTS

SECTION	TITLE	PAGE
1	**INTRODUCTION**	**1**
1.1	The Need for Multi-Hazard Considerations in Bridges	1
1.2	The Multi-Hazard Concept	2
1.3	Topics in the Field of Multi-Hazards	2
1.3.1	Mismatched Design Solutions	3
1.3.2	A System's Approach to Design	5
1.3.3	Calibration in Design	5
1.4	Challenge for the Multi-Hazard Concept	6
1.5	Scope of this Research	6
1.6	Organization of this Report	7
2	**HAZARD LOADS**	**9**
2.1	General	9
2.2	Earthquakes	10
2.2.1	SDOF Simplification	10
2.2.2	AASHTO Specifications	12
2.3	Vehicle Collisions	16
2.4	Tsunamis	16
2.4.1	Flow Velocity	17
2.4.2	Hydrostatic Forces	19
2.4.3	Hydrodynamic Forces	20
2.4.4	Breaking Wave Forces	21
2.4.5	Surge Forces	22
2.4.6	Debris Impact Forces	24
2.4.7	Load Combinations	25
2.5	Blast	26
2.5.1	Characterization of a Blast	26
2.5.2	Scaled Distance	27
2.5.3	Reflection	28
2.5.3.1	Normal Reflection	30
2.5.3.2	Regular and Mach Reflection	30
2.5.4	Blast Environments	31
2.5.4.1	Free-Air Burst	31
2.5.4.2	Air Burst	32
2.5.4.3	Surface Burst	33
2.5.4.4	Plausible Blast Environment for Bridges	33
2.5.5	Blast Wave Parameters for TNT Explosives	34
2.5.6	Strain Rate Effects	37
3	**STEEL PLATE SHEAR WALL APPLICATIONS, MECHANICS, AND DESIGN**	**39**
3.1	General	39

TABLE OF CONTENTS (CONT'D)

SECTION	TITLE	PAGE
3.2	Introduction to Steel Plate Shear Walls	40
3.2.1	Applications	40
3.2.2	Types of Infill Panels	40
3.3	Mechanics of Unstiffened SPSWs	41
3.3.1	Infill Plate Behavior	41
3.3.2	Forces on Boundary Frame	43
3.4	Simplified Modeling and Analysis	45
3.5	Design of Unstiffened SPSWs	47
4	**BRIDGE PIER SYSTEM DEVELOPMENT**	**51**
4.1	General	51
4.2	Retrofit Concepts for Existing Bridges	52
4.2.1	Prototype Bridge #1	52
4.2.2	Supplementary Walls Attached to Bent Cap	53
4.2.3	Supplementary Walls Integral with Reinforced Concrete Columns	55
4.2.4	Integral SPSWs with Perforations	56
4.3	New Bridge Concepts Using Box Pier Systems	57
4.3.1	Modification of Prototype Bridge #1 Geometry	57
4.3.2	Six-Column Wall Pier	58
4.3.3	Four-Column Pier	59
4.3.4	Prototype Bridge #2	60
4.3.5	Application of the Four-Column Pier System	61
4.3.6	Prototype Bridge #2 with Integral Pier Caps	63
4.3.7	Final Multi-Hazard Pier Concept	64
5	**SIMPLIFIED ANALYSIS AND DESIGN**	**67**
5.1	General	67
5.2	Interaction Equations	68
5.2.1	Onset of Yielding	68
5.2.2	Fully Plastic Yielding	69
5.3	Earthquake	70
5.3.1	Idealization of Behavior	71
5.3.2	Bridge Seismic Parameters	71
5.3.3	Method of Analysis and Design	72
5.3.3.1	Boundary Frame Details	72
5.3.3.2	Desired Boundary Frame Behavior	73
5.3.3.3	Plate Sizing and Representation	74
5.3.3.4	Constraints	75
5.3.3.5	Pushover Description	76
5.3.3.6	SAP2000 Model	78
5.3.3.7	SAP2000 Analysis and Design	78
5.3.4	Final Seismic Design and Analysis Results	80

TABLE OF CONTENTS (CONT'D)

SECTION	TITLE	PAGE
5.3.5	Relative Contributions to Total Strength	83
5.4	Vehicle Collision	84
5.4.1	Simplified Collision Analysis	84
5.4.2	Summary of Simplified Collision Analysis	86
5.5	Tsunami	87
5.5.1	Plate Analysis for Out-of-Plane Loads	87
5.5.2	Simplified Tsunami Analysis	93
5.5.2.1	Tsunami Loads Acting on Pier	93
5.5.2.2	Load Representation on Pier	95
5.5.2.3	SAP2000 Analysis	97
5.5.3	Summary of Simplified Tsunami Analysis	98
5.6	Blast	99
5.6.1	Plate Analysis for Out-of-Plane Impulse Loading	99
5.6.2	Simplified Blast Analysis	103
5.6.2.1	Plate Analysis	103
5.6.2.2	Effect of Plate Yielding on the VBEs	105
5.6.2.3	Blast Effects on the VBEs	106
5.6.3	Summary of Simplified Blast Analysis	109
6	**FINITE ELEMENT ANALYSIS**	**111**
6.1	General	111
6.2	Earthquake	111
6.2.1	Part Definitions	112
6.2.2	Material Definition	113
6.2.3	Part Assembly	113
6.2.4	Constraints	114
6.2.5	Boundary Conditions	115
6.2.6	Meshing	115
6.2.7	Initial Imperfections	116
6.2.8	Pushover Analysis	118
6.2.9	Results	119
6.2.10	Summary of Observations	123
6.3	Vehicle Collision	124
6.3.1	Boundary Conditions	124
6.3.2	Analysis	125
6.3.3	Results	125
6.3.4	Summary of Observations	128
6.4	Tsunami	129
6.4.1	Meshing	129
6.4.2	Analysis	130
6.4.3	Results	131
6.4.4	Summary of Observations	135

TABLE OF CONTENTS (CONT'D)

SECTION	TITLE	PAGE
6.5	Blast	136
6.5.1	Analysis	136
6.5.2	Results	137
6.5.3	Summary of Observations	140
7	**CONCLUSIONS**	**141**
7.1	Summary	141
7.2	Conclusions	141
7.3	Future Work	142
8	**REFERENCES**	**143**
APPENDIX A	**DERIVATION OF INTERACTION EQUATIONS**	**149**
A.1	General	149
A.2	Onset of Yielding	150
A.3	Fully Plastic Yielding	151
APPENDIX B	**SIMPLIFIED SEISMIC ANALYSIS AND DESIGN WORKSHEETS**	**155**
APPENDIX C	**FIBER HINGE STUDY**	**169**
C.1	General	169
C.2	Study Set-up and Results	170
APPENDIX D	**TORSION EFFECTS ON VBES**	**173**
D.1	General	173
D.2	Study Setup	173
D.3	Study Summary and Results	175
APPENDIX E	**COMPARISON OF SIMPLIFIED PLATE ANALYSIS WITH FINITE ELEMENT PREDICTIONS**	**177**
E.1	General	177
E.2	Study Setup and Results	177
E.2.1	Longitudinal Plate	177
E.2.2	Transverse Plate	181
E.3	Summary of Observations	184
APPENDIX F	**CALCULATION OF LOADS AND PLATE EDGE REACTIONS FOR TSUNAMI LOAD CASES**	187

LIST OF FIGURES

FIGURE	TITLE	PAGE
2-1	Single-Degree-of-Freedom System	11
2-2	Elastic Seismic Coefficient versus Period	13
2-3	Generic Force Deformation Curves (Bozorgnia and Bertero 2004)	15
2-4	Design Velocities	19
2-5	Tsunami Wave Pressure Distribution with/without Soliton Break-up (Okada et al. 2004)	23
2-6	Tsunami Wave Runup on a Rigid Wall (Haritos et al. 2005)	24
2-7	Tsunami Force on a Rigid Wall (Haritos et al. 2005)	24
2-8	Proposed Loading Combinations (Nouri et al. 2007)	25
2-9	Free-Field Pressure History (USDA 1990)	27
2-10	Pressure History (Reflected vs. Incident) (FEMA 2003a)	28
2-11	Reflected Pressure Coefficient vs. Angle of Incidence (Smith and Hetherington 1994)	29
2-12	Schematic of Mach Reflection (Smith and Hetherington 1994)	30
2-13	Mach Stem and Triple Point Development for Height of Burst Explosion (Smith and Hetherington 1994)	31
2-14	Free Air Burst Environment (USDA 1990)	32
2-15	Air Burst Environment (USDA 1990)	32
2-16	Surface Burst Environment (USDA 1990)	33
2-17	Plausible Blast Environment for Bridges (Winget et al. 2005)	34
2-18	Positive Phase Shock Wave Parameters for a Spherical TNT Explosion in Free Air at Sea Level (USDA 1990)	35
2-19	Positive Phase Shock Wave Parameters for a Hemispherical TNT Explosion on the Surface at Sea Level (USDA 1990)	36
2-20	Stress – Strain Curves for (a) Concrete, and; (b) Steel (USDA 1990)	37
3-1	Typical Steel Plate Shear Wall (Bruneau et al. 2005)	40
3-2	Idealized Tension Field Action in an Unstiffened SPSW (Sabelli and Bruneau 2006)	41
3-3	Light-gauge Steel Plate Shear Wall Prior to Testing (Berman and Bruneau 2003a)	42
3-4	Buckling of Infill Panel (Berman and Bruneau 2003a)	42
3-5	Inward Flexure of SPSW Boundary Elements (Sabelli and Bruneau 2006)	43
3-6	Free Body Diagram of SPSW Elements (Sabelli and Bruneau 2006)	44
3-7	Strip Model for Static (Linear and Nonlinear) Analysis of SPSWs (Sabelli and Bruneau 2006)	45
3-8	Strip Model Representation of a Steel Plate Shear Wall (Berman and Bruneau 2003b)	46
3-9	Single-Story Collapse Mechanism (Berman and Bruneau 2003b)	48
4-1	Prototype Bridge #1 Elevation	52
4-2	Prototype Bridge #1 Cross-Section Elevation at Pier	53

LIST OF FIGURES (CONT'D)

FIGURE	TITLE	PAGE
4-3	Single Wall	54
4-4	Two Walls	54
4-5	Integral Walls	55
4-6	Integral Walls with Perforations	56
4-7	Modified Version of Prototype Bridge #1	57
4-8	Elevation at Pier: Box Pier Concept No. 1	58
4-9	Elevation at Pier: Box Pier Concept No. 2	59
4-10	Bridge Elevation	60
4-11	Cross-Section of Bridge Superstructure (Adapted from Mast et al. 1996a)	61
4-12	Elevation of Proposed Pier Concept	62
4-13	Bridge with Final Pier Concept	64
4-14	Bridge Section Elevations at Pier	65
4-15	3-D Pier and Bridge Segment From Above	65
4-16	3-D Pier and Bridge Segment From Below	66
4-17	Exploded View of Proposed Pier Concept	66
5-1	Cross Section of a Thin Tube	68
5-2	Superposition of Bending and Axial Stress Distributions (Onset of Yielding)	68
5-3	Superposition of Bending and Axial Stress Distributions (Fully Plastic Yielding)	69
5-4	Plot of Interaction Curves for Thin Circular Tube	70
5-5	Bridge with Final Pier Concept	70
5-6	Idealized Bridge Behavior	71
5-7	Design Spectra	72
5-8	Boundary Frame Geometry	73
5-9	Fiber Hinge Locations	74
5-10	Constraint Assignments	75
5-11	(a) Initial Gravity Load; (b) Lateral Pushover Pattern	77
5-12	Pushover in the Transverse Direction	77
5-13	(a) Parallel to Transverse Direction; (b) Parallel to Longitudinal Direction; (c) 3-D View of Strip Model	78
5-14	Bi-Directional Pushover Analysis: (a) 3-D Undeformed Position; (b) Final State of the Structure	82
5-15	Bi-Directional Pushover Analysis (Transverse Direction Results): (a) Undeformed Position; (b) Final State; (c) Pushover Curve	82
5-16	Bi-Directional Pushover Analysis (Longitudinal Direction Results): (a) Undeformed Position; (b) Final State; (c) Pushover Curve	83
5-17	Undeformed, Simplified Pier for Vehicle Collision Study	84
5-18	Vehicle Collision Scenarios	85
5-19	Deformed Shape for a Vehicle Load: (a) Parallel to the Bridge's Transverse Direction; (b) Angled at 45 deg., and; (c) Parallel to the Bridge's Longitudinal Direction	86

LIST OF FIGURES (CONT'D)

FIGURE	TITLE	PAGE
5-20	Geometry of a Parabola	88
5-21	Angle of Inclination of a Tangent to the Parabola	89
5-22	Idealized Out-of-Plane Plate Deformation	90
5-23	Simplified Plate using Parabolic Strips	91
5-24	Plate Divided into Strips	91
5-25	Plate Forces Imposed on Boundary Elements	92
5-26	Hydraulic Load Distributions	94
5-27	Load Case 1 Pressure Representation	96
5-28	Load Case 2 Representation: (a) Hydrostatic Pressure; (b) Hydrodynamic and Hydrostatic, and; (c) Combination of Edge Reactions	97
5-29	Deformed Shape of Pier for Two Load Cases: (a) Load Case 1: Surge and Impact, and; (b) Load Case 2: Drag, Hydrostatic, and Impact	98
5-30	Plate Information for Simplified Blast Analysis: (a) Typical One-Way Strips; (b) Assumed Strip Material Behavior, and; (c) a Typical Strip Cross-Section	102
5-31	Idealized Blast Loading History	103
5-32	Blast Scenario Showing (a) a Section Through the Pier; (b) a FBD at a Typical VBE; (c) Load Distribution on a Typical VBE, and; (d) Moment Diagram for a Typical VBE	105
5-33	Reduction of a VBE to an SDOF for Blast Analysis	107
5-34	SDOF Response Charts (Biggs 1964)	108
6-1	Cutting Plane for HBEs	112
6-2	Finite Element Pier Geometry: (a) without Plates, and; (b) with Plates	114
6-3	Final Meshed Pier Finite Element Model	116
6-4	First Mode Shape for Transverse Plates and Longitudinal Plates	117
6-5	Deformed Shape Following Application of Dead Load (Deformation Scale Factor = 10)	119
6-6	Deformed Shape Following Lateral Displacement (Deformation Scale Factor = 1)	120
6-7	Pushover Curves: (a) Transverse Direction, and; (b) Longitudinal Direction	121
6-8	Pier Pushover Behavior	122
6-9	Resultant Pushover Curve	123
6-10	Deformed Shape for Resultant Load: (a) 1780kN (400kips); (b) 3560kN (800kips); (c) 5340kN (1200kips), and; (d) 7120kN (1600kips) (Deformation Scale Factor = 5)	126
6-11	von Mises Stress Contours for Resultant Loads: (a) 1780kN (400kips); (b) 3560kN (800kips); (c) 5340kN (1200kips), and; (d) 7120kN (1600kips) (Deformation Scale Factor = 5)	127
6-12	Basic Behavior of the Pier Subject to a Vehicle Collision	127
6-13	Effect of Plates on Deformation	128
6-14	Modified Mesh for Tsunami Hazard	130

LIST OF FIGURES (CONT'D)

FIGURE	TITLE	PAGE
6-15	Final Deformed Shape (Deformation Scale Factor = 2) for a Water Height up to: (a) First Level; (b) Second Level; (c) Third Level, and; (d) Top of Pier	132
6-16	von Mises Stress Contours (MPa) After Application of Hydrodynamic Pressure	133
6-17	von Mises Stress Contours (MPa): (a) After Application of Hydrostatic Pressure, and; (b) After Application of Hydrodynamic Pressure	134
6-18	Base Shear vs. Top Lateral Displacement	135
6-19	Deformed Shape of Pier (Deformation Scale Factor = 1): (a) VBE Loaded from Pier's Exterior, and; (b) VBE Loaded from Pier's Interior	138
6-20	Schematic Displacement of 1st Story VBE	139
6-21	Resultant Displacement at VBE Mid-Height	139
A-1	Cross Section for a Thin Tube	149
A-2	Superposition of Bending and Axial Stress Distributions (Onset of Yielding)	150
A-3	Superposition of Bending and Axial Stress Distributions (Fully Plastic Yielding)	151
A-4	Plot of Interaction Curves for a Thin Circular Tube	153
C-1	Fiber Hinge in a Circular Tube	169
C-2	Fiber Hinge Study Structure	170
C-3	Results of the Study	171
D-1	Torsion Study Setup: (a) Forces Acting on the Cross-Section; (b) the Study Structure, and; (c) the Internal Torsion Force Diagram	174
D-2	Torsion Demand-Capacity Ratio vs. Height	176
E-1	Longitudinal Plate Mesh	178
E-2	Pressure vs. Displacement Comparison Between Finite Element Modeling and Simplified Method (Longitudinal Plate)	178
E-3	Plate Edge Reactions: (a) along the Vertical Edge, and; (b) along the Horizontal Edge	179
E-4	Plate Edge Reactions: (a) along the Vertical Edge, and; (b) along the Horizontal Edge	180
E-5	Transverse Plate Mesh	181
E-6	Pressure vs. Displacement Comparison Between Finite Element Modeling and Simplified Method (Transverse Plate)	181
E-7	Plate Edge Reactions: (a) along the Vertical Edge, and; (b) along the Horizontal Edge	182
E-8	Plate Edge Reactions: (a) along the Vertical Edge, and; (b) along the Horizontal Edge	183
E-9	Elevation of Section Cut Through the Center of the Transverse Plate's Short Dimension	185
E-10	Elevation of Section Cut Through the Center of the Transverse Plate's Long Dimension	185

LIST OF TABLES

TABLE	TITLE	PAGE
1-1	Reinforcing and Conflicting Design Aspects (FEMA 2004)	4
2-1	Substructure Response Modification Factors (AASHTO 2007)	15
2-2	Drag Coefficients for Larger Obstructions (FEMA 2000)	21
2-3	Dynamic Increase Factors for Steel and Concrete (Mays and Smith 1995)	38
5-1	Final Design Parameters	81
5-2	Equivalent Uniform Pressure Acting on Plates	94
5-3	Load-Mass Factors for Elastic Behavior (Adapted from Biggs (1964))	100
5-4	Investigation of Plates Subjected to Blast Loading	104
C-1	Results of Fiber Hinge Study	171

CHAPTER 1

INTRODUCTION

1.1 The Need for Multi-Hazard Considerations in Bridges

Bridges are built in a variety of locations, many of which are susceptible to multiple extreme hazards. New York City and South Carolina, for example, are regions susceptible to hurricanes and earthquakes, and bridges in all regions are susceptible to vehicle collisions and blasts. In fact, numerous bridges have been damaged by extreme hazards. Bridge damage due to earthquakes has been substantial following many earthquakes, two examples being the 1994 Northridge and the 1995 Kobe earthquakes, which resulted in non-ductile flexure and shear failures of reinforced concrete bridge piers (Priestley et al. 1996). Bridge damage was also widespread as a result of storm surges, due to hurricanes (such as Hurricane Katrina) or tsunamis. In particular, relief efforts following the 2004 Sumatra earthquake and Tsunami were hindered by extensive damage to bridges (Saatcioglu et al. 2005). Vehicle collisions have also damaged bridge piers, and terrorist attacks destroying bridge substructure elements could also cripple bridges.

This exposure and vulnerability to multiple hazards underscores the need to develop an innovative design concept for bridges from a multi-hazard perspective, which is the objective of this research. Given that this is a rather large proposition, the scope was limited by focusing on developing a pier system that incorporated concepts from steel plate shear walls (SPSWs) design. Bridge piers, which are oftentimes only designed for one or two extreme hazards (e.g. earthquakes and vehicle collisions), are vulnerable elements whose failure could lead to bridge closure or even collapse if they are not sufficiently resilient to sustain the demands of multiple hazards. A system incorporating SPSWs was sought because of their ductile nature, because of the redundancy they offer, and because they are easy to repair. Such qualities of SPSWs make them a resilient structural system that, although unknown at this time, should be capable of

resisting multiple hazards. However, SPSW concepts, while already implemented in buildings, have never been developed for bridges, which creates an additional challenge.

Section 1.2 introduces the multi-hazard concept, Section 1.3 briefly describes topics within the multi-hazard field, and Section 1.4 discusses a challenge that the multi-hazard concept faces. Section 1.5 identifies the scope of this research, and Section 1.6 describes the organization of this report.

1.2 The Multi-Hazard Concept

The concept formally referred to as multi-hazard engineering has recently emerged as a new interest in the field of civil engineering. It addresses the anticipated cost implications of growingly complex structures required to resist the sometimes conflicting demands of multiple hazards (Ettouney et al. 2005).

Bruneau (2007) describes this concept as follows: "A true multi-hazard engineering solution is a concept that simultaneously has the desirable characteristics to protect and satisfy the multiple (contradicting) constraints inherent to multiple hazards." Accordingly, he states that multi-hazard engineering calls for holistic designs that encompass all hazards in an integrated framework, and that provide optimized, single cost/single concept solutions rather than a collection of multiple design schemes.

1.3 Topics in the Field of Multi-Hazards

There are three major topics in the emerging field of multi-hazard engineering: (i) mismatched design solutions; (ii) a system's approach to the design of structures to resist multiple hazards, and; (iii) calibration in design. These three topics are discussed further in Sections 1.3.1 to 1.3.3.

1.3.1 Mismatched Design Solutions

Favorable features for design against one hazard may inevitably be unfavorable for other hazards. In this sense, enhancing and optimizing a structure's design for one hazard could be detrimental to the same structure for the purpose of resisting another hazard.

Such conflicting outcomes are well illustrated in the Federal Emergency Management Agency document FEMA 424 (FEMA 2004), which focuses on improving school safety against three hazards, namely earthquakes, hurricanes, and floods. Although these hazards are different in terms of geographic exposure, warning time, frequency, and risk, they all have the potential to cause damage and loss. This document compares protection design methods and design aspects for each of the hazards from a standpoint of how they reinforce or conflict with one another. Table 1-1, which is taken from FEMA 424, provides this comparison for various aspects of structural systems with respect to blast and fire, in addition to earthquakes, floods, and hurricanes. In that table, a cross indicates that the corresponding protective design feature is undesirable, a checkmark indicates the design feature to be desirable, and a box indicates that the design feature is of no significance for the corresponding hazard. The trends in that table show that, most frequently, a specific design aspect or proposed protective system can be effective for one hazard and at the same time undesirable for another. FEMA 424 also provides other similar comparisons for design features related to site characteristics, architectural aspects, building envelopes, and mechanical building equipment.

Table 1-1 Reinforcing and Conflicting Design Aspects (FEMA 2004)

Building System Protection Methods: Reinforcements and Conflicts							
System ID	Existing Conditions or Proposed Protection Methods	The Hazards					
		Earth-quake	Flood	Wind	Security/Blast (FEMA 428)	Fire	Discussion Issues
3	**Structural Systems**						
	3-1 Heavy structure: reinforced concrete (RC) masonry, RC or masonry fireproofing of steel	✘	✔	✔	✔	✔	Increases seismic forces, but generally beneficial against other hazards.
	3-2 Light structure: steel/ wood	✔	✘	✘	✘	✘	Decreases seismic forces, but generally less effective against other hazards.
	3-3 URM exterior load bearing walls	✘	✘	✘	✘	✘	
	3-4 Concrete or reinforced CMU exterior structural walls	✔	✔	✔	✔	✔	
	3-5 Soft/weak first story	✘	✘ ✔	✘	✘	✘	Very poor earthquake performance, and vulnerable to blast. Generally undesirable for flood and wind. Elevated first floor is beneficial for flood if well constructed, but should not be achieved by a weak structure that is vulnerable to wind or flood loads.
	3-6 Indirect load path	✘	❑	✘	✘	✘	Undesirable for highly stressed structures, and fire weakened structure is more prone to collapse. Not critical for floods.
	3-7 Discontinuities in vertical structure	✘	❑	✘	✘	✘	Undesirable for highly stressed structures causes stress concentrations, and fire-weakened structure is more prone to collapse. Not critical for floods.
	3-8 Seismic separation joints	✔	❑	❑	❑	✘	Possible path for toxic gases to migrate to other floors.
	3-9 Ductile detailing and connections/steel	✔	❑	✔	✔	❑	Provides a tougher structure that is more resistant to collapse.
	3-10 Ductile detailing/RC	✔	❑	✔	✔	❑	Provides a tougher structure that is more resistant to collapse.
	3-11 Design for uplift (wind)	✔	❑	✔	✔	❑	Necessary for wind; may assist in resisting seismic or blast forces.
	3-12 Concrete block, hollow clay tile around exit ways and exit stairs	✘	❑	❑	✘	✔	May create torsional structural response and/or stress concentration in earthquakes in frame structures unless separated, and if unreinforced wall is prone to damage. Properly reinforced walls preserve evacuation routes in the event of fire or blast.

1.3.2 A System's Approach to Design

Multi-hazard engineering is not the consideration of demands from multiple hazards being imposed on a structure simultaneously, nor is it about addressing demands of multiple hazards in succession independent of each other as part of the design process; rather, it is optimization in design by simultaneously considering the demands of multiple hazards (MCEER 2007).

To make a design that is beneficial for one hazard while at the same time avoiding the possibility of making the structure vulnerable to other hazards, a system's approach to design must be undertaken. Such an approach necessitates designers to be knowledgeable of multiple hazards, and to consider the numerous and sometimes contradicting demands from the multiple hazards at the onset of the design process.

1.3.3 Calibration in Design

As a part of the emerging field of multi-hazard engineering, researchers have been and are seeking methods by which load and resistance factors can be determined and calibrated for multiple extreme hazards for use in LRFD specifications, such as the LRFD AASHTO Bridge Design Specification. LRFD specifications are reliability-based which consider statistical distributions of loads and resistances. On that basis, load and resistance factors should be calibrated to achieve uniform reliability levels for the design of components over a range of design aspects such as load effects, materials, and structure geometry, including extreme events. For example, Ghosn et al. (2003) conducted studies that considered live load, scour, wind, vessel collision, and earthquakes with the objective of developing design procedures for the consideration of extreme loads and their combinations to highway bridges. From the study, four extreme load combinations were recommended. Currently, research is underway by Lee et al. (2006) to establish commeasurable criteria by which the effects on bridges from various hazards can be compared based on the approach of the AASHTO LRFD.

1.4 Challenge for the Multi-Hazard Concept

A significant limitation to the application of the multi-hazard concept exists in that there is no set of tools (i.e. design guides and equations) available to facilitate multi-hazard design (Ettouney et al. 2005). There needs to be more objective-driven demonstration and technical substantiation of the concept, which would provide engineers with direction on how to employ the multi-hazard concept and how to incorporate it into the overall design of structures. By overcoming this limitation and by adhering to a multi-hazard design approach, more economical and safer structures can be obtained. Ettouney et al. (2005) provide a list of benefits for considering a multi-hazard approach, some of which include: potential for economic designs and constructions, a more accurate estimation of inherent resiliency of systems, a more accurate treatment/estimation of life cycle cost of systems, and a more accurate analysis of systems.

1.5 Scope of this Research

The research presented herein considers the engineering aspect of the field of multi-hazards. This report investigates how to modify and adapt a system originally conceived for seismic applications, more specifically steel plate shear walls, for bridge applications as a multi-hazard resistant system. To explore possible designs, a variety of concepts are proposed, and, based on the reinforcing and conflicting nature of the hazards being considered, a discussion of their possible applicability and limitations is provided. Ultimately, a design that accounts for the demands of all hazards being considered, which utilizes steel plate shear walls with round tubular steel sections for boundary elements in a box configuration, is chosen for further development as a bridge pier system. Following the design of the system for a seismic hazard and after investigation of the system for demands imposed by the other hazards (vehicle collision, tsunami, and blast) with simplified analyses, advanced finite element analysis methods are employed to further investigate the system for application as a multi-hazard conceptual design.

1.6 Organization of this Report

Chapter 2 provides an overview of the hazards considered in this research, namely earthquakes, vehicle collisions, tsunamis (and indirectly storm surge from hurricanes), and blasts. While bridge piers could be subjected to other hazards, in general, the hazards considered here are some of the most likely extreme loads of current interest nationwide. This is an important aspect of the multi-hazard design approach since an engineer must be familiar with the various hazards being considered to appropriately account for the demands they impose and to be aware of their reinforcing and/or conflicting nature.

Chapter 3 presents an overview of the structural behavior and design of steel plate shear walls (SPSWs) and provides information regarding SPSWs relevant to the system developed for this research. An understanding of what SPSWs are and how they behave is important in the conception of a multi-hazard design having SPSWs and in the analysis and design of the system being proposed. The mechanics of unstiffened SPSWs, along with an overview of methods of analysis and design is provided.

Chapter 4 illustrates various concepts that were conceived and attempted in the process of arriving at a final system simultaneously considering the constraints and demands germane to each hazard. For each concept, a discussion of reasons for its conception and reasons for its dismissal are provided. The final integrative concept (explored further in subsequent chapters) and justification for its expected satisfactory structural behavior are presented in this chapter.

Chapter 5 describes the simplified analyses undertaken to obtain a detailed design of the structural system considered and to gain a preliminary understanding of its global behavior when subjected to the multiple hazards considered. On the strength of knowledge from Chapter 4 that the selected system is workable in a multi-hazard perspective, detailed design considered each hazard individually. The system was designed for the seismic hazard using methods described in AASHTO (2007) and in the AISC Steel Plate Shear Wall Design Guide (2006). The loads of each of the other hazards considered were then imposed and observations regarding the system's behavior were made.

Chapter 6 uses nonlinear finite element analysis to investigate the validity of the proposed design. More specifically, trends in the system's behavior are observed to investigate how the proposed structural system resists multiple hazards, and its suitability as a multi-hazard design is assessed.

Chapter 7 offers conclusions based on the findings from this research. Included are comments on how well the system's anticipated behavior agreed with the results obtained from the advanced analyses. Finally, recommendations for future avenues of investigation based on the findings of this research are provided.

CHAPTER 2

HAZARD LOADS

2.1 General

This chapter's purpose is to briefly summarize current knowledge of the loads and how to determine the loads considered in structural analysis for the selected extreme hazards being considered for this research (i.e. earthquakes, vehicle collisions, tsunamis (and indirectly storm surges from hurricanes), and blasts). It is recognized that other hazards exist, such as wind (from tornadoes or hurricanes), fire, and bridge overload but these are beyond the scope of this study as bridge pier failures are less likely from these hazards, except fire for which protection could be achieved by the use of intumescent paint. Each section briefly discusses potential impacts of these hazards on bridges, reviews relevant literature regarding quantification of these loads, and describes current methods for imposing such loads on structures. In essence, this chapter provides information on how to account for the demands of each hazard in analysis and design. Section 2.2 provides information on the seismic hazard. Idealizations through which structures are simplified are introduced, which leads into a brief overview of how AASHTO treats seismic effects on bridges. A summary of AASHTO provisions regarding vehicle collision is provided in Section 2.3. Section 2.4 provides an overview of reviewed literature regarding tsunami demands on structures, and Section 2.5 provides information regarding the blast hazard.

It is recognized that it is unconventional for a research report to review basic principles of design. However, the understanding is that in the emerging field of multi-hazards, most engineers are familiar with one of these extreme loads and far less with the others. As this summary unfolds, reference to various sources where additional and more comprehensive information can be found is provided.

2.2 Earthquakes

In general, earthquakes occur when tectonic plates rupture and move in relation to one another resulting in a large release of energy, which is felt on the earth's surface as shaking. Their potentially devastating consequences make earthquakes a hazard that needs to be considered in the design of structures. Extensive damage to bridges has been observed in a large number of past earthquakes. Two recent earthquakes that have caused damage to bridges include the 1994 Northridge and the 1995 Kobe earthquakes. The Northridge earthquake occurred on January 17th, 1994 in the San Fernando Valley, about 20 miles northwest of downtown Los Angeles. The Kobe earthquake, which struck Japan exactly one year after the Northridge earthquake had struck California, caused major damage to bridges and elevated highways. The major types of damage to reinforced concrete bridge piers during both earthquakes resulted from non-ductile flexure and shear failures (Priestley et al. 1996). Damage to steel bridges was also observed during the Kobe earthquake, including non-ductile failure and local buckling of steel columns (Bruneau et al. 1996).

Satisfactory performance of bridge structures subjected to earthquakes can be achieved by conducting seismic design in compliance with codes such as the 2007 AASHTO LRFD Bridge Design Specification. The specifications in this code are briefly discussed in Section 2.2.2 following a brief review in Section 2.2.1 of how simple systems are typically idealized as single-degree-of-freedom systems, and how the equation describing their response to seismic excitation is derived.

2.2.1 SDOF Simplification

When analyzing a structure subjected to seismic loading, the structure is typically idealized. For instance, the simple linear single level bridge bent in Figure 2-1, shown at the instant in time, *t*, is composed of two columns for which axial deformations are considered negligible and a rigid beam which constitutes the majority of the system's mass. In this example, the two columns are considered fixed-fixed. Figure 2-1 also shows that the base of the structure is being subjected to ground accelerations. The effect of the ground accelerations can be treated as an effective external seismic excitation force, $-m\ddot{u}_g(t)$, that acts at the location of the mass, and which acts in

a direction opposite to the ground acceleration. Thus, the seismic problem transforms into one in which the ground is stationary, but the structure is subjected to an effective external seismic force (Chopra 2001). In Figure 2-1, the algebraic sign of the force denotes an effective seismic force acting to the left.

Making these assumptions allows a reduction of this structure to a single-degree-of-freedom (SDOF) system, which is shown in the right half of Figure 2-1. Effectively, this simple one-story frame can be thought of as acting like a cart on rollers (on a frictionless surface) with mass, *m*, connected with a linear spring (for a linear system) with stiffness, *k*, and with a dashpot (or linear, viscous damper) with a damping coefficient, c. The linear spring is used to account for the resistance that the columns provide against translation of the mass. Because the columns are in parallel, the system stiffness is simply the sum of that offered by each column. The dashpot is included to account for any inherent or intentional damping (energy dissipation) within the system.

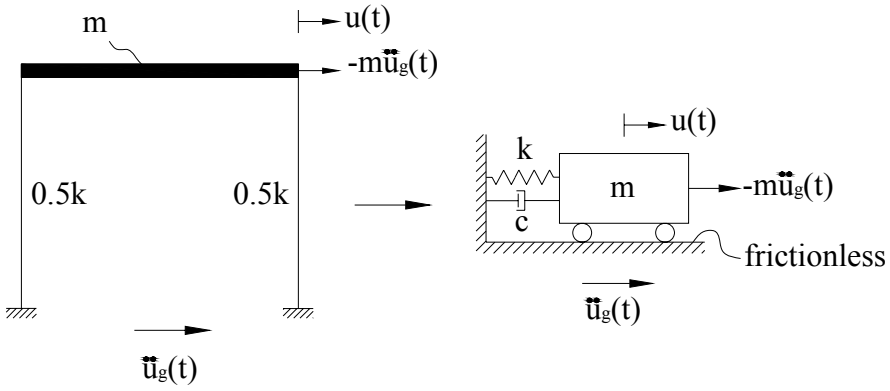

Figure 2-1 Single-Degree-of-Freedom System

With Newton's Second Law, an equation describing the motion of this system can be obtained. Consider the idealized representation of the system. If the cart is assumed to be displaced and moving to the right at time *t*, the spring and the damper resist the motion by providing resisting forces to the left. The resistance offered by the spring is in proportion to the relative displacement, *u(t)*, and the resistance offered by the damper is in proportion to the relative velocity of the system, $\dot{u}(t)$. By applying Newton's Second Law, which states that the sum of forces acting on an object equals the product of its mass and acceleration, (2-1) is obtained.

$$-ku(t) - c\dot{u}(t) - m\ddot{u}_g(t) = m\ddot{u}(t) \tag{2-1}$$

Through a simple arrangement of the terms in this equation, (2-2) is obtained.

$$m\ddot{u}(t) + c\dot{u}(t) + ku(t) = -m\ddot{u}_g(t) \tag{2-2}$$

Dividing each term by the system's mass, the familiar equation of motion of (2-3) is obtained,

$$\ddot{u}(t) + 2\zeta\omega_n\dot{u}(t) + \omega_n^2 u(t) = -\ddot{u}_g(t) \tag{2-3}$$

where ω_n is the natural angular frequency of the system:

$$\omega_n = \sqrt{\frac{k}{m}} \tag{2-4}$$

and where ζ is the damping ratio, expressed in terms of percentage of critical damping:

$$\zeta = \frac{c}{2\omega_n m} \tag{2-5}$$

While closed form solutions can be obtained for simple forcing functions, solutions to the equation of motion for the random forcing functions produced by earthquakes require the use of numerical methods to solve for the response of an SDOF. Using such procedures (for which much software is available), given an earthquake acceleration history and a specific amount of damping, a spectrum can be developed. A spectrum is a means of graphically displaying the maximum value of a response parameter (e.g. displacement, velocity, or total acceleration) for a number of SDOF systems, each with a different period, $T = 2\pi/\omega_n$, that are subjected to a specified earthquake acceleration record and that have a specified damping ratio. The maximum response parameter is typically plotted for a range of periods. For design purposes, a more general spectrum, which, in a sense, represents an average of a number of spectra for a set of earthquakes expected at a given site, is typically provided in codes.

2.2.2 AASHTO Specifications

AASHTO (2007) specifies a design spectrum to be used in seismic bridge design, expressed in terms of an elastic seismic response coefficient, C_{sm}. The elastic seismic response coefficient

can be written in the form of (2-6), where A is an acceleration coefficient, S is a site coefficient, and T_m is the period of vibration for the mth vibration mode.

$$C_{sm} = \begin{cases} \dfrac{1.2AS}{T_m^{2/3}} \le 2.5A \\ 2.5A \quad otherwise \end{cases} \tag{2-6}$$

The acceleration coefficient is site dependent and can be obtained from contour maps provided in Article 3.10.2 of the AASHTO specification, which shows values corresponding to earthquakes having a 475 year return period (also referred to as having a 10% probability of exceedance in a 50 year period) (AASHTO 2007). The site coefficient represents the effect of soil conditions on the elastic seismic response coefficient. Softer soils amplify the effect of earthquakes more than stiff soils. AASHTO provides site coefficients in Article 3.10.5 for four different soil profiles. Figure 2-2 shows a plot of the elastic seismic coefficient versus period considering an acceleration coefficient of 0.20, a site coefficient of 1.2 and a damping ratio of 5%.

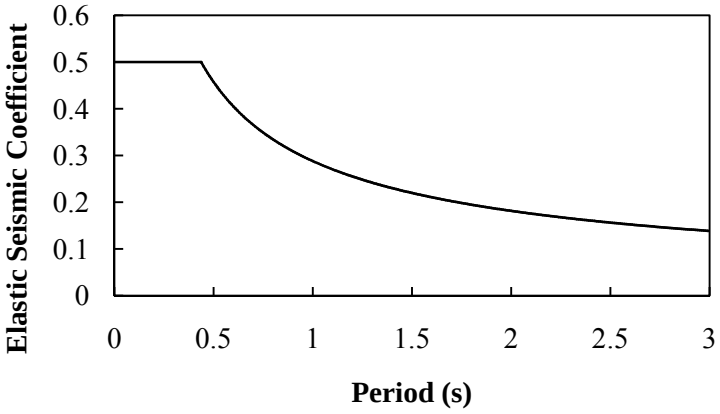

Figure 2-2 Elastic Seismic Coefficient versus Period

Other information that needs to be considered in the seismic design of a bridge is its importance and its seismic zone performance category. AASHTO (2007) addresses these in Articles 3.10.3 and 3.10.4, respectively. The seismic performance zone is used to specify certain methods of analysis and to specify design details, bridges in more severe seismic zones being subjected to more stringent requirements. Article 4.7.4 provides minimum analysis requirements for seismic effects on bridges, which are specified as a function of the seismic zone where the bridge is located, the importance of the bridge, and whether the bridge is regular or irregular. Available

methods of analysis listed in this article include the uniform load elastic method, the single-mode elastic method, the multimode elastic method, and the time history method. The uniform load elastic method will be considered here, as will be seen in subsequent chapters.

The uniform load elastic method is based on the fundamental vibration mode in either the longitudinal or transverse direction of the bridge (AASHTO 2007). The corresponding period is that of an equivalent SDOF oscillator whose stiffness is determined from the displacement resulting from an arbitrarily applied load. The elastic seismic response coefficient, obtained from (2-6), is then used to compute the equivalent uniform lateral seismic load acting on the bridge by multiplying it to the weight of the structure divided by the length over which it acts.

The above gives equivalent forces that would be imparted to the structure if it was to remain elastic. The AASHTO (2007) specification recognizes that it is generally uneconomical to design a bridge to remain elastic during a significant seismic event. Accordingly, the use of response modification factors is introduced.

Figure 2-3 displays two generic force displacement curves to illustrate the response modification factor concept. The dashed line is for a system that remains elastic and the other is for a system that is allowed to behave inelastically. In this figure, F_e is the elastic force demand that should be considered in design for structural systems to remain elastic, and F_s is the design strength obtained by dividing F_e by the response modification factor, R. By using an R value greater than unity in the design of a structural component, the component is designed for a force less than required by elastic analysis and is therefore anticipated to deform into the inelastic range.

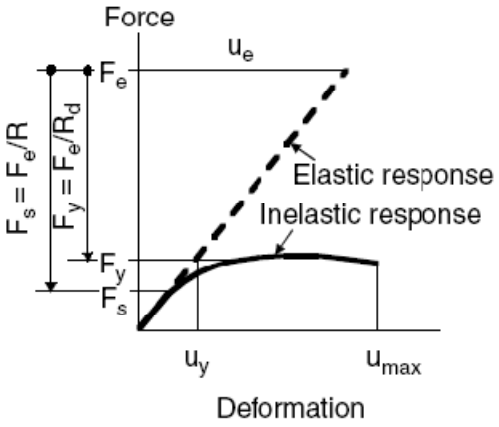

Figure 2-3 Generic Force Deformation Curves (Bozorgnia and Bertero 2004)

Article 3.10.7 of the AASHTO specification provides response modification factors for substructures, which are summarized in Table 2-1, and for connections. These different factors are intrinsically tied to specified detailing requirements to ensure that the components considered can develop the expected magnitude of inelastic response in a stable manner without loss of strength under repeated cyclic seismic excitation.

Table 2-1 Substructure Response Modification Factors (AASHTO 2007)

Substructure	Importance Category		
	Critical	Essential	Other
Wall-type piers - larger dimension	1.5	1.5	2.0
Reinforced concrete pile bents			
• Vertical piles only	1.5	2.0	3.0
• With batter piles	1.5	1.5	2.0
Single columns	1.5	2.0	3.0
Steel or composite steel and concrete pile bents			
• Vertical piles only	1.5	3.5	5.0
• With batter piles	1.5	2.0	3.0
Multiple column bents	1.5	3.5	5.0

Note that choice of a response modification factor depends on the direction in which the bridge is being analyzed. For instance, a wall may be assigned different R-factors for shaking in the transverse direction than for shaking in the longitudinal direction, on account of different structural behavior and ductility in those directions respectively. Following the determination of

the seismic demands, standard design principles must be employed to appropriately design the component or system under consideration.

2.3 Vehicle Collisions

AASHTO (2007) considers the impact of vehicles colliding into railings or barriers mounted to superstructures, as well as the possibility of vehicles colliding with piers and abutments. The focus of this research is on vehicles colliding with bridge substructures.

Guidance on how to load piers and abutments subject to vehicle collisions can be obtained from Article 3.6.5, *Vehicular Collision Force*, of the 2007 AASHTO LRFD Bridge Design Specifications. The specification states that abutments and piers located within a distance of 9000mm (30.0 ft) to the edge of a roadway shall be designed for an equivalent static force of 1800kN (400 kip). This equivalent static force is assumed to act at a height of 1200mm (4.0 ft) above the ground and in any direction in the horizontal plane. Moreover, the specification states that this equivalent static load can be idealized as a point load for individual columns, and as either a point load or, alternatively, an equivalent load considered to act over a reasonable area not greater than 1500mm (5.0 ft) wide by 600mm (2.0 ft) high for walls. Article C3.6.5.2 states that the 1800kN (400 kip) equivalent static force stems from information obtained from full-scale crash tests of barriers for redirecting 360kN (80.0 kip) tractor trailers, and from other truck collisions.

The specification states that the above equivalent static load procedure need not be followed if piers are protected by either of the following measures: an embankment, a structurally independent crashworthy ground-mounted 1370mm (54.0 in) high barrier located within 3000mm (10.0 ft) from the component being protected, or a 1070mm (42.0 in) high barrier located at more than 3000mm (10.0 ft) from the component being protected (AASHTO 2007).

2.4 Tsunamis

Tsunamis are rare events, but often result in devastation when they occur. In particular, damage to bridges resulting from spans being swept away or piers being destroyed can disrupt post

disaster relief efforts. In general, these events occur when a large volume of water is quickly displaced, as may be the case during an offshore earthquake. One such event was the Sumatra Earthquake and Tsunami that struck the coast of the Indian Ocean on December 26, 2004. This event, which was the result of a large earthquake, resulted in more than 310,000 casualties (Saatcioglu et al. 2005).

Available guidance for the determination of what loads to apply on structures and how to apply them when considering tsunami's include FEMA 55 (FEMA 2000) and the City and County of Honolulu Building Code (CCH) (CCH 2000). The ASCE document "Minimum Design Loads for Buildings and Other Structures" (i.e. ASCE 7-05) (ASCE 2006) provides some information on hydraulic loads for floods, and many of the equations provided in that document are similar to those presented in FEMA 55.

The forces typically resulting from such an event include hydrostatic forces, buoyancy forces, hydrodynamic forces, breaking wave forces, surge forces, debris impact forces, and effects of scour (not addressed in this research as this is a foundation design matter). Section 2.4.1 presents relationships for determining flow velocity, Section 2.4.2 provides information regarding the determination of hydrostatic forces, Section 2.4.3 covers hydrodynamic forces, Section 2.4.4 briefly discusses breaking wave forces, Section 2.4.5 reviews information regarding surge forces, Section 2.4.6 reviews information in regard debris impact forces, and Section 2.4.7 provides information on load combinations for this hazard.

2.4.1 Flow Velocity

Flow velocity is an integral part of determining the hydraulic forces on a structure, or on structural components. For instance, the calculation of hydrodynamic and debris impact forces depends on flow velocity. The velocity term in the equation for hydrodynamic pressure is squared which makes the choice of flow velocity critical in determining design loads since hydrodynamic loads account for much of the total tsunami-related force acting on structures (Nouri et al. 2007). Yet, as critical as determination of flow velocity may be, much uncertainty

exists in the estimates available at this time, based on current knowledge. As a result, conservatively high values for velocity are typically recommended by design codes.

For example, FEMA 55 presents some guidance on how to compute design flow velocities for floods and tsunamis; however, it warns that design velocities are subject to much uncertainty and recommends that conservative estimates be used. FEMA 55 presents equations, (2-7) through (2-9), for calculating design velocities, where h is the design stillwater depth and where t equals 1 second. The relationship in (2-7) is a lower bound velocity which could be used for determining flood velocities for structures far from any flood sources. The relationship in (2-8) is an upper bound relationship for determining flood flow velocities for use with sites that are located near a flood source or near obstructions that may intensify flood velocities. For design purposes, FEMA 55 recommends the use of flood velocities between these bounds. However, for extreme instances (e.g. tsunamis) an estimate of a design velocity is given by (2-9).

$$v_{LowerBound} = \frac{h}{t} \tag{2-7}$$

$$v_{UpperBound} = \sqrt{gh} \tag{2-8}$$

$$v_{tsunami} = 2\sqrt{gh} \tag{2-9}$$

These equations show that the tsunami flow velocity is twice the value of the upper bound design flood velocity. Figure 2-4 is a plot of the above three equations showing the variation of design velocity with the design stillwater depth.

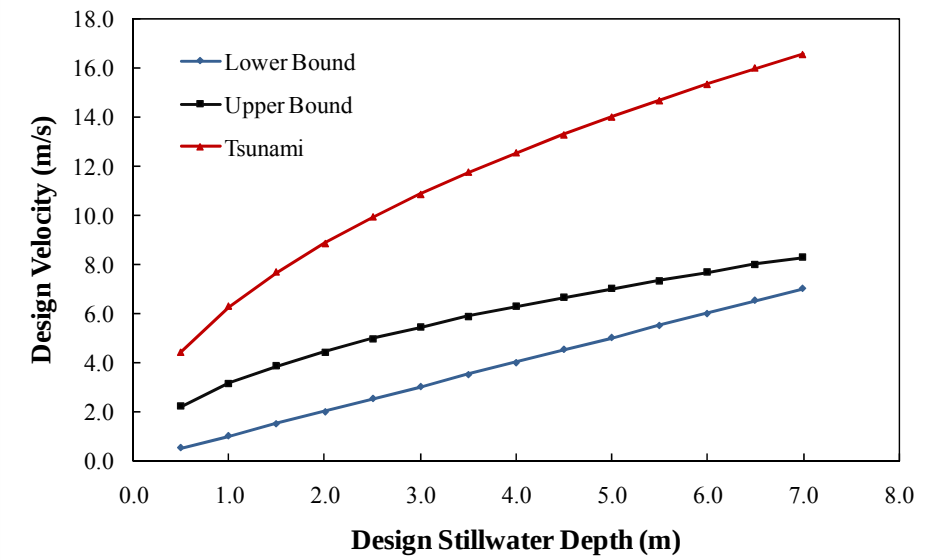

Figure 2-4 Design Velocities

2.4.2 Hydrostatic Forces

Hydrostatic forces result from standing (or slowly moving) water acting on an object. Hydrostatic forces present at a point are proportional to the depth of fluid above that point and act normally to the surface against which the fluid is in contact. FEMA 55 uses a linearly varying pressure distribution (as a function of depth) with the maximum pressure shown in (2-10) to define hydrostatic loads, where γ is the unit weight of the fluid being considered and h is the inundation depth.

$$P_h = \gamma h \tag{2-10}$$

The resultant of this pressure distribution on a vertical surface acts horizontally at a distance, measured from the base of the structure being considered, equal to one-third the water depth. The expression for hydrostatic force given in the CCH includes the addition of a velocity head term, which essentially accounts for the dynamic effect of flowing water.

Hydrostatic forces can also act vertically on submerged (or partially submerged) bodies. These forces are termed buoyancy forces and are proportional to the volume of a body that is submerged. The net upward buoyancy force stems from the fact that pressure increases with

water depth. Thus, the pressures resulting from beneath a volume are greater than the pressures acting above the volume. Buoyancy force is calculated according to (2-11) where V is the submerged volume of the object being considered.

$$F_b = \gamma V \tag{2-11}$$

2.4.3 Hydrodynamic Forces

When a body is immersed in fluid flowing around it, dynamic loads (or drag forces) are imposed, which are related to the interaction between the fluid and the object. The resulting forces can be described as impact loads on the front of the object, drag along the sides of the object, and suction on the downstream side the object. These forces are dependent on flow velocity and on geometry of the object. This is shown by (2-12), which is typically used to obtain hydrodynamic pressure where, ρ is the fluid's mass density, C_d is the drag coefficient, and v is the flow velocity.

$$P_D = \frac{1}{2}\rho C_d v^2 \tag{2-12}$$

In calculating hydrodynamic pressures, it is typically assumed that fluid flow is uniform; thus, the resultant of the pressure distribution acts at half the height over which the pressure is distributed. This assumed pressure distribution is common among FEMA 55, CCH, and AASHTO, with the exception of the recommended values for the drag coefficients. The CCH recommends a drag coefficient of 1.0 for circular piles, 2.0 for square piles, and 1.5 for walls, whereas FEMA 55 recommends 1.2 for round piles and 2.0 for square or rectangular piles. For larger obstructions, drag coefficient values based on width-to-depth ratios (or width-to-object height for completely submerged objects) are provided in FEMA 55, as shown in Table 2-2. For hydrodynamic loads on piers, AASHTO recommends a drag coefficient of 0.7 for semi-circular nosed piers, 1.4 for square ended piers, and 1.4 for debris lodged against piers.

Table 2-2 Drag Coefficients for Larger Obstructions (FEMA 2000)

Width to Depth Ratio	Drag Coefficient, C_d
From 1 - 12	1.25
13 - 20	1.30
21 - 32	1.40
33 - 40	1.50
41 - 80	1.75
81 - 120	1.80
> 120	2.00

Alternatively to (2-12), Yeh (2007) proposed (2-13) to calculate the total hydrodynamic force acting on structures as tsunamis run onshore, where *B* is the width of the structure in a plane normal to the direction of the flow.

$$F_d = \frac{1}{2}\rho C_d B(hv^2)_{\max} \tag{2-13}$$

This equation considers that the maximum flow depth, *h*, and the maximum flow velocity do not necessarily take place at the same time ($(hv^2)_{max} \neq h_{max}v^2_{max}$); rather, it suggests that the total hydrodynamic force be computed based on the maximum momentum flux, hv^2. Yeh presents (2-14) to roughly estimate $(hv^2)_{max}$, where *R* is the ground elevation at the maximum tsunami penetration measured from the initial shoreline, and *z* is the ground elevation at the location of interest.

$$\frac{(hv^2)_{\max}}{gR^2} = 0.125 - 0.235\frac{z}{R} + 0.11\left(\frac{z}{R}\right)^2 \tag{2-14}$$

Yeh emphasized that values obtained with this equation should be used as a guide since the formula is based on the assumption of a tsunami running up a uniformly sloping beach with no lateral variation in topography.

2.4.4 Breaking Wave Forces

FEMA 55 presents equations for determining the forces due to breaking waves and assumes them to act as loads at the stillwater level. The equations provided in FEMA 55 distinguish between breaking wave forces on piles and breaking wave forces on walls. Furthermore, the

cases where water is on both sides of a wall and where water is only on one side of a wall are considered separately. However, Nouri et al. (2007) comment that breaking wave equations are not applicable (in the same way they are for floods) when considering the effect of tsunamis.

Yeh (2007) commented on the consideration of breaking wave forces and the effects they have on structures inland, stating that they are the least likely of all the aforementioned hydraulic forces to affect onshore structures during tsunamis. After a wave breaks offshore it runs inland as a broken wave, or hydraulic-bore. As a tsunami-bore runs inland on dry ground it is referred to as a surge, which when initially impacting a structure produces a surge force rather than a breaking wave force (Yeh 2007).

2.4.5 Surge Forces

Surge forces are a result of the leading edge of a surge of water coming into contact with a structure or structural element being considered. Figure 2-5 depicts a proposed design force evaluation method for buildings located inland that are subjected to tsunami loading (Okada et al. 2004). Figure 2-5(a) shows the surge traveling as an unbroken soliton (a soliton being a wave that travels with maintained form), and Figure 2-5(b) represents the surge traveling as a broken soliton and striking a wall. The first case treats the effects with a hydrostatic pressure distribution that is three times the height of the surge, with a resultant force nine times the magnitude of a resultant hydrostatic force for the corresponding surge height. The second case uses the same distribution and superimposes an additional hydrostatic distribution at the base of the wall. This leads to a force factor of approximately 11 times the corresponding hydrostatic distribution (Haritos et al. 2005).

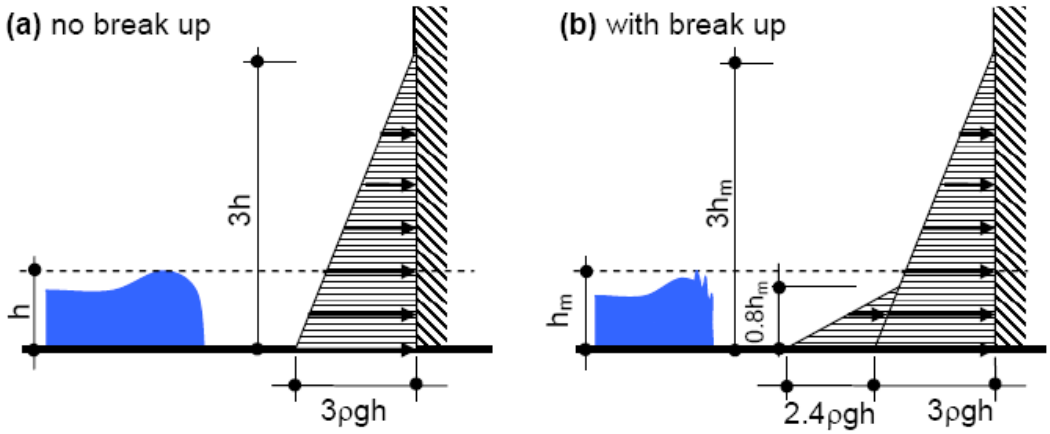

Figure 2-5 Tsunami Wave Pressure Distribution with/without Soliton Break-up (Okada et al. 2004)

The resultant surge force per unit width of wall corresponding to case (a) in Figure 2-5 is given by (2-15), where *h* is the surge height.

$$F_s = 4.5\rho g h^2 \tag{2-15}$$

This equation, adopted from Dames and Moore (1980), is specified by CCH. Note that this equation is only valid for wall heights greater than or equal to three times the surge height. Otherwise, it is recommended that the height of the pressure distribution be truncated at the height of the structure or the structural component being considered (Haritos et al. 2005).

Haritos et al. found (2-15) to be in agreement with their numerical findings. In their study, Haritos et al. numerically modeled a tsunami as a 5m high bore traveling along a flat horizontal surface with a velocity of 10m/s, eventually striking a rigid wall. Figure 2-6 shows the behavior of the model and Figure 2-7 shows a trace of the force per unit width acting on the wall. The force values observed in the "tail" portion of the force plot are in agreement with those corresponding to the proposed method by Okada et al.

Note, however, that Yeh (2007) argued that (2-15) is overly conservative for estimating surge forces. Rather, he suggested the use of (2-13) to estimate a design surge force, with a drag coefficient that is 150% the drag coefficient for the corresponding hydrodynamic force.

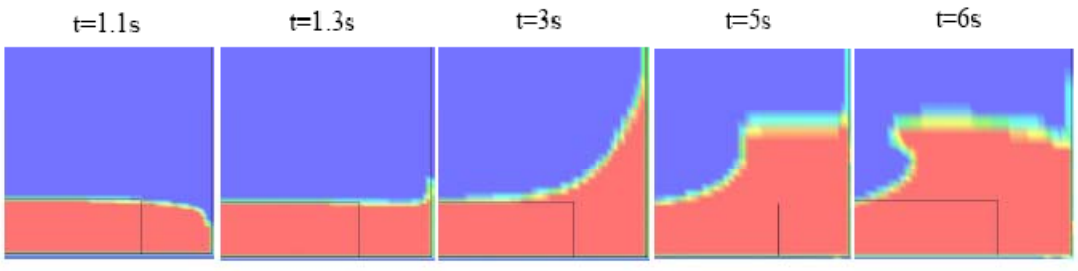

Figure 2-6 Tsunami Wave Runup on a Rigid Wall (Haritos et al. 2005)

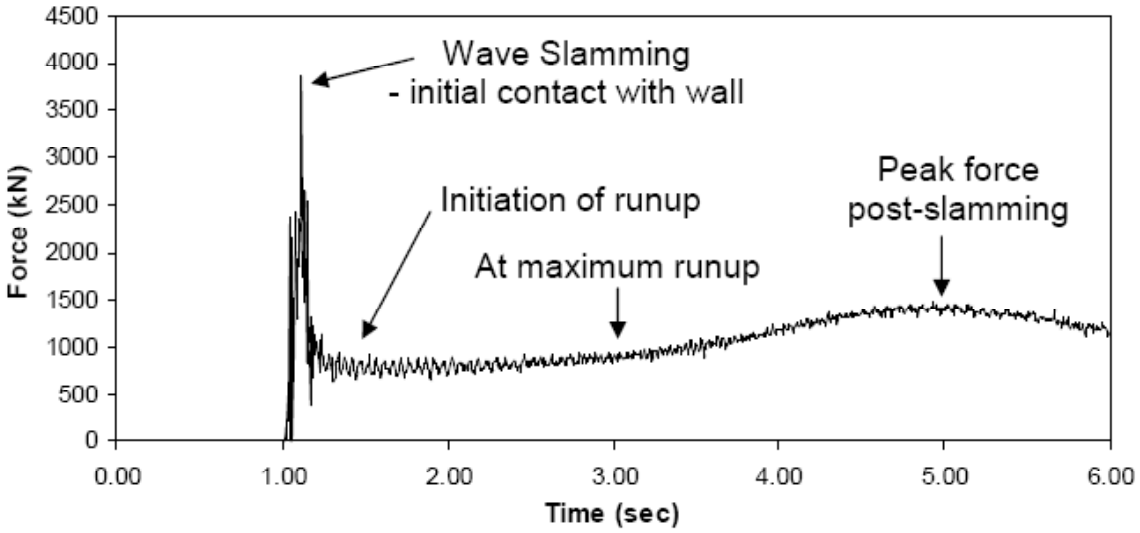

Figure 2-7 Tsunami Force on a Rigid Wall (Haritos et al. 2005)

2.4.6 Debris Impact Forces

When tsunamis travel inland, the swiftly moving water can carry debris such as automobiles, portions of buildings, utility poles, and driftwood (Nouri et al. 2007). Though this force is subject to considerable uncertainty, it must be considered as it has potential to severely damage debris-impacted structures. The formula, provided by FEMA 55 and the CCH, for estimating impact forces stems from an impulse-momentum approach and is shown by (2-16), where *m* is mass of the floating debris, *v* is the velocity of the debris, and Δt is the impact duration.

$$F_I = m\frac{v}{\Delta t} \tag{2-16}$$

In using (2-16), it is typically assumed that the debris is moving with the same velocity as the design flow velocity, which would be an overestimate for large objects. Additionally, FEMA 55 and the CCH alike recommend the use of an object weighing 455kg (1000lb) in the absence of more specific information. The duration of impact term in the above equation is most uncertain, and bound to have the biggest impact on the calculated debris impact forces (Yeh et al. 2005). Specifications typically suggest values based on type of material being impacted. For example, FEMA 55 recommends duration of impact values in the range of 0.2s to 0.4s for steel piles. For comparison, the CCH recommends an impact duration of 0.5s for steel construction.

2.4.7 Load Combinations

Although load combinations are established for design cases that include the actions resulting from floods, it would be inappropriate to apply the same load combinations that are used for floods to tsunamis (Nouri et al. 2007). For tsunamis, Nouri et al. (2007) suggested the use of the two load combinations shown in Figure 2-8, where F_i is an impact force, F_s is a surge force, F_d is a drag force, F_{HS} is a hydrostatic force, W is the weight of the object being considered, γ is the unit weight of water, and V is the submerged volume of the object being considered.

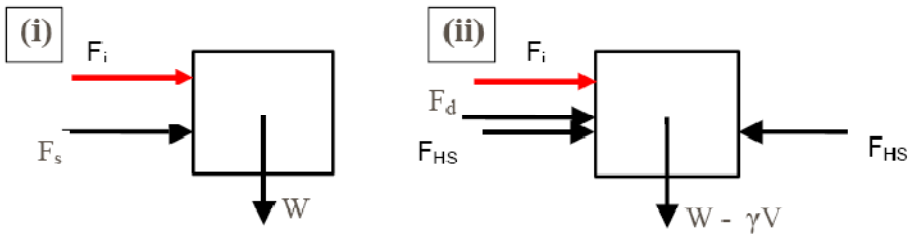

Figure 2-8 Proposed Loading Combinations (Nouri et al. 2007)

The first case considers an impact force and a surge force. The second considers a structure to be completely inundated and subjected to lateral hydrostatic forces, hydrodynamic forces, an impact force, and a buoyancy force. In this latter load combination, the hydrostatic force cancels itself out because it is assumed that the water levels on both sides of the element being considered are equal. In instances where the water levels on both sides are not equal, an unbalanced hydrostatic force would be present.

2.5 Blast

Significant attention has been given to buildings in regards to blast resistant design, particularly following events such as the 1995 bombing of the Alfred P. Murrah Federal Office Building in Oklahoma City, which claimed the lives of 168 people and injured hundreds more (FEMA 2003b). Bridges are, however, also potentially vulnerable when subjected to blasts. Winget et al.(2005) recognized this fact, but remark that most knowledge related to blast resistant structures is in regards to buildings. Accordingly, Winget et al. call for blast threat consideration in bridges and summarizes on-going research toward the development of performance-based blast design standards for bridges. Other research investigating blast implications for bridges includes research by Fujikura et al. (2007; 2008) who carried out experimental and analytical studies investigating the performance of seismically designed circular concrete filled steel tubes (CFSTs), for use in bridge bents, to blast loads. Analytical techniques based on methods utilizing an SDOF approach were employed to form a basis to compare the experimental results against. It was found that the seismically designed CFST columns adequately resisted blast loads in a ductile manner.

Note that blast is a hazard not often considered in design, and therefore many engineers may not be familiar with it. A basic understanding of this hazard requires knowledge of the loading environment and the significance of standoff. Section 2.5.1 provides information on how a blast load is characterized in terms of the resulting loading history. Section 2.5.2 introduces the concept of scaled distance. Section 2.5.3 provides information regarding blast wave reflection, and Section 2.5.4 provides an overview of general blast environments. Information regarding blast wave parameters and strain rate effects are provided in Section 2.5.5 and Section 2.5.6, respectively.

2.5.1 Characterization of a Blast

The detonation process converts the explosive material into a hot, dense, high-pressure gas, the volume of which creates a layer of compressed air – the blast wave – that expands outward from the center of the explosion's center. By analogy, it is similar to the ripples in a pond caused by dropping a stone into the water. The rise in pressure caused by an explosion in free air is termed

overpressure (also known as incident pressure or side-on pressure). The pressure history, which can last milliseconds, at a location in free air some distance from a detonation is schematically shown in Figure 2-9. At the arrival time, t_A, the pressure wave hits and causes a nearly instantaneous rise in pressure up to the peak overpressure, P_{so}. The pressure returns to the ambient pressure after time, t_o, where t_o is the duration of the pressure history's positive phase. The pressure history then enters a negative phase of longer duration, t_0^-, before returning to ambient pressure. For simplified design procedures, the positive phase is typically modeled with a triangular pressure distribution, and the negative phase of loading is neglected. The area under the pressure curve, p(t), from t_A to $(t_A + t_o)$ is equal to the positive phase specific impulse,i_s, and the area under the negative phase is equal to the negative phase specific impulse.

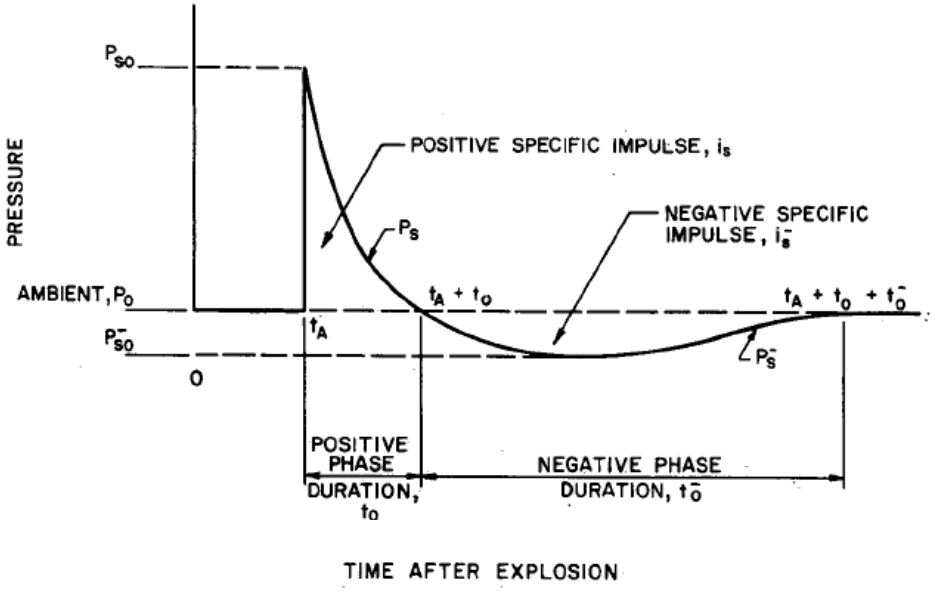

Figure 2-9 Free-Field Pressure History (USDA 1990)

2.5.2 Scaled Distance

For studies dealing with air blasts, scaling or modeling laws have been developed and are used to allow testing of scaled specimens to reduce the cost and effort required to perform blast experiments. Scaling laws increase the value and range of applicability of a single experiment. The most common form of scaling is Hopkinson, or "cube-root", scaling (Baker 1973). As stated by Baker (1973), "This law, first formulated by B. Hopkinson (1915), states that self-

similar blast (shock) waves are produced at identical scaled distances when two explosive charges of similar geometry and the same explosive, but different size, are detonated in the same atmosphere." The formulation for scaled distance, *Z*, is shown by (2-17).

$$Z = \frac{R}{W^{1/3}} \tag{2-17}$$

where *R* is the distance between the target and the explosive's center, and *W* is the total weight of a standard explosive. As will be seen in subsequent sections, the use of this scaled distance parameter allows for the organized presentation of various useful blast wave parameters.

2.5.3 Reflection

When a shock wave strikes a rigid surface, the wave reflects off of it and gets amplified forming a reflected wave that is at a pressure larger than the incident overpressure. Figure 2-10 illustrates the differences between the two types of pressure history. The various types of reflection, which include normal reflection, regular reflection, and Mach reflection, are presented in the next sections.

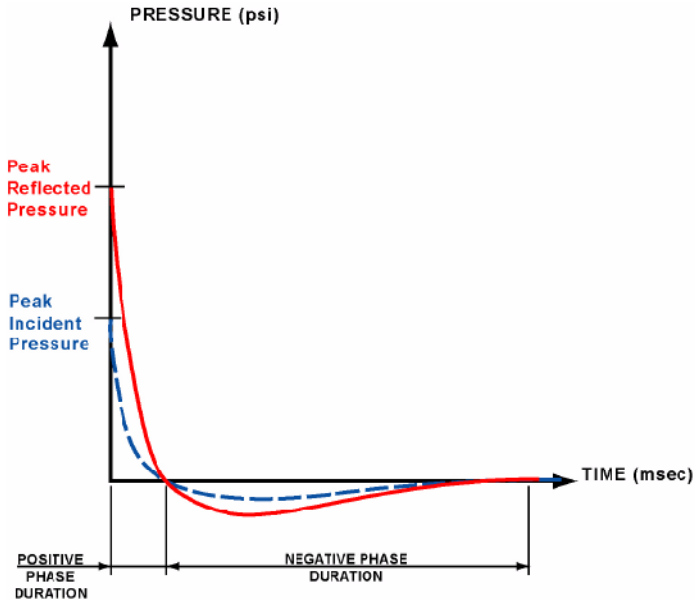

Figure 2-10 Pressure History (Reflected vs. Incident) (FEMA 2003a)

In the following, angle of incidence is the angle at which a shock wave strikes a surface. It is typically measured from an axis that is normal to the surface being struck. Reflection is quantified with a reflection coefficient, which is the ratio of reflected over pressure to the incident over pressure. This coefficient, which is plotted in Figure 2-11 as a function of angle of incidence, is shown to have values of up to about 13, but it has been measured up to 20 in certain cases because of gas dissociation and ionization at very close ranges (Smith and Hetherington 1994). When the angle of incidence is 90 degrees there is no reflection and the surface is loaded with the incident or side-on pressure.

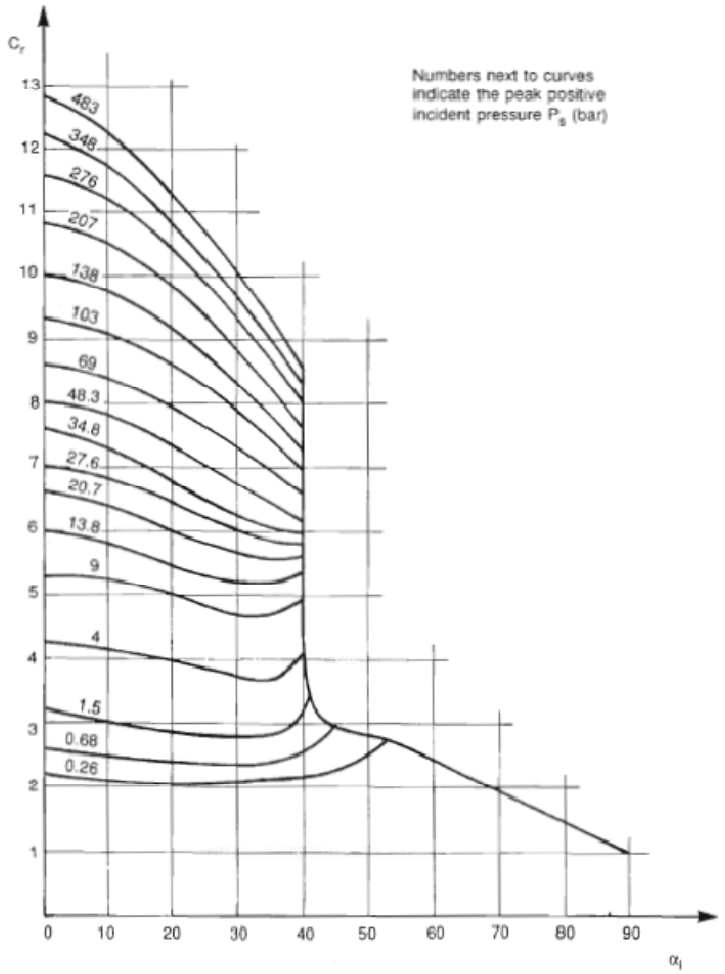

Figure 2-11 Reflected Pressure Coefficient vs. Angle of Incidence (Smith and Hetherington 1994)

2.5.3.1 Normal Reflection

Normal reflection occurs when an incident shock wave strikes a solid surface with an angle of incidence of zero. At the instant the shock wave strikes the surface, air molecules are brought to rest and compressed by the accumulation of pressure behind it creating a reflected pressure wave of higher magnitude than the original incident pressure wave (Smith and Hetherington 1994).

2.5.3.2 Regular and Mach Reflection

Regular reflection occurs when the angle of incidence ranges from 0 to approximately 40 degrees (Mays and Smith 1995). For angles of incidence greater than this and less than 90 degrees, there is a Mach reflection. This phenomenon is schematically illustrated in Figure 2-12, and in Figure 2-13 for a burst at a specified height. When the incident wave, I, strikes the surface it is reflected. Because a reflected shock wave, R, travels with a higher velocity than the incident shock wave, the reflected shock wave catches up with the incident shock wave and combines with it to form a third wave front called the mach stem, M (Bulson 1997). The point at which the three wave fronts merge in a plane is called the triple point (Smith and Hetherington 1994).

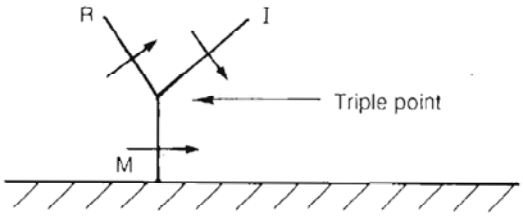

Figure 2-12 Schematic of Mach Reflection (Smith and Hetherington 1994)

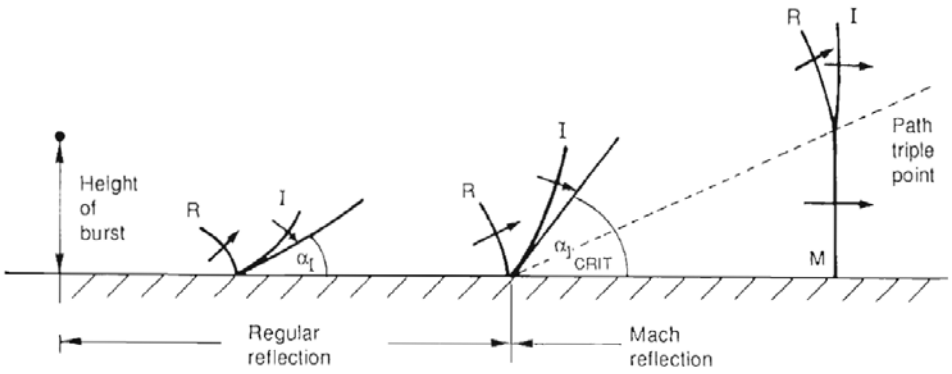

Figure 2-13 Mach Stem and Triple Point Development for Height of Burst Explosion (Smith and Hetherington 1994)

2.5.4 Blast Environments

The United States Department of the Army technical manual TM 5-1300 distinguishes between unconfined and confined explosions. An unconfined charge can occur in three different blast environments: free-air burst, air burst, and surface burst. Likewise, a confined charge can occur in three blast environments: fully vented, partially confined, and fully confined. For research on blast threats to bridges, unconfined blast environments are the primary concern, although consideration may need to be given to shock wave reflections off the underside of the superstructure for explosions that occur beneath the bridge. The three blast environments associated with unconfined explosions will be described in the following subsections.

2.5.4.1 Free-Air Burst

A free-air burst can be described as an explosion that occurs in free air with shock waves free to propagate radially outward from the center of the detonation. Figure 2-14 illustrates a free-air burst showing the spherical wave fronts at successive points in time. The explosion occurs at a height significantly far above the ground surface such that the shock front does not get amplified (or reflected) before arriving at a structure under consideration. Upon the shock wave arrival at the structure, the incident pressure waves are reflected to produce the aforementioned reflected pressure.

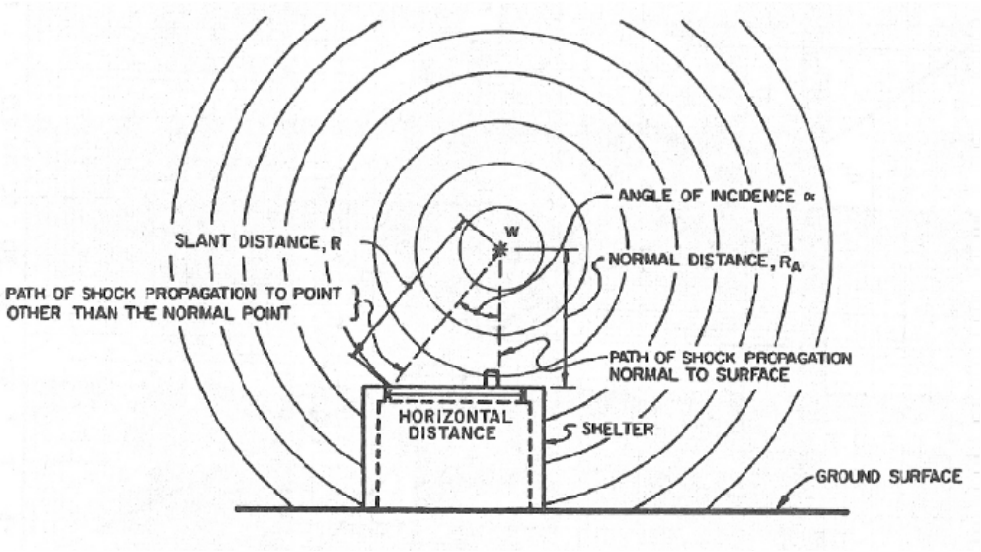

Figure 2-14 Free Air Burst Environment (USDA 1990)

2.5.4.2 Air Burst

An air burst, which is shown in Figure 2-15, occurs in air, as the free-air burst. However, an air burst is an explosion after which the incident shock wave, which initially propagates radially outward from the detonation, gets reflected and thus amplified before reaching a structure. Figure 2-15 also shows the Mach front and the triple point, which were introduced previously.

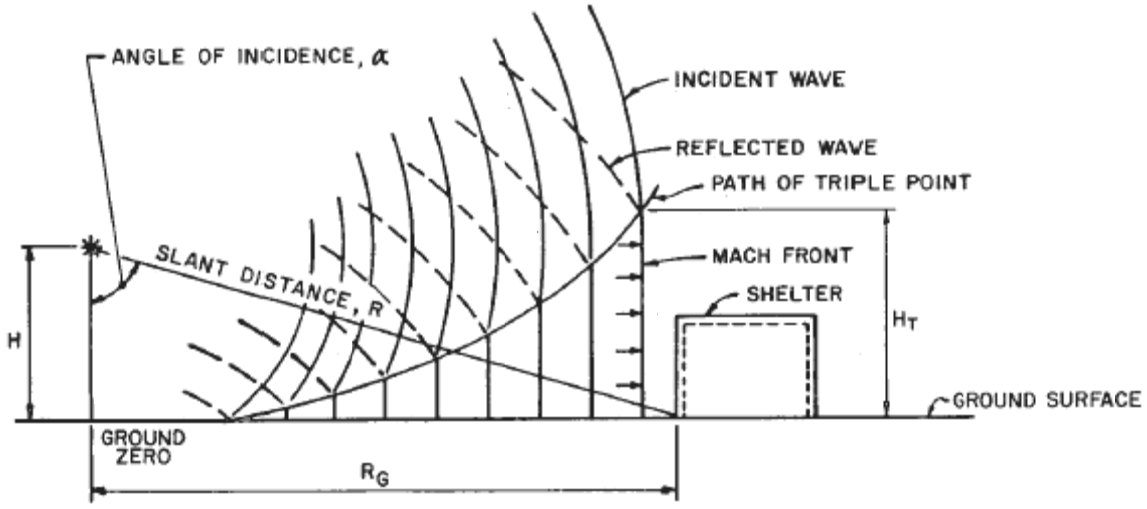

Figure 2-15 Air Burst Environment (USDA 1990)

2.5.4.3 Surface Burst

A surface burst is an explosion that occurs from the detonation of an explosive that is located at or close to the ground surface. This type of blast environment is shown in Figure 2-16. Due to the fact that detonation takes place on or close to the ground surface, the shock front that originates from detonation is immediately reflected resulting in a reflected shock wave propagating from the point of detonation in a hemispherical pattern.

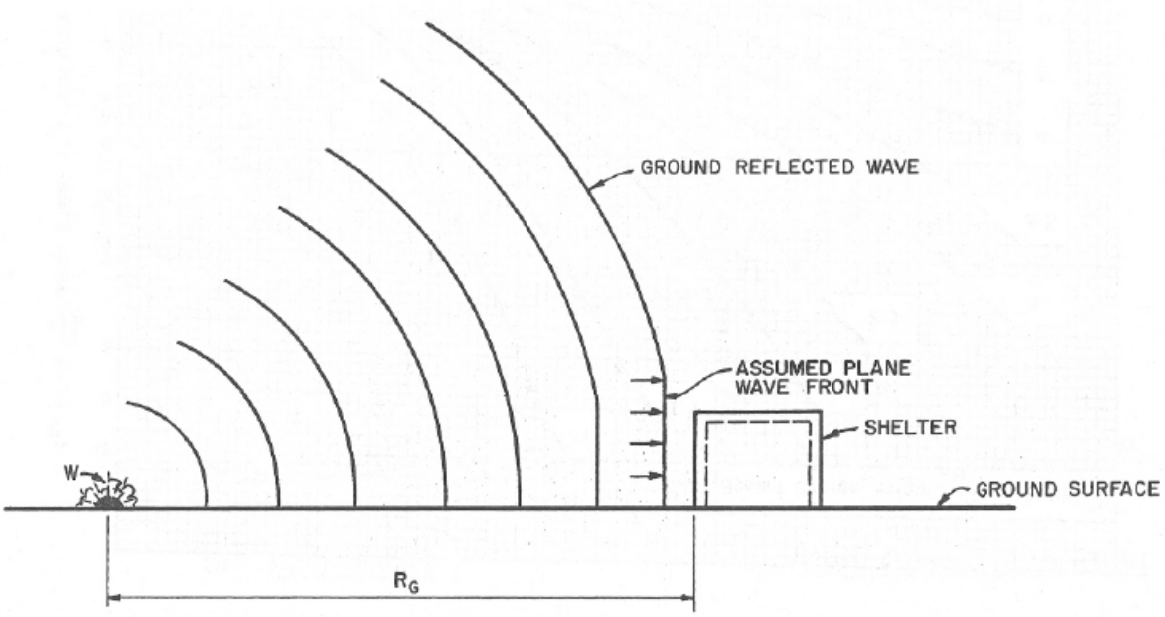

Figure 2-16 Surface Burst Environment (USDA 1990)

2.5.4.4 Plausible Blast Environment for Bridges

Figure 2-17 shows one conceivable blast environment that could be considered when designing bridge components for blast. This blast environment could be an air blast or a surface burst, depending on the location of the explosive. Actual placement of the charge in relation to the bridge superstructure and/or piers must be considered when determining the blast pressures on structural elements, accounting for possible shock wave reflections. Also, as shown by this figure, blast loading below the deck will subject the piers to lateral pressures, the deck to uplift pressures, and the piers to high axial loads.

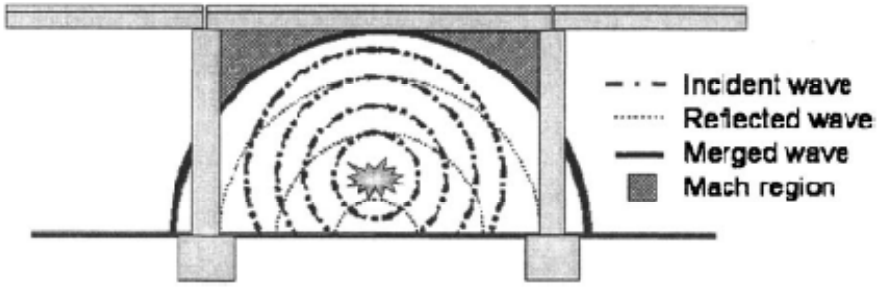

Figure 2-17 Plausible Blast Environment for Bridges (Winget et al. 2005)

2.5.5 Blast Wave Parameters for TNT Explosives

The scaled distance parameter provides a means to normalize and organize (in the form of charts) blast wave parameters, such as incident and reflected impulse, incident and reflected pressure, duration, and shock front velocity. Figure 2-18 and Figure 2-19 show two such charts, expressed in terms of scaled distance, which is obtained for a specific standoff distance, *R*, and a specified charge weight, *W*, in terms of equivalent TNT, by (2-17). Note that these graphs only give the blast wave parameters for the positive phase of the blast pressure history.

The graph shown in Figure 2-18 corresponds to the free air burst scenario (i.e. the case illustrated in Figure 2-14), and Figure 2-19 provides the blast wave parameters for surface bursts (i.e. the case illustrated in Figure 2-16). Note that the values for pressure and impulse are larger for the surface burst than for those corresponding to the free-air burst. This is due to the fact that hemispherical explosions release shock waves having more energy than that corresponding to spherical shock waves because of the reflection of shock wave on the ground (Smith and Hetherington 1994).

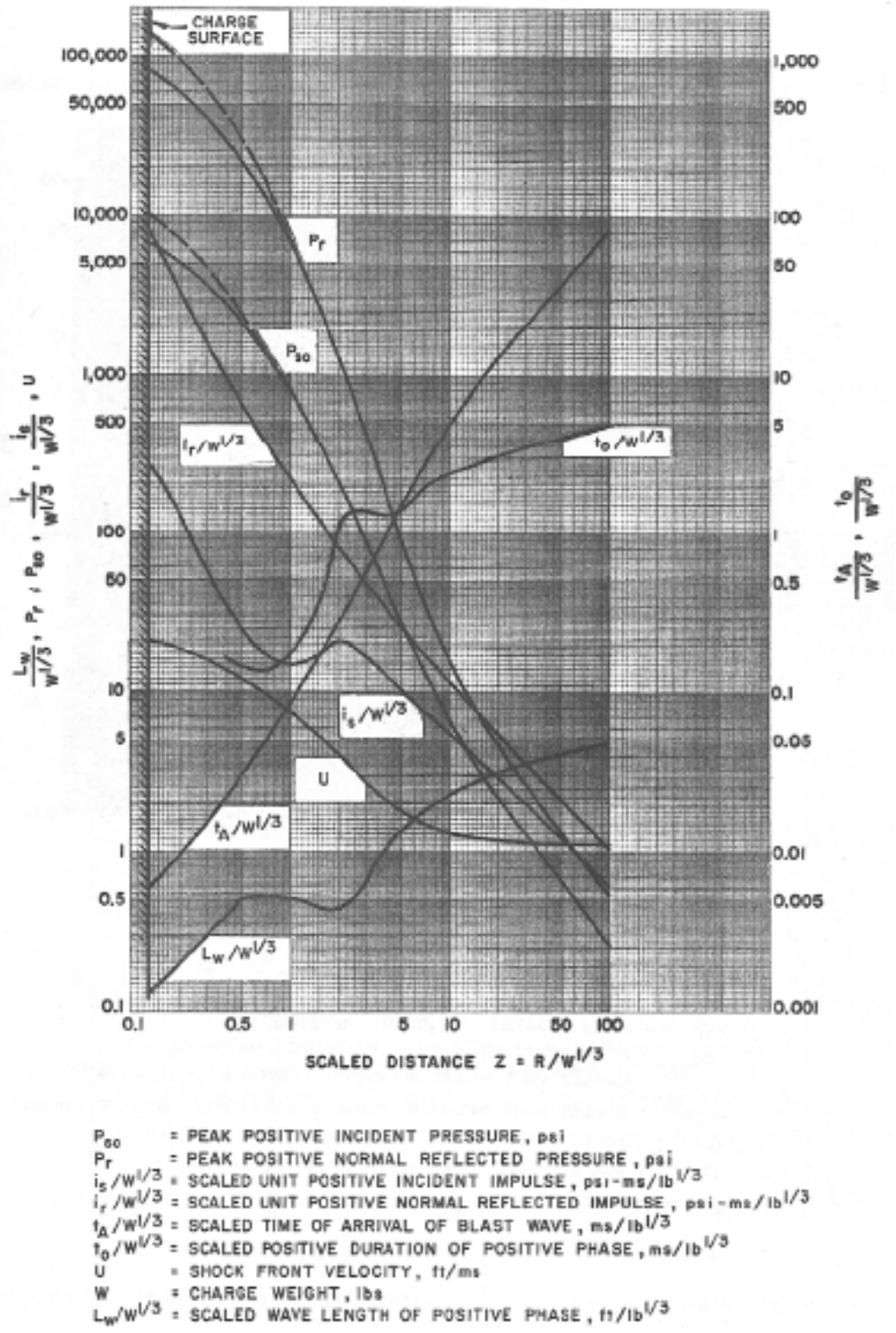

P_{so} = PEAK POSITIVE INCIDENT PRESSURE, psi
P_r = PEAK POSITIVE NORMAL REFLECTED PRESSURE, psi
$i_s/W^{1/3}$ = SCALED UNIT POSITIVE INCIDENT IMPULSE, psi-ms/lb$^{1/3}$
$i_r/W^{1/3}$ = SCALED UNIT POSITIVE NORMAL REFLECTED IMPULSE, psi-ms/lb$^{1/3}$
$t_A/W^{1/3}$ = SCALED TIME OF ARRIVAL OF BLAST WAVE, ms/lb$^{1/3}$
$t_o/W^{1/3}$ = SCALED POSITIVE DURATION OF POSITIVE PHASE, ms/lb$^{1/3}$
U = SHOCK FRONT VELOCITY, ft/ms
W = CHARGE WEIGHT, lbs
$L_W/W^{1/3}$ = SCALED WAVE LENGTH OF POSITIVE PHASE, ft/lb$^{1/3}$

Figure 2-18 Positive Phase Shock Wave Parameters for a Spherical TNT Explosion in Free Air at Sea Level (USDA 1990)

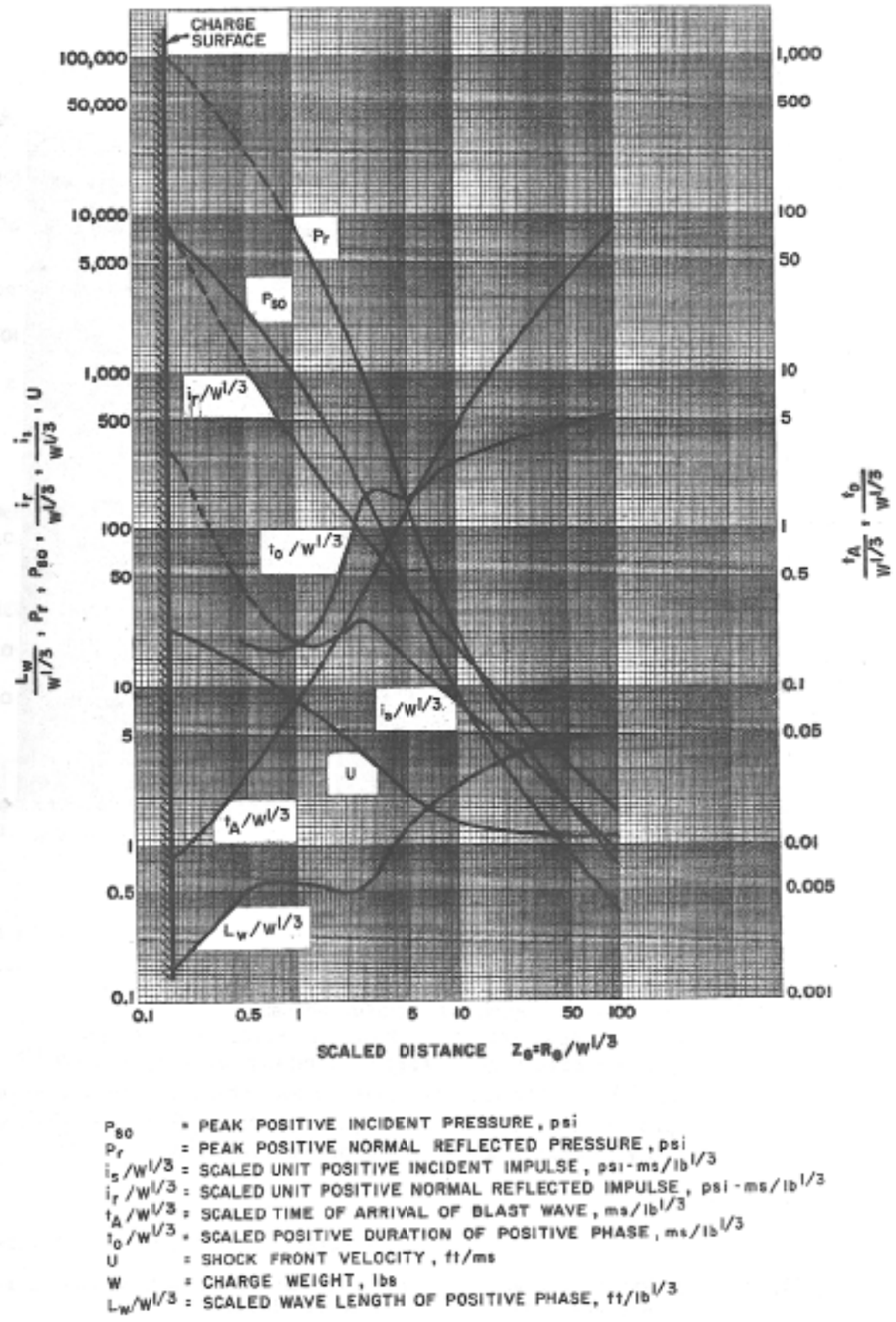

P_{so} = PEAK POSITIVE INCIDENT PRESSURE, psi
P_r = PEAK POSITIVE NORMAL REFLECTED PRESSURE, psi
$i_s/W^{1/3}$ = SCALED UNIT POSITIVE INCIDENT IMPULSE, psi-ms/lb$^{1/3}$
$i_r/W^{1/3}$ = SCALED UNIT POSITIVE NORMAL REFLECTED IMPULSE, psi-ms/lb$^{1/3}$
$t_A/W^{1/3}$ = SCALED TIME OF ARRIVAL OF BLAST WAVE, ms/lb$^{1/3}$
$t_o/W^{1/3}$ = SCALED POSITIVE DURATION OF POSITIVE PHASE, ms/lb$^{1/3}$
U = SHOCK FRONT VELOCITY, ft/ms
W = CHARGE WEIGHT, lbs
$L_w/W^{1/3}$ = SCALED WAVE LENGTH OF POSITIVE PHASE, ft/lb$^{1/3}$

Figure 2-19 Positive Phase Shock Wave Parameters for a Hemispherical TNT Explosion on the Surface at Sea Level (USDA 1990)

2.5.6 Strain Rate Effects

Since the duration over which a structural element experiences blast pressure loading is a matter of milliseconds, it is imperative to account for the effect of strain rates on material properties in determining a member's dynamic structural response. The figures shown in Figure 2-20 compare the static and dynamic compressive strength of concrete (f_c' and f_{dc}', respectively) as well as the static and dynamic yield strength and ultimate strength of steel (f_y and f_{dy}, and f_u and f_{du}, respectively).

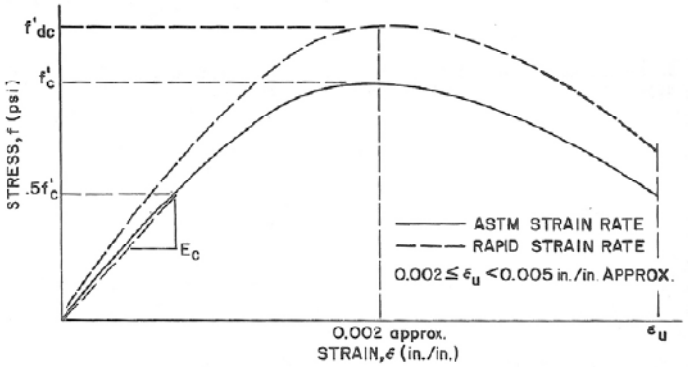

(a.) Stress – Strain Behavior for Concrete

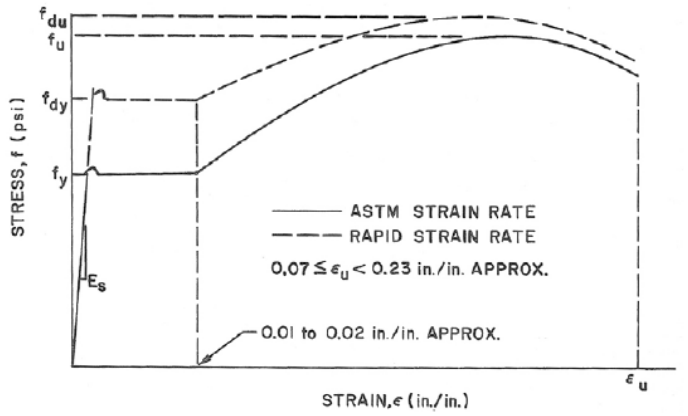

(b.) Stress – Strain Behavior for Steel

Figure 2-20 Stress – Strain Curves for (a) Concrete, and; (b) Steel (USDA 1990)

Dynamic increase factors (DIFs), are defined as the ratios of a material's dynamic property to its static property. Table 2-3 shows some DIFs for various construction materials. When analyzing a structure or any of its components, the material's static yield strength and ultimate strength should be multiplied by these factors.

Table 2-3 Dynamic Increase Factors for Steel and Concrete (Mays and Smith 1995)

Type of stress	Concrete	Reinforcing bars		Structural steel	
	f'_{dc}/f'_c	f_{dy}/f_y	f_{du}/f_y	f_{dy}/f_y *	f_{du}/f_y
Bending	1.25	1.20	1.05	1.20	1.05
Shear	1.00	1.10	1.00	1.20	1.05
Compression	1.15	1.10	---	1.10	---

* Minimum specified f_y for grade 50 steel or less may be enhanced by the average strength increase factor of 1.10.

CHAPTER 3

STEEL PLATE SHEAR WALL APPLICATIONS, MECHANICS, AND DESIGN

3.1 General

Research and applications involving steel plate shear walls (SPSWs) have focused on their use in buildings. These systems are well-known for the excellent ductility they provide against seismic loading. Moreover, if damaged, the plates are replaceable. Their applicability in bridges and their resilience to multiple hazards, however, remains to be determined.

This chapter provides a basic review of what steel plate shear walls are and how they behave. This knowledge will be used in the conception, analysis, and design of a multi-hazard resistant system composed of SPSWs, as discussed in Chapters 4 and 5. Section 3.2 provides a brief introduction to SPSWs. Section 3.3 summarizes the mechanics of unstiffened SPSWs, which are used in this research. Section 3.4 highlights one simplified modeling and analysis method, and Section 3.5 outlines the design of unstiffened SPSWs.

Many researchers have contributed to the development of steel plate shear walls, either in terms of experimental work or analytical work (Behbahanifard et al. 2003; Berman and Bruneau 2003a; Berman and Bruneau 2003b; Caccese et al. 1993; Driver et al. 1997; Elgaaly et al. 1993; Kharrazi et al. 2004; Lin and Tsai 2004; Lubell et al. 2000; Rezai 1999; Roberts and Sabouri-Ghomi 1992; Thorburn et al. 1983; Timler and Kulak 1983; Tromposch and Kulak 1987; Vian and Bruneau 2005; Xue and Lu 1994). Other references that provide guidance on how to analyze and design steel plate shear walls include the Seismic Provisions for Structural Steel Buildings (AISC 2005a) and American Institute of Steel Construction's Steel Plate Shear Wall Design Guide (Sabelli and Bruneau 2006).

3.2 Introduction to Steel Plate Shear Walls

3.2.1 Applications

A typical SPSW assembly is composed of three major components: columns (vertical boundary elements (VBEs)), beams (horizontal boundary elements (HBEs)), and infill plates. SPSWs have generally been implemented in buildings with individual plates spanning between stories. The VBEs and HBEs typically make up a moment resisting frame and serve as boundary elements to the plates. Figure 3-1 illustrates a four story SPSW system.

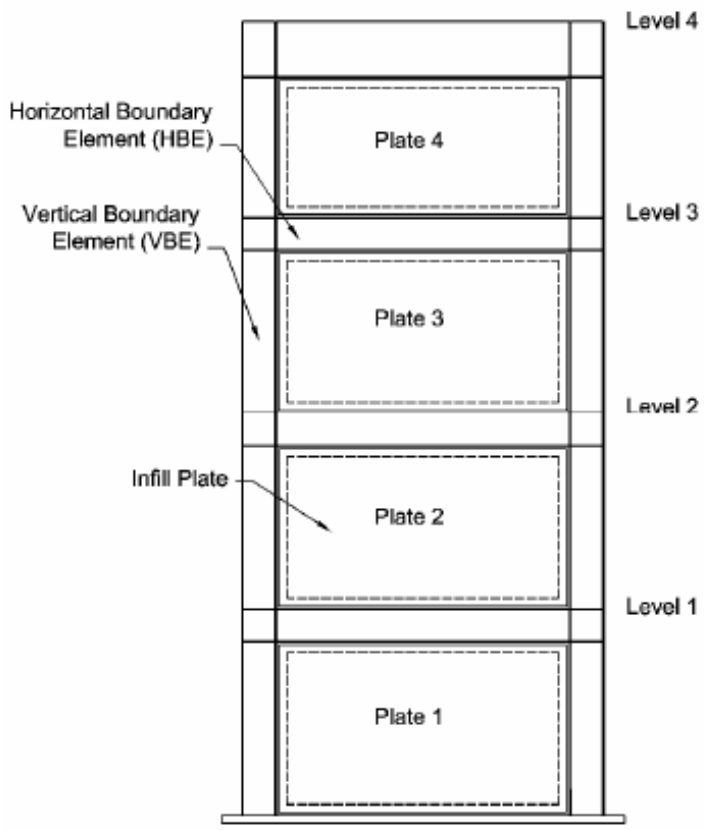

Figure 3-1 Typical Steel Plate Shear Wall (Bruneau et al. 2005)

3.2.2 Types of Infill Panels

Steel plate shear walls can be categorized into three general categories, in terms of infill panel type: (1) unstiffened, (2) stiffened, and (3) composite. Unstiffened SPSWs use slender steel plates for infill plates and utilize tension field action for resistance to lateral loads. Stiffened

SPSWs are similar to unstiffened SPSWs with the exception that stiffeners (vertically and/or horizontally oriented) are attached to the infill plate. Such stiffeners could be designed to allow the plate to develop significant compression forces, in addition to the tension field action seen with unstiffened SPSWs, but generally they are only designed to allow the plate to develop its full plastic shear strength. Composite SPSWs are those in which concrete is attached to the steel plates to offer out-of-plane restraint, as an alternate way for the plate to develop its plastic strength.

A variation of the unstiffened SPSW infill has also been investigated as a possible benefit for retrofitting buildings (Vian and Bruneau 2005). This type of infill uses perforations in the form of circular cutouts evenly spaced throughout the plate.

3.3 Mechanics of Unstiffened SPSWs

3.3.1 Infill Plate Behavior

Due to their slenderness, the plates of unstiffened SPSWs have little compressive strength. That strength is typically neglected in analysis and design. As SPSWs are laterally loaded, the infill plates buckle under the compressive forces acting along one diagonal direction and tension forces develop along the other diagonal direction (Sabelli and Bruneau 2006). Figure 3-2 illustrates an idealization of such tensile forces and points out plate buckling in the form of diagonal folds.

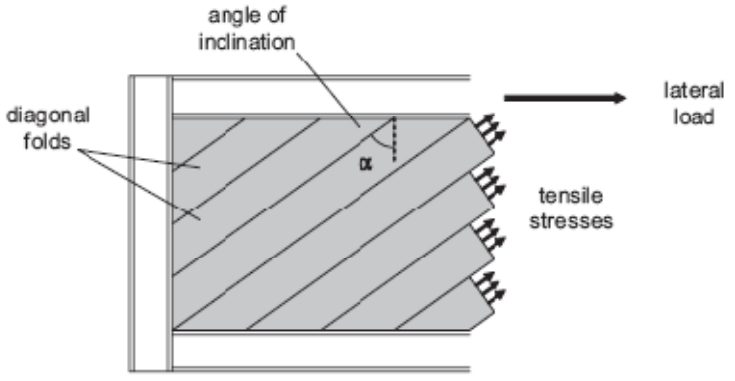

Figure 3-2 Idealized Tension Field Action in an Unstiffened SPSW (Sabelli and Bruneau 2006)

For illustration purposes, consider the setup shown in Figure 3-3 used to investigate light-gauge steel infill plates for seismic retrofitting of buildings (Berman and Bruneau 2003a). Figure 3-4 shows the deformed position of a similar specimen and illustrates the behavior of unstiffened SPSWs.

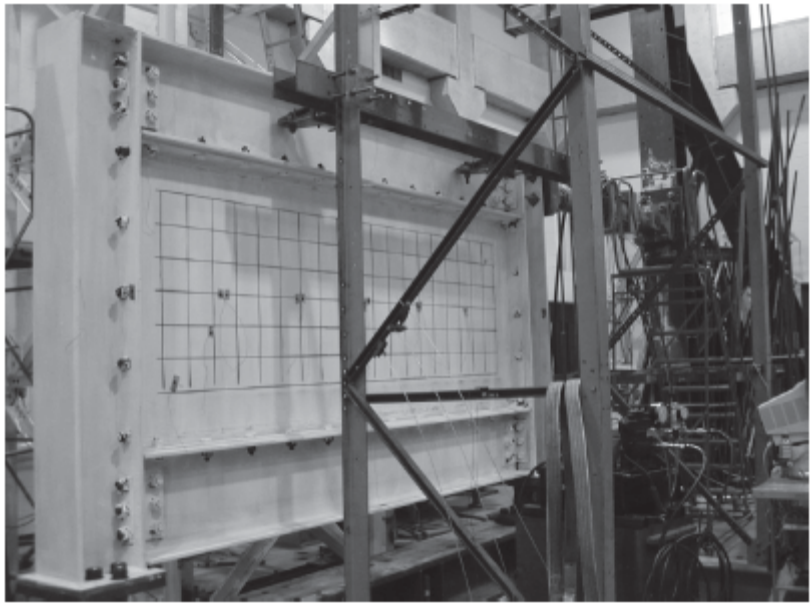

Figure 3-3 Light-gauge Steel Plate Shear Wall Prior to Testing (Berman and Bruneau 2003a)

Figure 3-4 Buckling of Infill Panel (Berman and Bruneau 2003a)

As the plates deform, they impose inward forces on the boundary elements. Figure 3-5 shows the severely deformed shape of a single story unstiffened SPSW resulting from pull-in of the plates on boundary elements of inadequate stiffness. If the plates are to be fully effective in resisting lateral loads, the boundary elements must be designed with adequate stiffness and must have adequate strength to resist the forces imposed on them by the plates. Therefore, a free-body diagram of the force distribution in a system incorporating SPSWs can be helpful and is presented in the next section.

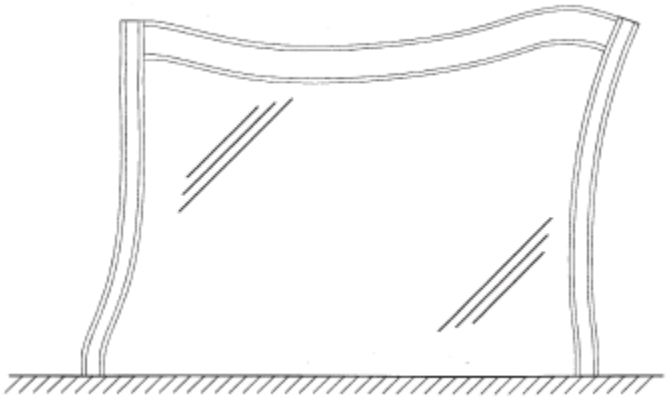

Figure 3-5 Inward Flexure of SPSW Boundary Elements (Sabelli and Bruneau 2006)

3.3.2 Forces on Boundary Frame

The AISC Design Guide for Steel Plate Shear Walls (Sabelli and Bruneau 2006) schematically provides information on the force distribution in a fully yielded SPSW, as illustrated in Figure 3-6 for a SPSW application in buildings subjected to lateral forces, F. From this figure, it can be seen that the fully yielded plates apply a uniformly distributed load (pull-in force) on the boundary elements (VBEs and HBEs) at the angle at which the tension strips develop. For simplicity, this figure has omitted the member end moments that would be present in the VBEs and in the HBEs if the boundary frame was designed as moment resisting; rather, this figure treats all connections as simple. Each of the members in this system develop moments and axial forces. The VBEs in particular develop moments from plate pull-in and from frame action (if designed as such) in addition to axial load from overturning. Note that t_w is the plate thickness, σ is the tension stress in the infill plate, and $P_{HBE(VBE)}$ is the axial force applied to the HBEs due to the pull-in load applied on the VBEs by the plate.

Inclusion of the HBEs, in addition to providing an anchoring boundary for plates, provides support for the VBEs in the form of reactions to resist the pull-in forces applied to the VBEs. As a result, the HBEs can develop significant axial forces due to the web plate tension forces acting on the VBEs (Sabelli and Bruneau 2006). In certain instances, intermediate horizontal struts are introduced to offer more support for VBEs.

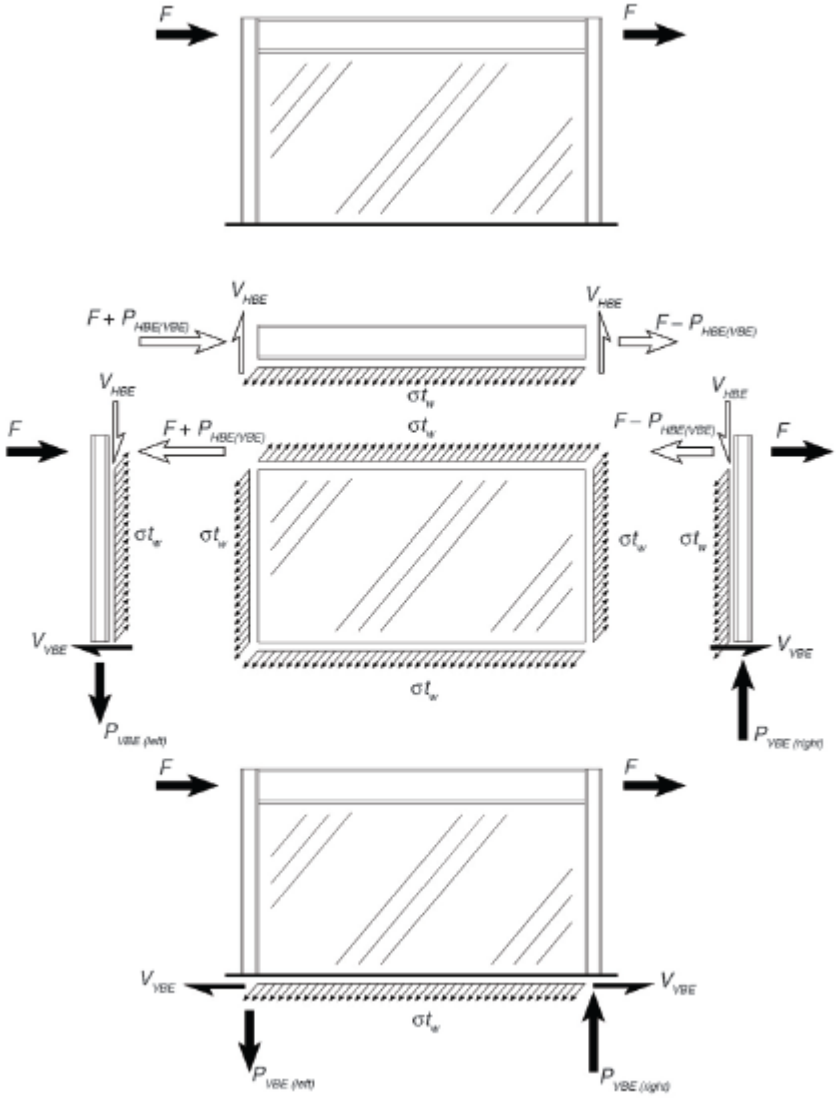

Figure 3-6 Free Body Diagram of SPSW Elements (Sabelli and Bruneau 2006)

3.4 Simplified Modeling and Analysis

Two simplified modeling methods presented in the SPSW design guide are the Orthotropic Membrane Model and the Strip Model. The model used in this research for simplified analysis is the strip model. The strip model reduces a SPSW system to a series of parallel, equally spaced, pin-ended, tension-only strips to represent the infill plate, and beam elements to represent the boundary elements. Figure 3-7 shows the transition of an unstiffened SPSW assembly into a simplified strip model.

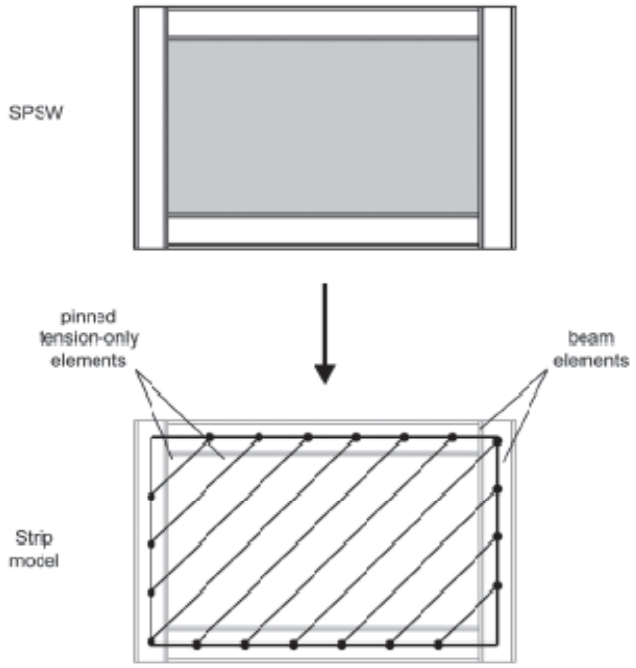

Figure 3-7 Strip Model for Static (Linear and Nonlinear) Analysis of SPSWs (Sabelli and Bruneau 2006)

Figure 3-8 shows another strip model for a four-story SPSW. In this model, the angle of the tension strips, α, is also shown. This angle, first introduced in Figure 3-2, is the angle of inclination of the diagonal folds. This angle can be found using (3-1) (AISC 2005a), where t_w is the plate thickness, A_c is the cross-sectional area of a VBE, A_b is the cross-sectional area of an HBE, I_c is the moment of inertia of a VBE taken perpendicular to the direction of the web-plate line, and L and h are the centerline-to-centerline dimensions of the VBEs and the HBEs, respectively.

$$\tan^4 \alpha = \frac{1 + \frac{t_w L}{2A_c}}{1 + t_w h\left[\frac{1}{A_b} + \frac{h^3}{360 I_c L}\right]} \tag{3-1}$$

This equation, put into the form shown here by Timler et al. (1988), was derived assuming simple beam-to-column connections and assuming that the plate could not resist compression.

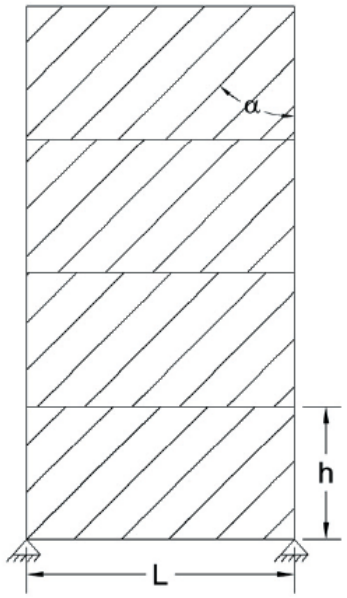

Figure 3-8 Strip Model Representation of a Steel Plate Shear Wall (Berman and Bruneau 2003b)

The area of each strip can be computed with (3-2), where *n* is the number of strips used to represent one plate (Sabelli and Bruneau 2006),

$$A_s = \frac{\left[L\cos(\alpha) + h\sin(\alpha)\right] t_w}{n} \tag{3-2}$$

where it is recommended that a minimum of 10 strips is required to adequately represent the distributed yielding force of a plate.

3.5 Design of Unstiffened SPSWs

In the perspective of selecting a plate thickness for a given story shear, it is worthwhile to review how the equation describing the ultimate capacity of a SPSW system is derived. The following is taken from Berman and Bruneau (2003a) based on plastic analysis principles.

Consider the single-story collapse mechanism shown in Figure 3-9, for a strip model of a SPSW with strips equally spaced of a perpendicular distance s. Using the method of virtual work, the story shear, V, that is needed to create a collapse mechanism can be determined. Note that this model considers the boundary elements to remain elastic and assumes their internal work to be negligible. It also considers simple beam-to-column connections (i.e. no plastic hinges form). The external work is calculated by the product of V and the frame displacement, Δ. Internal work for the system (neglecting any contribution from the boundary elements) is obtained by the product of the force in the strips and their elongation. This elongation can be obtained by summing the absolute displacement of the strips' attachment points. To make this process easier, the strip forces can be broken into their orthogonal components. The vertical component of the strip forces will not contribute to the internal work since the attachment points of the strips do not displace vertically. The horizontal components on the bottom beam do not displace, and those on the columns cancel since those on the left column are doing positive work and those on the right column are doing negative work. The internal work done by each strip's horizontal component on the top beam is given by the following equation when the plate is fully yielded, where σ_y is the yield strength of the plate:

$$W_{Istrip} = \sigma_y s t_w \sin(\alpha)\Delta \tag{3-3}$$

Multiplying (3-3) by the number of strips that intersect the top beam, n_b, and setting this total internal work equal to the external work, the following relationship is obtained,

$$V = n_b \sigma_y s t_w \sin(\alpha) \tag{3-4}$$

where the number of strips intersecting the top beam can be determined from (3-5) (Berman and Bruneau 2003a).

$$n_b = \frac{L\cos(\alpha)}{s} \tag{3-5}$$

By substituting (3-5) into (3-4) and by knowing the trigonometric identity $\sin(\alpha)\cos(\alpha) = (½)\sin(2\alpha)$, the following equation is obtained (Berman and Bruneau 2003a), which gives the plastic lateral capacity of the plate:

$$V_{ult} = \frac{1}{2} L\sigma_y t_w \sin(2\alpha) \tag{3-6}$$

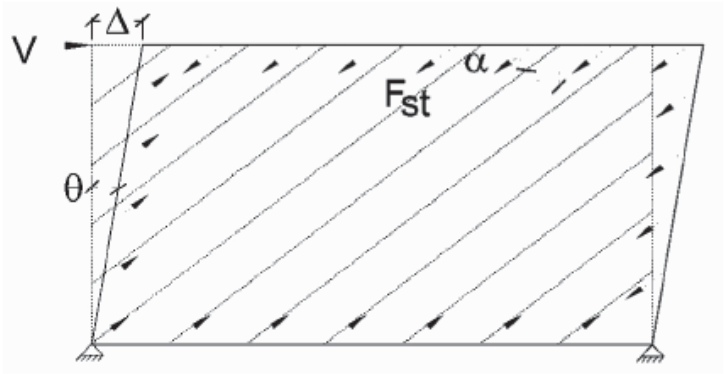

Figure 3-9 Single-Story Collapse Mechanism (Berman and Bruneau 2003b)

After multiplying the right side of (3-6) by a resistance factor, ϕ_v, and after dividing by an overstrength factor of 1.2 (Sabelli and Bruneau 2006), the following relationship is obtained for the ultimate strength of the plate, which was adopted the AISC Seismic Provisions (2005a), except that the L value used there recognized that the clear span of the plate between VBE flanges, L_{cf}, is the actual yielding length of the plate (as opposed to the centerline-to-centerline dimensions of the frame).

$$V_{ult} = 0.42\phi_v L_{cf}\sigma_y t_w \sin(2\alpha) \tag{3-7}$$

Various approaches may be employed to design a SPSW system. The AISC Design Guide provides comprehensive guidance and illustrates design methods through two examples. A brief summary of a possible design procedure is listed below.

- Establish the geometry of the system (e.g. boundary frame and plate dimensions) keeping in mind that the AISC Seismic Provision (2005a) restricts the aspect ratio, L/h, to be within the range of 0.8 to 2.5.
- Establish preliminary sizes for the boundary elements keeping in mind that they must be seismically compact.
- Determine the shear demand in the plates being designed.
- Assume an inclination angle for the tension strips, which typically ranges between 30˚ and 55˚ (Sabelli and Bruneau 2006).
- Determine the required plate thickness by rearranging (3-7) and assuming that the plate resists the full shear force at a given story (i.e. not accounting for the contribution of boundary elements).

$$t_w = \frac{V_{ult}}{0.42\phi_v L_{cf} \sigma_y \sin(2\alpha)} \tag{3-8}$$

- Check the selected boundary frame members against the stiffness requirements for VBEs and the HBEs that are shown by (3-9) and (3-10), respectively.

$$I_{VBE} \geq 0.00307 \frac{t_w h^4}{L} \tag{3-9}$$

$$I_{HBE} \geq 0.003 \frac{(\Delta t_w) L^4}{h} \tag{3-10}$$

- Calculate the tension strip inclination angle using (3-1) and check against the one initially assumed.
- Obtain the internal forces of the boundary elements. One method to achieve this, and the one used in this research project, involves nonlinear static pushover analysis of a strip model.
- Check these members for strength and for the desired performance.
- Check that any plastic hinging at an HBE/VBE interface occurs in the HBE rather than in the VBE (strong-column/weak-beam criterion).
- Check the plates' contribution to the system's overall resistance, and if more contribution of the plates is desired, further iteration could be conducted.

CHAPTER 4

BRIDGE PIER SYSTEM DEVELOPMENT

4.1 General

This chapter describes the evolution of the multi-hazard resistant bridge system that will be further investigated in this report. As specified in Chapter 1 a system composed of steel plate shear walls was sought. This is a system whose applicability in bridges and whose resistance to multiple hazards remains to be determined, as mentioned in Chapter 3. Obviously there are many ways to achieve the multi-hazard objective that is central to this research, but by focusing on concepts involving SPSWs and the ductility and resilience they offer, the range of possible systems was narrowed. Systems that are adaptable for retrofits and for new bridge design were considered for this research.

The system's approach to design, which was discussed in Chapter 1, was used in the development of the final design concept. The reinforcing and/or conflicting demands of the hazards being considered in this research, which were described in Chapter 2, were considered for each proposed concept, and the desirable and undesirable aspects of each concept were evaluated. In considering the seismic hazard, adequate resistance in each of a bridge's principal directions was desired. At the same time, protection of the system's ability to sustain gravity loads and maintain its integrity after occurrence of any of the other hazards was considered. Additionally, a design that had aesthetic appeal was sought.

Section 4.2 illustrates some design concepts that were thought of for retrofitting existing bridges. These design concepts (Section 4.2.2 to 4.2.4) were applied to the prototype bridge described in Section 4.2.1. The search for concepts involving retrofits was eventually dismissed and the search narrowed by focusing on box pier concepts for application in new bridges, as described in Section 4.3. Six and four column pier systems (Sections 4.3.2 and 4.3.3) were introduced into a

modified version of the prototype bridge, which is discussed in Section 4.3.1. A second prototype bridge is introduced in Section 4.3.4 and a design attempt of the four-column concept is discussed in Section 4.3.5 along with the difficulties encountered. Section 4.3.6 describes a modification to the second prototype bridge, and Section 4.3.7 provides the final design concept that will be investigated in the remainder of this report.

4.2 Retrofit Concepts for Existing Bridges

4.2.1 Prototype Bridge #1

The intent at this stage was to search for a system that incorporated the multi-hazard concept into existing bridge piers. Accordingly, the two-span continuous prototype bridge having a reinforced concrete pier at its center, shown in Figure 4-1 and Figure 4-2, was selected as a case study to modify for the purpose of developing a concept. This prototype bridge is an adaptation of the single span AASHTO precast girder bridge presented in the third seismic design example, which is a part of the series of seismic design examples developed for the Federal Highway Administration (Mast et al. 1996b). The superstructure dimensions (e.g. span length and bridge width) used for each span of the prototype bridge were taken from the single span AASHTO bridge example. A generic pier was chosen and placed at the center of the bridge. Arbitrary sizes for the cap beam and columns were chosen and were not designed for the purpose of this preliminary investigation.

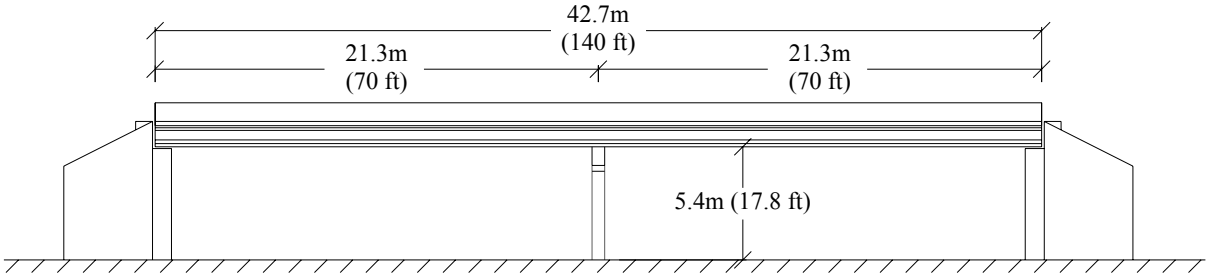

Figure 4-1 Prototype Bridge #1 Elevation

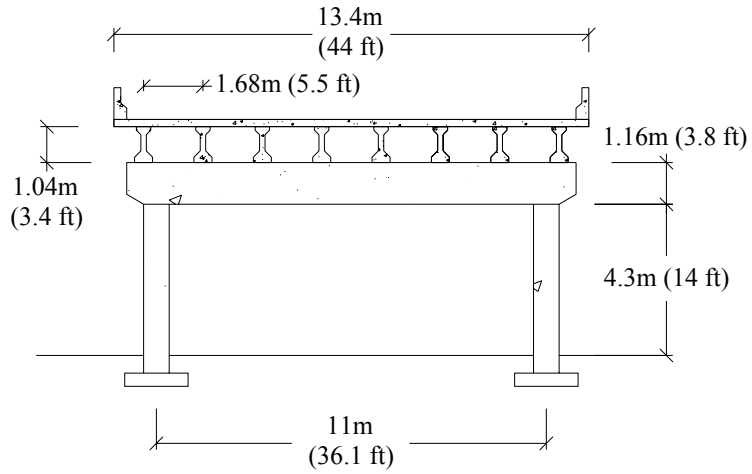

Figure 4-2 Prototype Bridge #1 Cross-Section Elevation at Pier

4.2.2 Supplementary Walls Attached to Bent Cap

As mentioned in Chapter 3, SPSWs are typically used in buildings. One way to implement them into bridges could be to connect them between a bent cap and a foundation (which is analogous to a single story SPSW) with the objective of providing lateral resistance, providing for simplicity in replacement, and providing redundancy. Two variations of this concept are shown in Figure 4-3 and Figure 4-4. These figures are intended to show preliminary concepts, so details of the connection between the bottom of the walls and the foundation are not considered. Figure 4-3 shows a case with two reinforced concrete columns and a SPSW placed between them. Figure 4-4 shows a modification of Figure 4-3 in which the bent could have three columns instead of two and multiple SPSWs instead of a single SPSW.

Both figures show the boundary elements of the SPSWs as being wide flange sections oriented such that pull-in forces of the plate bends them about their strong axis, as is normally the case in SPSW applications. The horizontal boundary elements at the bottom and top of the SPSW could be continuously attached to the foundation and to the bent cap, respectively. The reinforced concrete columns of the bent could be used for resisting gravity loads and the SPSWs for resisting the lateral inertial loading transferred through the bridge's superstructure during a seismic event. As a result of this decoupling, the SPSWs could be used as modules that could be removed and replaced with relative ease if damaged during an extreme event. Their replacement could be achieved without disrupting traffic since the columns would be capable of sustaining

gravity loads during the replacement process. Additionally, if one of the bent's reinforced concrete columns became critically damaged by an explosion, by a vehicle collision, or by some other extreme event, the VBEs of the SPSWs offer redundancy for resisting gravity loads, thus preventing collapse of the bridge.

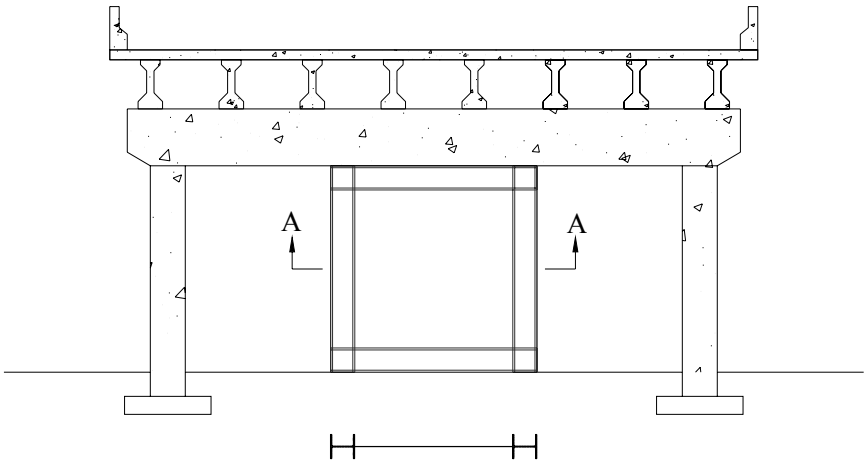

Section A-A

Figure 4-3 Single Wall

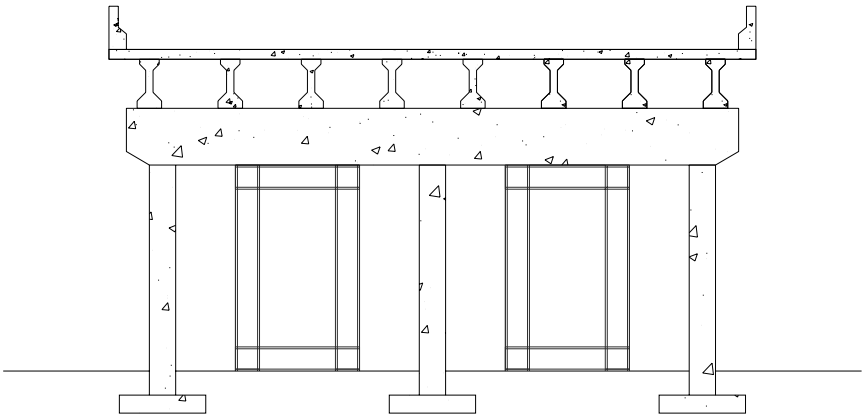

Figure 4-4 Two Walls

A shortcoming of these concepts is that they wouldn't provide an increase in longitudinal seismic resistance comparable to that in the bridge's transverse direction. The only increase in longitudinal resistance would come from the VBEs being bent about their weak axis. Moreover, it can be argued that these systems are not aesthetically appealing. Also the plate aspect ratio for the SPSWs in Figure 4-4 is outside of the limits discussed in Chapter 3. To establish proper aspect ratios for these plates one would have to introduce horizontal boundary elements at various heights along the wall.

4.2.3 Supplementary Walls Integral with Reinforced Concrete Columns

The structural implications of the concepts in Section 4.2.2 were directed towards the seismic hazard in terms of increased lateral resistance. In an effort to address protection against other hazards more directly, another concept that integrates SPSW assemblies with the bent columns was devised. This concept is depicted in Figure 4-5 with a bent that has three columns, two of which (the exterior columns) are integral with SPSW assemblies. Plates would be attached to each side of the column. Horizontal members would be necessary, and are schematically shown, to achieve proper aspect ratios for each panel of the plate. This figure introduces an interesting concept where the tension fields, which act on opposing faces of the columns, run through the column centerlines. The pull-in forces from the plates are equal and opposite on each side of the columns which, conceptually, would result in no net vertical force acting on the column (excluding gravity). However, the eccentricity of the vertical components of the pull-in forces from the column centerlines acting at the edge of the columns may induce some deformations.

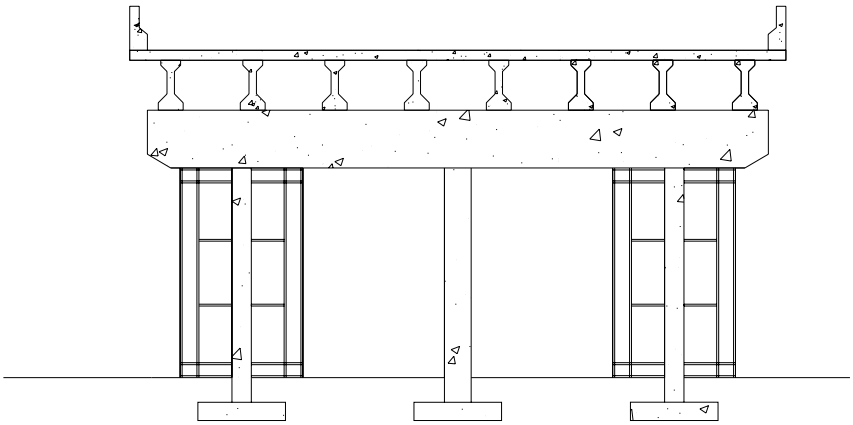

Figure 4-5 Integral Walls

This concept provides more protection to the bent columns for other hazards than did those in Section 4.2.2. For instance, if a vehicle was to collide with the assembly or if debris swept away by a tsunami bore struck the assembly, the plate (and to a minor extent the horizontal boundary elements) would buckle allowing the VBE to deform and to absorb the energy of the impact inelastically, and in doing so serve as a sacrificial element to protect the reinforced concrete bent column. Additionally, if a reinforced concrete column was removed by some sort of localized blast event, the SPSW assemblies could potentially offer sufficient redundancy to resist gravity

loads. Section 4.2.4 illustrates a modification to this concept that was thought of to minimize the susceptibility of the plates to pressure loading.

4.2.4 Integral SPSWs with Perforations

The concept illustrated Figure 4-6, which is the same as that shown in Figure 4-5 with different plates, uses perforated plates that could allow any pressure loads (e.g. blast) to vent through the plates.

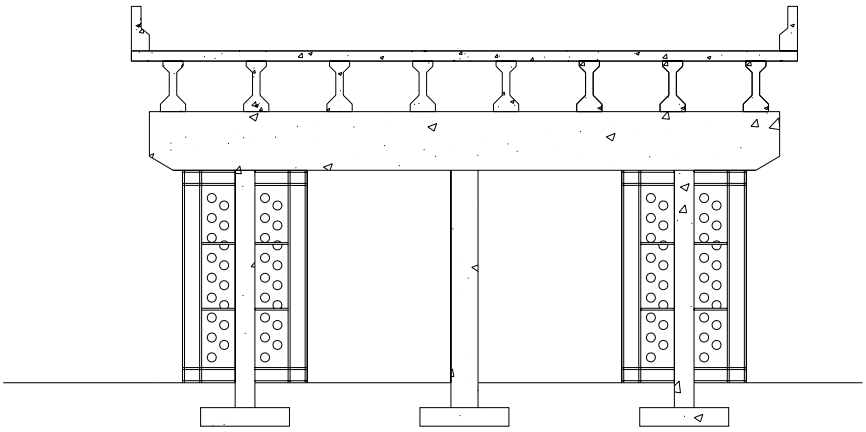

Figure 4-6 Integral Walls with Perforations

When methods of attaching the plates to the reinforced concrete columns were examined for this concept (and the one in Section 4.2.3) it was determined that the connection detail would not be trivial. Also, as was seen with the concepts in Section 4.2.2, the increase in longitudinal seismic resistance would not be comparable to the increase provided in the transverse direction. One possible alternative that could be used to increase the longitudinal resistance could be to rotate the wide flange sections so that they could be in weak-axis bending to resist the pull-in of the plate, but in strong-axis bending to resist longitudinal motion of the bridge. An alternative way to achieve this would be to use doubly symmetric sections such as cruciform shapes or pipes. Nonetheless, longitudinal seismic strength would still remain substantially less than in the transverse direction. Accordingly, this concept was discarded, and it was determined to explore other concepts and to focus primarily on systems that could be used in new bridge designs. These concepts, which use tubular boundary elements in a box configuration, will be investigated further in Section 4.3.

4.3 New Bridge Concepts Using Box Pier Systems

4.3.1 Modification of Prototype Bridge #1 Geometry

Considering that the main concern with each of the concepts introduced in Section 4.2 was that the increase in longitudinal seismic resistance would not be comparable to the increased resistance in the transverse direction, a box pier concept was pursued. Such a concept could be capable of providing increased seismic resistance in a bridge's longitudinal and transverse direction. Also, the plates of the system could be considered sacrificial for any of the other hazards being considered.

In order to use the box pier for the current prototype bridge, however, a relatively wide pier cap would be necessary, depending on the dimensions of the box pier. To visualize such a concept the geometry of the prototype bridge described in Section 4.2.1 was modified. More specifically, the height of the superstructure above grade was increased. This modified version of prototype bridge #1 is illustrated in Figure 4-7, which also depicts the box pier concept.

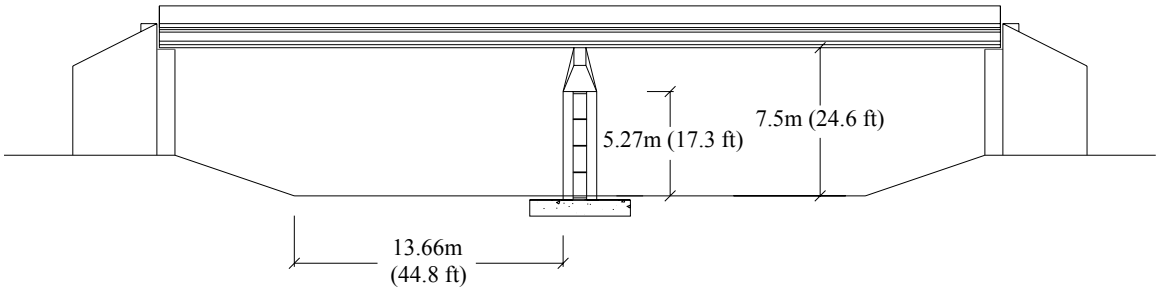

Figure 4-7 Modified Version of Prototype Bridge #1

Two variations of this concept were briefly considered. Section 4.3.2 depicts a six-column box pier and Section 4.3.3 depicts a four-column concept. The SPSW pier box assembly is composed of round tubular VBEs, HBEs (either wide flange shapes or hollow tubes), and steel plates. The plates are attached tangentially to the VBEs, as will be shown by the section views in Figure 4-8 and Figure 4-9 in Section 4.3.2 and 4.3.3, respectively. The HBEs would be attached to the VBEs and to the inner side of the plates. Therefore, the HBEs would not be visible to the public. The elevations in Figure 4-7 to Figure 4-9 show the pier box without the plates and

schematically reveal the placement of HBEs. Attaching the plates tangentially to the boundary frame also gets rid of the fish plate detail necessary to attach the plates in typical SPSW systems.

4.3.2 Six-Column Wall Pier

The concept shown in Figure 4-8 has a total of six columns. The six columns would share the gravity load, which would thus reduce their size. Also, this assembly would posses much redundancy if any one of the six columns was removed or critically damaged.

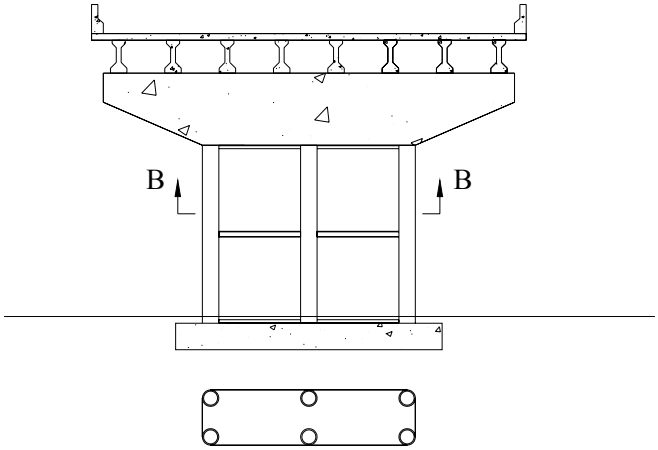

Figure 4-8 Elevation at Pier: Box Pier Concept No. 1

While this concept can provide more effective strength in the longitudinal direction, the pier remains longer in the transverse direction compared to the longitudinal direction, with seismic resistance for transverse ground shaking potentially far greater than that in the longitudinal direction, which, though not a deficiency, is not optimum. Moreover, since the required plate thickness depends on the width of the plate, the thickness of the plate required to resist the specified loads could become impractically small, depending on the superstructure's reactive mass and the ground motion considered. Section 4.3.3 considers a modification of this concept in which the transverse dimension is reduced.

4.3.3 Four-Column Pier

The six-column wall pier (Figure 4-8) was reduced in transverse width to resemble a large, single column pier. This concept reduces the length of the transverse plates to approach that of the longitudinal plates. This would provide comparable seismic lateral resistance in both directions. This concept, depicted in Figure 4-9, was also thought to be more aesthetically appealing than the other concepts considered to this point.

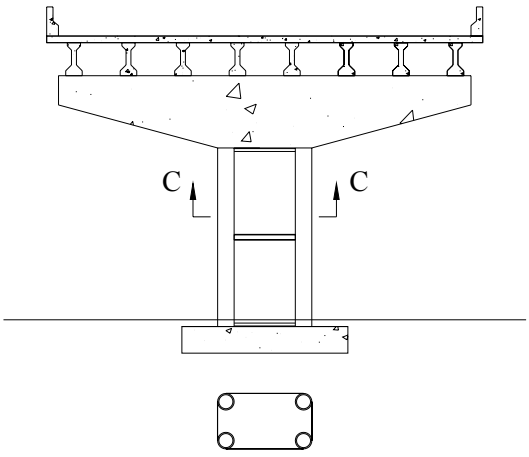

Figure 4-9 Elevation at Pier: Box Pier Concept No. 2

It was also judged that box-pier systems of the type considered here afforded the benefit of easily replacing damaged plates if needed after an extreme event. A possible negative aspect of this system, however, is that the center of mass, at which inertial forces act, is elevated high above the pier, which could cause large overturning axial force demands in the VBEs, with corresponding reductions in their moment capacity.

Of all the concepts conceived to this point this four-column box pier was deemed the most worthy of further developments because of its more balanced resistance to seismic forces in both directions and its potential to resist other hazards by treating the plates as sacrificial elements. Accordingly, the remainder of this chapter discusses such further developments of this concept. However, after preliminarily sizing some plates it was determined that this concept would be more effective for bridges having a larger reactive mass than available for the prototype

considered up to this point. Section 4.3.4 describes the new prototype bridge that was consequently considered.

4.3.4 Prototype Bridge #2

The bridge chosen for the second prototype bridge was the three-span continuous steel girder bridge presented in the second seismic design example in the series of seismic design examples developed for the Federal Highway Administration (Mast et al. 1996a).

Figure 4-10 shows an elevation of the bridge with the proposed four-column SPSW box piers in-place of the 11m tall wall piers that were considered in the FHWA design example. The figure shows the dimensions of the bridge, which are significantly increased from those of prototype bridge #1. The total height of the prototype bridge's substructure is approximately 12.5m from the foundation to the top of the pier cap, with the pier cap itself being approximately 3m in height. The bridge has one center span of 46.3m and two adjacent spans each of 37.8m for a total bridge length of 121.9m. The previous bridge prototype studied was only 42.7m in total length.

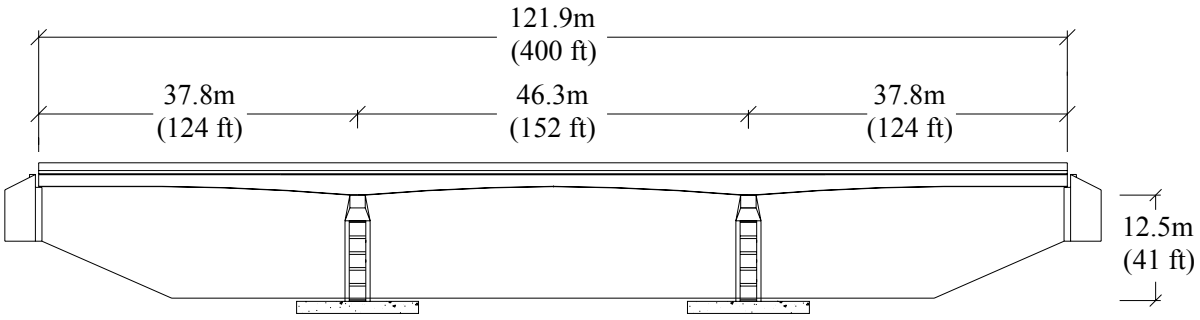

Figure 4-10 Bridge Elevation

This three-span bridge superstructure is composed of plate girders with varying depth that act compositely with a reinforced concrete deck. The alignment of the bridge's roadway is straight with no vertical curve. For the purposes of this study, it was assumed that the piers and abutments are oriented perpendicular to the longitudinal axis of the superstructure (i.e. no skew). Figure 4-11 illustrates the bridge's cross-section and overall dimensions. Notice the depth of the

plate girders at the piers in relation to those at the bridge's mid-spans. More specific information regarding details of the superstructure, including plate girder sizes and deck geometry can be found in the three-span continuous steel girder bridge seismic design example no. 2 (Mast et al. 1996a).

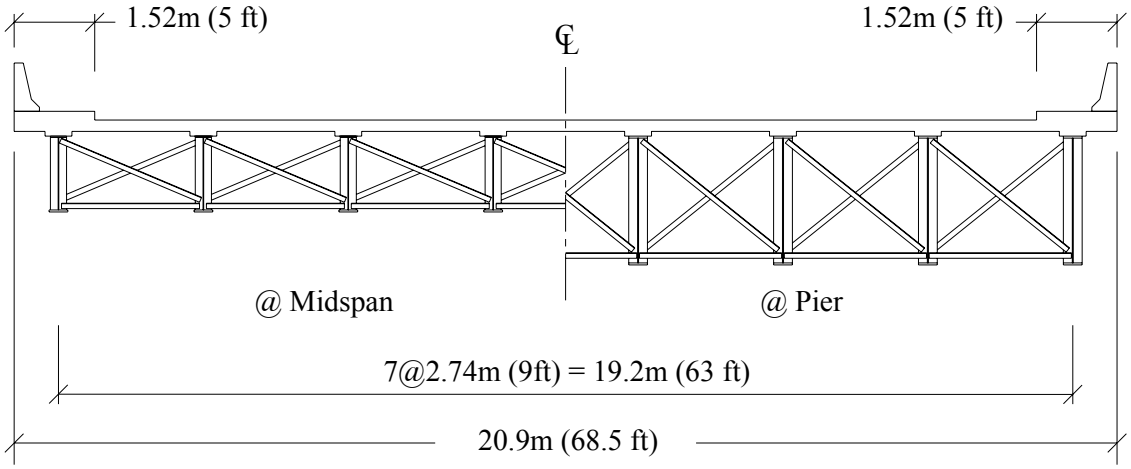

Figure 4-11 Cross-Section of Bridge Superstructure (Adapted from Mast et al. 1996a)

4.3.5 Application of the Four-Column Pier System

Elevations of the proposed pier concept are provided in Figure 4-12. The pier cap was taken indirectly from the FHWA seismic design example no. 2. The design example uses large reinforced concrete walls for piers. The height and width of the cap shown in Figure 4-12 was taken from that wall pier by removing the lower portion. In place of the wall portion, the four-column SPSW box pier was inserted. This pier uses four round hollow tubes for columns and round hollow tubes for horizontal boundary elements, which are shown as being spaced vertically at 1.9m. The connection details between the pier cap and the superstructure, though important, are not included in the scope of this study. Rather, it was assumed that the connection had sufficient capacity to restrain relative translation between the superstructure and the pier cap, in the bridge's longitudinal and transverse direction. Additionally, it was assumed that negligible moment capacity existed in the connection for moments about an axis perpendicular to the longitudinal direction of the bridge.

As is evident from Figure 4-12, the center of mass of the superstructure (and pier cap) is well above the top of the pier. This high center of mass coupled with the small width of the SPSW pier required to obtain reasonable plate thicknesses could potentially induce significant axial force demands in the VBEs when the reactive mass is excited during seismic events. Incidentally, this would also be a concern for any tall slender steel plate shear wall in an application having lateral forces applied at its top.

Note that making the pier narrow in both directions helps increase the plate thickness required to resist the specified seismic loads, which is often needed as required strength may be less than the minimum available hot rolled plate stock. Moreover, wide plates parallel to the bridge's longitudinal direction would catch more wave loads, which is undesirable, assuming water is flowing transversely the bridge's longitudinal direction. Despite the possible consequences, a design of this system was attempted.

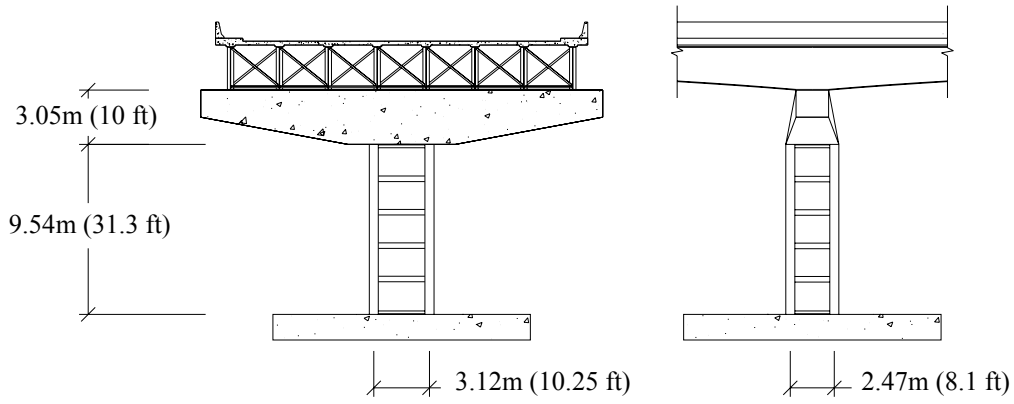

Figure 4-12 Elevation of Proposed Pier Concept

For design, a two-step, nonlinear pushover analysis was conducted using commercially available software, namely SAP2000. This method of analysis and design is further described in Chapter 5 (Section 5.3). As a brief summary, the boundary frame was modeled using linear beam elements and the plates were modeled using the nonlinear strip model discussed in Chapter 3. Nonlinear hinges were inserted at the ends of each of the members to allow for hinging in the expected hinge regions and in each of the strips to allow for the structure to reach its ultimate capacity and to develop a plastic mechanism. The bottom of the pier was modeled as a fixed boundary to replicate the presence of a foundation. The top of the pier was constrained, with a

diaphragm constraint, to replicate the presence of a pier cap. The top of the pier was allowed to translate and to rotate in both of the bridge's principal directions.

It was found through the analysis and design of this system that the axial force demand in the VBEs was indeed large, which made finding an acceptable design difficult. As the column size was increased, the ultimate capacity of the system also increased, with resulting increased axial force in the VBEs. Significant axial force resulted in reduced moment capacity of the VBEs' cross-sections. When the additional moment distribution from plate pull-in was applied to the VBEs it was found that the bi-axial moment/axial force interaction ratio tended to exceed that allowed by full plastification in some of the tubes' cross-sections. This resulted in probable plastic hinge formation at the mid-height of the first story, which was not desired. Therefore, the significant axial force in the VBEs made it difficult to find a design using available tube sections.

It was thought that perhaps increasing the size of the HBEs, with the intent of increasing the amount of frame action in the system, would prevent hinge formation at the members' mid-height; however, several attempts failed to successfully achieve this objective and to provide a satisfactory design with available tube sizes. This is an interesting observed behavior that deserves further attention and will be the subject of future studies. However, for the purpose of the current work, it was decided to reduce the height of the reactive mass above the box pier. This was done by making the pier cap integral with the superstructure, resulting in the rotation of the top of the pier being fixed for longitudinal motion. The remaining constraints imposed on the pier were kept the same. Section 4.3.6 discusses this modification to prototype bridge #2.

4.3.6 Prototype Bridge #2 with Integral Pier Caps

The final bridge prototype considered is shown in Figure 4-13. Note that the pier cap was moved into and made integral with the plate girders of the superstructure.

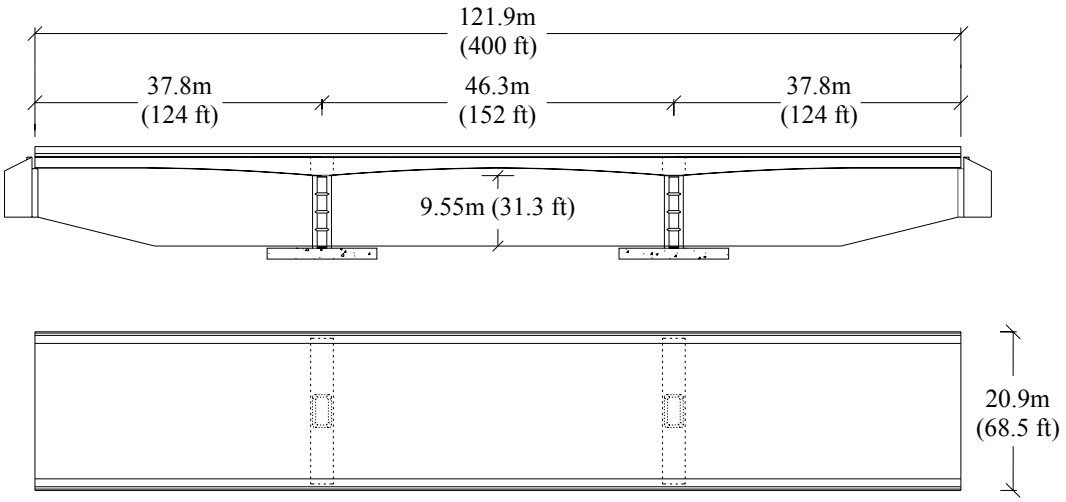

Figure 4-13 Bridge with Final Pier Concept

4.3.7 Final Multi-Hazard Pier Concept

Figure 4-14 shows two additional views of the bridge at the pier. The left elevation is looking down the longitudinal direction of the bridge, and the figure on the right is an elevation looking transversely at the pier. The transverse spacing of the VBEs was increased from 3.12m to 3.71m so that the columns would clear the girders. Also, the number of HBEs was reduced from four to three. Lastly, to reduce the demands on the longitudinal plates from wave forces, and because the rotation at the top of the pier was assumed fixed for longitudinal motion and overturning was no longer an issue in that direction, the spacing of the columns in the longitudinal direction was reduced from 2.47m to 1.88m. Note that all dimensions are center-to-center. Also, note that an approximately 86mm space was left at the pier's top and bottom to account for a continuous connection detail of the plates to the pier cap and foundation, respectively. In the design of the system, it was assumed that this detail could be worked out and was simply considered here as providing an infinitely rigid boundary.

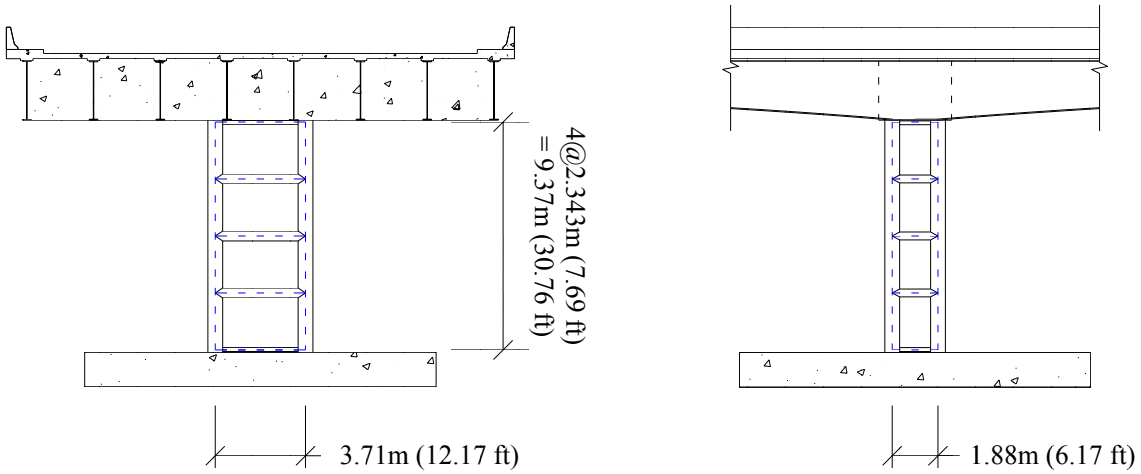

Figure 4-14 Bridge Section Elevations at Pier

To gain a better perspective on the proposed conceptual design, 3-D renderings were created. Note that the previous bridge elevations in Figure 4-14 showed the pier without the plates; however, the concept has been developed such that the plates essentially "wrap" the pier. This can be seen in Figure 4-15, which shows a view of a segment of the bridge at the pier. Figure 4-16 displays the same bridge section but from below, which displays the integrated pier cap. For simplicity, the cross frames were left out of the rendering.

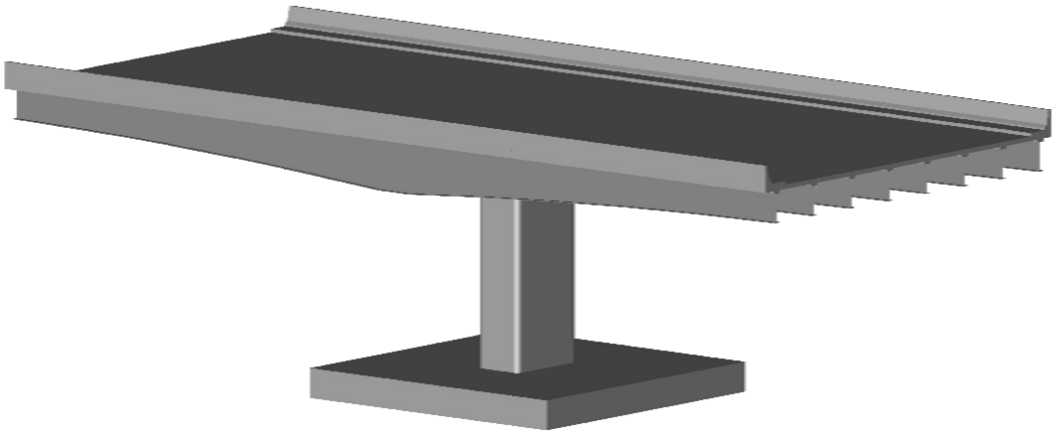

Figure 4-15 3-D Pier and Bridge Segment From Above

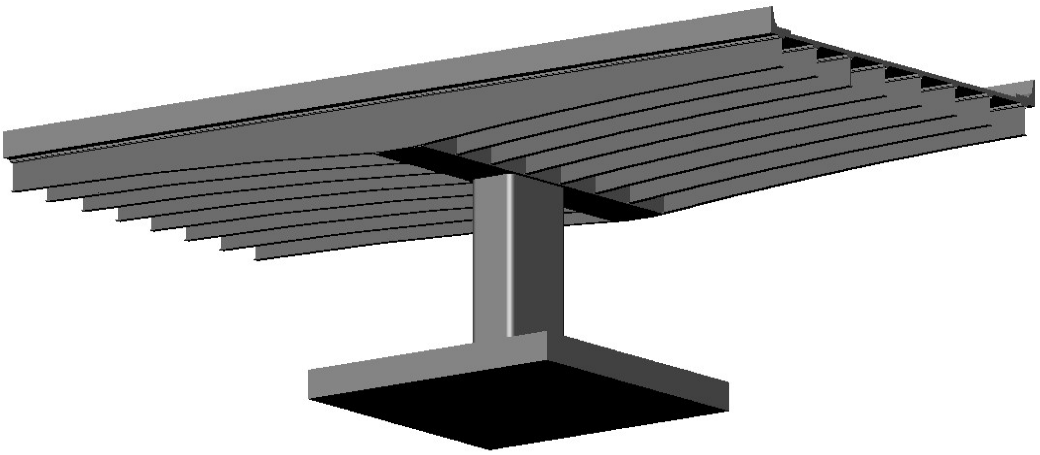

Figure 4-16 3-D Pier and Bridge Segment From Below

For a better understanding of how the pier itself is constructed, rather than how it fits into the bridge structure, an exploded view of the pier was created. This can be seen in Figure 4-17, which illustrates the fact that the plates are attached to the exterior of the pier's frame. Detailed information pertaining to the design and analysis of this pier concept is provided in Chapter 5.

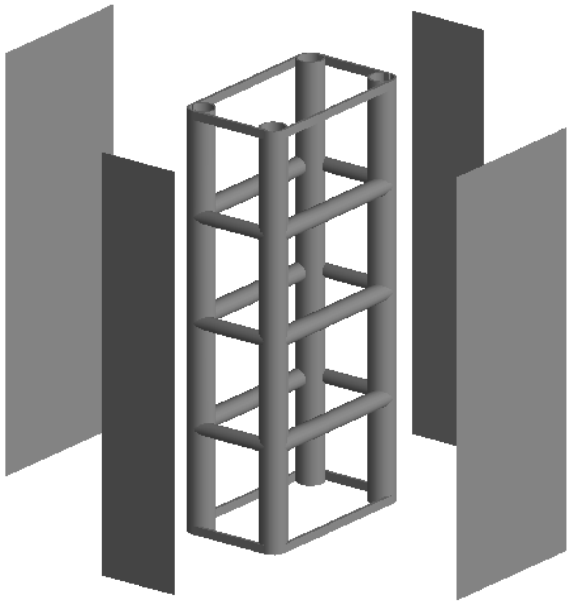

Figure 4-17 Exploded View of Proposed Pier Concept

CHAPTER 5

SIMPLIFIED ANALYSIS AND DESIGN

5.1 General

This chapter presents the simplified analyses, decisions, and assumptions made in designing the proposed multi-hazard resistant bridge pier system. While simplified approaches are appropriate for design, ultimate performance and trends in ultimate behavior of the resulting system will be investigated in the next chapter by using advanced finite element modeling techniques.

In general, the system was designed for a given seismic hazard and then analyzed for the other hazards using rational approaches and conservative assumptions. This was only possible because of the extent of the multi-hazard approach described in Chapter 4 to develop a concept that worked for all hazards considered here. The seismic hazard design was also used as the starting point of the detailed design because proven methods for the design and analysis of steel plate shear walls for seismic hazards are available in codes and design guides.

Section 5.2 introduces the interaction equations describing the cross-sectional behavior of round hollow steel tubes, which will be referenced throughout this document. Section 5.3 addresses the analysis and design of the pier considering the seismic hazard. Section 5.4 looks at the system's global behavior when subjected to vehicle collisions. Section 5.5 provides a simplified analysis for the tsunami hazard. Section 5.6 investigates the system's performance considering the blast hazard. Note that some of the details provided in this chapter are superfluous for engineers well versed in design for one respective hazard but are presented here to provide more accessibility for engineers having expertise in design for other hazards.

5.2 Interaction Equations

The corner members used in the proposed pier system are round hollow steel tubes, as illustrated in Figure 5-1. Sections 5.2.1 and 5.2.2 introduce the interaction equations used to express the ultimate capacity of these sections. It is assumed that the wall thickness of the tubes is small relative to the tube's diameter; thus, a "thin" tubular section is assumed for the derivation of these interaction equations. Interaction equations are provided for two cases: (1) for the onset of yielding in the section, and (2) full plastic yielding of the section. Detailed derivations of these interaction equations are provided in Appendix A.

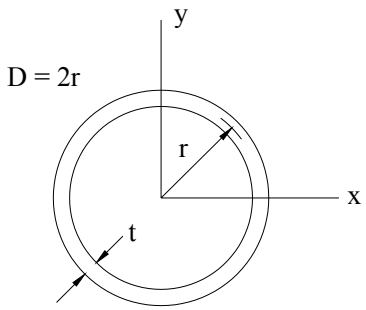

Figure 5-1 Cross Section of a Thin Tube

5.2.1 Onset of Yielding

A section is deemed to have reached the onset of yielding when the sum of the axial stress from axial load, P, and bending stress from bending moment, M, at one of the section's extreme fibers equals the section's material yield strength. This scenario is schematically illustrated in Figure 5-2.

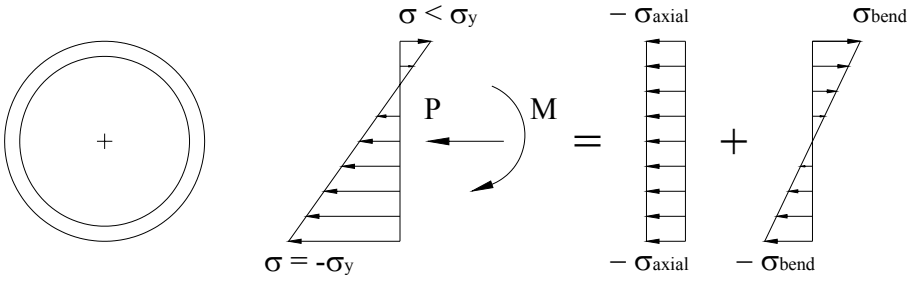

Figure 5-2 Superposition of Bending and Axial Stress Distributions (Onset of Yielding)

The equation describing the interaction between axial load and bending moment limiting the applied loads such as not to exceed the condition when yielding is initiated in an extreme fiber of the section is given by (5-1).

$$\frac{P}{P_y} = 1 - \frac{4}{\pi}\frac{M}{M_p} \tag{5-1}$$

5.2.2 Fully Plastic Yielding

When a member has hinged at a certain location, its cross section at that location has fully plastified, or fully yielded. This occurs when the axial load and bending moment is such that every fiber in the section develops the yielding capacity of the material. This scenario is schematically illustrated in Figure 5-3.

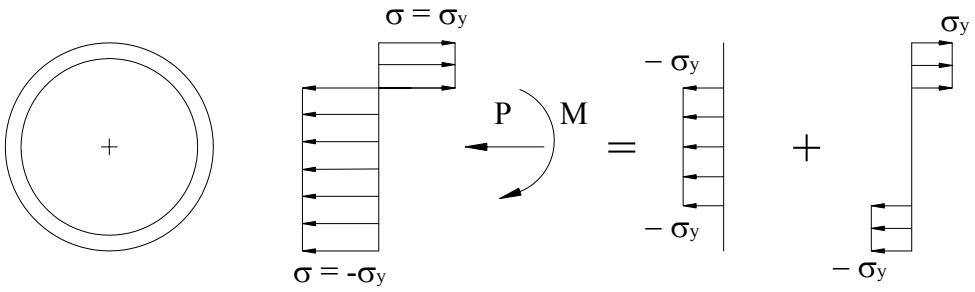

Figure 5-3 Superposition of Bending and Axial Stress Distributions (Fully Plastic Yielding)

The equation describing the interaction between axial load and bending moment for that condition is given by (5-2).

$$\frac{P}{P_y} = 1 - \frac{2}{\pi}\sin^{-1}\left(\frac{M}{M_p}\right) \tag{5-2}$$

In both cases, the cross section is assumed to meet the AISC compactness requirements. The resulting interaction equations are plotted in Figure 5-4.

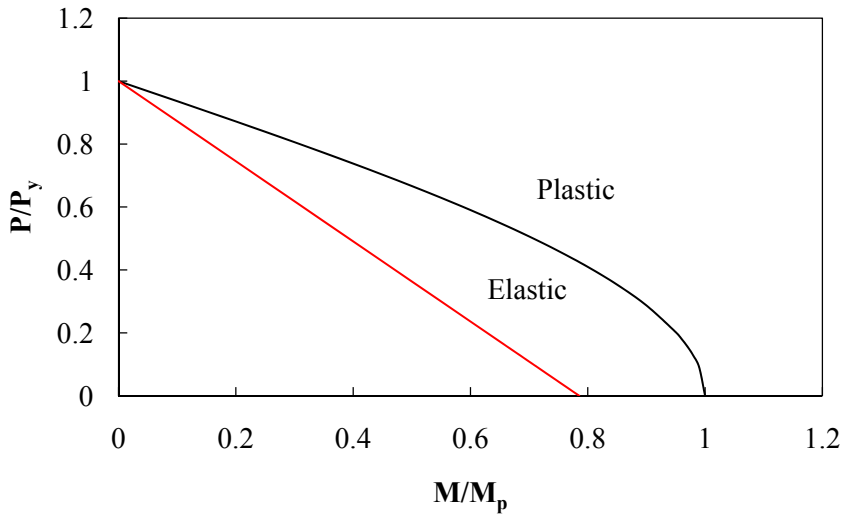

Figure 5-4 Plot of Interaction Curves for Thin Circular Tube

5.3 Earthquake

The prototype bridge selected for the current study was introduced in the preceding chapter and is presented anew in Figure 5-5.

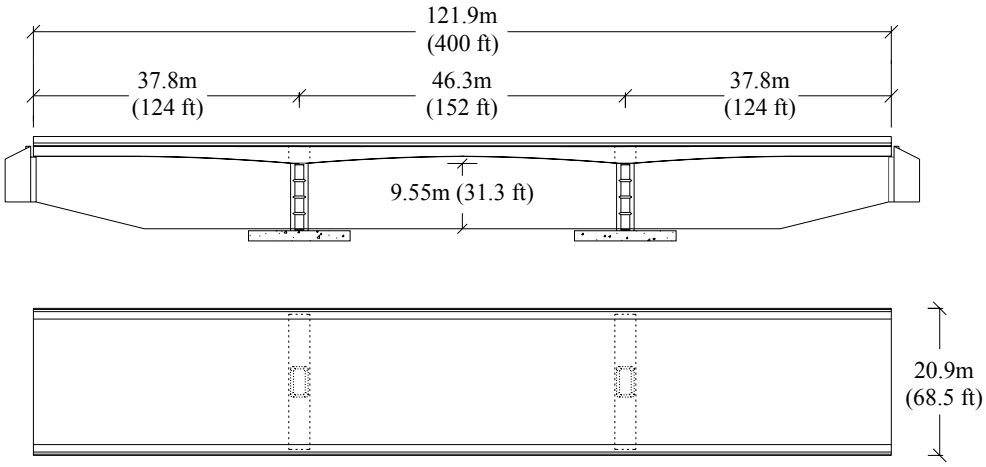

Figure 5-5 Bridge with Final Pier Concept

This section outlines the seismic analysis and design conducted and provides the final component sizes selected for the pier concept. More specifically, Section 5.3.1 illustrates the idealized bridge behavior, Section 5.3.2 provides the seismic parameters used for design, Section 5.3.3 details the method of analysis and design, and Section 5.3.4 provides the final design.

Detailed calculations are presented in Appendix B where Mathcad calculation sheets are provided.

5.3.1 Idealization of Behavior

For the purpose of this research, the bridge is considered to behave as shown in Figure 5-6. Motions in the longitudinal and transverse directions are only resisted by the two piers; the superstructure is considered rigid. The abutments are assumed to offer no lateral resistance to seismic forces, and it is assumed that there is sufficient space for movement at the abutments so that the piers can develop their ultimate strength. This idealization lends itself to treating the bridge as a single-degree-of-freedom system where the superstructure is the mass and the two piers act as springs in parallel.

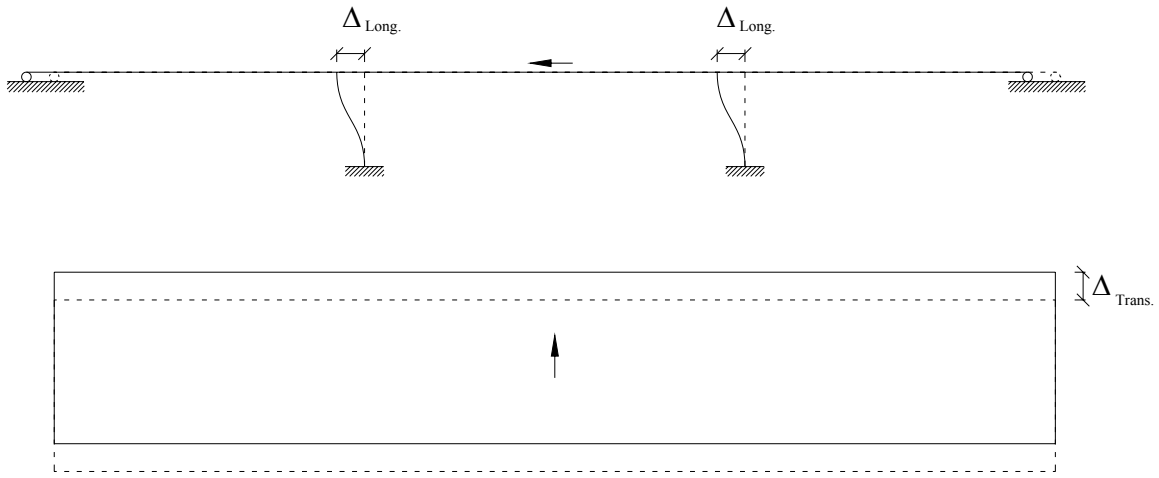

Figure 5-6 Idealized Bridge Behavior

5.3.2 Bridge Seismic Parameters

For the purpose of this research, the seismic acceleration coefficient was chosen to be 0.20, which places this bridge in seismic performance zone III. In addition, the bridge was classified as "regular", and its importance classification was chosen to be in the AASHTO category of "other bridge" (as opposed to "critical" or "essential"). The response modification factor, R, was chosen to be 5, and based on recommendations from AASHTO (Article 3.10.5.1) when the soil

profile is unknown, the site coefficient was chosen to be 1.2. The design spectrum for the site characterized with these parameters is provided in Figure 5-7.

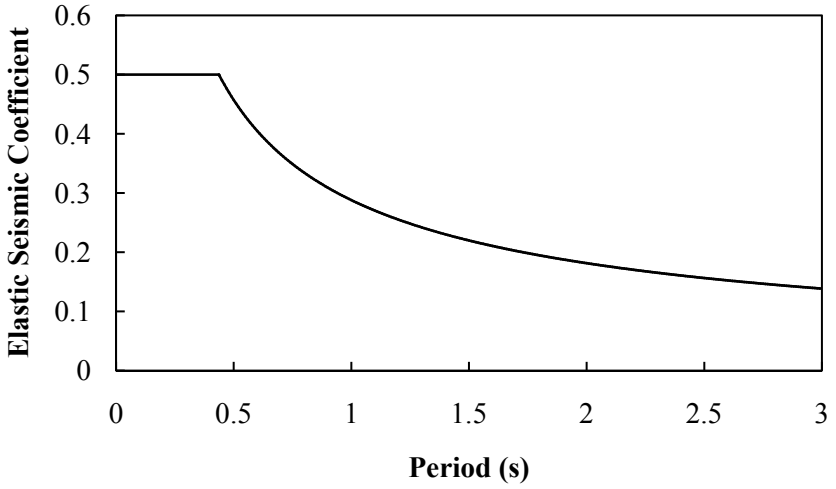

Figure 5-7 Design Spectra

5.3.3 Method of Analysis and Design

The method used to analyze and design the pier made use of a nonlinear pushover analysis with a commercially available structural analysis software, namely SAP2000 (v11.0.0). Details regarding the SAP model and the method of analysis and design are presented in the following subsections. Specifically, information regarding the setup of the SAP model and the pushover analysis is presented in Sections 5.3.3.1 through 5.3.3.6, and Section 5.3.3.7 provides details regarding the iterative analysis and design procedure followed.

5.3.3.1 Boundary Frame Details

The model's geometry was built using center-to-center dimensions (as shown in Figure 5-8) and linear frame elements. The eccentricity of the connection of the HBEs to the VBEs was neglected for the purpose of the simplified analyses. Only the middle 12 HBEs, (six parallel to the transverse direction and six parallel to the longitudinal direction) are able to deflect and were designed for the purposes of this research. The horizontal members at the top and bottom of the pier were considered continuously connected to the pier cap and to the foundation, respectively, and were assigned arbitrary sections having modified properties making them rigid.

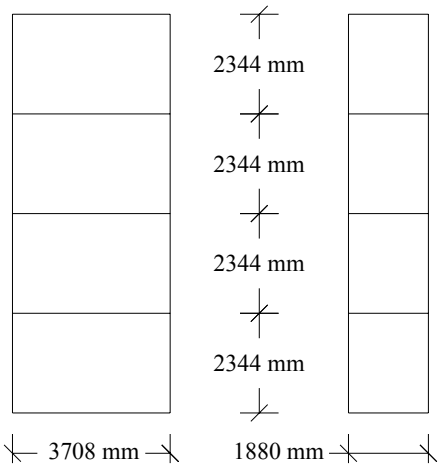

Figure 5-8 Boundary Frame Geometry

5.3.3.2 Desired Boundary Frame Behavior

For the purpose of this research, plastic hinging was allowed in the boundary frame at the ends of the VBEs and HBEs. This, along with complete yielding of the plates, constitutes the pier's ultimate behavior and plastic mechanism. To allow for this behavior to develop in the nonlinear pushover analysis, discrete nonlinear hinges were introduced at the ends of the boundary frame elements. Since the SAP model is built of linear elements located along the centerlines of the boundary frame members, the hinges were essentially placed where the centerlines of the HBEs meet the centerlines of the VBEs. Realistically, this is not the case since hinging will develop at some distance from the centerline. For the purpose of the initial simplified analysis, this was not accounted for, as it was not anticipated to have a significant effect on the overall behavior of the system.

The nonlinear hinge model chosen was the "Fiber P-M2-M3Hinge". This hinge, which is one of several models that SAP2000 offers, automatically accounts for the interaction between axial load and bi-axial moment, by its nature of being a fiber model. A short study verifying that the hinge model used provided desirable nonlinear behavior can be found in Appendix C. Note that the material model assumed for this research was assumed to be elastic-perfectly plastic. This was deemed adequate since this research focuses on determining trends in the proposed system's global behavior. The steel used for the tubular sections was A500 Gr. B (σ_y = 290MPa (42ksi)),

for which the ratio of expected yield strength to the specified yield strength, R_y, is 1.4 (AISC 2005a).

Figure 5-9 shows the geometry of the pier's boundary frame and the schematic location of the fiber hinges. As described in Appendix C, a total of 28 fibers were used in each of the fiber hinges while performing the SAP2000 analyses.

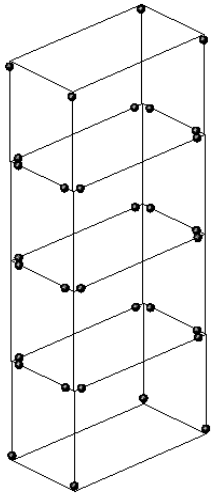

Figure 5-9 Fiber Hinge Locations

5.3.3.3 Plate Sizing and Representation

The plates were represented in the model by a series of strips. A description of these strips and how to determine their properties was provided in Chapter 3. The strips in this model were modeled as "tension-only" strips, without any compression strength. Additionally, a discrete ductile "axial-P" nonlinear hinge having elastic-perfectly plastic behavior was assigned to each strip. The material used for the plates was A36 (σ_y = 248MPa (36ksi)) steel, for which R_y is 1.3 (AISC 2005a).

The strips were connected to the centerlines of the bounding elements, again a simplification since the plates are actually attached tangentially to the boundary frame. It was assumed that the torsion induced in the VBEs would be negligible compared to the torsion capacity of the final

members. Also, since plates meet perpendicular to each other at the VBEs, the forces from the plates' pull on the VBEs would likely have a tendency to cancel out when both are yielding.

5.3.3.4 Constraints

The pier's connection to the foundation was accomplished by assigning fixed supports at the base of each of the VBEs and by assigning pin supports at the locations where the strips intersect the bottom members. To model the connection of the pier to a rigid pier cap, a *diaphragm constraint* was applied to each of the nodes located at the pier's top. To produce the boundary conditions illustrated in Figure 5-6 for longitudinal motion, *equal constraints* were assigned to each node located at the pier's top on the two members oriented parallel to the bridge's longitudinal direction. This constraint was used to constrain the nodes on each of these two members to have equal vertical translations. Figure 5-10 schematically indicates the members whose nodes were assigned *diaphragm* and *equal* constraints as described above. The intent of constraining the pier this way was to prevent rotation of its top for longitudinal translation, but to allow rigid rotation for transverse translation of the bridge's superstructure.

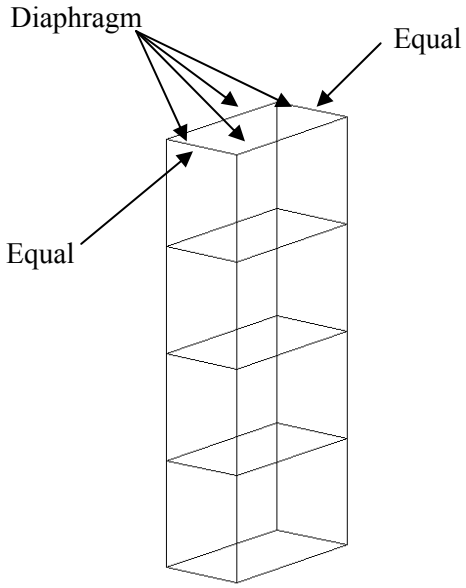

Figure 5-10 Constraint Assignments

5.3.3.5 Pushover Description

In this system, VBEs were thought to be most critically loaded when the pier was pushed simultaneously (or bi-directionally) in the transverse and longitudinal directions because as the strips yield in two plates oriented perpendicular to each other, they would each apply axial loads on the VBE to which they are attached. For pushover in some specific directions, these vertical axial forces could be additive. Therefore, for the purpose of this analysis, the pier was pushed bi-directionally to its ultimate capacity, which is reached when all anticipated hinging has developed in the HBEs, VBEs, and strips on all four sides of the pier.

The pushover analysis was achieved in two steps. The first step, a load-controlled nonlinear static pushover analysis, applied dead load (resulting from the pier cap and superstructure) to each VBE (referred to as P_{dead}). This load was then held constant as a lateral pushover analysis was performed. The lateral nonlinear displacement-controlled pushover analysis was performed by incrementally applying a given pushover pattern until a specified displacement limit was reached. This displacement limit was assigned to a node at the pier's top. The selected corresponding pushover load patterns chosen are schematically shown in Figure 5-11. Figure 5-11(a) illustrates the dead load being applied to the VBEs and Figure 5-11(b) illustrates the subsequent lateral pushover pattern applied.

The loads acting in the transverse direction of the bridge, P_{trans}, are equally applied at each of the four VBEs. Likewise, the loads in the longitudinal direction of the bridge, P_{long}, act equally at the four VBEs. Vertical forces producing a couple acting to overturn the pier about the bridge's longitudinal axis were also applied to account for the height of the center of mass above the pier. Figure 5-12 schematically illustrates how these forces were determined.

In that figure, P_{Pier} and P_{super} respectively represent the contribution of the lateral seismic forces attributed to the inertia force due to the pier cap and the superstructure. These were respectively applied at the centers of mass of the pier cap and the superstructure (the superstructure's centroid location being taken from the FHWA seismic design example from which the prototype superstructure is taken – see Section 4.3.4 of this report). Since only the pier was modeled, the combined lateral force that they produce was represented by lateral point loads, and the

overturning moment that they produce about the pier's centerline was replaced with equal and opposite vertical loads forming a couple. The lateral pushover pattern in the longitudinal direction did not include an overturning couple because of its fixed-fixed top and bottom boundary conditions.

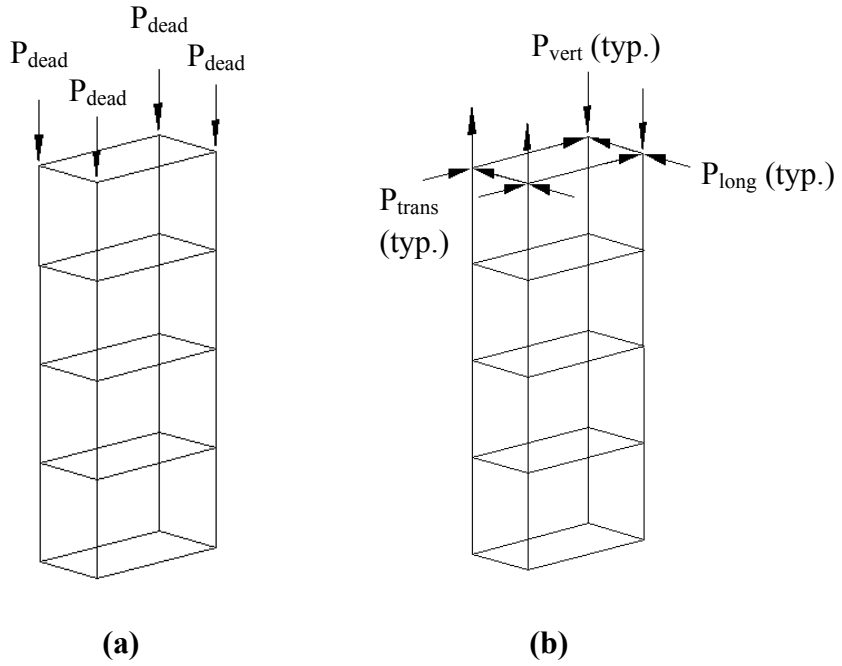

Figure 5-11 (a) Initial Gravity Load; (b) Lateral Pushover Pattern

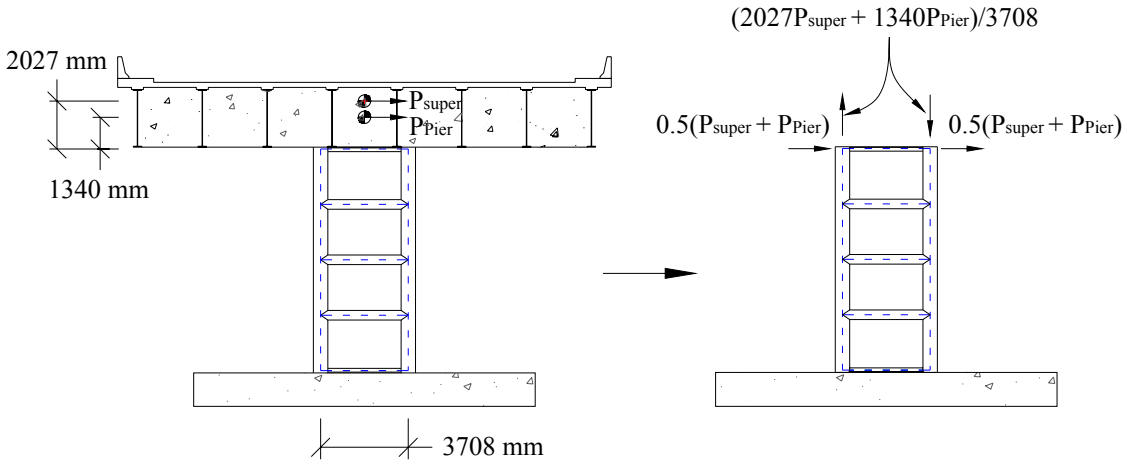

Figure 5-12 Pushover in the Transverse Direction

5.3.3.6 SAP2000 Model

The final SAP strip model is shown in Figure 5-13. Three views of the model are shown: (a) an elevation of the model looking at the side of the pier parallel to the bridge's transverse axis; (b) an elevation of the model looking at plates parallel to the bridge's longitudinal axis, and; (c) a 3-D view of the model.

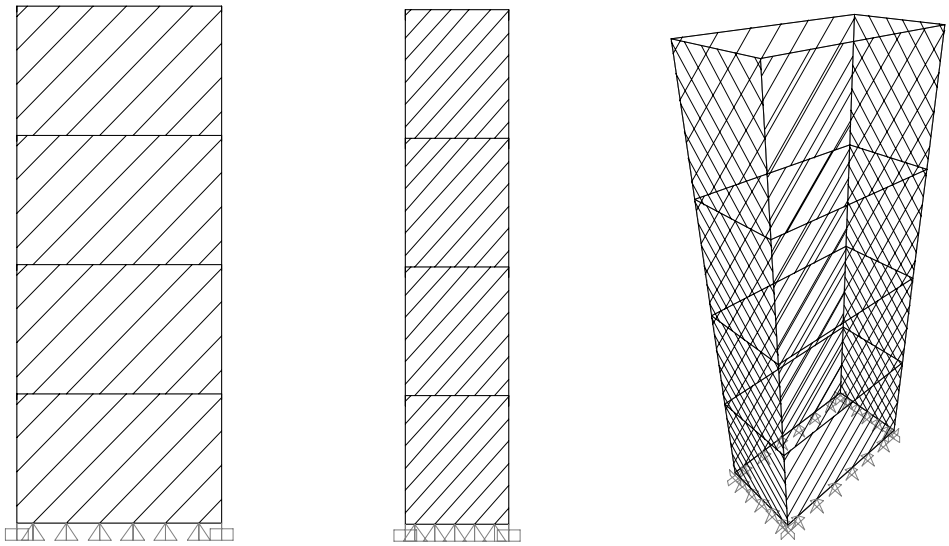

(a) **(b)** **(c)**

Figure 5-13 (a) Parallel to Transverse Direction; (b) Parallel to Longitudinal Direction; (c) 3-D View of Strip Model

5.3.3.7 SAP2000 Analysis and Design

To obtain the bridge's reactive mass, dead load was computed taking into account the average cross-sectional area of the girders, the deck, the sidewalks, the bridge overlay, the deck forms, the barriers, the cross-frames, and the pier caps. The distributed dead load for the superstructure was estimated as 0.207 kN/mm (1.18 kip/in) and the dead load per pier cap was estimated as 3369.5 kN (758 kip). Assuming each pier resisted tributary load, the dead load demand for the VBEs of each pier, P_{dead}, was calculated to be 3020.3 kN (679 kip). This does not include the self-weight of the pier's boundary frame, which was included in the SAP analysis.

To determine the period of the structure, and thus the seismic force from the spectrum presented in Section 5.3.2, an iterative analysis and design procedure was followed, starting with the selection of member sizes for the HBEs and VBEs. An initial lateral stiffness of the bridge structure was assumed in the transverse direction and in the longitudinal direction, from which the bridge's transverse and longitudinal periods were computed (using the total mass of the pier caps and the superstructure noting that this mass is identical for both directions). With these two periods, the elastic seismic coefficient, C_{sm}, was determined from the spectrum in Figure 5-7, which allowed for the determination of the shear demand on each pier taking into account the response modification factor given in Section 5.3.2. The mass of the piers themselves was neglected in the computation of lateral seismic force since it is small relative to that of the superstructure and pier caps.

Because the two piers have identical stiffness in each direction, they equally resist the equivalent lateral loads. Moreover, since each pier is constructed of steel plates on four sides (as described in the preceding chapter), there are two plates per direction per pier, and the lateral force demand on each pier (in each direction) must be halved to determine the shear demand for which each plate is designed. Since the seismic forces are applied to the pier's top, each of the plates between the HBEs in a given direction resist the same shear demand and are sized to be of identical thickness.

After establishing boundary frame member sizes and plate thicknesses, a nonlinear pushover analysis was performed on the SAP model with the procedure described in Section 5.3.3.5, where $P_{trans} = 1$, $P_{long} = 1$, $P_{vert} = 1.015$, and P_{dead} was given in the first paragraph of this section. Thus, the pier was pushed diagonally with a resultant force acting at 45 degrees. Following the pushover analysis, resulting member forces were checked for each member. The key strength checks included the following:

- The moment-axial force interaction was checked for each of the VBEs and HBEs with the interaction equation from Section 5.2.2, assuming that the tube sizes were such that their critical buckling stress was essentially equal to their yield strength, and such that secondary bending effects were small. When performing the pushover (and thus when designing the boundary frame), the expected yield strength, $R_y\sigma_y$, of the plates was

conservatively used. In practice, the expected yield strength of HBEs should also be used when checking the VBEs, and can be incorporated into the SAP model. This was not considered since an elastic-perfectly plastic material model was assumed for this study. However, additional checks conducted after the design was completed showed that the VBEs in this design would still be adequate if it was considered. Also, in practice, material strain hardening would need to be considered, but was not considered in this study.

- Shear capacity of the members was checked following specifications by AISC (2005b)
- The HBE-to-VBE moment connections were checked. However, specifications regarding this type of connection were not found in the reviewed literature. To have a sense for the connection capacities, however, information provided by AISC (2005b) and in the book titled "Hollow Structural Section" (Packer and Henderson 1997) was used. Packer states that design criteria have not been established for multi-planar moment connections, and AISC states that available testing for HSS-to-HSS moment connections is less abundant than for truss connections. Accordingly, the equations used were based on limit states used for planar, axially-loaded connections. In practice, connection matters would deserve more attention.

Stiffness of the resulting completed design was then checked against the assumed values taken to determine the bridge period and corresponding design forces. When the resulting stiffness became close to the one assumed, then the design and analysis procedure had converged to a satisfactory solution. When they differed, design iterations were executed with the above procedure.

5.3.4 Final Seismic Design and Analysis Results

For the resulting design, structural members obtained were as follows: the round hollow members for the VBEs have an outer diameter of 609.6mm (24 in) with a wall thickness of 46.0mm (1.812 in), the longitudinal HBEs have an outer diameter of 323.9mm (12.75 in) with a wall thickness of 12.7mm (0.5 in), and the transverse HBEs have an outer diameter of 406.4mm (16 in) with a wall thickness of 21.4mm (0.843 in). For the VBE sizes being used, torsion effects

were found to be negligible. A short study regarding torsion effects on the VBEs due to plate eccentricity can be found in Appendix D.

Table 5-1 shows the final design parameters, where L/h is a plate's aspect ratio, $k_{initial}$ is the bridge's elastic stiffness, C_{sm} is the elastic seismic coefficient, V_{pier} is the total lateral force demand per bridge pier, and V_{plate} is the plate shear demand. Note that V_{plate} is half of V_{pier} since there are two plates per pier per direction. Also, t_w is a plate thickness, α is a tension field's inclination angle, and A_{strip} are areas assigned to the strips in the strip model.

Table 5-1 Final Design Parameters

	Transverse Direction	**Longitudinal Direction**
L/h	1.582	0.802
$k_{initial}$	217.16 kN/mm (1240 k/in)	212.25 kN/mm (1212 k/in)
C_{sm}	0.343	0.340
V_{pier}	1096.5 kN (246.5 kip)	1088.0 kN (244.6 kip)
V_{plate}	548.0 kN (123.2 kip)	544.0 kN (122.3 kip)
t_w	1.588 mm (0.0625 in)	3.175 mm (0.125 in)
α	44.2 deg.	41.7 deg.
A_{strip}	681.3 mm^2 (1.056 in^2)	854.8 mm^2 (1.325 in^2)

Figure 5-14 to Figure 5-16 show results from the final bi-direction pushover analysis performed in SAP. Each figure displays the undeformed and deformed geometries. Additionally, Figure 5-15 and Figure 5-16 show graphs of the base shear versus displacement for the corresponding direction.

The curves presented in Figure 5-15 and Figure 5-16 show the transverse and longitudinal behavior and strength of the pier as it is pushed bi-directionally. The ultimate capacity is reached because each of the hinges introduced into the frame was assigned elastic-perfectly plastic behavior (i.e. no strain hardening).

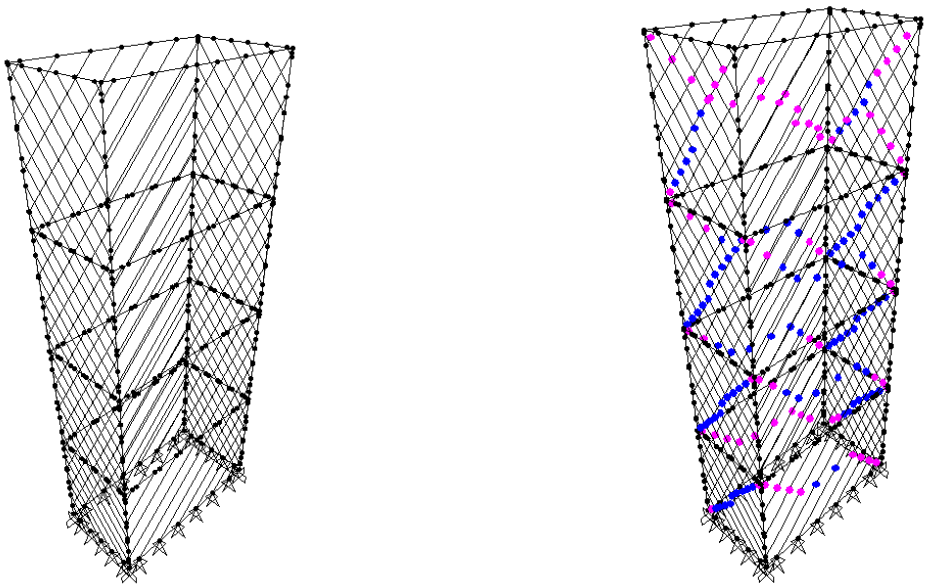

(a) **(b)**

Figure 5-14 Bi-Directional Pushover Analysis:
(a) 3-D Undeformed Position; (b) Final State of the Structure

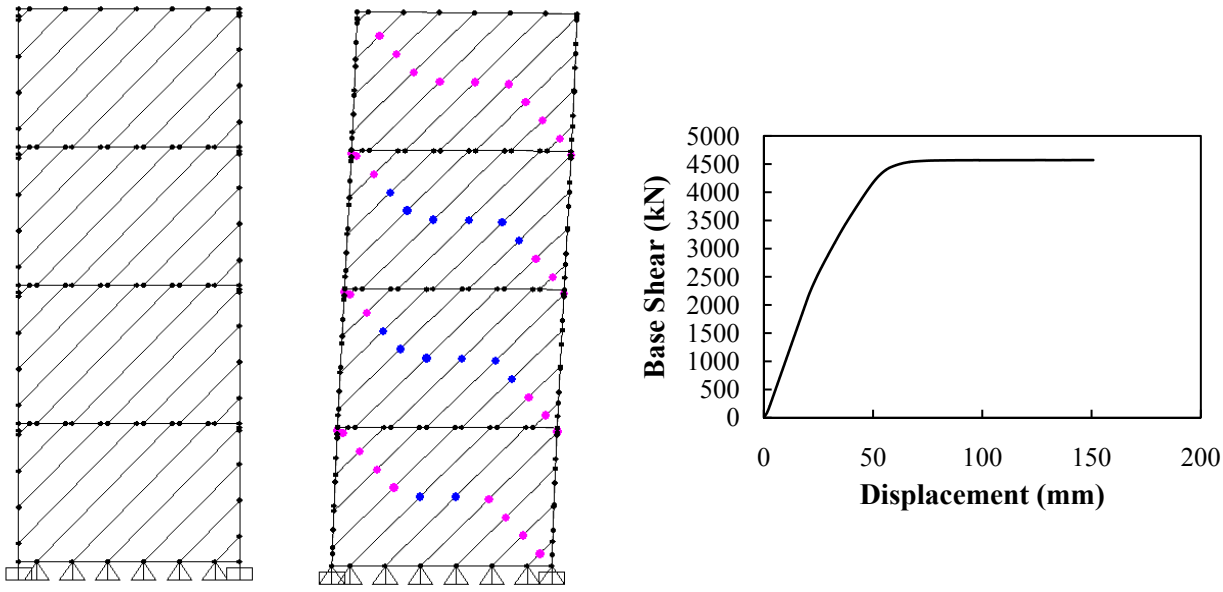

(a) **(b)** **(c)**

Figure 5-15 Bi-Directional Pushover Analysis (Transverse Direction Results):
(a) Undeformed Position; (b) Final State; (c) Pushover Curve

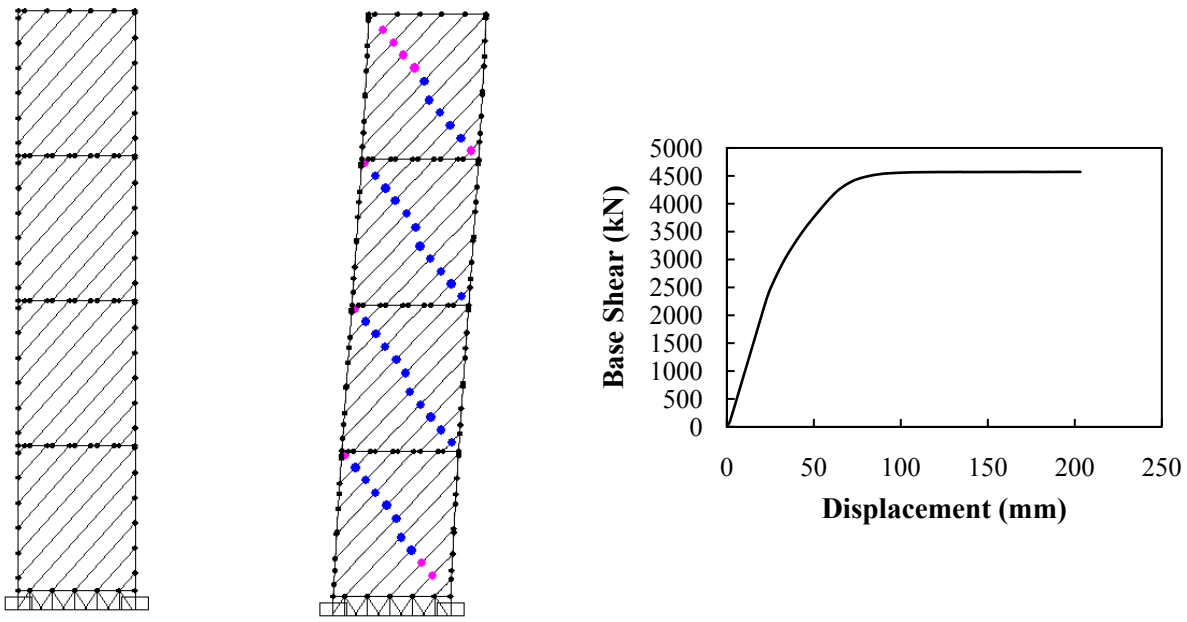

Figure 5-16 Bi-Directional Pushover Analysis (Longitudinal Direction Results): (a) Undeformed Position; (b) Final State; (c) Pushover Curve

5.3.5 Relative Contributions to Total Strength

The relative contribution of the plates and the boundary frame to the pier's ultimate resistance was quantified. This was accomplished by determining the total contribution of the plates relative to the ultimate resistance of the system based on the formulation discussed in Chapter 3. The ultimate resistance of the plates in each direction was determined with (5-3).

$$V_{Ult.Plates} = 2\left(\frac{1}{2} L\sigma_y t_w \sin(2\alpha)\right) \tag{5-3}$$

In both directions, the plate-to-boundary frame strength ratio was found to be the same. The plate contributed 32% of the total resistance in each direction and the frame contributed 68%. Since there are no rules at this time prescribing a distribution of forces between the plates and the frame, this measure of relative contribution was arbitrarily decided to be acceptable for the purpose of this study as the objective is to observe behavioral trends of this system when it is subjected to multiple hazards.

5.4 Vehicle Collision

With the design determined for the seismic hazard, the pier's behavior when subjected to vehicular collision loading, as defined by AASHTO (2007), was next investigated using a simplified method of analysis. The motivation behind this simplified analysis was to gain a general understanding, with simplifying assumptions, of the pier's response to this hazard.

5.4.1 Simplified Collision Analysis

For this analysis, the SAP2000 model used for the seismic analysis and design was re-used without the discrete nonlinear hinges. However, the contribution of the plates to the pier's resistance, which is unknown at this time, was conservatively neglected for this analysis, leaving just the boundary frame, as shown in Figure 5-17.

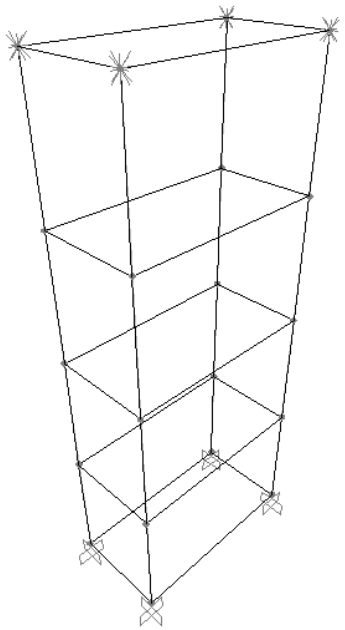

Figure 5-17 Undeformed, Simplified Pier for Vehicle Collision Study

All section sizes obtained from the seismic analysis were kept the same. The boundary conditions were altered from those assigned to the pier subjected to the seismic hazard. Although the vehicular collision hazard is characterized by a static point load in AASHTO, collision is actually an impact load. Therefore, because the bridge superstructure is believed to

have a negligible response until after the load has been applied and removed, the boundary condition at the top of the pier was modified to only allow translation vertically; otherwise, the top of the pier was fixed. Also, release of the vertical degree of freedom allowed for application of dead load to the model.

In reality, if a vehicle were to strike a pier, the collision load could be applied at any point. The vehicle could impact a plate parallel to the bridge's longitudinal direction, a plate perpendicular to the bridge's longitudinal direction, or any one of the pier's VBEs. For the purpose of this simplified analysis, the vehicular collision load was assumed to act on one of the VBEs. Side plates could be sacrificial for this purpose. The loading conditions were as shown in Figure 5-18 (i.e. either in directions parallel to the transverse and longitudinal directions of the bridge (cases a and c, respectively), or at a 45 degree angle (case b)). A vehicle collision load of 1800kN (400 kip) acting at 1200mm (4 ft) from the pier base was imposed at each location shown. Moreover, an axial load of 3020kN (679 kips) representing the dead load of the superstructure was placed on each of the VBEs, as was done for the seismic hazard.

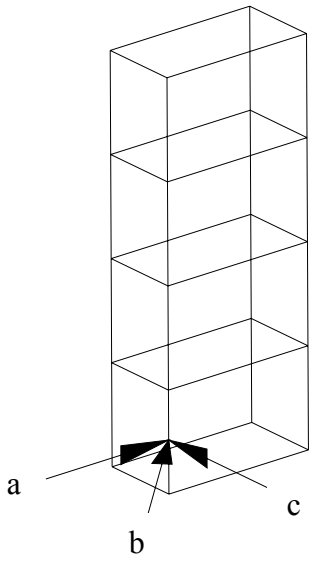

Figure 5-18 Vehicle Collision Scenarios

For each of the load cases shown in Figure 5-18, a linear static analysis was performed with SAP2000. Figure 5-19 shows the deformed shape of the pier for each of the loading scenarios considered.

The deformed shapes in these figures are scaled by a factor of 500 so that the effect of the load can be seen. For each of the cases considered, the displacement of the node located above the point of load application was less than 2mm in the direction of the applied load. The frame also remained elastic under the specified collision loading, based on the internal axial force and moments in each of the VBEs and the interaction equation introduced in Section 5.2.1.

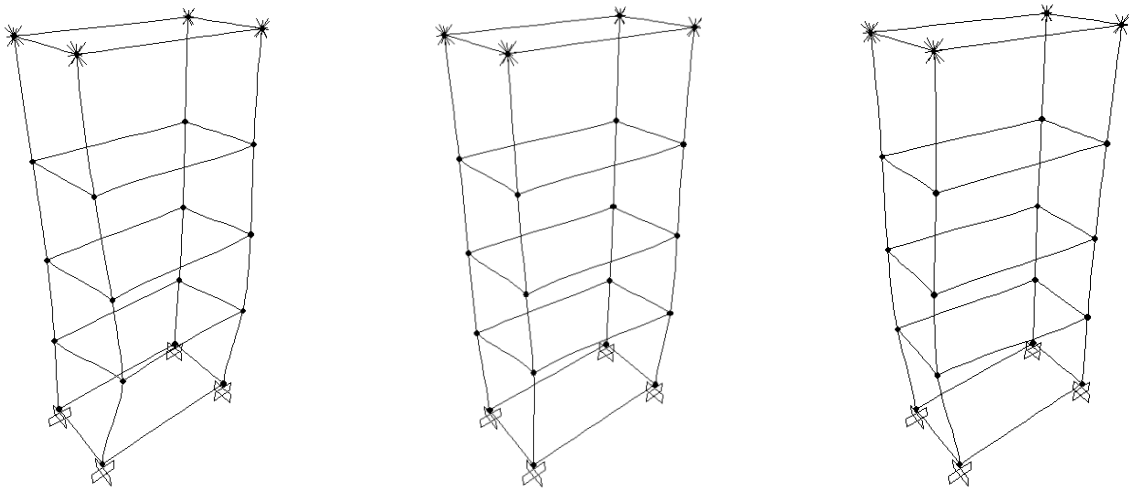

(a) **(b)** **(c)**

Figure 5-19 Deformed Shape for a Vehicle Load: (a) Parallel to the Bridge's Transverse Direction; (b) Angled at 45 deg., and; (c) Parallel to the Bridge's Longitudinal Direction

5.4.2 Summary of Simplified Collision Analysis

Though the internal forces found from the three loading cases considered suggested that the members remained elastic, the local effects of a point load acting normal to a tube's surface could not be captured using the simplified SAP2000 analyses. Finite element analyses would be required to determine the local effect of this assumed point load that represents the vehicle collision on the wall of a tube.

From this simplified analysis, the hazard to the proposed pier design when subjected to a vehicle collision is low, neglecting any possible local failure of the tubes near the point of load application. As a result, design is governed by other hazards. Particularly, design resulting from the demands of the seismic hazard led to pier properties adequate to resist a vehicular collision

load, as specified by AASHTO, for a load applied to a VBE. The vehicular collision load was not considered applied to the plates as those were considered sacrificial in this load case.

5.5 Tsunami

Further simplified analysis of the proposed pier concept is next described for the tsunami hazard. To perform a simplified analysis in the absence of advanced finite element software, a simplified method to analyze the plates, which are loaded out-of-plane, was used. Section 5.5.1 provides a discussion of this simplified method. Then, to gain a preliminary understanding of tsunami force effects on the proposed pier system, the structure was subjected to a specific tsunami hazard (namely, an event corresponding to a 3m design stillwater depth with flow parallel to the bridge's transverse direction) and evaluated, as described in Section 5.5.2. The calculation of these forces was based on the relationships provided in existing codes, which were introduced in Chapter 2.

5.5.1 Plate Analysis for Out-of-Plane Loads

For the tsunami hazard, a major factor that contributes to the behavior and effectiveness of the proposed system is the fact that the plates are loaded out-of-plane. In the absence of special measures to allow water penetration to the interior of the pier assembly, even the plates parallel to water flow will be loaded because the space enclosed by the plates on each of the four sides will be assumed to remain dry. The out-of-plane loading of the plates is anticipated to result in large deformations, which must be accounted for in computing the resistance of the plates. These loads are then transferred to the boundary frame through the plate edge reactions.

Yield line theory was first attempted to capture the out-of-plane strength of the plates. However, calculations showed the out-of-plane resistance calculated using yield line theory to be impractically small due to the small thicknesses of the plates used, but also because yield line theory relies on plastic hinge formation along yield lines and does not capture the catenary type of behavior expected from the thin plates used in this research. Thus, a method of analysis that accounts for the two components (i.e. normal and pull-in) of plate edge reactions acting on the boundary elements (the "normal" component being that which is normal to the initial plate's

surface and the "pull-in" component being that which is acting in the plane of a initial plate's surface) must be employed to obtain a reasonable approximation of the plate and boundary frame behavior. The simplified method used in analyzing out-of-plane loads on the plates is based on a method used by Warn and Bruneau (2008) in an investigation of the blast resistance of steel plate shear walls. The method by which they approximated the capacity of steel plates for out-of-plane blast loads made use of the plate's yield strength, parabolas to approximate the deformed shape of the plate, and the corresponding plate edge rotations to calculate the resistance. To illustrate this idea, a typical parabolic shape is shown in Figure 5-20, where L is the length of the parabola below the x-axis referred to herein as the deformed length, z is the maximum depth of the parabola measured from the x-axis, and L_o is the distance between the zero points referred to as the undeformed length.

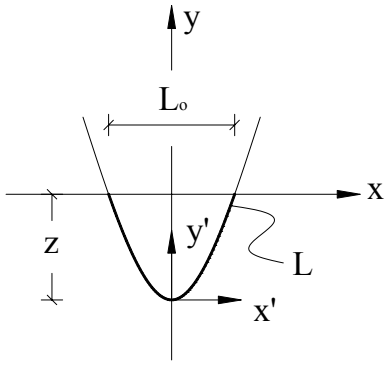

Figure 5-20 Geometry of a Parabola

The deformed length, L, is given by (5-4).

$$L = \sqrt{4z^2 + \frac{L_o^2}{4}} + \frac{L_o^2}{8z} \ln\left[\frac{2z + \sqrt{4z^2 + L_o^2/4}}{L_o/2}\right] \tag{5-4}$$

Referencing the deformed shape by coordinates from the x'-y' axes (as shown in Figure 5-20), the following relationship describes the curve.

$$y' = \frac{4z}{L_o^2}(x')^2 \tag{5-5}$$

Using (5-5) and taking the derivative of *y'* with respect to *x'*, one obtains the relationship shown by (5-6), which represents the angle of rotation at any point along the curve.

$$\frac{dy'}{dx'} = \frac{8z}{L_o^2} x' \tag{5-6}$$

Consider Figure 5-21, which shows a tangent to a point on the curve some distance to the right of the x'-y' coordinate system's origin.

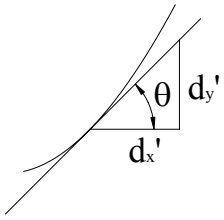

Figure 5-21 Angle of Inclination of a Tangent to the Parabola

Using trigonometry, the relationship shown in (5-7) is obtained.

$$\tan\theta = \frac{dy'}{dx'} = \frac{8z}{L_o^2} x' \tag{5-7}$$

By simple use of this equation one can obtain the angle of inclination at the point where the parabola intersects the x-axis. The resulting relationship is given by (5-8).

$$\theta(x' = L_o/2) = \tan^{-1}\left(\frac{4z}{L_o}\right) \tag{5-8}$$

In the simplified method used by Warn and Bruneau, the plate is assumed to be completely yielded for a given out-of-plane displacement at the center of the plate. The plate's yield strength and thickness, and this angle are then used to compute the normal reaction component for each edge, assuming a constant angle along each edge to simplify calculations. The total normal reaction divided by the plate's area is used to approximate the plate's capacity.

The method used for this research attempts to refine this method by taking into consideration the varying edge rotation along the plate boundaries, and does not assume the plate to be fully yielded for every level of deformation, as this would overestimate the plate's capacity for small deformations. Figure 5-22 illustrates how the plates are assumed to deform in this study. The deformation of the plate is represented by a series of parabolic strips spanning each direction.

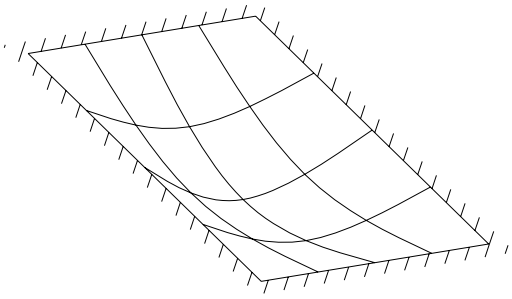

Figure 5-22 Idealized Out-of-Plane Plate Deformation

The simplified analysis procedure begins by specifying a center out-of-plane deformation of the plate and by assuming a uniform pressure load, and thus a symmetrical deformation of the plate. For a known center displacement, the deformed length of the two main parabolas, which span horizontally and vertically at the center of the plate (as shown in Figure 5-23) can be calculated using (5-4). The main parabolas are defined here as being those at the center width of the plate on each side, and that intersect the central point of maximum out-of-plane deformation.

Once the geometry of the main parabolas has been established, a grid of other parabolas can be set across the plate; the geometry of these subsequent parabolas spanning perpendicular to the main parabolas can be assumed as shown in Figure 5-23. From this figure, it can be seen that the point of maximum out-of-plane deflection for each of these parabolas (labeled for reference as V1, V2 and H1, H2) can be taken as located on one of the main parabolas. For instance, point P1 and P2 on M1are used to obtain the deformation at the center of H1 and H2. Similarly, P3 and P4 on M2 are used to specify the center deformation of V1 and V2. The depth of P1-P4 can be determined from (5-5), using the offset, Δ (= x'), of the parabola under consideration from the center of the corresponding main parabola. With this information, the deformed length of each parabola subsequent to the main parabolas can be calculated using (5-4). Spreadsheets can be used to calculate the deformed shape of a plate represented by any number of parabolas, resulting in a web of parabolas that approximate a plate's deformed shape.

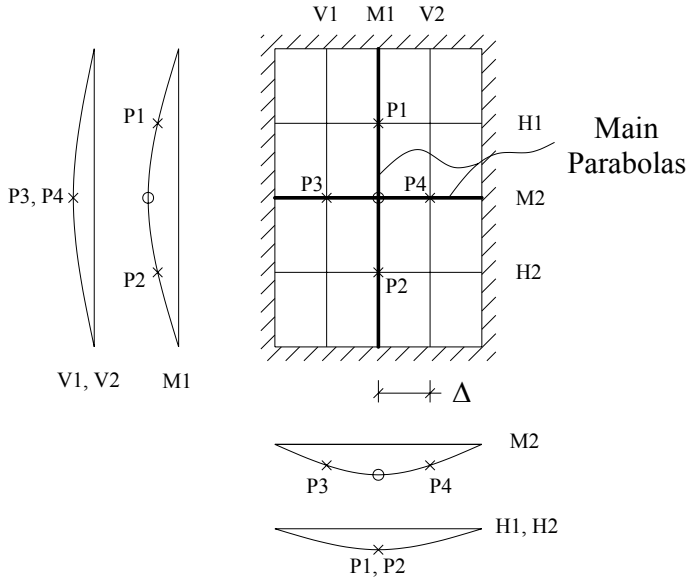

Figure 5-23 Simplified Plate using Parabolic Strips

Once the deformed position of each main parabola and each subsequent parabola being considered is determined, they can be assigned a tributary width (W_T), which, when multiplied by the thickness of the plate, results in each parabola (or strip) having a specific cross-sectional area. Figure 5-24 shows the same plate as previously considered, except with more strips.

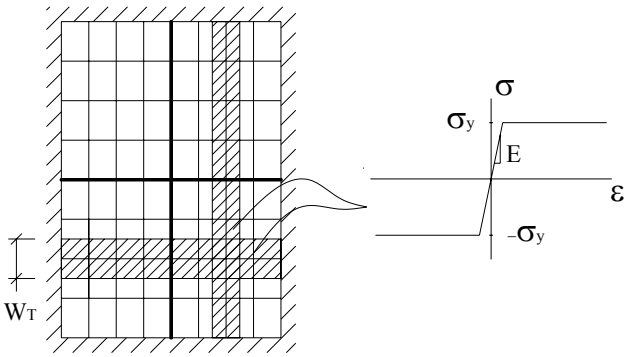

Figure 5-24 Plate Divided into Strips

With the undeformed and the deformed length of each strip known, the strain in each strip can be calculated, assuming constant strain along the strip for simplicity. From this calculation, and assuming elastic-perfectly plastic behavior, the stress in each strip corresponding to the calculated strain can be obtained. The stress is also assumed to be constant throughout the strip's length.

With the deformed shape of the strips in each direction known, the rotation at the plate's edge can be determined with (5-8). For a strip force (calculated as the product of the stress in the strip and the cross-sectional area of the strip) acting at this angle at the plate edge, the normal and pull-in components of the force can be determined. This is schematically shown in Figure 5-25 for the main parabolas, where F_s is the force in the strip, and F_{sy} and F_{sx} are the normal and pull-in components, respectively.

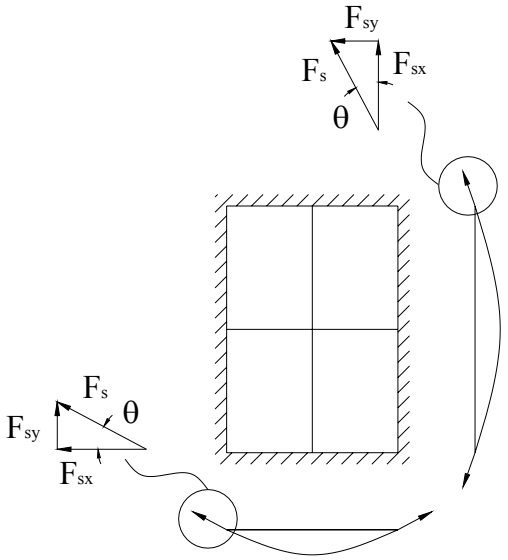

Figure 5-25 Plate Forces Imposed on Boundary Elements

In order to compute the uniform pressure that a plate sustains for given center displacement, the "normal" component of each strip's force is summed to obtain a total reaction force. The resultant of the pressure acting on the plate must equal this total reaction. Thus, the uniform pressure required to deform a plate to a specific center displacement is obtained by dividing the total reaction force by the area of the plate, as was done in the simplified method by Warn and Bruneau.

Finding equilibrium for a given applied pressure by the above procedure is an iterative process. Given a uniformly distributed pressure applied to a plate, the procedure begins by choosing a displacement for the center of the plate and determining reactions as described above. The uniform pressure corresponding to those reactions is obtained. Iterations on the value of center displacement for the plate are required until convergence to the specified pressure demand. At

this point, the approximate deformed shape (as assumed by the analysis) of the plate for a given uniform pressure is known. Note that because the plate deformation is assumed to be symmetric, only one-quarter of the plate was considered in calculations.

To approximate the distribution of forces at the edges of a plate, only the main parabolas are considered. After the center displacement corresponding to the uniform pressure being imposed on the plate is known, the deformation of the main parabolas is also known, and correspondingly their stresses. Multiplying this stress by the plate's thickness, one obtains a force per unit length applied to the plate edges. This uniformly distributed edge reaction obtained from the main parabolas is assumed to act uniformly over the entire edge to which it connects, thus approximating the force imposed on the plate's edges as uniformly distributed loads. The two components of this distributed force per unit length can also be determined. A brief study comparing results obtained using this simplified method with corresponding finite element results can be found in Appendix E. This study, and all analyses done with this simplified procedure, considers strips that have tributary widths equal to 0.5% of the corresponding perpendicular edge's length.

5.5.2 Simplified Tsunami Analysis

5.5.2.1 Tsunami Loads Acting on Pier

For the purpose of this preliminary study, the design stillwater depth was assumed to be 3m and water flow was assumed parallel to the bridge's transverse direction. The two load cases considered include: (1) surge plus debris impact (Load Case 1), and; (2) hydrostatic plus hydrodynamic and debris impact (Load Case 2). Associated with these load cases are the following pressure distributions: hydrostatic, hydrodynamic, and surge. The debris impact was considered as a point load acting at the water surface. An illustration of these forces is shown in Figure 5-26. In many cases found in the reviewed literature, the hydrostatic load was not considered since it was assumed that there was no imbalance of hydrostatic force acting on the element being considered. For this pier system, the space enclosed by the plates was assumed to remain dry, necessitating the consideration of hydrostatic pressure. The hydrodynamic pressure was assumed to only act on the upstream side of the pier. Likewise, the surge pressure

distribution was assumed to act on the upstream plates. Note that suction on the transverse plates and on the downstream longitudinal plate was not considered for the purpose of this research.

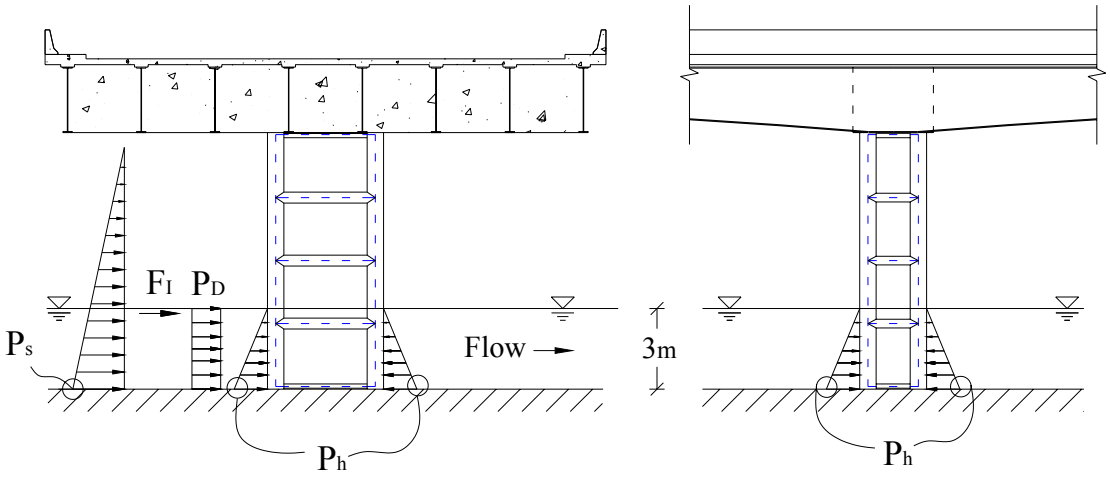

Figure 5-26 Hydraulic Load Distributions

For a design stillwater depth of 3m, the design velocity was calculated as 10.8m/s, the maximum hydrostatic pressure, P_h, was computed as 29.4 kPa, the hydrodynamic pressure, P_D, as 117.6 kPa (assuming C_d=2), the peak surge pressure, P_s, as 88.2 kPa, and the impact force was computed as 61.5kN. Calculations of these pressures are provided in Appendix F. For the linear pressure distributions shown in Figure 5-26 (i.e. hydrostatic and surge), equivalent uniform pressures were computed for each plate and were taken as being equal to the average pressure acting on the plates. Having an equivalent uniform pressure distribution makes possible the use of the simplified plate analysis introduced in Section 5.5.1. The equivalent uniform pressures calculated for each plate, for Load Cases 1 and 2 are listed in Table 5-2, where the plates are numbered with 1 for the bottom plates and 4 for the top plates.

Table 5-2 Equivalent Uniform Pressure Acting on Plates

	Plate	Load Case 1	Load Case 2
Longitudinal Plates (Upstream)	4	9.7 kPa (1.4 psi)	-
	3	30.8 kPa (4.47 psi)	-
	2	53.9 kPa (7.82 psi)	-
	1	77.2 kPa (11.2 psi)	132.4 kPa (19.21 psi)
Longitudinal Plate (Downstream)	1	-	14.7 kPa (2.13 psi)
Transverse Plates	1	-	14.7 kPa (2.13 psi)

5.5.2.2 Load Representation on Pier

For the purpose of this simplified analysis, the boundary frame from the SAP2000 seismic analysis was considered without the plates since their contribution in resisting the demands of this hazard is unknown, and was subjected to the loads described in Section 5.5.2.1. Additionally, gravity loads from the pier cap and superstructure were considered for this hazard and were applied as shown in Figure 5-11(a). The impact load was applied to the same VBE and in the same direction as scenario (a) in Figure 5-18. The plates that are loaded by water pressure were replaced by the corresponding edge reactions. This essentially decouples the analyses of the plates and frame.

For the equivalent uniform pressures provided in Table 5-2, the edge reactions resulting from the deformed plates, obtained by the simplified analysis method described in Section 5.5.1 (using the expected yield strength of the plates), were applied to the boundary frame. Additionally, for conservatism, there was an allowance made for pressure acting on half the projected width of the VBEs. Calculations are included in Appendix F. This is schematically shown in Figure 5-27 and Figure 5-28 respectively for Load Cases 1 and 2. The numbers provided in these figures are in reference to the loads calculated in Appendix F. There, the edge reactions for the two load cases are provided.

The pressure load representation for Load Case 1 is illustrated in Figure 5-27, where each of the plates is replaced with the edge reactions that they produce from being loaded. For clarity, the "pull-in" forces acting along the horizontal edges of the plates are shown for a typical plate by the figure to the right. Referencing Appendix F, the numbers 14 and 15 are the edge reactions for the bottom plate, 16 and 17 are the reactions for the plate above that, and so on. The net vertical reaction being transferred to the HBEs is anticipated to be small since plates on both side of the tubes act to cancel each other out.

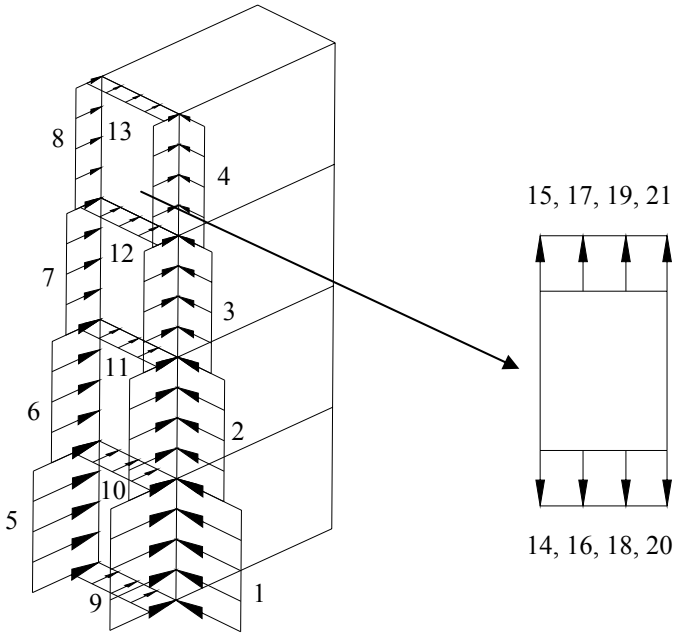

Figure 5-27 Load Case 1 Pressure Representation

Figure 5-28 illustrates how the pressure loading for Load Case 2 was assumed to transfer from the plates to the boundary frame. Figure 5-28(a) shows the transverse plate and downstream longitudinal plate edge reactions from hydrostatic pressure loading, Figure 5-28(b) shows the upstream longitudinal plate edge reactions from combined hydrostatic and hydrodynamic pressure, and Figure 5-28(c) shows the combination of (a) and (b). For Load Case 2, only the bottom plates experience significant pressure loading (as shown in Figure 5-26), and the plates above are unloaded. To account for the presence of these plates, however, the pull-in edge reactions acting along the HBEs will be assumed to transfer directly to the top of the pier, which is shown by the vertical arrows pointing to where the loads will be assumed to act. It is realized that the actual load transfer is more complex; however, assuming this load transfer conservatively subjects the entire VBE to this "pull-in" effect by applying the load to the top of the VBEs as shown by the arrows. Realistically, the HBEs will resist a portion of the pull-in and some of the load will be transferred to the VBE through the plate. Further insight regarding this issue can be obtained with finite element analyses, which will be used next chapter.

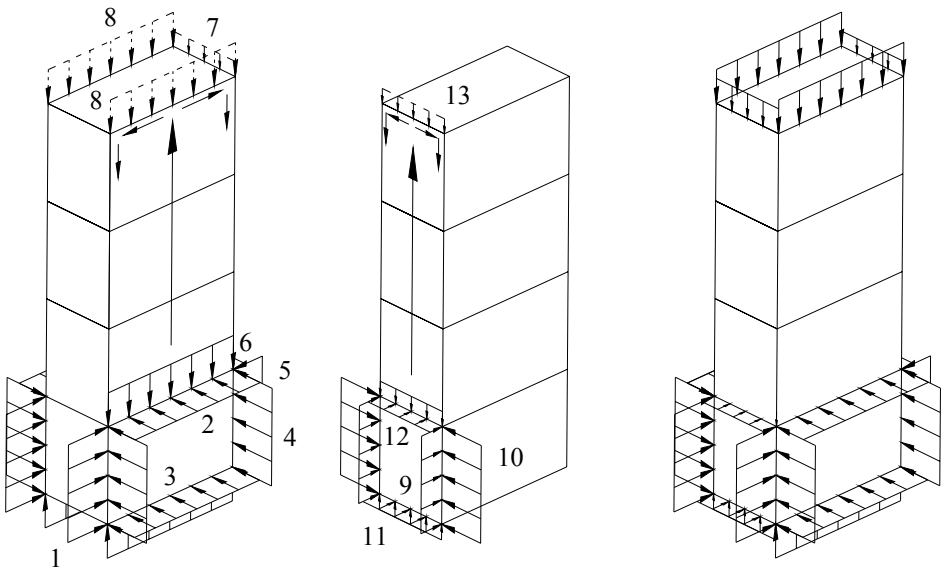

Figure 5-28 Load Case 2 Representation: (a) Hydrostatic Pressure; (b) Hydrodynamic and Hydrostatic, and; (c) Combination of Edge Reactions

5.5.2.3 SAP2000 Analysis

As was done for the other hazards being considered, for the SAP2000 analyses, attention was paid to the boundary conditions at the top of the pier. For the tsunami hazard, the pier's top was assigned the same constraints that were used for the seismic hazard, allowing for overturning of the pier's top about the longitudinal axis of the bridge.

Figure 5-29 shows the resulting defected shapes obtained from a linear static SAP2000 analysis for both load cases, respectively scaled by factors of 90 and 300. The transverse displacements at the top of the pier are approximately 9mm and 1.3mm for Load Cases 1 and 2 respectively. Load Case 1 produces more global effects on the pier, as expected from front face loading, whereas Load Case 2 shows concentrated effects on the structure around the submerged base of the pier where water is flowing.

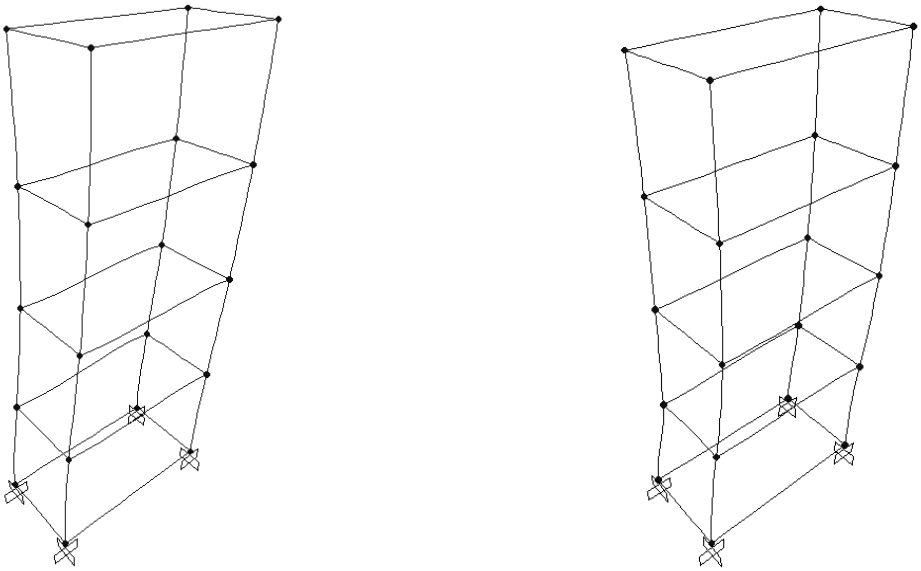

(a) **(b)**

Figure 5-29 Deformed Shape of Pier for Two Load Cases: (a) Load Case 1: Surge and Impact, and; (b) Load Case 2: Drag, Hydrostatic, and Impact

Following the analysis of the frame for both load cases, internal forces were checked with the interaction equation derived for full yielding of a cross-section (Section 5.2.2). It was found that none of the HBEs or VBEs developed plastic hinges and, with the exception of the plates, the proposed pier system remained elastic. This was in agreement with the intended behavior for this hazard whereas the plates were meant to be sacrificial elements while the boundary frame was meant to remain intact. The effect of the debris impact load is not visible from these deflected shapes.

5.5.3 Summary of Simplified Tsunami Analysis

For tsunami-induced hydraulic pressures, the plates subjected to transverse pressures were modeled using a simplified analysis, and the resulting edge reactions were used in place of the plates in the SAP model of the pier. In this uncoupled analysis, behavior of the unloaded plates on global system performance was conservatively neglected. During the surge, the SAP model shows the pier to displace as a frame in the direction of flow. At this time, it is unknown if some form of tension field action (as seen with seismic loading) would develop in the transverse plates to offer added resistance for the system.

The results from simplified analysis provided preliminary insight into the system's behavior for the tsunami hazard, and showed satisfactory performance. Further investigation in the next chapter will allow consideration of the coupled system and will determine if global performance differs from that observed here.

5.6 Blast

Simplified analysis of the proposed pier concept is next described for the blast hazard. The simplified method of analysis used for analysis of out-of-plane loading for the tsunami hazard is built upon to obtain a preliminary understanding of the blast resistance of the plates. This concept is discussed in Section 5.6.1. Section 5.6.2 provides a discussion of the pier's potential for resisting blast loads. Here, some concerns and observations regarding its ability to resist blast pressures are highlighted.

5.6.1 Plate Analysis for Out-of-Plane Impulse Loading

The dynamic behavior of a relatively complex system subjected to impulse loading can be obtained by transforming the system into an equivalent SDOF such that the displacement of the equivalent SDOF represents the displacement of a particular point on the actual structure (Biggs 1964). Such a point, for instance, could be at a plate's center. Transformation factors are used to transform the properties of the actual structure (i.e. mass, stiffness, and load) into equivalent properties for use in the SDOF idealization. Through the use of these factors, Biggs introduced a "load-mass" factor, allowing an equation of motion to be written by only modifying the total mass of the actual system, as is shown by (5-9), where damping is typically neglected for short duration loading.

$$K_{LM} M\ddot{u}(t) + ku(t) = P(t) \tag{5-9}$$

In this equation, M is the total mass of the actual system, k is the stiffness of the actual system for the corresponding load being considered, and $P(t)$ is the total load acting on the system (for distributed loads this is the corresponding resultant).

The load-mass factor, K_{LM}, depends on the deflected shape corresponding to the particular load distribution being considered, and on the mode of structural deformation, which depends on elastic or inelastic behavior. Biggs provided values for two-way elements, including slabs with simple supports along each edge and for slabs with fixed edges. For both cases, a uniform load is assumed to cause the deflected shape being considered. As discussed in Section 5.5.1, which described the simplified plate analysis being used for this research, the deformed shape of the plate (for any range of behavior) is approximated with a specified number of parabolas spanning each direction. This would resemble the elastic deformed shape of the two-way elements with pinned edges provided by Biggs. Table 5-3 shows the load-mass factors provided by Biggs for such a slab subjected to uniform loading as a function of the slab aspect ratio, H/L, or L/H, where H is the slab height and L is its width. These load-mass factors are used later to describe the impulse that can be resisted by a steel plate. Note that the transformation factors that Biggs considers for slabs behaving in the plastic range are based on deformed shapes obtained from yield line analysis in which the segments between the yield lines are assumed to be planar, which does not correspond to the deflected shape assumed for the plates considered in this study.

Table 5-3 Load-Mass Factors for Elastic Behavior (Adapted from Biggs (1964))

H/L	L/H	K_{LM}
1.0	1.0	0.68
0.9	1.1	0.70
0.8	1.3	0.71
0.7	1.4	0.73
0.6	1.7	0.74
0.5	2.0	0.75

To calculate the response of plates, following principles used by Fujikura et al. (2007), it was assumed that the kinetic energy imparted to the plate by a blast's impulsive loading was absorbed by the plate as internal work. Given that the duration of a blast load is short compared to the natural period of the component being considered, the impulse imparts an initial velocity to the component. Consider the system described by (5-9). For load durations much shorter than the natural period, the maximum deformation is controlled by the pulse area, I, or the area under

the loading curve P(t) (Chopra 2001). The displacement response of the system that is subjected to such an impulsive loading is given by (5-10).

$$u(t) = I\left(\frac{1}{K_{LM} M \omega_n} \sin \omega_n t\right) \tag{5-10}$$

By taking the derivative of this expression with respect to time one obtains the corresponding velocity of the system by (5-11).

$$\dot{u}(t) = \frac{I}{K_{LM} M} \cos \omega_n t \tag{5-11}$$

From this expression, the initial velocity imparted to the system is $\dot{u}_o = I/\left(K_{LM} M\right)$. Using this relationship, one can obtain the kinetic energy imparted to the system by (5-12), where I is the area under the resultant load curve, and M is the total mass of the system.

$$KE = \frac{1}{2} m v^2 = \frac{1}{2} K_{LM} M \left(\frac{I}{K_{LM} M}\right)^2 = \frac{I^2}{2 K_{LM} M} \tag{5-12}$$

This kinetic energy must be absorbed as internal work of the component being considered as it deforms; i.e. $KE = W_{\text{int}_{total}}$. The simplified plate analysis introduced in Section 5.5.1 is used to compute the internal work done.

The simplified analysis used for the blast hazard uses the deformed shape of each parabolic strip and its corresponding strain. Figure 5-30 schematically illustrates this strip segmentation, showing typical strips that span each direction of the plate, the assumed elastic-perfectly plastic material model for each strip, and the cross-section of a typical strip.

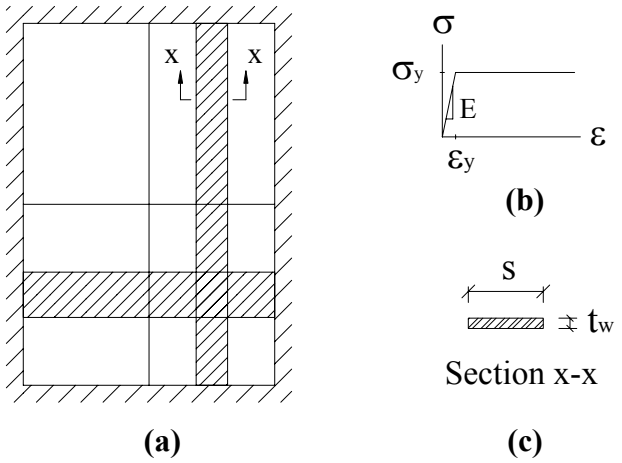

Figure 5-30 Plate Information for Simplified Blast Analysis: (a) Typical One-Way Strips; (b) Assumed Strip Material Behavior, and; (c) a Typical Strip Cross-Section

For an infinitesimal element in a typical strip behaving in the elastic range, the work done can be represented by (5-13). For the same infinitesimal element behaving plastically, the work done is given by (5-14).

$$dW = \frac{1}{2}\sigma\varepsilon dV \tag{5-13}$$

$$dW = \sigma_y \varepsilon_{plastic} dV \tag{5-14}$$

For a given center displacement of the plate, and thus a deformed shape of the plate, the deformed shape of each strip is available. The corresponding constant stress and strain within the strip is used to calculate the internal work of each strip. For a strip that remains elastic, the work can be calculated by (5-15).

$$W_{\text{int}} = \int_V \frac{1}{2}\sigma\varepsilon dV = \frac{1}{2}E\varepsilon^2 t_w s L_{o\,strip} \tag{5-15}$$

If the strain in the strip is greater than the yield strain ($\varepsilon > \varepsilon_y$), the internal work can be computed by (5-16).

$$W_{\text{int}} = W_{elastic} + W_{plastic} = \frac{1}{2}E\varepsilon_y^2 t_w s L_{o_{strip}} + \int_V \sigma_y \varepsilon_{plastic} dV = \left(\frac{1}{2}E\varepsilon_y^2 + \sigma_y\left(\varepsilon - \varepsilon_y\right)\right) t_w s L_{o_{strip}} \tag{5-16}$$

For a given deformed shape of the plate, the internal work of the strips spanning each direction can be computed using the appropriate equations. The sum of internal work for each strip gives the total internal work of the plate. The load impulse necessary to obtain the specified displacement can be computed using (5-17). Dividing this by the plate's area gives the pressure impulse of the blast pressure distribution.

$$I = \sqrt{2K_{LM}MW_{\text{int}_{total}}} \tag{5-17}$$

The idealized loading used in this preliminary study neglects the negative phase of loading and approximates the positive phase of loading with a linear distribution as shown in Figure 5-31, where P(t) is the resultant of the pressure distribution applied to the plate.

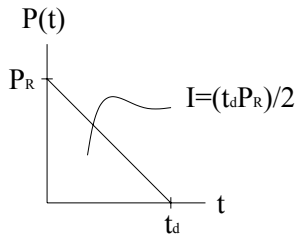

Figure 5-31 Idealized Blast Loading History

5.6.2 Simplified Blast Analysis

5.6.2.1 Plate Analysis

The method described in Section 5.6.1 was used to investigate the effects of blast loads on the plates chosen for the proposed pier concept. The public domain software A.T.-Blast was used to obtain blast load parameters used for this preliminary analysis. The bottom transverse plate and the bottom longitudinal plate were subjected to a blast load equivalent to W of TNT at a standoff of X[1]. This threat results in a peak reflective pressure of 29.2MPa (4228 psi), a reflective impulse of 9.7MPa-msec (1407 psi-msec), and a load duration of 0.67 msec. The height of the charge was assumed to be located at the mid-height of the plates and the pressure history at their center was conservatively assumed to be the same over their area. To account for strain rate

[1] The charge weight and standoff, represented by W and X, respectively, have been omitted in the body of this report, and were included in a special Appendix made available to selected individuals.

effects in the analyses, the expected yield strength of the plates was multiplied by a dynamic increase factor (DIF) of 1.2 (Mays and Smith 1995).

After performing analyses of the plates, it was found that their capacity to resist blast loads was relatively small. Table 5-4 summarizes the results of the study, in which the maximum plate energy dissipation, obtained by limiting the strain of the strip spanning the short side of the plates to 20%, was converted into the impulse capacity.

Table 5-4 Investigation of Plates Subjected to Blast Loading

Plate	Dimensions mm (in)	Center Displacement mm (in)	Impulse Capacity MPa-msec (psi-msec)	Impulse Demand MPa-msec (psi-msec)	C/D
Transverse	3708 x 2343.7 (146 x 92.27)	693 (27.3)	1.3 (192)	9.7 (1407)	0.13
Longitudinal	1880 x 2343.7 (74 x 92.27)	556 (21.9)	2.8 (408)	9.7 (1407)	0.29

For strains in the plates as large as those considered, the impulse capacity was less than 30% of the demand (C/D < 0.30). This shows that the energy dissipation capacity of the plates is small relative to the demand considered. While assuming the same pressure history over the entire plate is quite conservative, the above results provide a sense that the plates are likely to have little resistance to blast and would be best considered as sacrificial.

It should be noted that strain hardening was not considered in this plate analysis, nor was capacity of the connections. It is unknown how to design connections to resist the extreme strains that could develop at the edges of the plate during the blast. Nonetheless, for conservatism, the VBEs were analyzed assuming they would be subjected to the forces that develop during yielding of the plates. This is investigated in the following section. Note that since the HBEs are not critical members for the gravity resisting system, beyond the fact that they provide some lateral bracing to the VBEs, their performance under blast loading is not investigated here.

5.6.2.2 Effect of Plate Yielding on the VBEs

The worst blast loading scenario considered here for the analysis of a typical first-story VBE happens when both longitudinal and transverse plates yield simultaneously, as is schematically shown in Figure 5-32(a). This figure represents a section through the proposed pier system between HBEs. If the plates have the capability to deform as shown in Figure 5-32(a), both the longitudinal and transverse plates could end-up pulling in the same direction (Figure 5-32(b)). Accounting for the expected yield strength and the dynamic increase factor of the plates, the demand to consider on a typical VBE could be represented by a distributed load summing the forces acting on that VBE. Imposing this load on a typical VBE of the system, and treating the junction where the HBEs frame into the VBE as a fixed support, the resulting system to analyze could be idealized as shown in Figure 5-32(c), with the resulting moment diagram as shown in Figure 5-32(d).

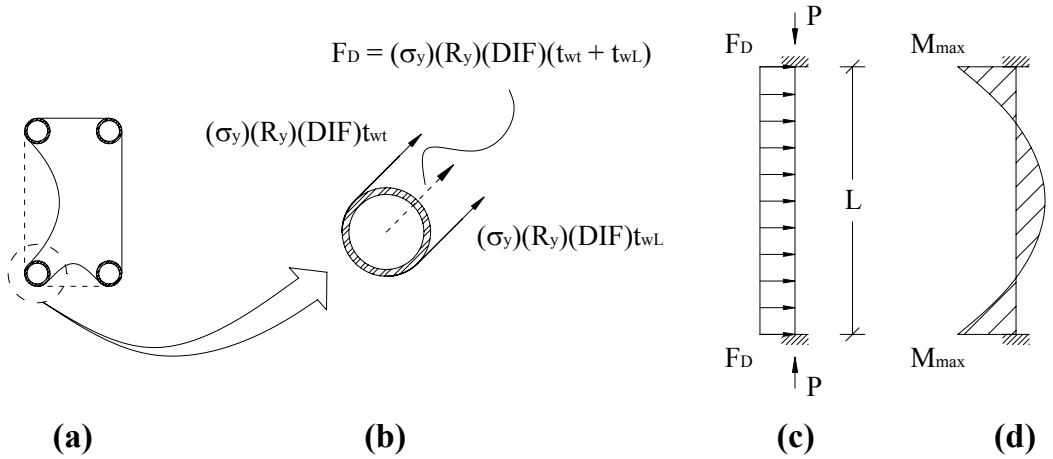

Figure 5-32 Blast Scenario Showing (a) a Section Through the Pier; (b) a FBD at a Typical VBE; (c) Load Distribution on a Typical VBE, and; (d) Moment Diagram for a Typical VBE

To keep the VBEs elastic, the moment at the fixed ends, $M_{\max} = F_D L^2 / 12$, should be less than the plastic moment of the VBE, reduced to account for axial loads. As a result, the maximum distributed load that can be applied to the VBE is:

$$F_{D\max} = \frac{12 M_{pr}}{L^2} \tag{5-18}$$

where M_{pr} is the reduced moment capacity of the section calculated according to (5-19), which is derived from the plastic interaction equation established in Section 5.2.2. Given that the loading is impulsive, the yield strength can be increased by a dynamic increase factor when calculating M_p.

$$M_{pr} = M_p \left[\sin\left(\frac{\pi}{2}\left(1 - \frac{P}{P_y} \right) \right) \right] \tag{5-19}$$

For the VBE size established in Section 5.3.4, a member length, L, of 2344mm (92.27 in), and an axial dead load from the superstructure and pier cap (P = P_{dead} = 3020kN (679 kips)), the reduced plastic moment capacity of the section is $M_{pr} = 0.98M_p$ = 4989 kN-m (44152 kip-in). From (5-18), the maximum allowable distributed load that can be imposed on this VBE such that no hinging develops is 10.9 kN/mm (62 kip/in). However, considering shear capacity at the VBE's supports, calculated per AISC (2005b) as $V_n = (0.6\sigma_y)A_g/2$ where A_g is the VBE's gross cross-sectional area, the maximum strength of the VBE is limited by a distributed load of 7.25kN/mm (41 kip/in).

Note that from Figure 5-32(b), which represents a worst case scenario for a typical VBE, the applied distributed load from two plates yielding is 1.84 kN/mm (10.5 kip/in). This is approximately 25% of the maximum strength calculated above. This suggests that the VBEs would be sufficiently strong to resist the loads imposed by the transverse and longitudinal yielding plates, noting that the effect of blast pressures applied simultaneously to the VBE was not considered in this analysis. Effects of blast loads directly applied to the VBEs are considered in the next section.

5.6.2.3 Blast Effects on the VBEs

Section 5.6.2.1 suggested that the plates could be sacrificial for blast loads, and Section 5.6.2.2 showed that the VBEs have sufficient strength to resist the pull-in from the yielding plates, conservatively applied as a statically distributed force. This section investigates the resistance of the VBEs themselves to direct blast loads. The same idealized SDOF concept used in Section 5.6.1 for analyzing the plates is used for analyzing the VBEs. More specifically, the response of

a typical VBE's midpoint (Figure 5-33) is represented with an equivalent SDOF system. In this figure, p(t) is the pressure history and P(t) was defined in Section 5.6.1. The response of this SDOF system is governed by (5-9).

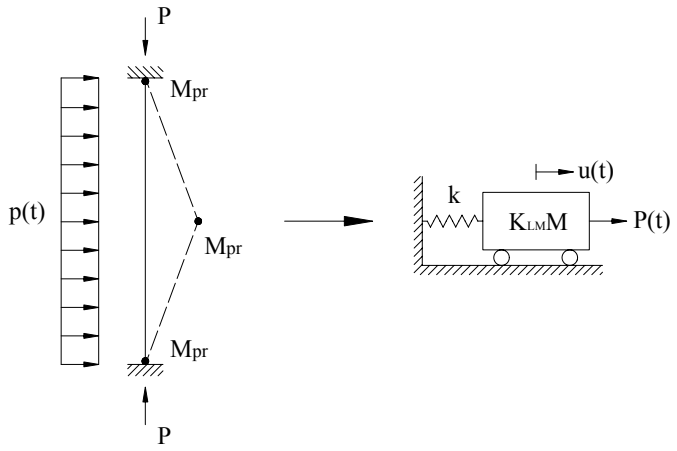

Figure 5-33 Reduction of a VBE to an SDOF for Blast Analysis

The plots in Figure 5-34(a) and (b), respectively, provide a convenient way of obtaining an SDOF's ductility, and time of maximum displacement for a triangular load history, given information such as the ratio of load duration to the SDOF's period (t_d/T), and the ratio of the SDOF's maximum resistance to the peak load applied (R_m/F_1), where the idealized SDOF's period can be obtained by $T = 2\pi\sqrt{K_{LM}M/k}$.

For this analysis, the system will be assumed to remain elastic. Therefore the system's maximum resistance is determined by $R_m = 12M_{pr}/L$, and K_{LM} is chosen to be 0.77, as specified by Biggs (1964) for elastic behavior of a uniformly loaded fixed-fixed member. The reduced moment capacity, M_{pr} was computed per (5-19), where M_p was increased by a DIF to account for strain rate effects. Assuming the blast pressure loading to be the same over the height of the VBE, and assuming a pressure reduction factor of 0.45 (Fujikura et al. 2007) to account for the circular shape of the VBE, the peak load was computed as $F_1 = 0.45p_rD_oL$, where p_r is the peak reflected pressure. Also, assuming elastic behavior, the stiffness is provided by (5-20).

$$k = \frac{384EI}{L^3} \tag{5-20}$$

Assuming a VBE height of 2344mm (92.27 in), the natural period, T, was computed as 1.53msec and the duration, t_d, was provided in Section 5.6.2.1. The resulting t_d/T ratio is 0.44. The maximum resistance was computed as 25 542kN (5742 kip) and F_1 was computed as 18 740kN (4213 kip), resulting in an R_m/F_1 ratio of 1.36. Entering the chart in Figure 5-34(a), the ductility of the VBE was determined as 0.8. Therefore, the flexural strength is adequate since no plastic hinges develop, resulting in the VBE remaining elastic, as assumed.

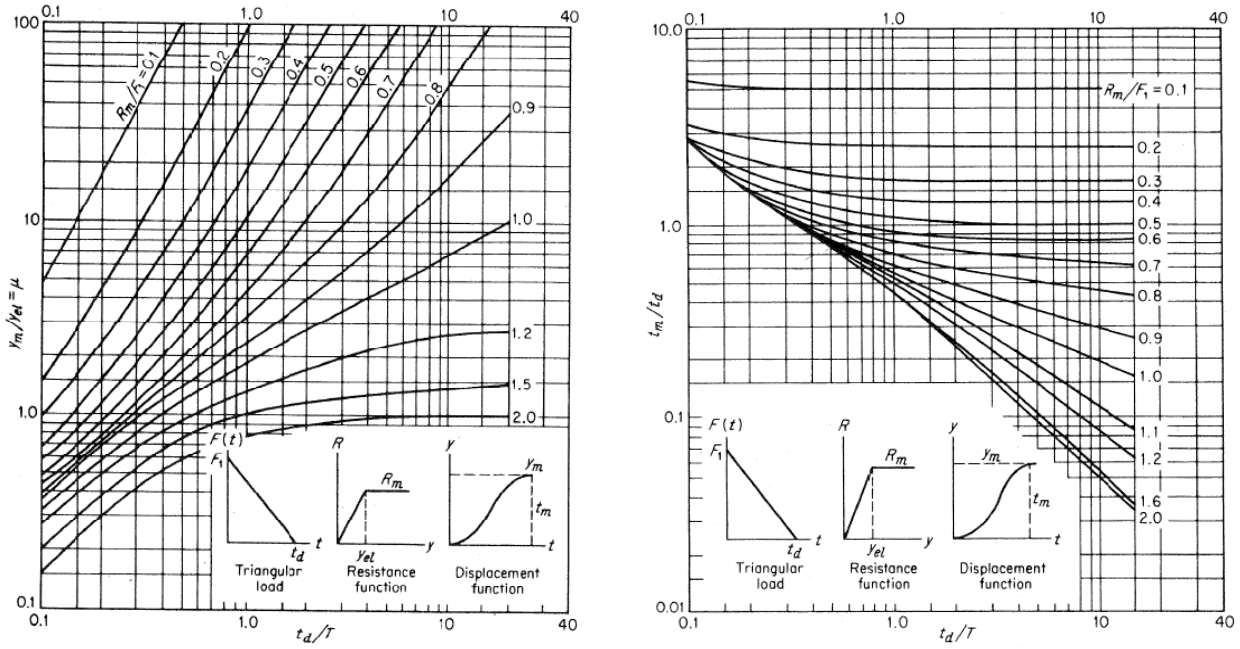

Figure 5-34 SDOF Response Charts (Biggs 1964)

The maximum displacement at the center of the VBE was computed to be 1.1mm (0.042 in) occurring approximately 0.54 msec (from Figure 5-34(b)) after the initial load application. The resistance corresponding to this displacement ($R = k*u_{max}$) was estimated as 20 435kN (4594 kip), and load, F, acting on the VBE at the time of maximum displacement was 3750kN (843 kip). Assuming the maximum dynamic reaction (i.e. maximum shear) to occur at the time of maximum displacement, the maximum shear demand at the supports of the VBE was determined by $V = 0.36R + 0.14F$ (Biggs 1964), resulting in a value of approximately 7882kN (1772 kip). Using the relationship for shear capacity introduced in Section 5.6.2.2, and a DIF of 1.2, the shear capacity of the VBE was determined as 8496kN (1910 kip). Therefore, the shear capacity of the VBE is adequate.

5.6.3 Summary of Simplified Blast Analysis

Although the bare VBE was shown through approximate analysis, and the conservative assumption of uniformly distributed pressure, to have adequate resistance to blast pressures, note that this analysis did not consider the effect of plates being loaded at the same time as the VBE. Also, although analysis showed flexural ductility demands to be relatively low, the shear demand was high in comparison, and governed response.

The simplified analyses presented here provided a basic understanding of the capacity of the system against the blast hazard where a uniform pressure distribution was conservatively assumed. The plates were found to have little resistance to realistic blast loads, and were therefore considered to be sacrificial. The VBEs were found able to resist the pull-in forces from the yielding plates deformed such as to even pull together in the same direction (as a worst case scenario). This was expected since the VBEs were originally designed to resist the forces from plate yielding. Additionally, the VBEs were shown to have adequate capacity against direct blast pressure, assuming no plates were attached. Interaction between the plates and the exposed surface of the VBE being simultaneously loaded should be investigated further to determine the impact on VBE demands. Analyses revealed that shear demands may govern over flexure demands.

As with all hazards, the demands on the system depend on the magnitude of the event (i.e. charge size and standoff distance in the case of blast loading). The intent of the simplified analysis was not to validate the system's adequacy against general blast hazards, but rather to highlight some important aspects that should be considered when analyzing demands on the pier for blast loads. Building on this simplified analysis that considered individual components of the entire system, the global response of the structure to the blast hazard will be investigated in the next chapter.

CHAPTER 6

FINITE ELEMENT ANALYSIS

6.1 General

Chapter 5 established and investigated a design for the proposed pier system conceived in Chapter 4, which considered demands of multiple hazards from the onset of the design process. For the investigation in Chapter 5, simplifications were made to gain a preliminary understanding of the system's behavior to the multiple hazards being considered. This chapter further investigates the behavior of the system to gain a better understanding of how the system resists multiple hazards.

In Section 6.2, a description of how the finite element model was developed for the seismic hazard is provided. This model is then altered, if necessary, according to the needs of the other hazards, as described in their respective sections. Section 6.2 also provides the results obtained from the finite element model for the seismic hazard and compares them with those expected from the simplified seismic analysis using SAP2000. Section 6.3 investigates the pier's behavior when subjected to the vehicle collision hazard, and Section 6.4 explains the modeling of the tsunami hazard and describes the resulting behavior of the system. Section 6.5 explains the modeling of the blast hazard and provides observations of the resulting behavior.

6.2 Earthquake

This section describes the assembly of the finite element model that was used to further investigate the trends in behavior of the system when subjected to multiple hazards. Sections 6.2.1 through 6.2.8 describe how the finite element model was assembled, and Section 6.2.9 presents the results of the analysis, and compares the results to those expected from the simplified analysis. Section 6.2.10 offers several observations of the pier's seismic resistance.

6.2.1 Part Definitions

The graphical interface program ABAQUS/CAE (v6.5-1) was used to build the finite element model of the pier, and ABAQUS/Standard (v6.5-1) was used to analyze the model. Each of the structure's components (longitudinal HBEs, transverse HBEs, VBEs, transverse plates, and longitudinal plates) were first created as deformable shell "parts". The VBEs and HBEs were modeled as having diameters equal to the mid-thickness of the actual members. The VBEs were assigned a diameter of 563.6mm (22.188 in), the longitudinal HBEs a diameter of 311.2mm (12.25 in), and the transverse HBEs a diameter of 385mm (15.157 in). The VBEs were 9.37m (369.08 in) in length, the transverse HBEs were 3.71m (146 in), and the longitudinal HBEs were 1.88m (74 in). To achieve the connection between the HBEs and the VBEs, the ends of the HBE parts were cut to match the shape of the VBEs. Figure 6-1 schematically shows how this was accomplished, where L_{HBE} is the length of the HBE and D_{HBE} is the diameter of the HBE. One can think of this figure as showing a plan view of one side of the pier with the VBEs used as cutting profiles. The resulting shape of the HBE part is outlined.

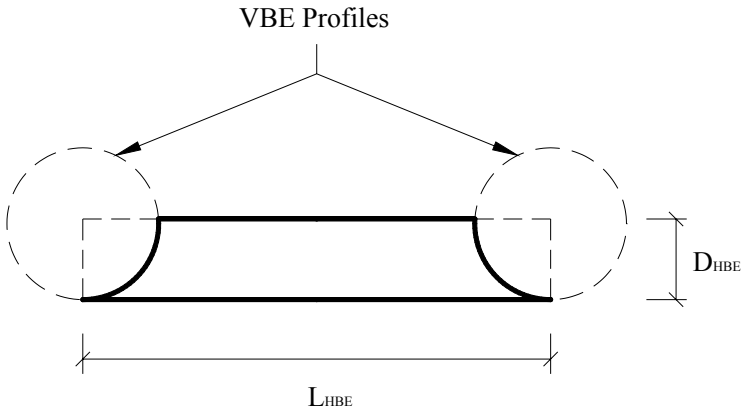

Figure 6-1 Cutting Plane for HBEs

The dimensions of the transverse plates were 3.71m (146 in) x 9.37m (369.08 in), and of the longitudinal plates were 1.88m (74 in) x 9.37m (369.08 in). Each of these parts was assigned section thicknesses equal to that of the actual elements, as defined in Section 5.3.4.

One additional part, chosen to be a plate, was created to model the pier cap boundary at the top of the pier. This part was created as a deformable solid part, and was arbitrarily assigned a

thickness of 25.4mm (1in). The plate's plan dimensions were 2.44m (96.188 in) x 4.27m (168.188 in).

6.2.2 Material Definition

For the purpose of this research, which is to establish trends in behavior of the pier system being developed, elastic-perfectly plastic nominal stress-strain material behavior was assumed for each material used (A36 (σ_y = 248MPa (36ksi)) and A500 Gr. B (σ_y = 290MPa (42ksi))). For calculating element behavior, however, ABAQUS/Standard uses "true" stress (Cauchy stress) and logarithmic strain, σ_{true} and $\varepsilon_{\ln}^{pl}$, respectively (HKS 2002). Therefore, the assumed elastic-perfectly plastic nominal stress-strain data for a uniaxial test of isotropic material was converted into "true" stress and logarithmic strain by use of (6-1) and (6-2), where *E* is Young's modulus.

$$\sigma_{true} = \sigma_{nom}(1 + \varepsilon_{nom}) \tag{6-1}$$

$$\varepsilon_{\ln}^{pl} = \ln(1 + \varepsilon_{nom}) - \frac{\sigma_{true}}{E} \tag{6-2}$$

As described in Section 5.3.3, A500 Gr. B was used for all tubes of the boundary frame and A36 was used for the plates.

6.2.3 Part Assembly

Following part and material definitions, ABAQUS/CAE allows users to work with part instances (which can be thought of as representations of the original parts) in an assembly space where the part instances can be positioned as desired. Centerline-to-centerline dimensions were used to position each part instance. The VBEs were spaced 1.88m (74 in) from each other in the longitudinal direction and 3.71m (146 in) in the transverse direction. The HBEs were spaced vertically at 2.34m (92.27 in) on center. The transverse and longitudinal plates were positioned so that their vertical edges met tangentially with the VBEs. Also, the pier cap plate was positioned so that its bottom surface rested on top of the VBEs. Figure 6-2 shows the geometry of the final model. Figure 6-2(a) shows only the bare frame so that the placement of the HBEs can clearly be seen, and Figure 6-2(b) shows the model with plates included. Note that the pier cap plate was partitioned using the "Partition" option available in ABAQUS/CAE with lines

parallel to each edge, which cross at the centerline of the VBEs. This was done so that point loads representing the initial dead load could eventually be applied at the centerlines of the VBEs. Also, Figure 6-2(b) shows that the plates were partitioned at locations where they were to be attached to the HBEs. This was done to allow for a small cutout in the plate at the point where an HBE instance, a VBE and a plate meet to alleviate probable over constraints when tying the individual part instances together (as will be discussed in Section 6.2.4).

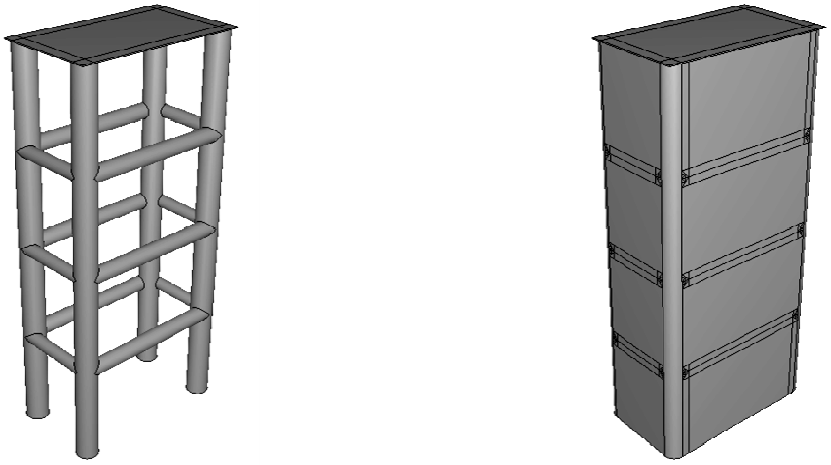

(a) **(b)**

Figure 6-2 Finite Element Pier Geometry: (a) without Plates, and; (b) with Plates

6.2.4 Constraints

To connect the HBEs and plates to the VBEs, the VBEs and plates to the pier cap plate, and the plates to the HBEs, the *Tie* constraint available in ABAQUS/CAE was used. The tie constraint allows two regions (one being a "slave" and one a "master") to have distinct meshes and to be effectively fused together (ABAQUS 2006).

To replicate the rigid boundary provided at the top of the pier in the actual structure by the pier cap, the *Rigid Body* constraint option available with ABAQUS/CAE was used. The option constrains regions in a model to the motion of a single reference point. The relative motion of all points within a selected region is held constant throughout an analysis (ABAQUS 2006). The pier cap plate defined in Section 6.2.1 was assigned a rigid body constraint with the reference point placed at its center of mass.

6.2.5 Boundary Conditions

To simulate the boundary condition at the pier's top, where rotation about an axis perpendicular to the bridge's longitudinal direction is restrained, a boundary condition that prohibited rotation about the bridge's transverse axis was placed on the reference point introduced in Section 6.2.4.

The base of the pier was assumed to be fixed. To simulate this boundary condition, the edges of each of the plates and VBEs located at the base of the pier were assigned boundary conditions in which all translations and rotations were restrained, namely the ABAQUS *Encastre* boundary condition.

6.2.6 Meshing

Meshing of the pier model was accomplished by meshing each part individually. The meshing technique used to mesh each part varied. The longitudinal plate, the transverse plate, and the pier cap plate used the "structured" meshing technique with the minimizing mesh transition algorithm option. The VBEs were meshed using the "swept" meshing technique, and the longitudinal and transverse HBEs were meshed using the "free" meshing technique with the medial axis algorithm. The structured meshing technique uses simple predefined mesh topologies in generating meshes. The swept meshing technique produces a mesh in two steps. First, ABAQUS/CAE creates a mesh on one side (the source side) of the region to be meshed. ABAQUS/CAE then copies the nodes of that mesh, one layer at a time, until the final (target) side is reached. In doing so, ABAQUS/CAE copies nodes along a sweep path. The free meshing technique does not use predefined mesh patterns like the structured meshing technique, and, therefore, allows more flexibility in meshing that the structured meshing technique (ABAQUS 2006).

Each of the parts, exclusive of the pier cap plate, was meshed with quadratic quadrilateral S8R elements. This is an 8-noded, doubly curved thick shell element with reduced integration. Each of the nodes has six active degrees of freedom: three translational (u_x, u_y, u_z) and three rotational (θ_x, θ_y, θ_z). The pier cap plate was meshed with quadratic, hexahedral C3D20R elements. The C3D20R element is a 20-node quadratic brick element with reduced integration.

Figure 6-3 shows the final meshed pier finite element model created using ABAQUS/CAE. The middle of the figure shows the complete model, and the section elevations to the left and right of it allow one to view the pier's inside. These figures also show how the plates are attached to the outside of the boundary frame, which would not be viewable by the public.

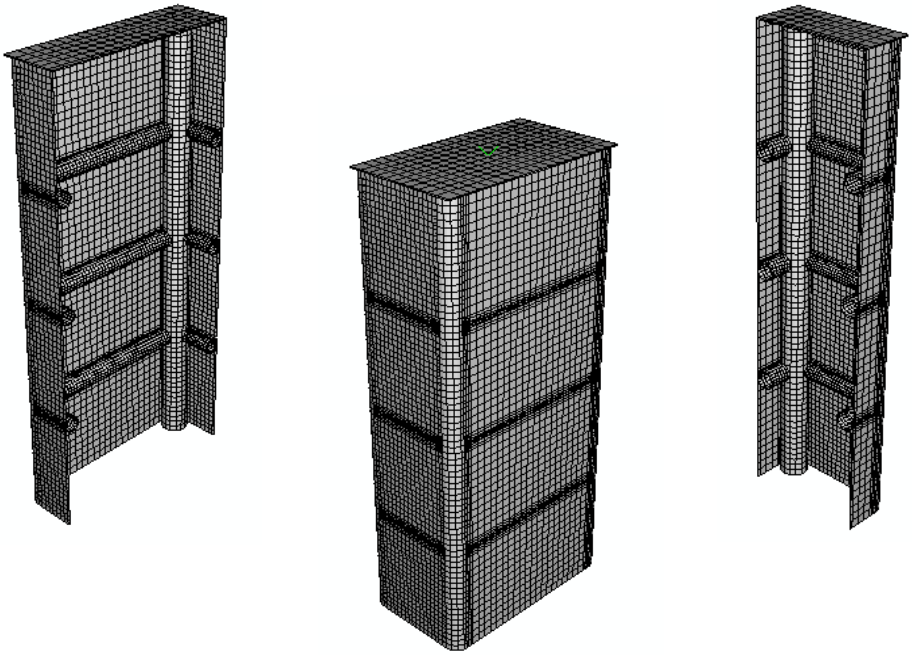

Figure 6-3 Final Meshed Pier Finite Element Model

6.2.7 Initial Imperfections

As discussed in Section 3.3.1, unstiffened SPSW infill plates buckle as they are loaded laterally. Therefore, the behavior of unstiffened SPSWs relies on their post-buckled state. Solutions to post-buckling problems, however, cannot be obtained directly due to a discontinuous response at the point of buckling. To obtain solutions to such problems, the model must be changed to ensure continuous behavior. This can be accomplished by introducing initial imperfections into the initially "perfect" model geometry (HKS2002).

One of the methods available for introducing imperfections is through a linear superposition of eigen-mode shapes, which can be obtained using an "Eigenvalue Buckling Prediction" analysis. The two methods available in ABAQUS/Standard for extracting buckling mode shapes are the

Lanczos method and the subspace iteration method; the Lanczos method being better for extracting a large number of buckling mode shapes (HKS2002).

As a result of the eigenvalues of the transverse and longitudinal plates being significantly separated due to the difference in their relative stiffness, it was difficult to obtain mode shapes using the subspace method for each of the sixteen plates of the pier. The Lanczos method worked well, however, and was used to obtain the structure's first 200 eigenmodes. Two such mode shapes are shown in Figure 6-4. The first mode obtained was in one of the top transverse plates, as shown in the left side of the figure. One of the mode shapes obtained for the longitudinal plates is shown in the right side of the figure.

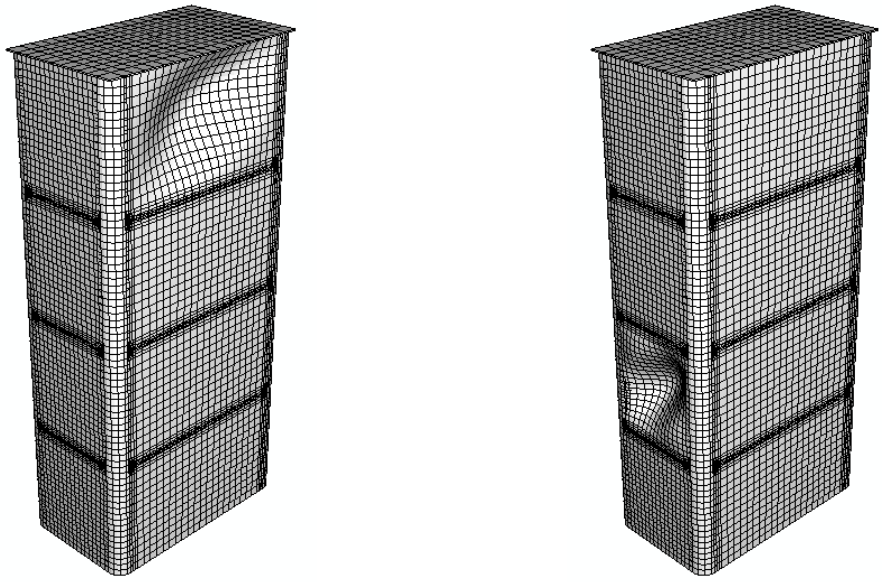

Figure 6-4 First Mode Shape for Transverse Plates and Longitudinal Plates

When introducing the initial imperfections into the model, the first two mode shapes of each of the eight transverse plates were used. A total of ten mode shapes were used for the longitudinal plates: the first two mode shapes for the bottom two plates on each side, and the first mode shape for plates on both sides located third from the bottom. The scale factor for the first mode shapes was taken as 5% of the corresponding plate's thickness and the second mode shape (where applicable) was taken as 80% of that.

6.2.8 Pushover Analysis

ABAQUS/Standard (v6.5-1) was used to analyze the model assembled in ABAQUS/CAE. As was done when analyzing and designing this pier system for the seismic hazard in Chapter 5 (Section 5.3), a bi-directional pushover was performed. The pushover was achieved in two steps. The first step applied dead load to the pier. This included the self-weight of the boundary elements (VBEs and HBEs), the weight of the bridge superstructure, and the weight of the pier cap. The self-weight of the HBEs and VBEs was applied using the ABAQUS *Gravity* load type. The weight of the superstructure and pier cap were applied to the pier cap at the nodes created by the partitioning described in Section 6.2.3 as concentrated loads having magnitudes identical to the point loads used in the SAP2000 model described in Section 5.3. These forces were applied statically to the structure and, following their application, held constant through the following lateral loading analysis step.

The second step was to laterally push the pier bi-directionally. This step was initially attempted by using the ABAQUS *Riks* method. This method can be used to predict the unstable and nonlinear collapse of structures. This method is applicable for cases in which the magnitudes of the loads applied to the structure are proportional and governed by a single scalar parameter (HKS2002). Therefore, this method would allow the application of the lateral force pushover pattern described in Section 5.3.3.5. However, in performing the lateral pushover of this model with this analysis method, there were difficulties in achieving convergence to a reasonable solution. Therefore, this method was dismissed and another approach was taken.

The alternate method used to complete the lateral pushover step included the use of a displacement controlled pushover. A statically imposed 203mm (8 in) displacement was applied simultaneously in the transverse and longitudinal direction at the reference point located within the pier cap plate. By using this approach to displace the pier laterally, the overturning couple resulting from the height of the reactive mass above the pier (Section 5.3.3.5) was neglected. For this pier concept, as opposed to the tall slender pier investigated in Section 4.3.5, the overturning couple was found to have an insignificant effect on the system's ultimate behavior when pushed bi-directionally. This was determined by comparing results obtained from the SAP2000 model used for the simplified analysis in Section 5.3 with and without the overturning couple.

6.2.9 Results

The first step of the two-step nonlinear static pushover was to apply dead load to the pier to simulate the presence of the bridge superstructure and the pier cap. The resulting deformed shape following the application of the dead load is shown in Figure 6-5, with a deformation scale factor set to 10 so that the deflected shape could be clearly seen. This figure shows the plates buckling; however, all elements remained elastic. Note that if the plates were attached to the boundary frame after the pier cap and superstructure were constructed, then this buckling of the plates would not occur.

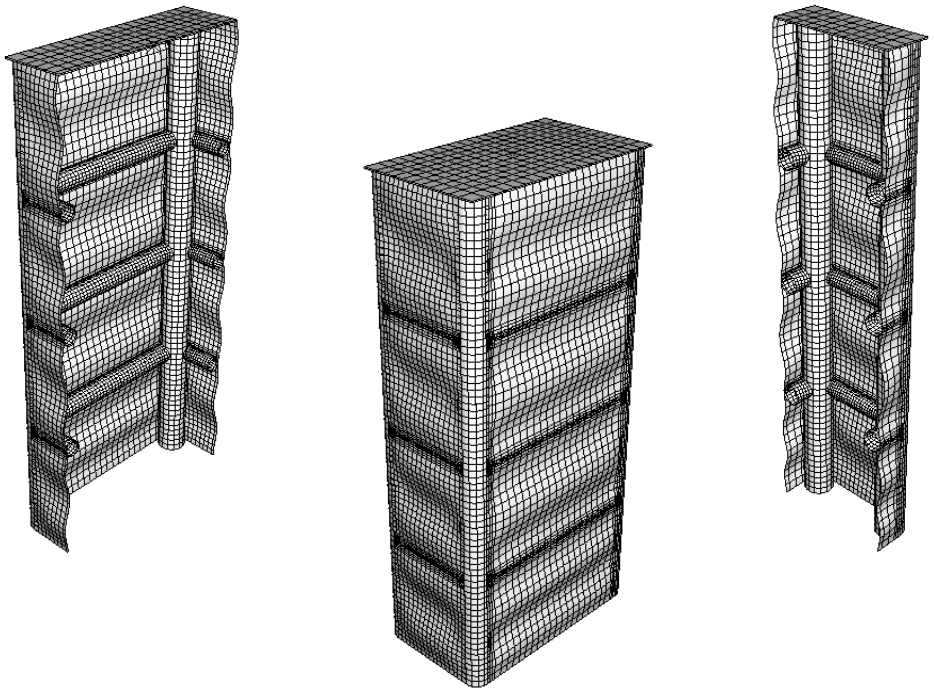

Figure 6-5 Deformed Shape Following Application of Dead Load (Deformation Scale Factor = 10)

The final state of the structure following the imposed lateral displacement at the pier's top is shown in Figure 6-6. This figure shows the final deformed shape of the pier system with a deformation scale factor set to unity. As expected, the plates buckle in compression and the lateral load is resisted by tension field action. Also note how plates parallel to each other on opposing sides of the pier box behave in an identical fashion.

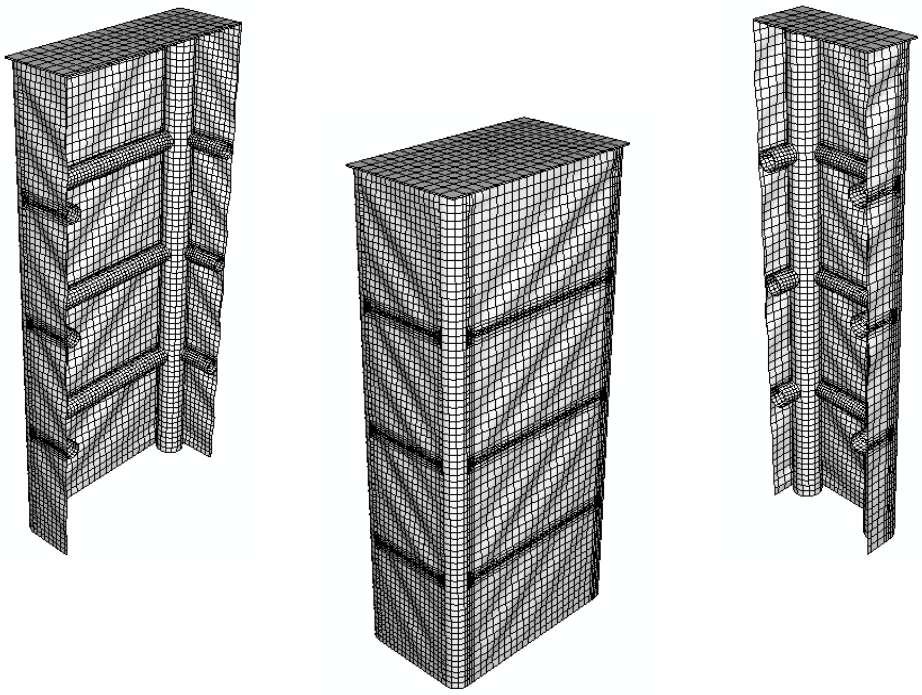

Figure 6-6 Deformed Shape Following Lateral Displacement (Deformation Scale Factor = 1)

In the simplified analysis and design of the system for the seismic hazard (Section 5.3), the pushover curves for each direction were obtained after performing the bi-directional pushover analysis. These curves are reproduced in Figure 6-7 where they are plotted against the pushover curves obtained from the ABAQUS analysis. Note that the simplified analysis initially assumed the hinges in the HBEs to be located at their ends, which would effectively locate them at the centerline of the VBEs. It was recognized, however, that the hinges would realistically form some distance from the VBE centerlines, which would result in a slightly greater ultimate capacity in each direction. Accordingly, Figure 6-7 also shows the results obtained from SAP2000 pushover analyses considering the hinges in the HBEs to be located at the face of the VBEs.

The pushover curves obtained from ABAQUS matched those obtained from SAP when the pier was behaving linearly. There was some slight difference, however, between the SAP model and the finite element model results with regards to the ultimate capacity in each direction. The ABAQUS model resulted in transverse and longitudinal ultimate base shears that were respectively greater than and less than that expected from results obtained with SAP.

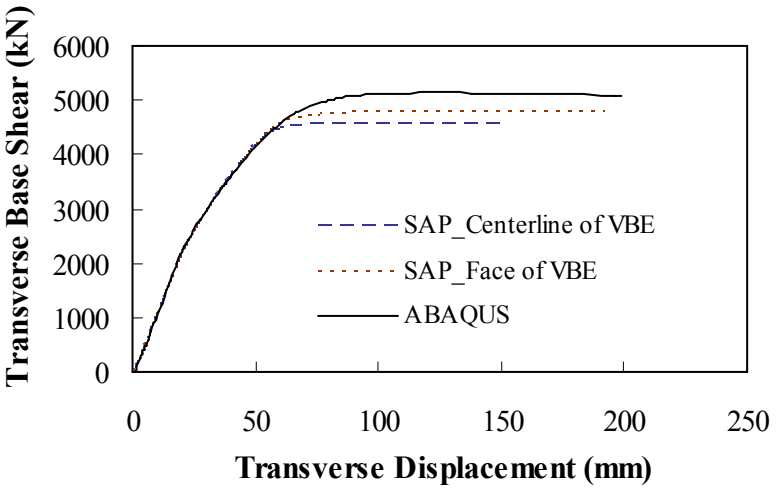

(a)

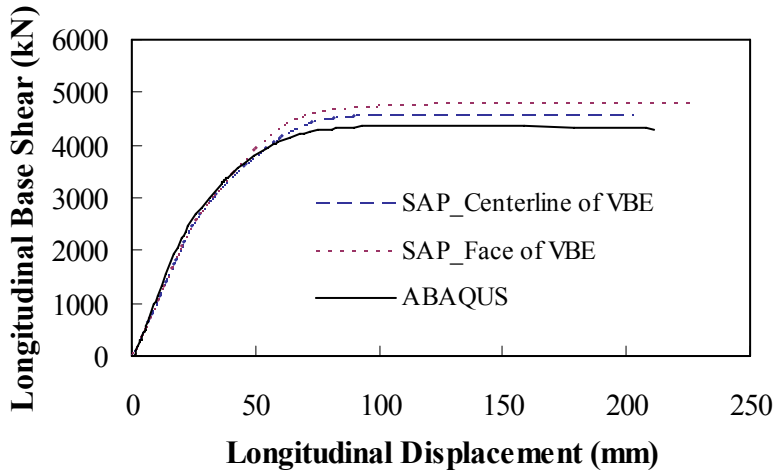

(b)

Figure 6-7 Pushover Curves: (a) Transverse Direction, and; (b) Longitudinal Direction

The discrepancy shown in these plots is likely a result of the methods used to perform the pushover analyses in SAP2000 and in ABAQUS. When the pier was pushed using SAP2000, a given lateral load pattern, chosen to be the same in both directions and applied together with an overturning couple, was incrementally applied until a specified displacement was reached. This type of analysis was necessary to account for overturning that would be caused by the height of the superstructure above the pier, a concern that was problematic for the earlier concept in Section 4.3.5, but of little consequence for the design being considered here. This is reflected in Figure 6-7 as the ultimate capacity reached in both directions by the SAP analysis is identical,

namely 4573kN (1028 kip) and 4786kN (1076 kip) respectively for the cases with hinges at the centerline and face of the VBEs. However, this approach of keeping orthogonal loads proportional throughout the nonlinear pushover analysis resulted in the structure being pushed more in the longitudinal direction than in the transverse direction following the onset of yielding in the pier.

As mentioned in Section 6.2.8, a similar analysis using ABAQUS could not be performed, and a displacement-based pushover, which imposed bi-directional displacements at the top of the pier was used instead, displacing it equally in the transverse and longitudinal direction. This is reflected in Figure 6-7 in that the ultimate strength in the transverse direction is greater (5142kN (1156 kip)) than that in the longitudinal direction (4373kN (983 kip)), which is reasonable since the HBEs in the transverse direction have a greater plastic section modulus than those in the longitudinal direction.

Figure 6-8 schematically illustrates the dissimilar behavior between the SAP and ABAQUS models. When behaving elastically, the SAP model was displaced in essentially the same direction as it was being forced. After reaching its ultimate capacity, however, the pier was being pushed in a direction that was approximately 36 degrees from the longitudinal axis, as opposed to the 45 degree direction of the load resultant. When the ABAQUS model was behaving elastically, the resultant base shear was in the same direction it was being displaced (approximately 45 degrees), but after reaching its ultimate capacity the resultant force became oriented at approximately 49 degrees from the longitudinal axis.

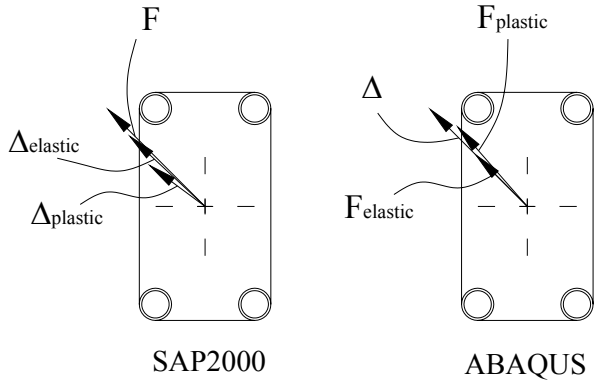

Figure 6-8 Pier Pushover Behavior

To reflect on the behavior of the pier, and being able to decouple issues related to the direction in which it is being pushed, the resultant behavior and strength of the system was considered. Figure 6-9 shows the resultant base shear versus the corresponding resultant displacement, obtained from the values plotted in the bi-directional curves shown in Figure 6-7. This figure shows that the ultimate behavior of the system obtained with the SAP2000 model agrees well with the behavior observed using the finite element model. Plots for the case assuming the hinges to be at the centerline of the VBEs was included for comparison with the more realistic case of placing the hinges at the face of the VBEs.

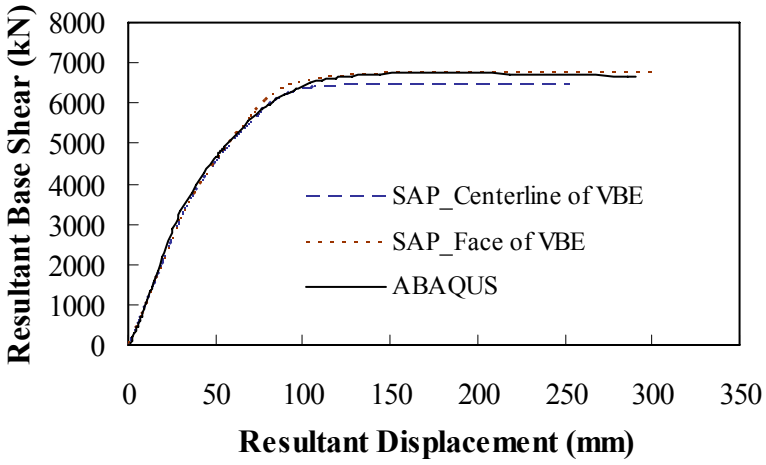

Figure 6-9 Resultant Pushover Curve

6.2.10 Summary of Observations

The behavior of the system resulting from the bi-directional pushover analysis conducted in ABAQUS resulted in transverse and longitudinal ultimate base shears that were respectively slightly greater than and less than those expected from results obtained with SAP. This is a result of the type of analysis used in each analysis. The SAP analysis was conducted by incrementally increasing a force pattern until a given displacement was reached, whereas the analysis in ABAQUS simultaneously imposed displacements in both directions. Overall, however, the analysis presented for the seismic hazard showed the pier to behave as expected based on the simplified analysis conducted in Chapter 5, and showed the pier to achieve the anticipated ultimate strength in terms of resultant behavior.

Note that the point at which these plots were terminated was arbitrary since all that was of interest for this research was the pier's fully yielded state. Therefore, determination of the system's maximum displacement capacity is unknown.

6.3 Vehicle Collision

This section investigates the behavior of the pier system subjected to the vehicle collision hazard. The model used in this investigation is the same as that used in investigating the seismic hazard, with the exception that the VBEs were assigned a slightly finer mesh as a result of partitioning that was necessary to accommodate the loading used. The constraints used to connect the model remained the same, but the boundary condition for the top of the pier changed as discussed in Section 6.3.1. As was done when analyzing the seismic hazard, initial imperfections were introduced into the plates to ensure they could buckle.

Application of the vehicle loading is discussed in Section 6.3.2. The dead load of the superstructure and pier cap were not included in this analysis, nor was self-weight of the boundary frame. This was deemed appropriate since the axial force in each of the VBEs was approximately 13% of the compressive yielding capacity. Moreover, neglecting this step in the analysis significantly reduced the total run time, and it was thought that the benefit of including it, in terms of the system's overall behavior, would be inconsequential. Section 6.3.3 provides results of the analysis and Section 6.3.4 provides a summary of observations related to this analysis.

6.3.1 Boundary Conditions

As mentioned in Section 5.4.1, the vehicle load is generated by an impact, which would likely have a duration sufficiently short so that the superstructure would not have enough time to globally respond. Therefore, all degrees of freedom at the top of the pier were considered fixed except for the vertical degree of freedom, to simulate the stationary superstructure. A released vertical degree of freedom was considered in the event that dead load was to be applied to the pier.

6.3.2 Analysis

The first attempt at loading the structure was made with the vehicle collision load as described in Section 2.3, which considered a point load as an equivalent static vehicular collision load. This horizontal load was applied to one of the VBEs at a 45degree angle directed into the pier, which is labeled in Figure 5-18 as load (b). Using a concentrated point load resulted in large stress concentrations at the point of load application. When increased from 1780kN (400 kip) to 3560kN (800 kip) the load resulted in excessive wall deformations in the VBE. It was deemed at this point that a single concentrated nodal load was not appropriate for this analysis method, nor was it representative of actual collisions. It was therefore decided to distribute the horizontal point load over a 442mm x 442mm (17.4 in x 17.4 in) area on the VBE, still angled at 45 degrees, such that the resultant remained at 1200mm (4ft) above the ground.

6.3.3 Results

The simple analysis presented in Section 5.4 showed that the 1780kN (400 kip) point load specified by AASHTO was not anticipated to cause any damage to the VBEs. A similar observation was made when the 1780kN (400 kip) load was applied to the finite element model of the structure. At no point in the structure were there signs of yielding. It was then determined to increase the magnitude of the load to observe trends and to see how the structure would ultimately behave under larger collision loads as larger demands could result from such a hazard. The pier was subjected to three other magnitudes of the horizontal load, namely a 3560kN (800 kip) load, a 5340kN (1200 kip) load, and a 7120kN (1600 kip) load. The resulting deformed shapes are displayed in Figure 6-10.

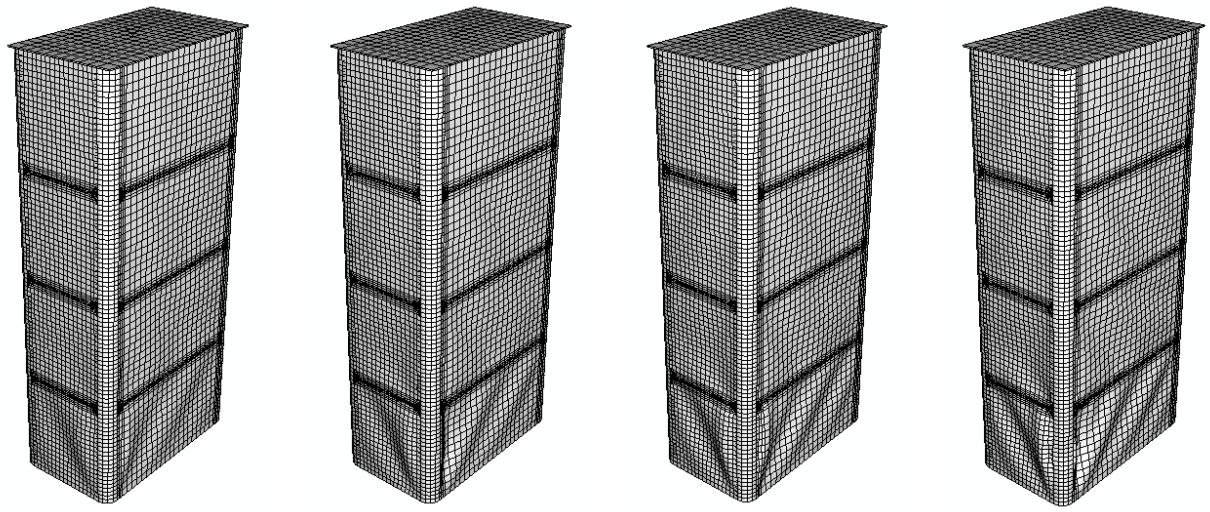

(a) **(b)** **(c)** **(d)**

Figure 6-10 Deformed Shape for Resultant Load: (a) 1780kN (400kips); (b) 3560kN (800kips); (c) 5340kN (1200kips), and; (d) 7120kN (1600kips) (Deformation Scale Factor = 5)

This figure shows that the bottom plates were affected most by these large collision loads. In regions near the load application point, the plates buckled. Further from the load, the plates tended to behave as they do when resisting seismic induced forces. The plates buckled in compression but resisted translation of the first level of HBEs by developing tension field action.

The von Mises stress contours shown in Figure 6-11 provide additional insight into the behavior of the system. As the load is increased, the bottom longitudinal and transverse plates are engaged more than any of the other structural components. Even for the 7120kN (1600kip) load case, the plates above the first level of HBEs, though they do become stressed, appeared to be much less engaged than the bottom plates. In Figure 6-11, the regions with lighter colored contours are more stressed than those of darker shades. Figure 6-11(d) shows the VBE to be significantly yielded compared to the case when the 1780kN (400kip) was applied. Nonetheless, even when considering the 7120kN (1600 kip) load case, the plates experienced little yielding overall, and by-and-large remained elastic. The plates on the opposing side of the pier were affected only negligibly compared to the plates shown in these figures.

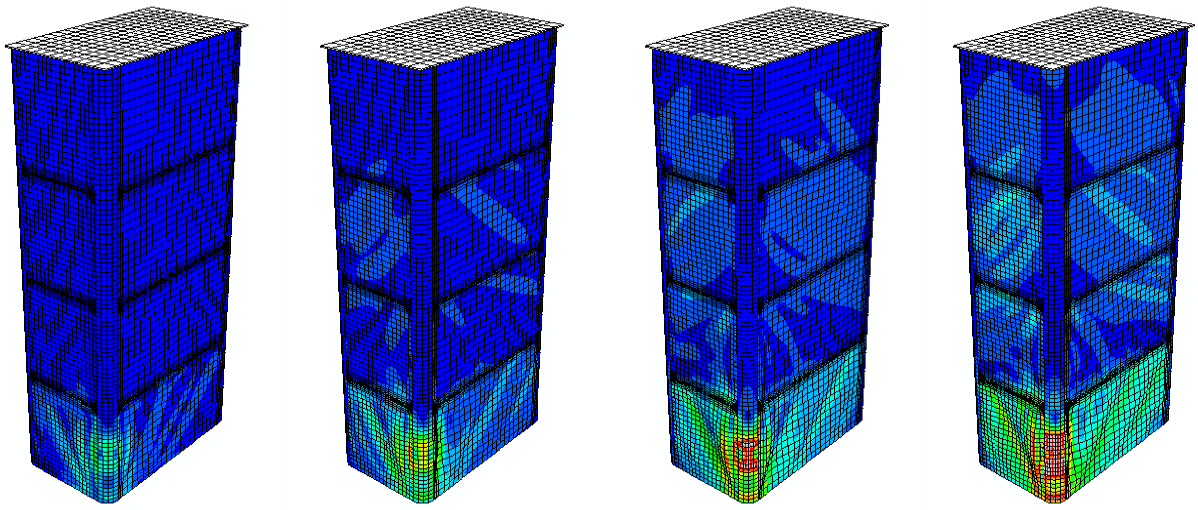

(a) **(b)** **(c)** **(d)**

Figure 6-11 von Mises Stress Contours for Resultant Loads: (a) 1780kN (400kips); (b) 3560kN (800kips); (c) 5340kN (1200kips), and; (d) 7120kN (1600kips) (Deformation Scale Factor = 5)

From these figures, the bottom plates seem to mitigate deformation in the boundary frame, beyond the VBE being loaded, by developing tensile stresses acting to restrain the motion of the first level of HBEs. In a basic sense, the observed behavior of the system is as shown in Figure 6-12, which shows the junction above the point of load application tending to displace in both the longitudinal and transverse direction. Assuming negligible contribution from the plates above, this motion is resisted by tension in the bottom plates.

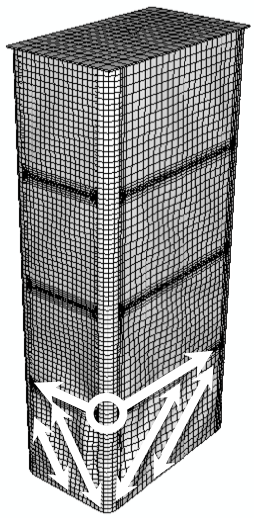

Figure 6-12 Basic Behavior of the Pier Subject to a Vehicle Collision

To gain an understanding of how much the plates influence the pier's behavior compared to the case when the plates are not present, the displacement of the junction above the load, which is indicated by a circle in Figure 6-12, was compared for both cases for the same four load cases already considered. The plot in Figure 6-13 shows the resulting displacement behavior in both the longitudinal and transverse directions. The quantities along the vertical axis refer to the total force being applied to the VBE horizontally at a 45 degree angle directed into the pier. Corresponding displacements in both directions, considering the cases when plates are present and when they are not, are provided as a function of this total load.

This figure shows that the observed junction tends to displace slightly more in the longitudinal direction than in the transverse direction for a given load, regardless of whether the plates are attached or not. Furthermore, inclusion of the plates reduces the transverse displacement of the junction by approximately 17%, and reduces its longitudinal displacement by approximately 20%.

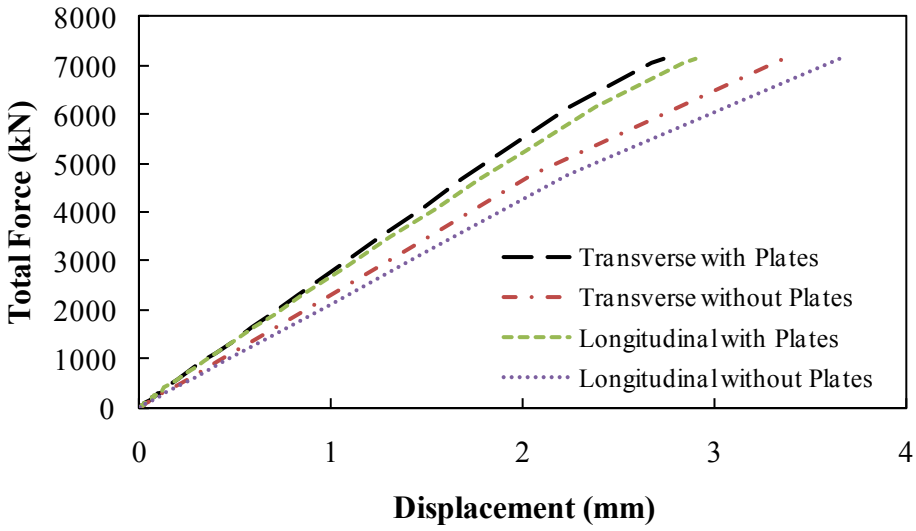

Figure 6-13 Effect of Plates on Deformation

6.3.4 Summary of Observations

The analysis presented in this section showed the proposed pier concept to have significant resistance to the vehicle collision hazard for impact applied to the VBE. Finite element analysis demonstrated that the pier could resist the specified AASHTO vehicular impact load, as well as a

load four times greater than that specified. It was also established that the plates in fact contributed roughly 20% to the pier's resistance to the vehicle collision hazard in terms of mitigating global deformation in the boundary frame.

6.4 Tsunami

This section investigates the behavior of the pier system subjected to the tsunami hazard. With changes to be discussed as follows, the same finite element model previously used for evaluating the seismic hazard was used again here. This includes the boundary condition assigned to the reference point in the pier cap, which allows the pier cap to rotate freely about the bridge's longitudinal axis. With the exception of the transverse and longitudinal plates, the pier's mesh remained unchanged. Modifications of the mesh are discussed in Section 6.4.1. Note that because the loads are applied normal to the plates for this hazard, no initial imperfections were introduced into the plates.

Application of the tsunami loading is discussed in Section 6.4.2. As with the collision hazard, dead load of the superstructure and pier cap, and self-weight of the boundary frame were not included in this analysis since the resulting axial force in each VBE is small in comparison to their capacity, and it would significantly reduce the analysis run time. Section 6.4.3 provides results of the analysis, and Section 6.4.4 provides a summary of observations related to this analysis.

6.4.1 Meshing

Difficulties with convergence when loading the plates prompted investigation of an alternate meshing strategy. Ultimately, it was decided to use a different element for the plates, namely the S4R element. The 4-noded S4R element is a general purpose, doubly-curved shell with reduced integration. Each node has six active degrees of freedom: three translational (u_x, u_y, u_z) and three rotational (θ_x, θ_y, θ_z). Additionally, it was decided to use a finer mesh than was used with S8R elements in the previous two hazards. Figure 6-14 shows the modified mesh used in analyzing this hazard.

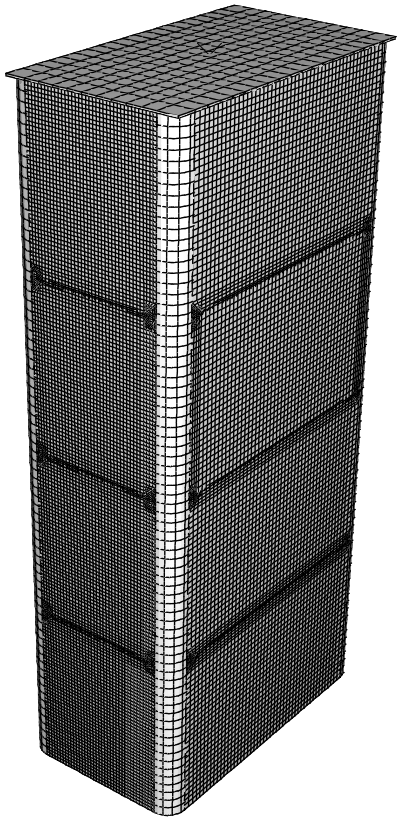

Figure 6-14 Modified Mesh for Tsunami Hazard

6.4.2 Analysis

Load Case 1, as introduced in Section 5.5.2, was not considered in this analysis since accounting for it with current codes (as considered in simplified analysis) would result in interaction with the superstructure for water depths greater than one-third the pier's height. Accordingly, this load case is left for future research. This analysis considers the pier subjected to loads for four different scenarios corresponding to Load Case 2 without the debris impact load since the VBEs of this system were shown to have significant resistance to impact through the vehicle collision analysis. Each scenario considered a different stillwater depth. Specifically, the first considered the depth to be at the centerline of the first HBE from the pier's base, the second considered the depth to be at the centerline of the second HBE, the third considered the depth to be at the centerline of the third HBE, and the fourth considered the depth to be at the top of the pier. For each scenario, loading was only applied to the plates, and no load was accounted for on the VBEs.

The loading was applied in two steps for each scenario. The first step applied hydrostatic pressure simultaneously on all faces of the pier using the ABAQUS *Hydrostatic Pressure* distribution, and the second step applied hydrodynamic pressure to the upstream longitudinal plates with the ABAQUS *Uniform Pressure*. The hydrostatic pressure distribution was applied in accordance with the relationship provided in Section 2.4.2, where the pressure increased linearly from zero at the water surface to a computed value at the pier's base. The hydrodynamic pressure was computed using the relationship provided at the beginning of Section 2.4.3, where the tsunami velocity was taken from Section 2.4.1, and assuming a drag coefficient of two. From the velocity relationship, the hydrodynamic pressure imposed on the pier increases as the depth being considered increases. Each step was applied with a "ramp" loading type that applies the pressure distributions linearly from zero to the maximum value being considered.

6.4.3 Results

Figure 6-15 shows the final deformed shape of the pier when subjected to each of the loading scenarios. Note that contact between the plates and the boundary frame members was not accounted for in this model. It was thought that neglecting the contact would not have a significant effect on the global behavior of the structure, and would reduce the computational demand. Therefore, in some instances, these figures show the plates to pass through the boundary elements. Note, however, that these figures show the deformed shape with a scale factor of two, so the degree to which this is occurring is exaggerated. In reality, the plates would wrap smoothly around the VBEs and HBEs, reducing the localized stresses at the ends of the plates, per design intent.

Figure 6-15(a) shows the pier to be relatively unaffected by the pressure distributions imposed on it for a design water depth up to the first HBE. The remaining figures show that as the water depth is increased, and thus the pressure imposed on the pier, the plates deform more. Note that no significant deformations develop in the boundary frame.

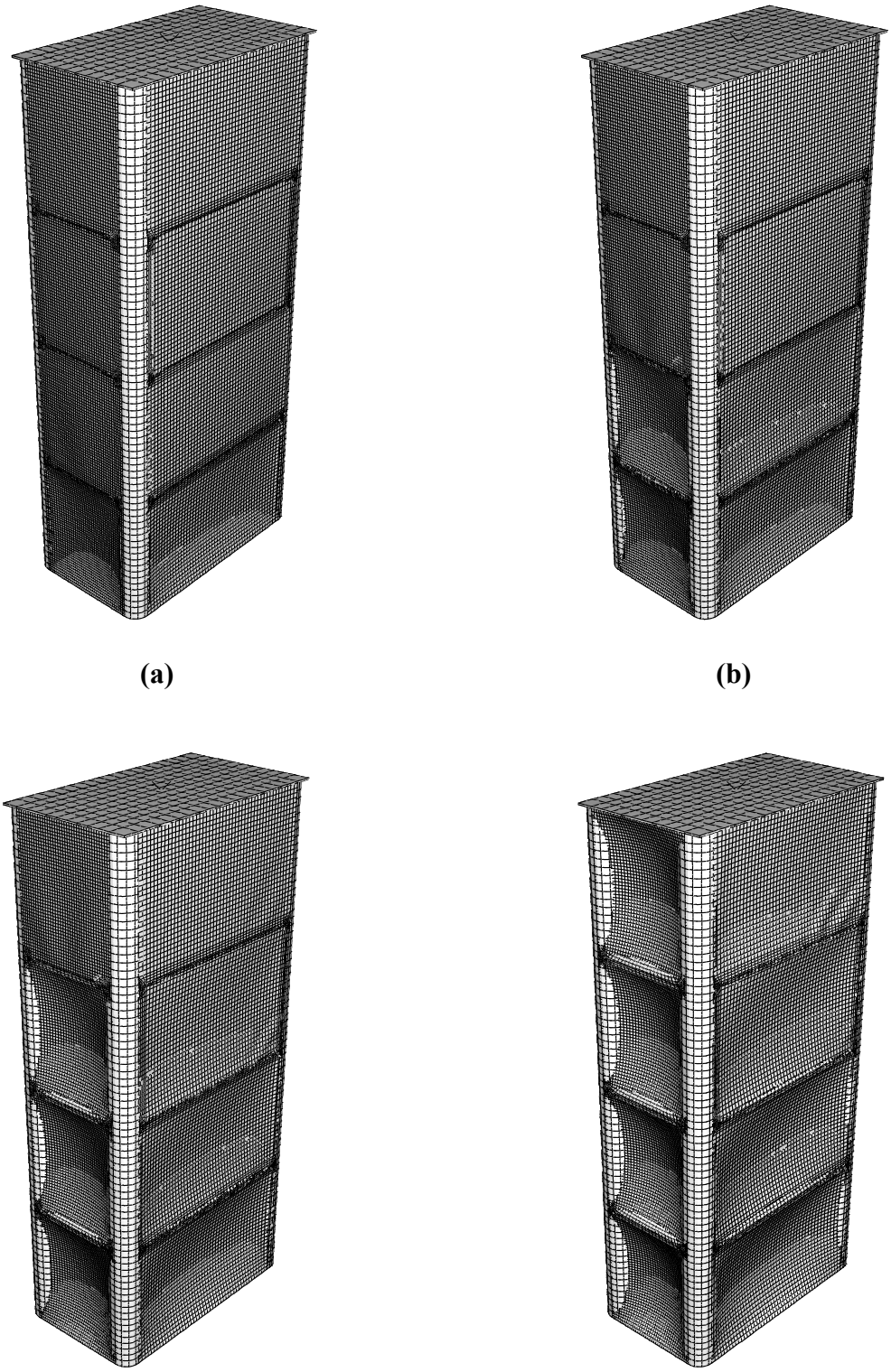

(a) **(b)**

(c) **(d)**

Figure 6-15 Final Deformed Shape (Deformation Scale Factor = 2) for a Water Height up to: (a) First Level; (b) Second Level; (c) Third Level, and; (d) Top of Pier

For simplified analysis, the pull-in forces acting on the HBEs from loaded plates were idealized as transferring directly to the top of the pier (as described in Section 5.5.2.2). However, it was observed from the finite element analysis results that some of these pull-in forces would be transferred to the HBEs due to their stiffness relative to the plates. Figure 6-16 shows the scenario for when the stillwater depth is at the second HBE level, and provides the corresponding von Mises stress contours for the top surface of the plates (for surfaces as defined in the figure). This figure reveals that some of the pull-in forces acting on the middle HBEs from the second longitudinal and transverse plates are transferred to the plate above. However, these stress contours illustrate that the pull-in forces do not entirely transfer to the top of the pier, as was initially conservatively assumed.

Figure 6-17 shows von Mises stress contours for stresses on the top surface of the plates, for the scenario when the stillwater depth is at the top of the pier. Figure 6-17(a) shows the pier after being subjected to hydrostatic loading on all sides, and Figure 6-17(b) shows the pier after being subjected to the hydrodynamic pressure.

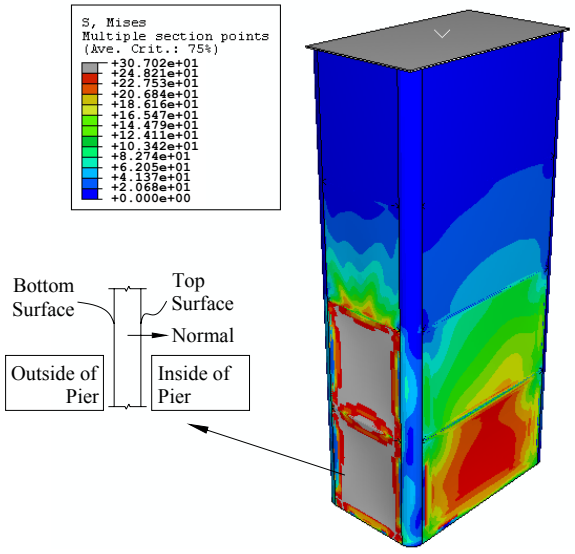

Figure 6-16 von Mises Stress Contours (MPa) After Application of Hydrodynamic Pressure

In all scenarios, except for the first, the loaded longitudinal plates were completely yielded. For the first two loading scenarios, the transverse plates experienced no yielding. For the third and fourth loading scenarios, the bottom two and three plates, respectively, were largely yielded.

This yielding of the plates is in agreement with the intent of this pier concept where the plates were intended to be sacrificial. Important to note is that while the plates yielded, particularly for the fourth case, the VBEs remained elastic. The longitudinal HBEs attached to the loaded plates, however, did experience some yielding but did not develop any plastic hinges. This could be a result of the way the plates were connected to the HBEs. Because no contact was modeled, the plate edge reactions were applied as concentrated distributed loads at the center of the HBEs.

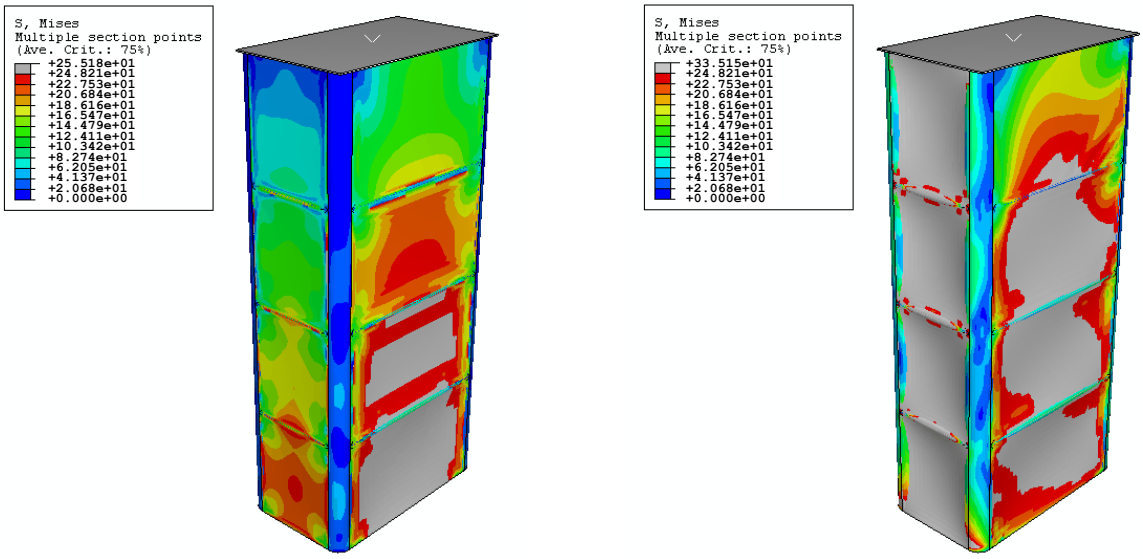

(a) **(b)**

Figure 6-17 von Mises Stress Contours (MPa): (a) After Application of Hydrostatic Pressure, and; (b) After Application of Hydrodynamic Pressure

For each scenario considered, the lateral displacement at the pier's top was also monitored. Figure 6-18 displays the pier's global behavior in terms of base shear (which is also the resultant of the applied hydrodynamic pressure) versus the pier's top displacement. The three curves represent water depths at the second HBE (Level 2), the third HBE (Level 3), and at the top of the pier (Level 4). For a depth at the first HBE, the pier was found to have a negligible response and is not included in Figure 6-18. This plot shows that as the depth being considered increased, the base shear increased. This is a result of the increase in depth, and thus in applied hydrodynamic pressure from an increased flow velocity. Also, the structure's initial stiffness (based on the pier's top displacement) decreases with increasing depth because the pressure is more distributed over the pier's height. From these plots, it is apparent that there is no loss in strength of the pier for the scenarios considered.

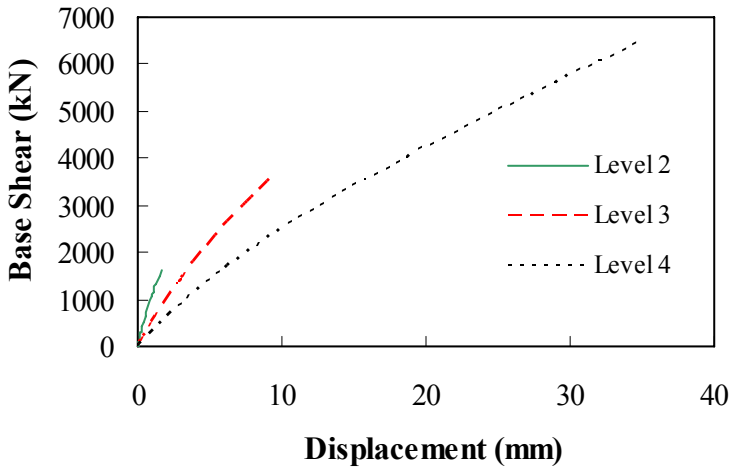

Figure 6-18 Base Shear vs. Top Lateral Displacement

6.4.4 Summary of Observations

This investigation showed the pier to have significant resistance to the hydrostatic and hydrodynamic loads, as expected from simplified analysis. With increased water depth, and corresponding increased lateral load, the longitudinal plates loaded with the hydrodynamic pressure increasingly deformed. For the most extreme case considered (stillwater depth to the top of the pier), the loaded longitudinal plates were fully yielded and the VBEs remained essentially elastic. Yielding of the plates (making them sacrificial) demonstrates the design intent of this pier concept. It was also shown that the pier's top displaced somewhat uniformly as the applied pressure increased, with no apparent loss in strength of the pier.

The transverse plates did not appear to contribute to the lateral resistance, in the form of tension field action, in any of the scenarios considered. However, from Figure 6-17, the plates appeared to contribute to the lateral resistance, which was conservatively neglected in the simplified analysis. The degree to which the plates contribute to lateral resistance, although possibly marginal, is unknown at this time and determination of this effect is left for future research.

6.5 Blast

This section investigates the behavior of the pier system subjected to the blast hazard. With changes to be discussed as follows, the model used for evaluating the collision hazard was re-used in evaluating this hazard. The boundary condition placed on the reference point in the pier cap remained fixed in all directions except for the vertical direction. This was done for this hazard because the loading is impulsive, and the global response of the bridge superstructure would not be affected until after the blast loads have been removed. As was done for the tsunami hazard, the mesh of the transverse and longitudinal plates was refined, and was assigned S4R elements. Note that no initial imperfections were introduced into the plates for this hazard.

As with the analyses for collision and for tsunamis (and for the same reason), dead load of the superstructure and pier cap, and self-weight of the boundary frame were not included. Section 6.5.1 provides information regarding the analyses undertaken for this hazard, Section 6.5.2 provides the resulting behavior observed during these analyses, and Section 6.5.3 provides a summary of observations.

6.5.1 Analysis

The first analysis considered a first story VBE and two adjacent first story plates to be simultaneously statically loaded with a ramp loading function. The intent was to determine the significance of the loaded plates pulling on the VBEs as the plates were loaded simultaneously with the VBEs.

Analysis of the VBEs was then conducted to determine the system's behavior assuming no additional load being transferred to them through the plates. This was done by considering the structure with plates attached, but only with load applied to a VBE. The presence of the plates would have a negligible effect on the capacity of the first story VBE as the plates readily buckle locally around the loaded VBE. This analysis indirectly takes into account a failure sequence of the system's components in the sense that the plates are not loaded and will not transfer additional loads to the VBEs. In essence, the sequence of load cases considered reflects the fact

that the plates transfer their capacity to the VBEs by being sacrificial, and then after this load has been removed, a VBE alone is loaded.

For this analysis, a uniformly distributed static load directed into the pier at a 45 degree angle was applied to the same VBE loaded in the collision analysis. The load was first applied to the exposed face of the VBE on the pier's exterior along the VBE's height between the pier's base and the first HBE. This resulted in a loaded area of 0.44m x 2.34m = 1.04m^2 (17.43in x 92.27in = 1608 in^2). Note that the simplified analysis of the blast effects on the VBEs assumed pressures to be acting on 45% of the VBE's projected width to reflect the pressure shape factor of 0.45 recommended for blast on columns of circular cross-section, whereas this analysis loaded an area that was one quarter the VBE's circumference, which is greater than 45% of the projected width, but was deemed acceptable considering only trends in ultimate behavior were of interest. Finally, an additional analysis was conducted (for reasons discussed in Section 6.5.2), where a distributed load acting over the same area was again applied to the VBE, but to the surface of the VBE located inside the pier assembly.

6.5.2 Results

When running the first analysis, the model experienced convergence difficulties when the uniformly distributed load simultaneously being applied to the plates and to the VBE reached approximately 359kPa (52psi). This load resulted in negligible deformation of the VBE, but the plates were deformed, and completely yielded. The center of the transverse plate displaced approximately 686mm (27 in), and the center of the longitudinal plate displaced approximately 140mm (5.5 in). At this point, the VBEs were observed to remain elastic. This was expected since it was observed from the tsunami analysis that the VBEs were undamaged for the case where all longitudinal plates had yielded (the worst case scenario considered for the tsunami hazard). This suggested that the VBEs were only marginally affected when the plates and the VBEs were simultaneously loaded. In reality, if the plates were to be further loaded, they would likely fail. At this point, only the VBE would be loaded and the plates would not be simultaneously pulling on the VBE. This suggests that a sequence of failures should perhaps be taken into consideration, in which loading of the VBE progresses further after failure of plates.

To circumvent the computational difficulties in accurately modeling this sequence the behavior of the system considering the plates as not being loaded was studied, which is discussed next.

Figure 6-19(a) shows the deformed shape of the pier for the load applied on the VBE's exterior. This loading scenario resulted in the wall of the VBE collapsing inward, a behavior that initiated when the uniform surface load reached approximately 16MPa (2.3 ksi). At this point, the wall of the VBE began "snapping" through, and the system's corresponding resistance dropped significantly. The inset in Figure 6-19(a) schematically shows this behavior.

At this point, it was decided to load the VBE differently. More specifically, the load was instead applied to the VBE (acting over the same VBE surface area and in the same direction as the previous analysis) from the interior of the pier. The intent was to alleviate the issue of having the wall of the VBE collapse by pulling on the VBE rather than pushing on it. The observed behavior from this load application was thought to be more representative of a case where the VBE was loaded from the exterior but would have a cross-section stiffened to prevent its inward caving (such as would be the case if the VBE was filled with concrete). The deflected shape for this load application is shown in Figure 6-19(b).

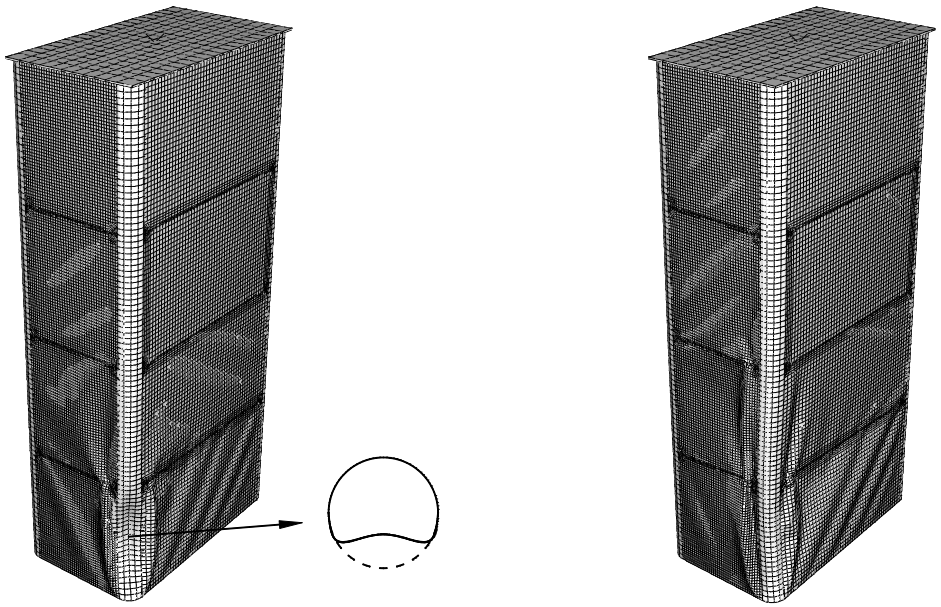

(a) **(b)**

Figure 6-19 Deformed Shape of Pier (Deformation Scale Factor = 1): (a) VBE Loaded from Pier's Exterior, and; (b) VBE Loaded from Pier's Interior

To better understand the demand on the first story VBE, the deformation at its center was observed. This is schematically shown in Figure 6-20. In this figure, Δ_j is the displacement of the joint at the top of the first "story" VBE, and Δ_m is the displacement at the VBE's mid-height, both of which are measured relative to the undeformed position. Deformation of the VBE's center, Δ_{vbe}, however, was measured relative to a chord connecting the base of the VBE to the joint at which Δ_j is measured. It was taken as being the difference between Δ_m and half of Δ_j.

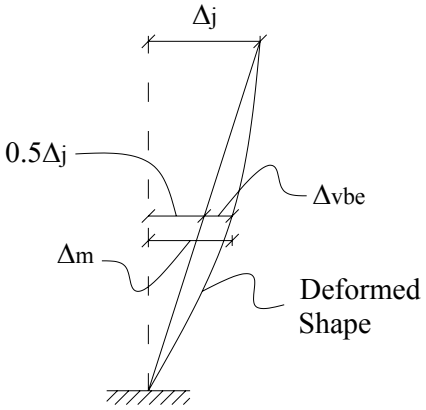

Figure 6-20 Schematic Displacement of 1st Story VBE

Because the VBE was displaced in both the transverse and longitudinal directions, the calculation of Δ_{vbe} was made for each direction (considering the Δ_j and Δ_m for those directions). The resultant of Δ_{vbe} for each direction was then taken and compared to the corresponding uniformly distributed load being statically applied to the VBE. This is shown by Figure 6-21.

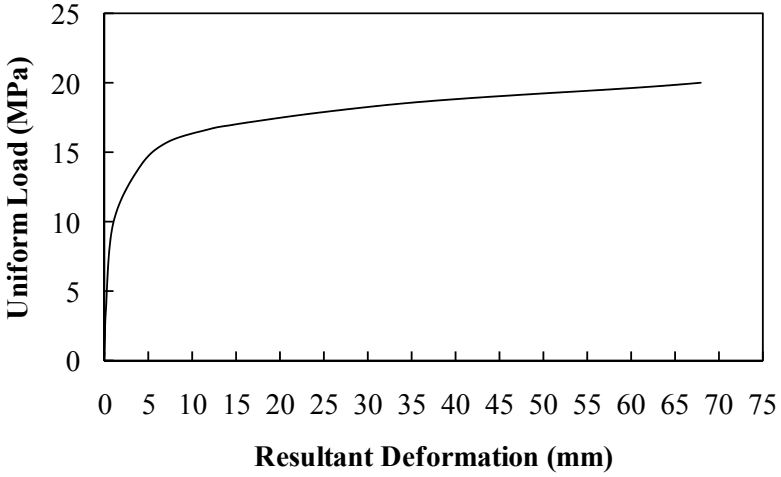

Figure 6-21 Resultant Displacement at VBE Mid-Height

From this figure, it is observed that the VBE undergoes yielding at a relatively small center deformation, but does not loose strength when undergoing larger deformation. For a sense of the demand on the VBE due to the blast hazard, recall that the simplified analysis in Chapter 5 investigating blast effects on a bare VBE estimated a mid-height deformation of the VBE of 1.1mm (0.04 in). From Figure 6-21, the VBE is shown to be approximately at the onset of yielding for a deformation of this magnitude. Note the finite element analysis did not consider any dynamic increase factors to account for strain rate effects, as was done in simplified analysis. The inelastic part of the pushover curve shown in Figure 6-21 could be roughly factored up by 1.2 to account for this effect.

6.5.3 Summary of Observations

The finite element analyses of the proposed pier subjected to blast loading, building upon the simplified analysis from Chapter 5, suggest that the plates could be considered sacrificial without consequence to the VBEs. Therefore, subsequent analyses considered a uniformly distributed load applied to a VBE of this system. Although the slender plates remained attached to the VBE in the model, they did not contribute to the resistance as they buckled upon being compressed by the VBE deflections. On the basis of calculated mid-height deformation of the VBE, the finite element blast analysis showed that the first story VBE could undergo significant deformations, and that the deformation of the VBE obtained from simplified analysis roughly corresponds to the onset of yielding. Analysis also exposed the risk of local failure of the VBE's wall under large compressive pressures.

It is recognized that the blast hazard is associated with a complex dynamic loading environment, which deserves more detailed investigation. In particular, further research should experimentally investigate local and global behavior of the proposed system to verify the analytical model and its underlying assumptions.

CHAPTER 7

CONCLUSIONS

7.1 Summary

This research simultaneously considered the demands and constraints germane to four extreme hazards (earthquakes, vehicle collisions, tsunamis (and indirectly storm surge), and blasts) in the development of a SPSW box bridge pier system from a multi-hazard perspective. Through means of simplified analysis and design approaches, a detailed design of this concept was achieved, which was then analyzed for the demands of each hazard to investigate the system's anticipated global behavior and resistance to each hazard. For a better understanding of the system's behavior in resisting the hazards, nonlinear finite element analyses were conducted.

7.2 Conclusions

The system was found to have adequate ductile performance and strength for each hazard considered. More specifically, from the simplified analyses, and with a design of the pier for the seismic hazard, it was observed that: (i) the AASHTO vehicle collision load applied to the pier, neglecting any contribution from the plates, remained elastic; (ii) for the tsunami hazard, the boundary elements were able to resist both the directly applied water pressures and the forces from the out-of-plane plate deformations, and; (iii) the system was found to have adequate resistance to the blast hazard.

The pier system was further investigated to determine trends in behavior using nonlinear finite element analyses. From these analyses, it was observed that: (i) the system behaved as expected in resisting the seismic hazard; (ii) the pier resisted the vehicle collision hazard, as expected, and it was found that the plates contributed roughly 20% to the pier's resistance by mitigating deformation in the boundary frame through the development of tension field action in the bottom

plates; (iii) the pier had significant resistance to the tsunami hazard, where it was shown that the plates could in fact be sacrificial while at the same time leaving the boundary frame intact, and that the plates appeared to contribute to the pier's resistance, but not through tension field action, and; (iv) barring local failure, the VBEs had significant deformation capacity for resisting the blast hazard, which was investigated with statically distributed loads.

7.3 Future Work

The scope of this research was intended to establish trends in behavior of a new system developed from a multi-hazard perspective. Building on the work presented here, validation of the performance of the proposed system requires more in-depth detailed investigation, particularly through experimental work, to further investigate the system's performance for each hazard. As with any new system being researched, a number of assumptions have been made. Therefore, further investigation is warranted to assess the validity of these assumptions. In particular, the blast hazard, which is a complex loading environment, requires special attention. Also, inter-disciplinary collaboration is strongly encouraged in evaluating the system for each hazard.

Note that all analyses here considered elastic-perfectly plastic material, without strain limits. It is not anticipated that the trends observed in this research will vary much when considering other types of material behavior, but future research should consider such matters. Moreover, this research focused only on one pier. It is recommended for future research that this system be incorporated into a total bridge system and the resulting system be evaluated as a whole. It is also suggested that more refinement be used to analyze the structure with finite element models as in some of the analyses a coarse mesh was used to reduce computational time. While this captured global behavior (and trends) adequately for the purpose of this study, questions remain on whether this captured well all important local behaviors. Additionally, there were instances in which convergence of the models was problematic, particularly in analyzing the seismic hazard and in hazards involving loading of the plates, supporting the need for further mesh refinement.

CHAPTER 8

REFERENCES

AASHTO. (2007). *AASHTO LRFD Bridge Design Specifications (4th Edition)*. American Association of State Highway and Transportation Officials, Washington, D.C.

ABAQUS. (2006). "ABAQUS/CAE User's Manual (version 6.6)."

AISC. (2005a). *Seismic Provisions for Structural Steel Buildings*, American Institute of Steel Construction, Inc., Chicago, IL.

AISC. (2005b). *Steel Construction Manual (13th edition)*, American Institute of Steel Construction, Inc., Chicago, IL.

Applied Research Associates, Inc. (2004). "A.T.-Blast (version 2.2)."

ASCE. (2006). "Minimum Design Loads for Buildings and Other Structures." American Society of Civil Engineers.

Baker, W. E. (1973). *Explosions in Air*, University of Texas Press, Austin, Texas.

Behbahanifard, M. R., Grondin, G. Y., and Elwi, A. E. (2003). "Experimental and Numerical Investigation of Steel Plate Shear Wall." *Structural Engineering Report No. 254*, Department of Civil Engineering, University of Alberta.

Berman, J. W., and Bruneau, M. (2003a). "Experimental Investigation of Light-Gauge Steel Plate Shear Walls for the Seismic Retrofit of Buildings." *Technical Report MCEER-03-0001*, Multidisciplinary Center for Earthquake Engineering Research, Buffalo, NY.

Berman, J. W., and Bruneau, M. (2003b). "Plastic Analysis and Design of Steel Plate Shear Walls." *ASCE Journal of Structural Engineering*, 129(11), 1448-1456.

Biggs, J. M. (1964). *Introduction to Structural Dynamics*, McGraw-Hill.

Bozorgnia, Y., and Bertero, V. V. (2004). *Earthquake Engineering: From Engineering Seismology to Performance-Based Engineering*, CRC Press.

Bruneau, M. (2007). "The 4 R's of Resilience and Multi-Hazard Engineering (The Meta-Concept of Resilience)." AEI/MCEER/Steel Institute of NY Symposium on Emerging Developments in Multihazards Engineering, New York City, NY.

Bruneau, M., Berman, J., Lopez-Garcia, D., and Vian, D. (2005). "Steel Plate Shear Wall Buildings: Design Requirements and Research." *Proceedings of 2005 North American Steel Construction Conference*, Montreal, Canada.

Bruneau, M., Wilson, J. C., and Tremblay, R. (1996). "Performance of steel bridges during the 1995 Hyogo-ken Nanbu (Kobe, Japan) earthquake." *Canadian Journal of Civil Engineering*, 23(3), 678 - 713.

Bulson, P. S. (1997). *Explosive Loading of Engineering Structures*, E & FN Spon.

Caccese, V., Elgaaly, M., and Chen, R. (1993). "Experimental Study of Thin Steel-Plate Shear Walls Under Cyclic Load." *Journal of Structural Engineering*, 119 (2), Feb. 1993, 573-587.

CCH. (2000). Department of Planning and Permitting of Honolulu Hawaii. City and County of Honolulu Building Code, Chapter 16 Article 11.

Chopra, A. K. (2001). *Dynamics of Structures - Theory and Applications to Earthquake Engineering (2nd ed.)*, Prentice Hall, Upper Saddle River, New Jersey.

Dames, and Moore. (1980). "Design and Construction Standards for Residential Construction in Tsunami-Prone Areas in Hawaii." Prepared for the Federal Emergency Management Agency.

Driver, R. G., Kulak, G. L., Kennedy, D. J. L., and Elwi, A. E. (1997). "Seismic Behavior of Steel Plate Shear Walls." *Structural Engineering Report No. 215*, Department of Civil Engineering, University of Alberta, Edmonton, Alberta, Canada.

Elgaaly, M., Caccese, V., and Du, C. (1993). "Postbuckling Behavior of Steel-Plate Shear Walls Under Cyclic Loads." *Journal of Structural Engineering*, 119 (2), Feb. 1993, 588-605.

Ettouney, M. M., Alampalli, S., and Agrawal, A. K. (2005). "Theory of Multihazards for Bridge Structures." *Bridge Structures*, 1(3), 281-291.

FEMA. (2000). "FEMA 55 - Coastal Construction Manual."

FEMA. (2003a). "FEMA 427 - Primer for Design of Commercial Buildings to Mitigate Terrorist Attacks."

FEMA. (2003b). "FEMA 428 - Primer to Design Safe School Projects in Case of Terrorist Attacks."

FEMA. (2004). "FEMA 424 - Design Guide for Improving School Safety in Earthquakes, Floods, and High Winds."

Fujikura, S., Bruneau, M., and Lopez-Garcia, D. (2007). "Experimental Investigation of Blast Performance of Seismically Resistant Concrete-Filled Steel Tube Bridge Piers." *Technical Report MCEER-07-0005*, Multidisciplinary Center for Earthquake Engineering Research, Buffalo, NY.

Fujikura, S., Bruneau, M., and Lopez-Garcia, D. (2008). "Experimental Investigation of Multihazard Resistant Bridge Piers having Concrete-Filled Steel Tube under Blast Loading." *Journal of Bridge Engineering*. ASCE (In press).

Ghosn, M., Moses, F., and Wang, J. (2003). "Design of Highway Bridges for Extreme Events." NCHRP 489.

Haritos, N., Ngo, T., and Mendis, P. "Modeling Tsunami Wave Force Effects on Structures." Earthquake Engineering in Australia - Conference 2005, Albury, New South Wales.

Hibbitt, Karlsson & Sorensen, Inc. (HKS). (2002). *ABAQUS/Standard User's Manual (version 6.3)*, Pawtucket, Rhode Island.

Hopkinson, B. (1915). British Ordnance Board Minutes 13565.

Kharrazi, M. H. K., Ventura, C. E., Prion, H. G. L., and Sabouri-Ghomi, S. "Bending and Shear Analysis and Design of Ductile Steel Plate Walls." *Proceedings of the 13th World Conference on Earthquake Engineering*, Vancouver, B.C., Canada, August 1-6, 2004, Paper No. 77.

Lee, G. C., Tong, M., and Yen, P. (2006). "Multi-hazards Design Criteria of Highway Bridge."

Lin, Y. C., and Tsai, K. C. (2004). "Seismic Responses of Steel Shear Wall Constructed with Restrainers." *Technical Report NCREE-04-015*, National Center for Research on Earthquake Engineering, Taipei, Taiwan, R.O.C., September 2004.

Lubell, A. S., Prion, H. G. L., Ventura, C. E., and Rezai, M. (2000). "Unstiffened Steel Plate Shear Wall Performance Under Cyclic Loading." *Journal of Structural Engineering*, 126(4), April 2000, 453-460.

Mast, R., Marsh, L., Spry, C., Johnson, S., Griebenow, R., Guarre, J., and Wilson, W. (1996a). "Seismic Design of Bridges Design Example No. 2: Three-Span Continuous Steel Girder Bridge." *FHWA-SA-97-007*, Federal Highway Administration.

Mast, R., Marsh, L., Spry, C., Johnson, S., Griebenow, R., Guarre, J., and Wilson, W. (1996b). "Seismic Design of Bridges Design Example No. 3: Single Span AASHTO Precast Girder Bridge." *FHWA-SA-97-008*, Federal Highway Administration.

Mays, G. C., and Smith, P. D. (1995). *Blast Effects on Buildings - Design of Buildings to Optimize Resistance to Blast Loading*, Thomas Telford.

MCEER. (2007). "Defining Multi-Hazard Engineering." A Summary of the Symposium on Emerging Developments in Multi-Hazard Engineering. 26 April 2008 <http://www.mceer.buffalo.edu/meetings/aei/default.asp>.

Nouri, Y., Nistor, I., Palermo, D., and Saatcioglu, M. (2007). "Tsunami-Induced Hydrodynamic and Debris Flow Force on Structural Elements." Ninth Canadian Conference on Earthquake Engineering Ottawa, Ontario, Canada.

Okada, T., Sugano, T., Ishikawa, T., Ohgi, T., Takai, S., and Hamabe, C. (2004). "Structural Design Method of Building for Tsunami Resistance (proposed)." Building Technology Research Institute, The Building Center of Japan.

Packer, J. A., and Henderson, J. E. (1997). *Hollow Structural Sections: Connections and Trusses (A Design Guide)*, Canadian Institute of Steel Construction.

Priestley, M. J. N., Seible, F., and Calvi, G. M. (1996). *Seismic Design and Retrofit of Bridges*, John Wiley &Sons, Inc.

Rezai, M. (1999). "Seismic Behaviour of Steel Plate Shear Walls by Shake Table Testing," PhD Dissertation, Department of Civil Engineering, University of British Columbia, Vancouver, Canada.

Roberts, T., and Sabouri-Ghomi, S. (1992). "Hysteretic Characteristics of Unstiffened Perforated Steel Plate Shear Panels." *Thin Walled Structures*, 14, 139-151.

Saatcioglu, M., Ghobarah, A., and Nistor, I. (2005). "Reconnaissance Report on The December 26, 2004 Sumatra Earthquake and Tsunami." The Canadian Association for Earthquake Engineering.

Sabelli, R., and Bruneau, M. (2006). *Steel Plate Shear Walls, AISC Steel Design Guide.* American Institute of Steel Construction, Inc.

SAP2000. (2007). "SAP2000 v.11.0.0." Computer and Structures, Inc., Berkeley, CA.

Smith, P. D., and Hetherington, J. G. (1994). *Blast and Ballistic Loading of Structures*, Butterworth-Heinemannn Ltd.

Thorburn, L. J., Kulak, G. L., and Montgomery, C. J. (1983). "Analysis of Steel Plate Shear Walls." *Structural Engineering Report No. 107*, Department of Civil Engineering, University of Alberta, Edmonton, Alberta, Canada.

Timler, P. A. (1988). "Design Procedures Development, Analytical Verification and Cost Evaluation of Steel Plate Shear Wall Structures." *Technical Report No. 98-01*. Earthquake Engineering Research, Facility, Department of Civil Engineering, University of British Columbia, Canada.

Timler, P. A., and Kulak, G. L. (1983). "Experimental Study of Steel Plate Shear Walls." *Structural Engineering Report No. 114*, Department of Civil Engineering, University of Alberta, Edmonton, Alberta, Canada.

Tromposch, E. W., and Kulak, G. L. (1987). "Cyclic and Static Behaviour of Thin Panel Steel Plate Shear Walls." *Structural Engineering Report No. 145*, Department of Civil Engineering, University of Alberta, Edmonton, Alberta, Canada.

USDA. (1990). *Structures to Resist the Effects of Accidental Explosions, Technical Manual TM 5-1300*, US Department of the Army, Washington, DC.

Vian, D., and Bruneau, M. (2005). "Steel Plate Shear Walls for Seismic Design and Retrofit of Building Structures." *Technical Report MCEER-05-0010*, Multidisciplinary Center for Earthquake Engineering Research, Buffalo, New York.

Warn, G. P., and Bruneau, M. (2008). "Blast Resistance of Steel Plate Shear Walls Designed for Seismic Loading." *Journal of Structural Engineering*, Submitted for Review, April 2008.

Winget, D. G., Marchand, K. A., and Williamson, E. B. (2005). "Analysis and Design of Critical Bridges Subjected to Blast Loads." *Journal of Structural Engineering*, 131(8), 1243 - 1255.

Xue, M., and Lu, L.-W. (1994). "Interaction of Infilled Steel Shear Wall Panels with Surrounding Frame Members." *Proceedings of the Structural Stability Research Council Annual Technical Session*, Bethlehem, PA, 339-354.

Yeh, H. (2007). "Design Tsunami Forces for Onshore Structures." *Journal of Disaster Research*, 2(6).

Yeh, H., Robertson, I., and Preuss, J. (2005). "Development of Design Guidelines for Structures that Serve as Tsunami Vertical Evacuation Sites." *Open File Report 2005-4*, Washington Division of Geology and Earth Resources.

APPENDIX A

DERIVATION OF INTERACTION EQUATIONS

A.1 General

The subsequent discussion introduces the interaction equations that are referenced in analyzing the round tubular steel sections, as shown in Figure A-1, being used in the proposed pier system. Derivations of the analytical expressions describing the relationship between moment, *M*, and axial force, *P*, for onset of yielding (Section A.2) and for full plastic yielding (Section A.3) are provided.

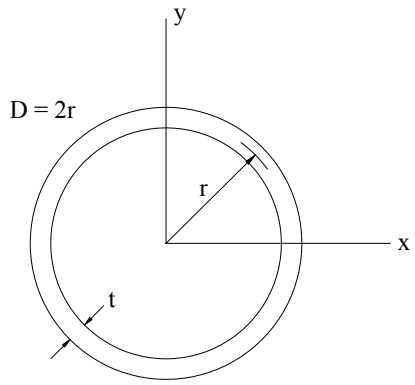

Figure A-1 Cross Section for a Thin Tube

For a thin ring (small t), the moment of inertia and the cross-sectional area are given by (A-1) and (A-2), respectively. Variables not defined in Figure A-1 will be defined as they are used in the derivations.

$$I_x = I_y = \pi r^3 t = \frac{\pi D^3 t}{8} \tag{A-1}$$

$$A = 2\pi rt = \pi Dt \tag{A-2}$$

A.2 Onset of Yielding

The derivation in this section provides the interaction equation for the instant at which yielding of an extreme fiber has initiated. This is shown in Figure A-2.

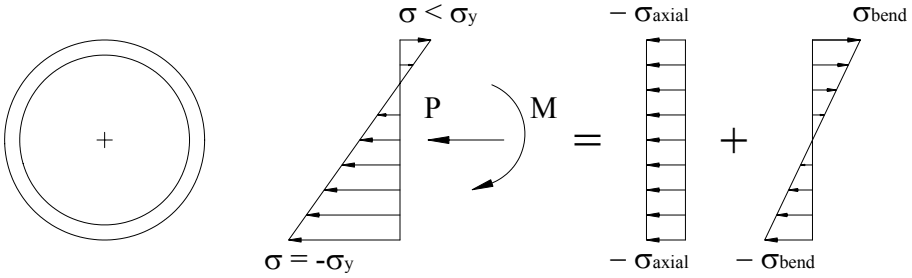

Figure A-2 Superposition of Bending and Axial Stress Distributions (Onset of Yielding)

For the onset of yielding at the section's extreme fiber, the sum of the axial stress, σ_{axial}, and bending stress, σ_{bend}, equals the material's yield stress, σ_y.

$$\sigma_{axial} + \sigma_{bend} = \sigma_y \tag{A-3}$$

Knowing that the axial force, P, is equal to the product of the axial stress and the section's area, A, and that the axial force required to yield the section in compression, P_y, is the product of the yield stress and the section's area, the following relationship can be determined:

$$\frac{P}{P_y} = \frac{\sigma_{axial}}{\sigma_y} \tag{A-4}$$

By substituting (A-3) into (A-4), with some rearranging, the following relationship is obtained:

$$\frac{P}{P_y} = 1 - \frac{\sigma_{bend}}{\sigma_y} \tag{A-5}$$

Knowing the classic bending stress equation where the bending stress is equal to moment divided by the section's elastic section modulus, the following expression is obtained:

$$M = \sigma_{bend} S \tag{A-6}$$

where:

$$S = \frac{\pi}{4} D^2 t \tag{A-7}$$

Also, the plastic moment can be determined, and is expressed by (A-8), where y_b is the centroid location for a semicircular ring measured from the center of the circle:

$$M_p = 2\left(\frac{A}{2}\sigma_y y_b\right) = A\sigma_y \frac{D}{\pi} = D^2 t \sigma_y \tag{A-8}$$

Expressions (A-6) and (A-8) can be combined and rearranged to form the following expression:

$$\frac{\sigma_{bend}}{\sigma_y} = \frac{4}{\pi}\frac{M}{M_p} \tag{A-9}$$

Combining (A-5) and (A-9), the following expression, which relates interaction between axial force and bending moment to the instant of first yield, is arrived at:

$$\frac{P}{P_y} = 1 - \frac{4}{\pi}\frac{M}{M_p} \tag{A-10}$$

A.3 Fully Plastic Yielding

The derivation in this section provides the interaction equation for the cross section shown in Figure A-1 at its fully plastic state. This is shown in Figure A-3.

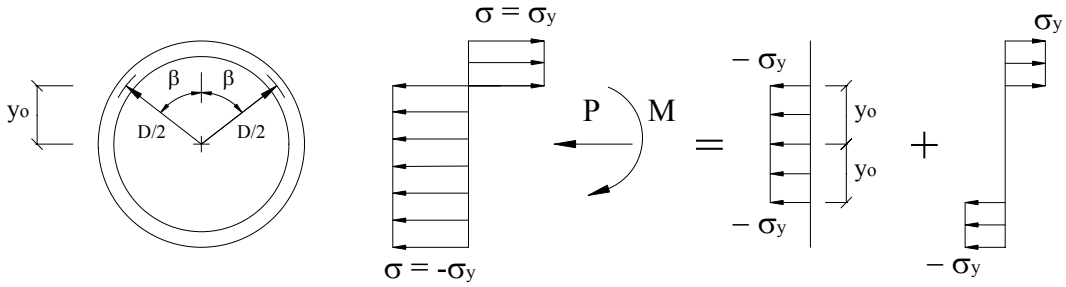

Figure A-3 Superposition of Bending and Axial Stress Distributions (Fully Plastic Yielding)

From the procedure used in determining the interaction equation for the onset of yielding the following expressions, which are restated for completeness of this section, have already been established:

$$P_y = A\sigma_y \tag{A-11}$$

$$M_p = D^2 t\sigma_y \tag{A-12}$$

The area of the ring above a height of y_0 from the center of the circle is defined in the following expression:

$$A_T = \beta Dt = \cos^{-1}\left(\frac{2y_o}{D}\right)Dt \tag{A-13}$$

where:

$$\beta = \cos^{-1}\left(\frac{2y_o}{D}\right) \tag{A-14}$$

Also, the centroid of this circular arc (above y_o) is located a distance y_b from the circle's center. The equation that provides this distance was used to determine y_b in (A-8) and is shown below.

$$y_b = \frac{r\sin(\beta)}{\beta} = \frac{D\sin\left(\cos^{-1}\left(\frac{2y_o}{D}\right)\right)}{2\cos^{-1}\left(\frac{2y_o}{D}\right)} \tag{A-15}$$

Therefore, the moment capacity of this section (accounting for the effect of axial load) is:

$$M = 2y_b A_T\sigma_y = \sigma_y D^2 t\sin\left(\cos^{-1}\left(\frac{2y_o}{D}\right)\right) \tag{A-16}$$

In dividing (A-16) by the expression for the plastic moment of the section, the following expression is defined:

$$\frac{M}{M_p} = \sin\left(\cos^{-1}\left(\frac{2y_o}{D}\right)\right) \tag{A-17}$$

Knowing that the axial force, P, is equal to the product of the yield stress, σ_y, and the area of the section that is considered to be resisting axial load (that which is within $\pm y_o$ of the circle's center) the following expression can be determined:

$$P = \sigma_y A_c = \sigma_y \left(A - 2A_T \right) = \sigma_y Dt \left[\pi - 2\cos^{-1}\left(\frac{2y_o}{D} \right) \right] \tag{A-18}$$

Dividing the expression for P shown in (A-18) by P_y the following expression is defined:

$$\frac{P}{P_y} = 1 - \frac{2}{\pi}\cos^{-1}\left(\frac{2y_0}{D} \right) \tag{A-19}$$

After rearranging (A-17) and plugging it into (A-19) the plastic interaction equation for this cross-section, which relates the interaction between axial force and bending moment to the fully yielded section, is shown to be the following:

$$\frac{P}{P_y} = 1 - \frac{2}{\pi}\sin^{-1}\left(\frac{M}{M_p} \right) \tag{A-20}$$

The resulting interaction curves are shown in Figure A-4:

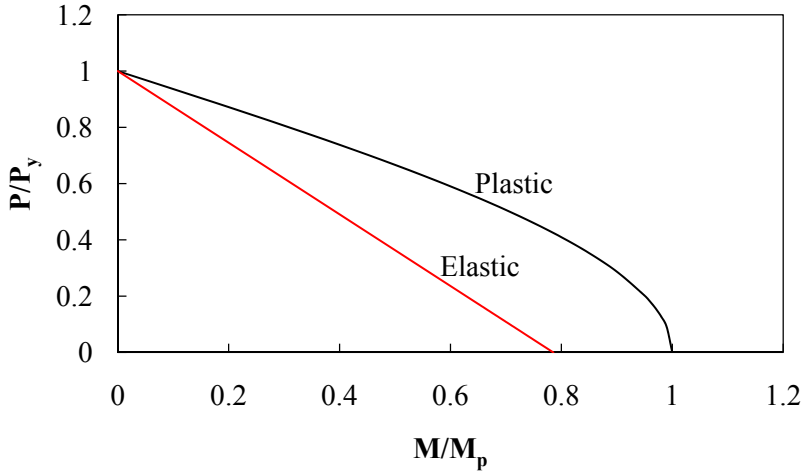

Figure A-4 Plot of Interaction Curves for a Thin Circular Tube

APPENDIX B

SIMPLIFIED SEISMIC ANALYSIS AND DESIGN WORKSHEETS

The worksheets provided in this appendix are those that were used in the iterative analysis and design procedure for the seismic hazard. These worksheets were used in conjunction with the nonlinear pushover results from SAP2000 (v11.0.0). Details regarding the following aspects of the analysis and design procedure are provided: load determination, pier geometry, member properties, pushover pattern, strip model development, and compactness checks.

Analysis and Design of a Box Steel Plate Shear Wall Pier for Bridge Applications

Basic Bridge Information

$L_{span1} := 124ft$ Length of bridge's first span

$L_{span2} := 152ft$ Length of bridge's second span

$L_{span3} := 124ft$ Length of bridge's third span

$L_{bridge} := L_{span1} + L_{span2} + L_{span3} = 400 \cdot ft$

$width_{bridge} := 68.5ft$ Width of Bridge in Transverse Direction

$N_{barriers} := 2$ Number of barriers on the bridge

$N_G := 8$ Number of Girders in Bridge Superstructure

$A_{g.pier} := 111.75in^2$ Cross-sectional area of girders over the piers

$A_{g.min} := 60in^2$ Cross-sectional area of girders at the minimum depth

$A_{g.ave} := 0.5 \cdot (A_{g.pier} + A_{g.min}) = 85.9 \cdot in^2$ Average cross-sectional area of bridge girders across the bridge

$\gamma_{conc} := 150 \frac{lbf}{ft^3}$ Unit Weight of RC

$\gamma_{steel} := 490 \frac{lbf}{ft^3}$ Unit Weight of Steel

Determine Dead Load - Estimate the Weight of the Bridge's Superstructure

$W_G := A_{g.ave} \cdot \gamma_{steel} \cdot N_G = 2.3 \cdot \frac{kip}{ft}$ Total weight of bridge's girders

$W_D := 8.16 \frac{kip}{ft}$ Bridge's deck and sidewalks

$W_{misc} := 3.69 \frac{kip}{ft}$ Weight of bridge's overlay, deck forms, barriers, and cross-frames/stiffeners

Total dead load of superstructure to be considered for seismic loading:

$W_{super} := (W_G + W_D + W_{misc}) \cdot L_{bridge}$ $\boxed{W_{super} = 5675.1 \cdot kip}$

Determine Dead Load - Estimate the Weight of the Bridge's Pier Caps

$V_{g.PierCap} := 5050.24ft^3 = 187 \cdot yd^3$ Volume of concrete for a single pier cap

$W_{PierCap} := V_{g.PierCap} \cdot \gamma_{conc}$ $\boxed{W_{PierCap} = 757.5 \cdot kip}$ Total Estimated Weight of a Pier Cap

Estimate Dead Load a Pier will be Required to Resist Between the Four VBEs

$P_{Pier.Dead} := \frac{W_{super}}{2L_{bridge}} \cdot (L_{span1} + L_{span2}) + W_{PierCap}$ $\boxed{P_{Pier.Col.Dead} := \frac{P_{Pier.Dead}}{4} = 678.9 \cdot kip}$

Site Seismic Characteristics & Seismic Forces (AASHTO - 4th ed.)

$A_s := 0.20$ Acceleration Coefficient

$IC := "Other"$ Importance Classification

$Type := "Regular"$ In addition to being an "Other" type of bridge, it is also a "Regular" bridge (Article 4.7.4.3 of AASHTO (2007))

$SZ := 3$ Seismic Zone based on the Acceleration Coefficient (0.19 < A < 0.29)

$S_{soil} := 1.2$ Site Coefficient based on the assumption of a Soil Profile of Type II for lack of better information

$R_{AASHTO} := 5$ Reduction Factor chosen for multiple column bents from Table 3.10.7.1-1 (AASHTO (2007))

Relationship Between Elastic Seismic Response Coefficient and Period

$$Transition_{Tm} := \left[\left(\frac{1.2}{2.5}\right)\cdot S_{soil}\right]^{\frac{3}{2}} s$$

$$T1F := 0, 0.001s .. Transition_{Tm}$$

$$T2F := Transition_{Tm}, Transition_{Tm} + 0.001s .. 3s$$

$$S_{cm1F}(T1F) := 2.5\cdot A_s$$

$$S_{cm2F}(T2F) := \frac{1.2\cdot A_s\cdot S_{soil}}{\left(T2F\cdot\frac{1}{s}\right)^{\frac{2}{3}}}$$

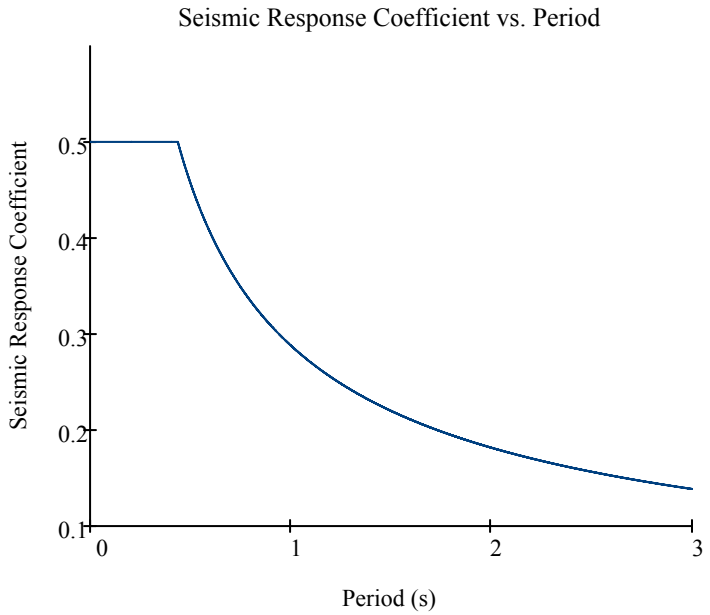

Determine the Elastic Seismic Coefficient

In order to obtain the seismic coefficient for a given direction the stiffness and thus the period in that direction must be known.

Exceptions: *As per Article 3.10.6.2 of AASHTO, for bridges on soil profiles III or IV and in areas where the coefficient A is not less than 0.30, C_{sm} need not exceed 2.0A. For soil profiles III and IV, and for modes other than the fundamental mode that have periods less than 0.3sec., C_{sm} shall be taken as $C_{sm} = A(0.8+4.0T_m)$. If the period of vibration for any mode exceeds 4.0sec., the value of C_{sm} for that mode shall be taken as $C_{sm}=3AS/T_m\text{^}(4/3)$*

Bridge Stiffness in the Transverse Direction:

$k_{trans} := 1240 \frac{kip}{in}$

$m_{trans} := \frac{1}{g} \cdot \left(W_{super} + 2 \cdot W_{PierCap}\right)$

Bridge Stiffness in the Longitudinal Direction:

$k_{long} := 1212 \frac{kip}{in}$

$m_{long} := \frac{1}{g} \cdot \left(W_{super} + 2 \cdot W_{PierCap}\right)$

Note: The mass of the steel plate assemblies (i.e. the piers) themselves have been neglected in the calculation of the mass.

$T_{trans} := 2 \cdot \pi \cdot \sqrt{\frac{m_{trans}}{k_{trans}}} = 0.77\,s$

$T_{long} := 2 \cdot \pi \cdot \sqrt{\frac{m_{long}}{k_{long}}} = 0.779\,s$

$C_{sm.trans} := \frac{1.2 \cdot A_s \cdot S_{soil}}{\left(T_{trans} \cdot \frac{1}{s}\right)^{\left(\frac{2}{3}\right)}}$

$C_{sm.long} := \frac{1.2 \cdot A_s \cdot S_{soil}}{\left(T_{long} \cdot \frac{1}{s}\right)^{\left(\frac{2}{3}\right)}}$

$C_{sm.trans} := \begin{cases} 2.5 \cdot A_s & \text{if } C_{sm.trans} > 2.5 \cdot A_s \\ C_{sm.trans} & \text{otherwise} \end{cases}$

$C_{sm.long} := \begin{cases} 2.5 \cdot A_s & \text{if } C_{sm.long} > 2.5 \cdot A_s \\ C_{sm.long} & \text{otherwise} \end{cases}$

$C_{sm.trans} = 0.343$

$C_{sm.long} = 0.34$

For multispan bridges that are classified as "Other" and are "Regular" (Article 4.7.4.3 of AASHTO) the Uniform Load Elastic Method of analysis is allowed in addition to the Single Mode Elastic Method. The Uniform Load Elastic Method shall be based on the fundamental mode of vibration in either the longitudinal or transverse direction.

Determine the Seismic Force on a Pier in both the Longitudinal & Transverse Direction

Equiv. Static **Transverse** Force on Superstructure

$V_{super.trans} := \frac{C_{sm.trans} \cdot W_{super}}{R_{AASHTO} \cdot L_{bridge}} \cdot \left(L_{span1} + 0.5 \cdot L_{span2}\right)$

$V_{super.trans} = 194.552 \cdot kip$

Equiv. Static **Transverse** Force on Pier Cap

$V_{PierCap.trans} := \frac{C_{sm.trans} \cdot W_{PierCap}}{R_{AASHTO}}$

$V_{PierCap.trans} = 51.94 \cdot kip$

Equiv. Static **Long.** Force on Superstructure

$$V_{super.long} := \frac{C_{sm.long} \cdot W_{super}}{2R_{AASHTO}}$$

$V_{super.long} = 193.08 \cdot kip$

Equiv. Static **Long.** Force on Pier Cap

$$V_{PierCap.long} := \frac{C_{sm.long} \cdot W_{PierCap}}{R_{AASHTO}}$$

$V_{PierCap.long} = 51.55 \cdot kip$

Material Properties

A500 Gr. B steel will be used for the VBE's & HBEs: $F_{ye} := 42 \cdot ksi$ $F_{ue} := 58 \cdot ksi$

A36 steel will be used for the web plates: $F_{yp} := 36 \cdot ksi$ $F_{up} := 58 \cdot ksi$

From the AISC seismic provisions (Table I-6-1): $R_{ye} := 1.4$ VBEs & HBEs

These "R" factors are the ratio of the expected yield stress to the minimum yield stress. $R_{yp} := 1.3$ Infill plate

Modulus of elasticity for steel: $E := 29000 \cdot ksi$

Steel Plate Shear Wall Design *(Transverse Direction)*

Steel Plate Shear Wall Geometry & Subsequent Design

Distance between HBE centerlines: $CtC_{HBE.t} := 92.27in$

Distance between VBE centerlines: $CtC_{VBE.t} := 146.00in$

According to Section 17.2b of the seismic provisions, the aspect ratio of the SPSW should be limited to $0.8 < L/h < 2.5$:

$$ratio_t := \frac{CtC_{VBE.t}}{CtC_{HBE.t}} \qquad Check_{R.t} := \begin{cases} \text{"OK"} & \text{if } ratio_t \geq 0.8 \wedge ratio_t \leq 2.5 \\ \text{"NG"} & \text{otherwise} \end{cases}$$

$Check_{R.t} = \text{"OK"}$

Relevant Section Properties for Boundary Elements:

Trial VBE: **24" x 1.812" Pipe**

$D_{o.vbe} := 24in$ $t_{vbe.wall} := 1.812in$ $D_{i.vbe} := D_{o.vbe} - 2 \cdot t_{vbe.wall} = 20.376 \cdot in$

$$A_{vbe} := \frac{\pi}{4} \cdot \left(D_{o.vbe}^{\ 2} - D_{i.vbe}^{\ 2} \right) \qquad A_{vbe} = 126.3 \cdot in^2$$

$$I_{vbe} := \frac{\pi}{64} \cdot \left(D_{o.vbe}^{\ 4} - D_{i.vbe}^{\ 4} \right) \qquad I_{vbe} = 7824.6 \cdot in^4$$

$$Z_{vbe} := \frac{1}{6} \cdot \left(D_{o.vbe}^{\ 3} - D_{i.vbe}^{\ 3} \right) \qquad Z_{vbe} = 894 \cdot in^3$$

$$\lambda_{vbe} := \frac{D_{o.vbe}}{t_{vbe.wall}} \qquad \lambda_{vbe} = 13.245$$

$$r_{vbe} := \sqrt{\frac{I_{vbe}}{A_{vbe}}} \qquad r_{vbe} = 7.871 \cdot in$$

Relevant Section Properties for the Horizontal Tubes in the Transverse Direction:

Trial Tube Size: **16" x 0.843" Pipe**

$D_{o.stiff.t} := 16in$ $t_{stiff.wall.t} := 0.843in$ $D_{i.stiff.t} := D_{o.stiff.t} - 2 \cdot t_{stiff.wall.t} = 14.314 \cdot in$

$$A_{stiff.t} := \frac{\pi}{4} \cdot \left(D_{o.stiff.t}^{2} - D_{i.stiff.t}^{2} \right) \qquad A_{stiff.t} = 40.1 \cdot in^2$$

$$I_{stiff.t} := \frac{\pi}{64} \cdot \left(D_{o.stiff.t}^{4} - D_{i.stiff.t}^{4} \right) \qquad I_{stiff.t} = 1156.3 \cdot in^4$$

$$Z_{stiff.t} := \frac{1}{6} \cdot \left(D_{o.stiff.t}^{3} - D_{i.stiff.t}^{3} \right) \qquad Z_{stiff.t} = 193.9 \cdot in^3$$

$$\lambda_{stiff.t} := \frac{D_{o.stiff.t}}{t_{stiff.wall.t}} \qquad \lambda_{stiff.t} = 18.98$$

$$r_{stiff.t} := \sqrt{\frac{I_{stiff.t}}{A_{stiff.t}}} \qquad r_{stiff.t} = 5.367 \cdot in$$

Relevant Section Properties for the Horizontal Tubes in the Longitudinal Direction:

Trial Tube Size: **12" x 0.50" Pipe**

$D_{o.stiff.L} := 12.75in$ $t_{stiff.wall.L} := 0.50in$ $D_{i.stiff.L} := D_{o.stiff.L} - 2 \cdot t_{stiff.wall.L} = 11.75 \cdot in$

$$A_{stiff.L} := \frac{\pi}{4} \cdot \left(D_{o.stiff.L}^{2} - D_{i.stiff.L}^{2} \right) \qquad A_{stiff.L} = 19.2 \cdot in^2$$

$$I_{stiff.L} := \frac{\pi}{64} \cdot \left(D_{o.stiff.L}^{4} - D_{i.stiff.L}^{4} \right) \qquad I_{stiff.L} = 361.5 \cdot in^4$$

$$Z_{stiff.L} := \frac{1}{6} \cdot \left(D_{o.stiff.L}^{3} - D_{i.stiff.L}^{3} \right) \qquad Z_{stiff.L} = 75.1 \cdot in^3$$

$$\lambda_{stiff.L} := \frac{D_{o.stiff.L}}{t_{stiff.wall.L}} \qquad \lambda_{stiff.L} = 25.5$$

$$r_{stiff.L} := \sqrt{\frac{I_{stiff.L}}{A_{stiff.L}}} \qquad r_{stiff.L} = 4.335 \cdot in$$

Determine a Plate Thickness Based on the Information Previously Provided:

Width of the plate, not clear distance between the tubes since the plate is connected tangentially to the VBEs: $L_{cVBE.t} := CtC_{VBE.t} = 12.167 \cdot ft$

Height of the plate, not clear distance between the tubes since the plate is connected tangentially to the HBEs: $L_{cHBE.t} := CtC_{HBE.t} = 7.689 \cdot ft$

Recall from the seismic analysis that the shear force applied to each pier in the transverse direction is: $V_{Pier.Trans} := V_{super.trans} + V_{PierCap.trans}$ $V_{Pier.Trans} = 246.5 \cdot kip$

Because there are two plates resisting seismic forces per pier, the plate shear force is as follows:

$$V_{Plate.Trans} := \frac{V_{Pier.Trans}}{2} \qquad V_{Plate.Trans} = 123.2 \cdot kip$$

As per Section 3.4.1 of the *AISC Steel Plate Shear Wall Design Guide*, the panel design shear strength is ϕV_n where $\phi = 0.90$ and $V_n = 0.42\, F_y\, t_w\, L_{cf} \sin 2\alpha$. Also, an initial angle of inclination for the tension field will initially be assumed, but must be checked.

Assumed angle of inclination of the tension field: $\alpha_t := 44.2deg$

Resistance factor for the SPSW: $\phi_v := 0.90$

$$t_{w.t} := \frac{V_{Plate.Trans}}{\phi_v \cdot L_{cVBE.t} \cdot 0.42 \cdot F_{yp} \cdot \sin\left(2 \cdot \alpha_t\right)} \qquad t_{w.t} = 0.0621 \cdot in$$

In reference to Table 7-2 of the SPSW Design Guide, say: $t_{w.t} := 0.0625in$

Using the guideline presented in AISC 341 (i.e. $I_c >= 0.00307 t_w * h^4/L$), the VBE's should have a minimum moment of inertia to provide adequate stiffness:

$$I_{c.min.t} := 0.00307 \cdot \frac{t_{w.t} \cdot CtC_{HBE.t}^{\,4}}{CtC_{VBE.t}} \qquad I_{c.min.t} = 95.3 \cdot in^4$$

$$Check_{I.vbe.t} := \begin{cases} \text{"OK"} & \text{if } I_{vbe} \geq I_{c.min.t} \\ \text{"NG"} & \text{otherwise} \end{cases} \qquad Check_{I.vbe.t} = \text{"OK"}$$

Using the guideline presented in the AISC Design Guide (i.e. $I_{HBE} >= 0.003\, \Delta t_w * L^4/h$), the HBE's should have a minimum moment of inertia to provide adequate stiffness:

$$I_{b.min.t} := 0.003 \cdot \frac{\Delta t_{w.t} \cdot CtC_{VBE.t}^{\,4}}{CtC_{HBE.t}} \qquad I_{b.min.t} = 0 \cdot in^4$$

$$Check_{I.hbe.t} := \begin{cases} \text{"OK"} & \text{if } I_{stiff.t} \geq I_{b.min.t} \\ \text{"NG"} & \text{otherwise} \end{cases} \qquad Check_{I.hbe.t} = \text{"OK"}$$

Compute the tension field angle and check the tension field angle that was assumed previously:

$$\alpha_t := \operatorname{atan}\left[\sqrt[4]{\frac{1 + \frac{t_{w.t}\cdot CtC_{VBE.t}}{2\cdot A_{vbe}}}{1 + t_{w.t}\cdot CtC_{HBE.t}\cdot\left(\frac{CtC_{HBE.t}^{3}}{360\cdot I_{vbe}\cdot CtC_{VBE.t}} + \frac{1}{A_{stiff.t}}\right)}}\right] \qquad \alpha_t = 44.2\cdot deg$$

Note that since essentially every "story" sees the same shear force due to the fact that the shear is applied at the top of the pier, and because every panel has the same dimensions, this tension field angle applies to every panel.

Compute the forces imposed on the boundary elements:

Note: These forces were one of the ways used to check SAP model

Distributed Loads on the HBE's from yielding of plate

$$\omega_{xB.t} := \frac{1}{2}\cdot R_{yp}\cdot F_{yp}\cdot t_{w.t}\cdot\sin\left(2\cdot\alpha_t\right) \qquad \omega_{xB.t} = 17.5\cdot\frac{kip}{ft}$$

$$\omega_{yB.t} := R_{yp}\cdot F_{yp}\cdot t_{w.t}\cdot\cos\left(\alpha_t\right)^2 \qquad \omega_{yB.t} = 18\cdot\frac{kip}{ft}$$

Distributed Loads on the VBE's from yielding of plate

$$\omega_{xC.t} := R_{yp}\cdot F_{yp}\cdot t_{w.t}\cdot\sin\left(\alpha_t\right)^2 \qquad \omega_{xC.t} = 17.1\cdot\frac{kip}{ft}$$

$$\omega_{yC.t} := \frac{1}{2}R_{yp}\cdot F_{yp}\cdot t_{w.t}\cdot\sin\left(2\cdot\alpha_t\right) \qquad \omega_{yC.t} = 17.5\cdot\frac{kip}{ft}$$

Strip Model Setup and Strip Dimensions For Transverse Wall Plates:

Length of a diagonal angled at -α from the vertical:

$$L_{\alpha.t} := CtC_{HBE.t}\cdot\sin(\alpha_t) + CtC_{VBE.t}\cdot\cos(\alpha_t) \qquad L_{\alpha.t} = 14.082\cdot ft$$

Number of Strips: $n_t := 10$

Perpendicular Strip Spacing: $s_{strip.t} := \frac{L_{\alpha.t}}{n_t}$ $s_{strip.t} = 1.408\cdot ft$

Strip Spacing in the x Direction (Along HBEs): $s_{x.t} := \frac{s_{strip.t}}{\cos(\alpha_t)}$ $s_{x.t} = 23.58\cdot in$

Half Spacing (Needed for Corners): $\frac{s_{x.t}}{2} = 11.79\cdot in$

Strip Spacing in the z Direction (Along VBEs): $s_{z.t} := \frac{s_{strip.t}}{\sin(\alpha_t)}$ $s_{z.t} = 24.228\cdot in$

Half Spacing (Needed for Corners): $\frac{s_{z.t}}{2} = 12.114\cdot in$

Strip cross sectional area:

NOTE: The area of each strip shall be the web thickness times these spacings. The figure below shows a general strip model setup and how the strips were spaced for the purpose of this study. Check to assure that the chosen number of strips is being provided.

Area of strips: $A_{strip.t} := t_{w.t}\cdot s_{strip.t}$ $A_{strip.t} = 1.056\cdot in^2$

Angle with horizontal:

$\alpha_{SAPModel.t} := 90deg - \alpha_t$

$\alpha_{SAPModel.t} = 45.776\cdot deg$

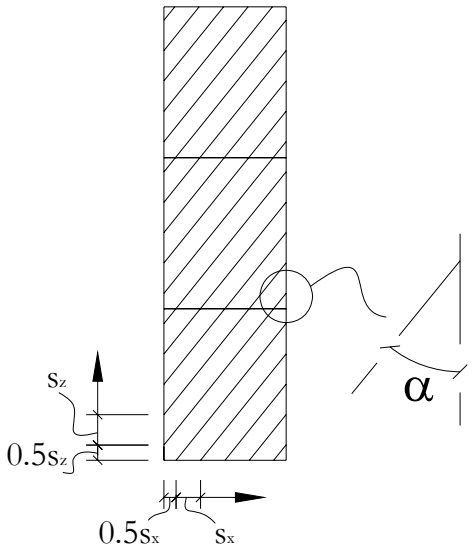

Compute the Normalized Forces Required for the Pushover Analysis

Transverse $P_{super.trans} := 0.5 \cdot V_{super.trans}$ $P_{PierCap.trans} := 0.5 \cdot V_{PierCap.trans}$

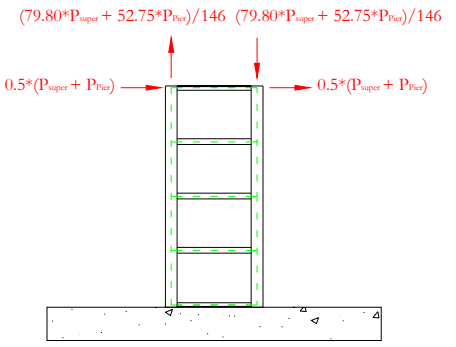

Horizontal Forces

$$P_{Horizontal.trans} := 0.5 \cdot \left(P_{super.trans} + P_{PierCap.trans}\right)$$

$$P_{Horizontal.trans} = 61.6 \cdot kip$$

Vertical Forces

$$P_{Vertical.trans} := \frac{1}{146} \cdot \left(79.80 P_{super.trans} + 52.75 P_{PierCap.trans}\right)$$

$$P_{Vertical.trans} = 62.6 \cdot kip$$

$$NormP_{H.trans} := \frac{P_{Horizontal.trans}}{P_{Horizontal.trans}} = 1$$

$$NormP_{V.trans} := \frac{P_{Vertical.trans}}{P_{Horizontal.trans}} = 1.015$$

Check the Compactness of the Sections

The AISC seismic provisions provide guidance as to how to limit the compactness of a round HSS steel section in axial and/or flexural compression. According to Table I-8-1, the limiting width to thickness ratio for a round HSS section is $0.044*E/F_y$.

Check the VBE:

$$Check_{vbe\lambda} := \begin{cases} \text{"OK"} & \text{if } \lambda_{vbe} \le 0.044 \cdot \frac{E}{F_{ye}} \\ \text{"NG"} & \text{otherwise} \end{cases}$$

$Check_{vbe\lambda} = \text{"OK"}$

Check the Horizontal Tubes in the Transverse Direction:

$$Check_{stiff.t.\lambda} := \begin{cases} \text{"OK"} & \text{if } \lambda_{stiff.t} \le 0.044 \cdot \frac{E}{F_{ye}} \\ \text{"NG"} & \text{otherwise} \end{cases}$$

$Check_{stiff.t.\lambda} = \text{"OK"}$

Check the Horizontal Tubes in the Longitudinal Direction:

$$Check_{stiff.L.\lambda} := \begin{cases} \text{"OK"} & \text{if } \lambda_{stiff.L} \le 0.044 \cdot \frac{E}{F_{ye}} \\ \text{"NG"} & \text{otherwise} \end{cases}$$

$Check_{stiff.L.\lambda} = \text{"OK"}$

Check the horizontal tube for required transverse stiffness

$h_t := CtC_{VBE.t} - D_{o.vbe}$ $a_t := CtC_{HBE.t}$ $j_t := 2.5 \cdot \left(\frac{h_t}{a_t}\right)^2 - 2$

$$j_t := \begin{cases} j_t & \text{if } j_t \ge 0.5 \\ 0.5 & \text{otherwise} \end{cases}$$

Thus: $I_{st.t} := a_t \cdot t_{w.t}^{3} \cdot j_t$

$$Check_{st.t} := \begin{cases} \text{"OK"} & \text{if } I_{stiff.t} \ge I_{st.t} \\ \text{"NG"} & \text{otherwise} \end{cases}$$

$Check_{st.t} = \text{"OK"}$

Steel Plate Shear Wall Design *(Longitudinal Direction)*

Steel Plate Shear Wall Geometry & Subsequent Design

Distance between HBE centerlines: $CtC_{HBE.L} := 92.27in$

Distance between VBE centerlines: $CtC_{VBE.L} := 74.00in$

According to Section 17.2b of the seismic provisions the aspect ratio of the SPSW should be limited to $0.8 < L/h < 2.5$:

$$ratio_L := \frac{CtC_{VBE.L}}{CtC_{HBE.L}} \qquad Check_{R.L} := \begin{cases} \text{"OK"} & \text{if } ratio_L \geq 0.8 \wedge ratio_L \leq 2.5 \\ \text{"NG"} & \text{otherwise} \end{cases}$$

$Check_{R.L} = \text{"OK"}$

Relevant Section Properties for Boundary Elements:

Use the same structural members as listed previously in this worksheet. Accordingly, if the members were shown to be seismically compact previously then they will still be seismically compact and don't have to be checked again.

Determine a Plate Thickness Based on the Information Previously Provided:

Width of the plate, not clear distance between the tubes since the plate is connected tangentially to the VBEs: $L_{cVBE.L} := CtC_{VBE.L} = 6.167 \cdot ft$

Height of the plate, not clear distance between the tubes since the plate is connected tangentially to the HBEs: $L_{cHBE.L} := CtC_{HBE.L} = 7.689 \cdot ft$

Recall from the seismic analysis that the shear force applied to each pier in the longitudinal direction is:

$$V_{Pier.long} := V_{super.long} + V_{PierCap.long} \qquad V_{Pier.long} = 244.6 \cdot kip$$

Because there are two plates resisting seismic forces per pier, the plate shear force is the following:

$$V_{Plate.long} := \frac{V_{Pier.long}}{2} \qquad V_{Plate.long} = 122.3 \cdot kip$$

As per Section 3.4.1 of the *AISC Steel Plate Shear Wall Design Guide* the panel design shear strength is ϕV_n where $\phi = 0.90$ and $V_n = 0.42\, F_y\, t_w\, L_{cf} \sin 2\alpha$. Also, an initial angle of inclination for the tension field will initially be assumed, but must be checked.

Assumed angle of inclination of the tension field: $\alpha_L := 41.7deg$

Resistance factor for the SPSW: $\phi_v := 0.90$

$$t_{w.L} := \frac{V_{Plate.long}}{\phi_v \cdot L_{cVBE.L} \cdot 0.42 \cdot F_{yp} \cdot \sin(2 \cdot \alpha_L)} \qquad t_{w.L} = 0.122 \cdot in$$

In reference to Table 7-2 of the SPSW Design Guide, say: $t_{w.L} := 0.125in$

Using the guideline presented in AISC 341 (i.e. $I_c >= 0.00307 t_w * h^4/L$), the VBE's should have a minimum moment of inertia to provide adequate stiffness:

$$I_{c.min.L} := 0.00307 \cdot \frac{t_{w.L} \cdot CtC_{HBE.L}^{4}}{CtC_{VBE.L}} \qquad I_{c.min.L} = 375.9 \cdot in^4$$

$$Check_{I.vbe.L} := \begin{cases} \text{"OK"} & \text{if } I_{vbe} \geq I_{c.min.L} \\ \text{"NG"} & \text{otherwise} \end{cases}$$

$Check_{I.vbe.L} = \text{"OK"}$

Using the guideline presented in the AISC Design Guide (i.e. $I_{HBE} >= 0.003\ \Delta t_w * L^4/h$), the HBE's should have a minimum moment of inertia to provide adequate stiffness:

$$I_{b.min.L} := 0.003 \cdot \frac{\Delta t_{w.L} \cdot CtC_{VBE.L}^{4}}{CtC_{HBE.L}} \qquad I_{b.min.L} = 0 \cdot in^4$$

$$Check_{I.hbe.L} := \begin{cases} \text{"OK"} & \text{if } I_{stiff.L} \geq I_{b.min.L} \\ \text{"NG"} & \text{otherwise} \end{cases}$$

$Check_{I.hbe.L} = \text{"OK"}$

Compute the tension field angle and check the tension field angle that was assumed before:

$$\alpha_L := \operatorname{atan}\left[\sqrt[4]{\frac{1 + \frac{t_{w.L} \cdot CtC_{VBE.L}}{2 \cdot A_{vbe}}}{1 + t_{w.L} \cdot CtC_{HBE.L} \cdot \left(\frac{CtC_{HBE.L}^{3}}{360 \cdot I_{vbe} \cdot CtC_{VBE.L}} + \frac{1}{A_{stiff.L}}\right)}}\right]$$

$\alpha_L = 41.7 \cdot deg$

Note that since every "story" sees the same shear force due to the fact that the shear is applied at the top of the pier, and because every panel has the same dimensions this tension field angle applies to every panel.

Strip Model Setup and Strip Dimensions For Longitudinal Wall Plate:

Length of a diagonal angled at -α from the vertical:

$$L_{\alpha.L} := CtC_{HBE.L}\cdot\sin(\alpha_L) + CtC_{VBE.L}\cdot\cos(\alpha_L) \qquad L_{\alpha.L} = 9.72\cdot ft$$

Number of Strips: $n_L := 11$

Perpendicular Strip Spacing: $s_{strip.L} := \frac{L_{\alpha.L}}{n_L}$ $\qquad s_{strip.L} = 0.884\cdot ft$

Strip Spacing in the x Direction (Along HBEs): $s_{x.L} := \frac{s_{strip.L}}{\cos(\alpha_L)}$ $\qquad s_{x.L} = 14.203\cdot in$

Half Spacing (Needed for Corners): $\frac{s_{x.L}}{2} = 7.102\cdot in$

Strip Spacing in the z Direction (Along VBEs): $s_{z.L} := \frac{s_{strip.L}}{\sin(\alpha_L)}$ $\qquad s_{z.L} = 15.936\cdot in$

Half Spacing (Needed for Corners): $\frac{s_{z.L}}{2} = 7.968\cdot in$

Strip cross sectional area:

NOTE: The area of each strip shall be the web thickness times these spacings. The figure below shows a general strip model setup and how the strips were spaced for the purpose of this study. Check to assure that the chosen number of strips is being provided.

Area of strips: $A_{strip.L} := t_{w.L}\cdot s_{strip.L}$ $\qquad A_{strip.L} = 1.325\cdot in^2$

Angle with horizontal:

$\alpha_{SAPModel.L} := 90deg - \alpha_L$

$\alpha_{SAPModel.L} = 48.291\cdot deg$

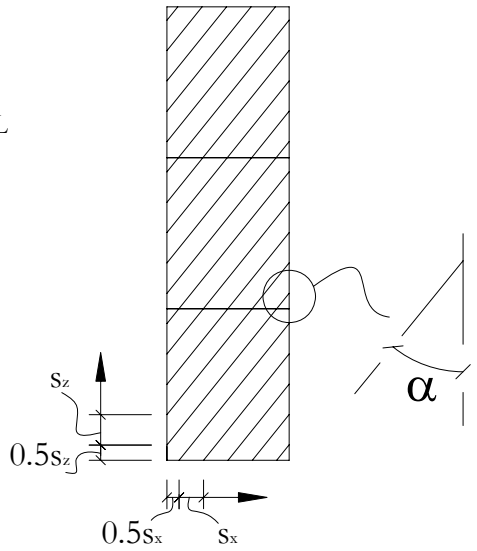

Compute the Normalized Forces Required for the Pushover Analysis

Longitudinal $P_{super.long} := 0.5 \cdot V_{super.long}$ $P_{PierCap.long} := 0.5 \cdot V_{PierCap.long}$

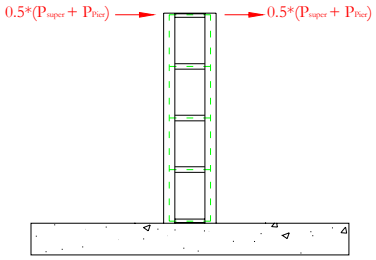

Horizontal Forces

$P_{Horizontal.long} := 0.5 \cdot \left(P_{super.long} + P_{PierCap.long}\right)$

$P_{Horizontal.long} = 61.2 \cdot kip$

Vertical Forces

$P_{Vertical.long} := 0$

$P_{Vertical.long} = 0 \cdot kip$

$NormP_{H.long} := \frac{P_{Horizontal.long}}{P_{Horizontal.long}} = 1$

$NormP_{V.long} := \frac{P_{Vertical.long}}{P_{Horizontal.long}} = 0$

Compute the forces imposed on the boundary elements:

Note: These forces were one of the ways used to check SAP model

Distributed Loads on the HBE's from yielding of plate

$\omega_{xB.L} := \frac{1}{2} \cdot R_{yp} \cdot F_{yp} \cdot t_{w.L} \cdot \sin\left(2 \cdot \alpha_L\right)$ $\omega_{xB.L} = 34.9 \cdot \frac{kip}{ft}$

$\omega_{yB.L} := R_{yp} \cdot F_{yp} \cdot t_{w.L} \cdot \cos\left(\alpha_L\right)^2$ $\omega_{yB.L} = 39.1 \cdot \frac{kip}{ft}$

Distributed Loads on the VBE's from yielding of plate

$\omega_{xC.L} := R_{yp} \cdot F_{yp} \cdot t_{w.L} \cdot \sin\left(\alpha_L\right)^2$ $\omega_{xC.L} = 31.1 \cdot \frac{kip}{ft}$

$\omega_{yC.L} := \frac{1}{2} R_{yp} \cdot F_{yp} \cdot t_{w.L} \cdot \sin\left(2 \cdot \alpha_L\right)$ $\omega_{yC.L} = 34.9 \cdot \frac{kip}{ft}$

Check the horizontal tube for required transverse stiffness

$h_L := CtC_{VBE.L} - D_{o.vbe}$ $a_L := CtC_{HBE.L}$ $j_L := 2.5 \cdot \left(\frac{h_L}{a_L}\right)^2 - 2$

$j_L := \begin{cases} j_L & \text{if } j_L \geq 0.5 \\ 0.5 & \text{otherwise} \end{cases}$

Thus, $I_{st.L} := a_L \cdot t_{w.L}^{\ 3} \cdot j_L$

$Check_{st.L} := \begin{cases} \text{"OK"} & \text{if } I_{stiff.L} \geq I_{st.L} \\ \text{"NG"} & \text{otherwise} \end{cases}$

$Check_{st.L} = \text{"OK"}$

APPENDIX C

FIBER HINGE STUDY

C.1 General

The subsequent discussion provides a short study of the fiber hinge available for use in SAP2000, and verifies that the hinge provides the desirable ultimate behavior sought for this study. Moreover, this study investigated how the hinge's behavior was affected by the number of fibers used in defining the hinge, which was accomplished by comparing the hinge's ultimate behavior to the interaction curve derived for a fully yielded cross-section (see Appendix A).

The "Fiber P-M2-M3 Hinge" models member cross-sectional behavior by using the axial behavior of a number of fibers placed at specified locations in the cross-section of a given frame element. If the hinge model is manually created, rather than taking one that is automatically generated by SAP, each fiber is assigned a tributary area and a stress-strain curve by the user. Figure C-1 illustrates a fiber hinge applied to a circular tube's cross-section, where each of the fibers is placed at the center of the tube's wall, and where each fiber is assigned its own stress-strain behavior. As shown in Figure C-1, the stress-strain behavior was considered elastic-perfectly plastic for tension and compression.

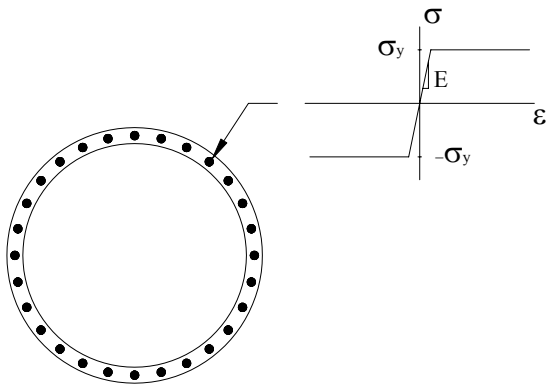

Figure C-1 Fiber Hinge in a Circular Tube

C.2 Study Set-up and Results

The structure used in the study is illustrated in Figure C-2. The structure was chosen to be a vertical cantilever as this made the determination of reactions, which will be related to the behavior of the hinge, a simple task.

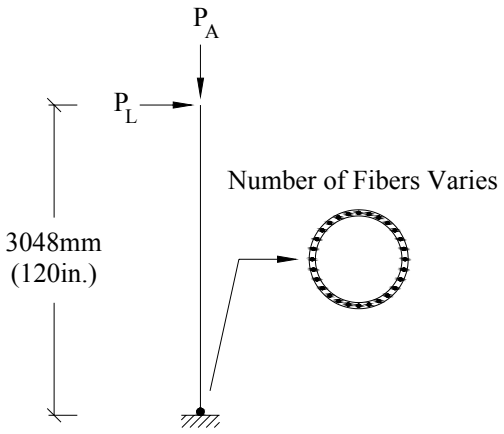

Figure C-2 Fiber Hinge Study Structure

The section chosen was a tube with an outer diameter of 559mm (22 in) and a wall thickness of 47.6mm (1.875 in), and the height of the tube was arbitrarily chosen to be 3048mm (120 in). The self-weight of the vertical tube was set to zero and the hinge length was chosen to be sufficiently small so that it was essentially a point hinge located at the fixed support (it was observed that the hinge length did not affect the ultimate capacity). Each of the fibers was assigned material with a yield strength, $\pm \sigma_y$, of 290MPa (42 ksi). Four different hinges were evaluated: one that used a total of 12 fibers, one a total of 20 fibers, one a total of 28 fibers, and one a total of 36 fibers. For each hinge, six axial load/lateral load combinations were used in nonlinear static pushover analyses. The axial load, P_A, was held constant as the structure was pushed by the lateral load, P_L, until the structure could no longer resist lateral load. The moment in the hinge was then found by multiplying the maximum lateral load by the member's height. The axial load was divided by the axial yielding strength of the section, $\sigma_y A$, to obtain P/P_y. Similarly, the moment at the member's base was divided by the member's plastic moment to obtain M/M_p. These two ratios were obtained for each of the axial load/lateral load combinations, for each hinge and were superimposed on the graph showing the interaction curves derived in Appendix A. Table C-1 displays the results of the study.

Table C-1 Results of Fiber Hinge Study

	M/M_p			
P/P_y	36 Fibers	28 Fibers	20 Fibers	12 Fibers
0.0	0.995	0.993	0.989	0.974
0.2	0.947	0.948	0.941	0.948
0.4	0.807	0.804	0.800	0.791
0.6	0.586	0.584	0.581	0.578
0.8	0.307	0.308	0.306	0.306
1.0	0.000	0.000	0.000	0.000

A plot of the results is provided in Figure C-3. It is important to realize the findings of this investigation. From this figure, it can be seen that the fiber hinge's ultimate behavior agrees well with the interaction equation derived using plastic analysis. The only significant deviation of the fiber hinge's behavior from the plastic interaction curve is when the axial load is zero, at which point the 12 fiber hinge deviates the most. Regardless, this investigation confirms the behavior of the fiber hinge to be satisfactory for the purpose of this study. With as few as 12 fibers composing the hinge, the behavior of the hinge in a circular tube provides desirable ultimate behavior.

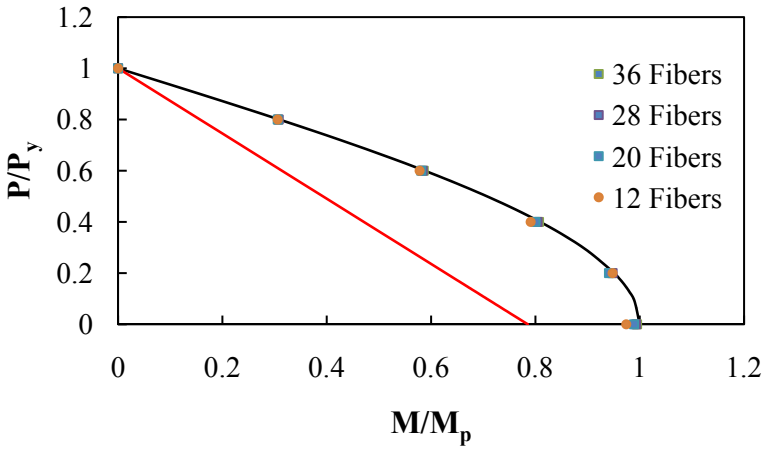

Figure C-3 Results of the Study

A second tube size that had an outer diameter of 219mm (8.625 in) and a wall thickness of 12.7mm (0.5 in) was also investigated and was found to produce results identical to those displayed in Figure C-3.

APPENDIX D

TORSION EFFECTS ON VBES

D.1 General

In the simplified analysis and design of the proposed pier system, torsion resulting from attaching the plates tangentially to the VBEs was assumed to be negligible compared to the capacity of the tubes. This appendix provides a short study looking at the effect of a yielding plate producing torsion on a round tube, and discusses how the induced torsion compares to the capacity of the section chosen for the final pier design.

D.2 Study Setup

The general study setup is as shown in Figure D-1. Figure D-1(a) shows the plate forces acting on the cross-section, neglecting any contribution from perpendicular plates. The horizontal component of the distributed force from plate yielding, F_D, is shown to be acting tangentially at the VBE's outer surface. The other two forces shown represent this force broken into an equivalent system of forces acting at the centerline of the VBE. To maintain that the sum of the forces in the lateral direction remains the same in the equivalent system the distributed force from plate yielding, F_D, is repositioned to the center of the section. Similarly, to maintain the sum of moments about the centerline of the VBE to be the same between the equivalent system and the actual system of forces, a distributed moment (or torque), T_D, acts about the centerline of the VBE. Since this study investigated the effect of torque on the VBE, the distributed torque will be the focus for the remainder of this appendix. The scenario to be studied is shown in Figure D-1(b), where the torsion reactions required for equilibrium are defined as T_R. From the internal torsion force distribution shown in Figure D-1(c) it can be seen that T_R will produce the greatest torsion stresses.

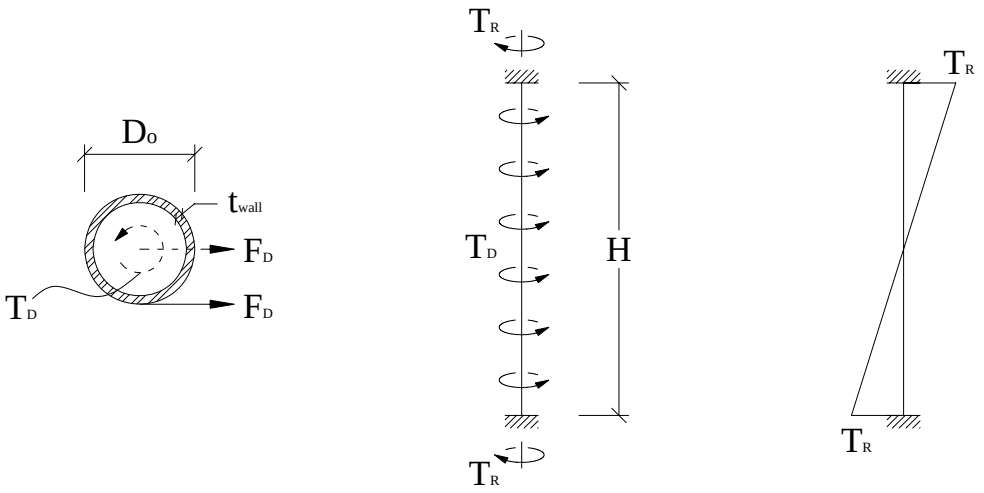

Figure D-1 Torsion Study Setup: (a) Forces Acting on the Cross-Section; (b) the Study Structure, and; (c) the Internal Torsion Force Diagram

From the AISC SPSW Design Guide (Sabelli and Bruneau 2006) the lateral component of the distributed force arising from plate yielding is given by (D-1), where the angle α is measured from the vertical, and where $R_y\sigma_y$ will be for A36 steel.

$$F_D = R_y \sigma_y t_w \sin^2 \alpha \tag{D-1}$$

Knowing the distributed force on the VBE from a yielding plate and the eccentricity at which it acts, (D-2) can be used to compute the distributed torque on the VBE, where t_w is the thickness of the plate. Note that the distributed force is considered as acting at the centerline of the plate.

$$T_D = \frac{(D_o + t_w)}{2} F_D = \frac{(D_o + t_w)}{2} R_y \sigma_y t_w \sin^2 \alpha \tag{D-2}$$

From statics, the torsion reaction can be determined from the relationship shown by (D-3).

$$T_R = T_D \frac{H}{2} = \frac{(D_o + t_w)H}{4} R_y \sigma_y t_w \sin^2 \alpha \tag{D-3}$$

According to the AISC Steel Construction Manual (AISC-LRFD Eq. H3-1) the nominal torsion resistance of a round HSS is $\phi_T T_n = \phi_T F_{cr} C$, where F_{cr} is given by (D-4) (AISC-LRFD Eq.H3-2a - Eq.H3-2b) and C is given by (D-5). Since the design of this pier system considers ultimate capacity, the strength reduction factor was set to unity.

$$F_{cr} = \max\left[\frac{1.23E}{\sqrt{\frac{H}{D_o}}\left(\frac{D_o}{t_{wall}}\right)^{5/4}}, \frac{0.60E}{\left(\frac{D_o}{t_{wall}}\right)^{3/2}}\right] \leq 0.6\sigma_{y(tube)} \quad \text{(D-4)}$$

$$C = \frac{\pi\left(D_o - t_{wall}\right)^2 t_{wall}}{2} \quad \text{(D-5)}$$

Moreover, the AISC-LRFD manual, Section H3.2, states that torsion effects can be neglected when $T_u / \phi_T T_n \leq 0.20$.

D.3 Study Summary and Results

The study presented in this appendix investigated torsion effects on the VBE section chosen for the final design. Accordingly, the section chosen for the study was a round tube having an outer diameter equal to 610mm (24 in) and a wall thickness of 46mm (1.812 in). From (D-3) it can be determined that the torsion demand on the member increases as the height increases. Also, as the tension field angle and the plate thickness vary, the torsion demand on the VBE is affected. To capture these variations, two plate thicknesses were investigated; one that was 3.175mm (0.125 in) thick and one that was 1.588mm (0.0625 in) thick. The bounds of the typical range for inclination angle, as stated in the AISC SPSW Design Guide, were considered for the tension field angle; the inclination angles considered were 30˚ and 55˚.

Figure D-2 displays the results of the study with a plot of torsion demand-capacity ratio versus the height of the tube. The range of height increases from zero to 9144mm (360 in), which is close to the total height of the pier. From this plot, it is evident that the torsion demand, when compared to the capacity of the section, is negligible. The worst case for each plate thickness occurs for larger inclinations of the tension field; in this instance, the worst case is with an inclination angle of 55˚. This plot shows that for a free-standing VBE with a 3.175mm (0.125 in) fully yielded plate attached to it, and with a tension field inclination of 55˚, the torsion would be negligible up to a height of 7400mm.

In the final design, the tension field is somewhere between these bounds. Also, there is another plate, oriented perpendicularly, that is attached tangentially to the same VBE, which would resist some of the torsion demand on the VBE. Moreover, recall that there are HBEs spaced at approximately 2344mm which would provide significant relief of the torsion demand on the VBE. Therefore, as expected, it was appropriate to neglect torsion effects from the plate being connected tangentially to the VBEs.

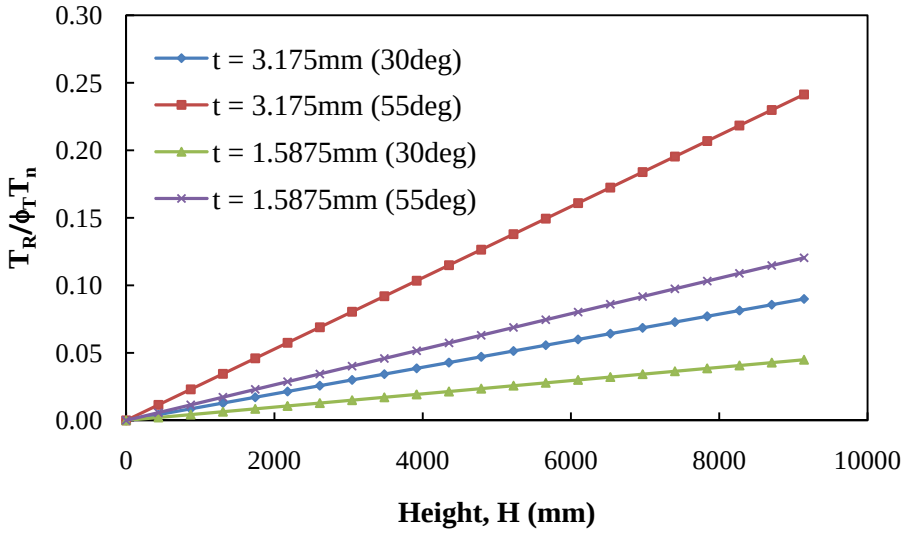

Figure D-2 Torsion Demand-Capacity Ratio vs. Height

APPENDIX E

COMPARISON OF SIMPLIFIED PLATE ANALYSIS WITH FINITE ELEMENT PREDICTIONS

E.1 General

In the simplified analysis and design of the proposed pier system, for loads that are applied normal to the plates, a simplified method was employed to gain a preliminary understanding of the plates' behavior and to determine the corresponding forces transferred to the boundary frame. To compare this method with finite element (FE) analyses, the two plates used in the proposed pier system were modeled using ABAQUS/CAE (v6.5-1). One model (Section E.2.1) represents the longitudinal plate of the pier. It has dimensions of 74in x 92.27in and a thickness of 0.125 in. The second model (Section E.2.2) represents the pier's transverse plate. It has dimensions of 146in x 92.27in and a thickness of 0.0625 in. These sections present a comparison between each plate's load versus displacement behavior, as obtained from FE analyses and the simplified method, assuming elastic-perfectly plastic material, with a yield stress of 36ksi. Additionally, a comparison of the edge reactions obtained with the simplified method and with the FE models is made. Section E.3 offers a summary of observations.

E.2 Study Setup and Results

E.2.1 Longitudinal Plate

The finite element model of the longitudinal plate is shown in Figure E-1. The plate was meshed with the structured meshing technique available in ABAQUS/CAE. The elements used to mesh the plate were S4R elements, which are 4-noded doubly curved general-purpose shell elements with reduced integration. Each node of this element contains six degrees of freedom.

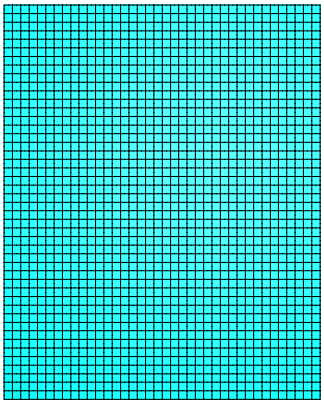

Figure E-1 Longitudinal Plate Mesh

To look at the influence of boundary conditions on the plate, two sets of edge boundary conditions were investigated (pinned and fixed). This plate was subjected to uniform loading twice, once considering pinned edges and once considering fixed edges. Figure E-2 provides the resulting behavior of the plate. This plot displays the uniform pressure required to displace the center of the plate a specified amount. This figure also shows a plot of the prediction made using the simplified method. The two FE analyses (one with pinned edges and one with fixed edges) are labeled "Pinned Edges" and "Fixed Edges".

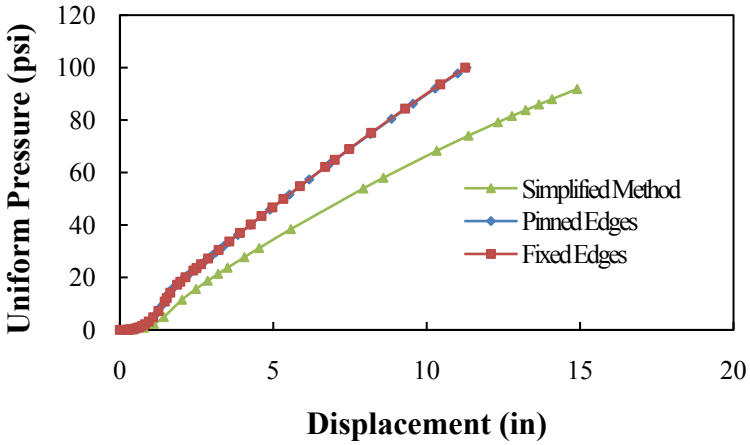

Figure E-2 Pressure vs. Displacement Comparison Between Finite Element Modeling and Simplified Method (Longitudinal Plate)

This figure shows the simplified method to follow the general behavior of that obtained from the finite element models. However, with increasing uniform pressure, the simplified method increasingly overestimates the displacement at the plate's center. Also, from this figure, it is evident that the difference in behavior between the case where the edges of the plate are pinned

and where the edges are fixed is essentially the same, which was expected considering the plate thickness relative to the plate size.

The reaction forces the plate will impose on the boundary frame were also investigated. Figure E-3 shows such reactions along the plate's vertical and horizontal edges. These distributions represent edge reactions for a pinned plate that is loaded with a uniform pressure of 5 psi, which results in a center displacement of 1.1 in. The curved distributions represent those obtained from finite element analysis, and the distributions with constant magnitude are those obtained with the simplified method. Note that reactions obtained from the finite element analysis were computed by dividing the edge node reactions by their tributary edge width.

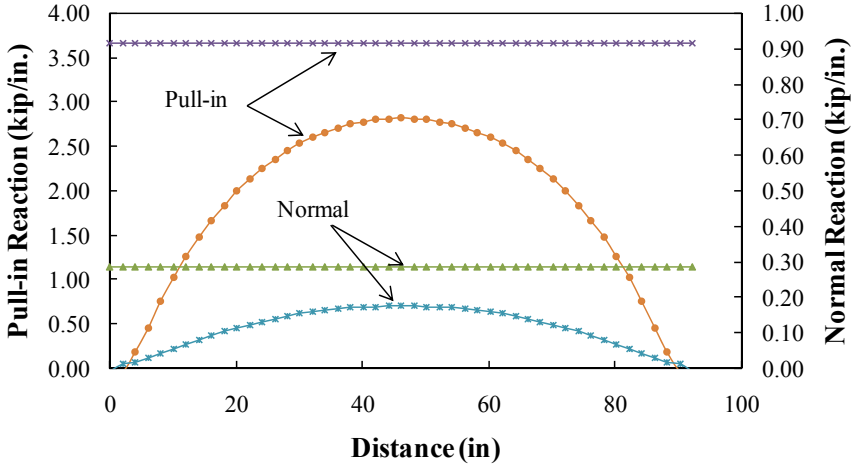

(a)

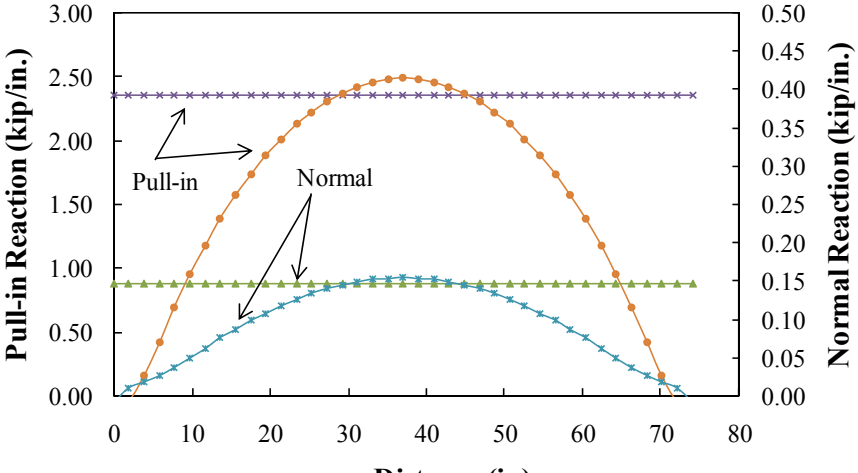

(b)

Figure E-3 Plate Edge Reactions: (a) along the Vertical Edge, and; (b) along the Horizontal Edge

The plate was also subjected to a uniform pressure of 50 psi, which produced a 5.4 in center displacement. Figure E-4 shows the edge reaction distributions for this case, where the FE plate reactions were computed in the same manner as those in Figure E-3.

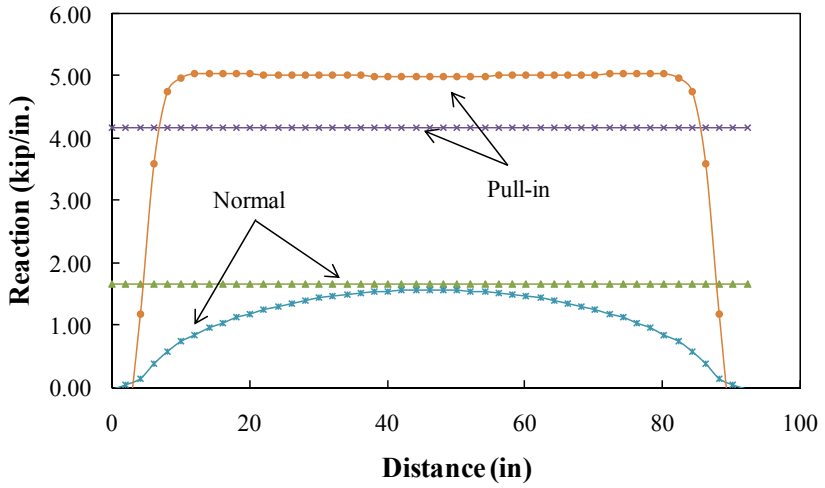

(a)

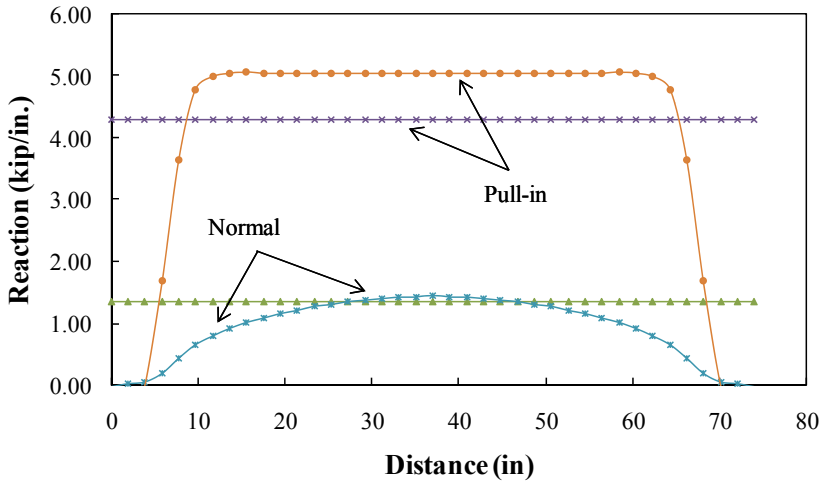

(b)

Figure E-4 Plate Edge Reactions: (a) along the Vertical Edge, and; (b) along the Horizontal Edge

From this figure, inelastic behavior of the plate is evident from the somewhat constant edge reactions in the middle of the plate. Also, from this figure it is evident that the peak normal reactions predicted by the simplified method are reasonably close to those obtained using finite element analysis. The pull-in edge reactions predicted by the simplified method, however, underestimate the reactions.

E.2.2 Transverse Plate

The second plate investigated was the transverse plate. The finite element model of it is shown in Figure E-5. The plate was meshed in the same way as the longitudinal plate, and it was meshed with the same of element.

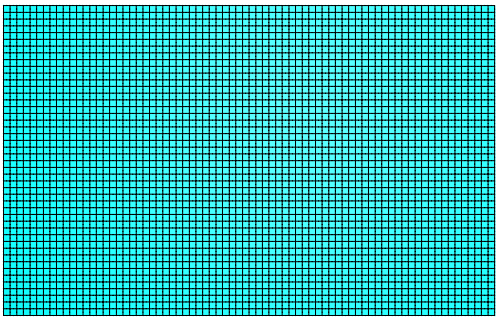

Figure E-5 Transverse Plate Mesh

In the same way that the longitudinal plate was investigated, pinned and fixed boundary conditions were assigned to the edges of the plate. Figure E-6 provides the resulting behavior of the plate for both cases. This plot displays the uniform pressure required to displace the center of the plate a specified amount, the FE results being labeled as "Pinned Edges" and "Fixed Edges." This figure also shows a plot of the predictions made using the simplified method. The results are similar to those seen with the longitudinal plate. The simplified method follows the general trend in behavior of the plate but deviates increasingly with increasing pressure.

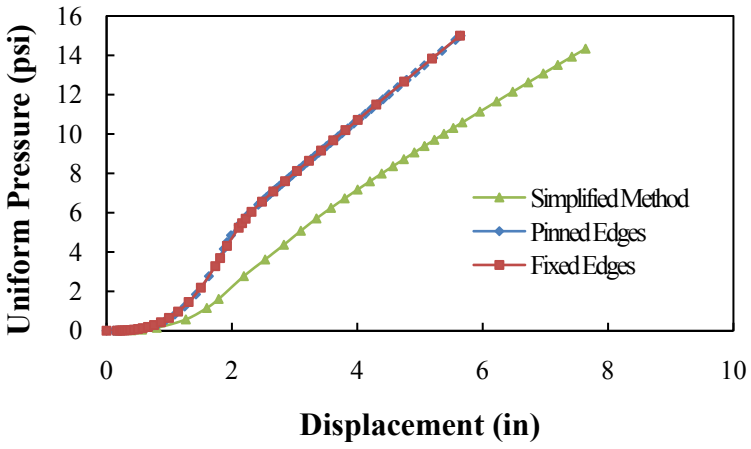

Figure E-6 Pressure vs. Displacement Comparison Between Finite Element Modeling and Simplified Method (Transverse Plate)

One analysis that was conducted on this plate to investigate the plate edge reactions (for the plate having pinned edges) considered a uniform pressure of 0.5 psi, which resulted in a center displacement of approximately 1 in. The resulting FE plate edge reaction distributions (calculated the same way as those in Section E.2.1) are provided in Figure E-7. It is evident from this figure that the simplified method underestimates the distribution of reactions along the vertical edges of the plate and overestimates the reaction forces of the horizontal edges of the plate.

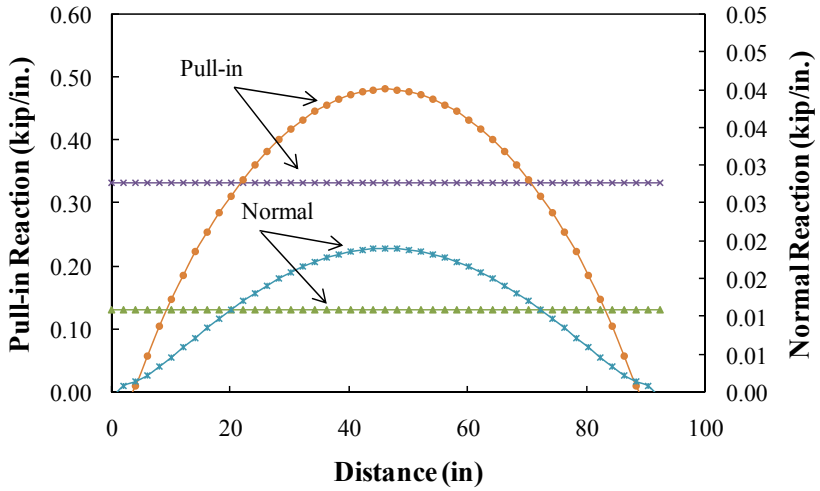

(a)

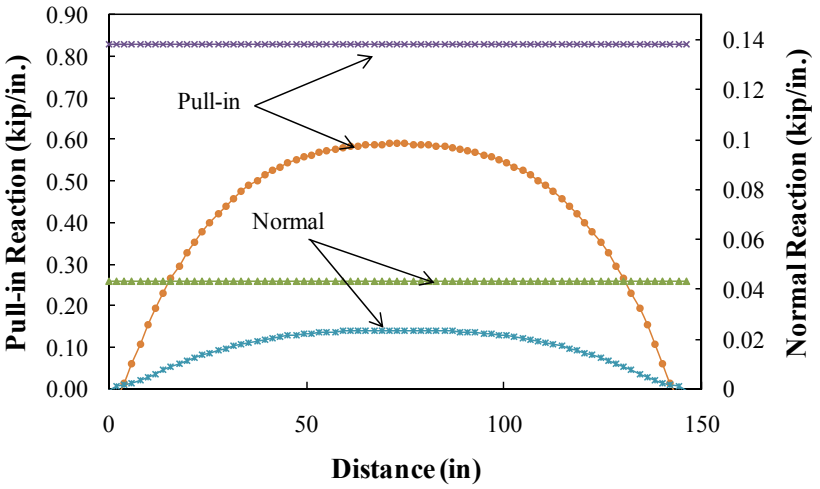

(b)

Figure E-7 Plate Edge Reactions: (a) along the Vertical Edge, and; (b) along the Horizontal Edge

The plate was also subjected to a uniform pressure of 8 psi, which produced an approximately 3 in center displacement. Figure E-8 shows the edge reaction distributions for this case. Again, it is evident that the simplified method predicts the normal edge reactions obtained from the finite element analysis reasonably well. However, the simplified analysis underestimates the pull-in edge reaction forces, as was seen with the longitudinal plate.

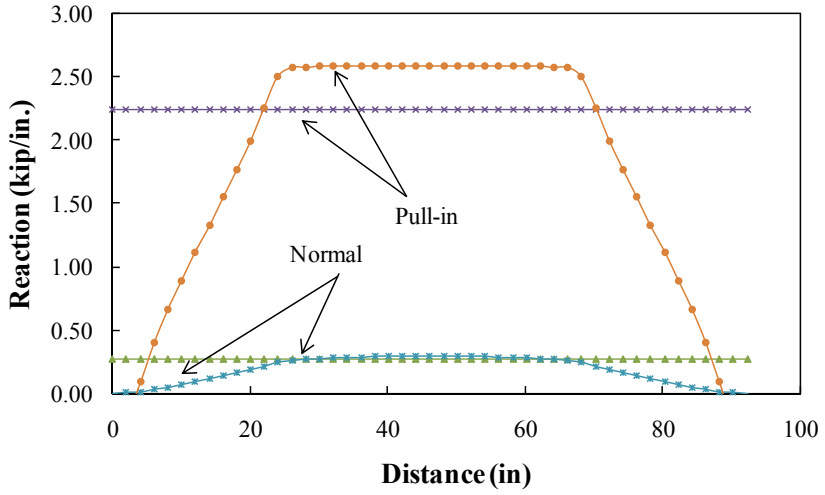

(a)

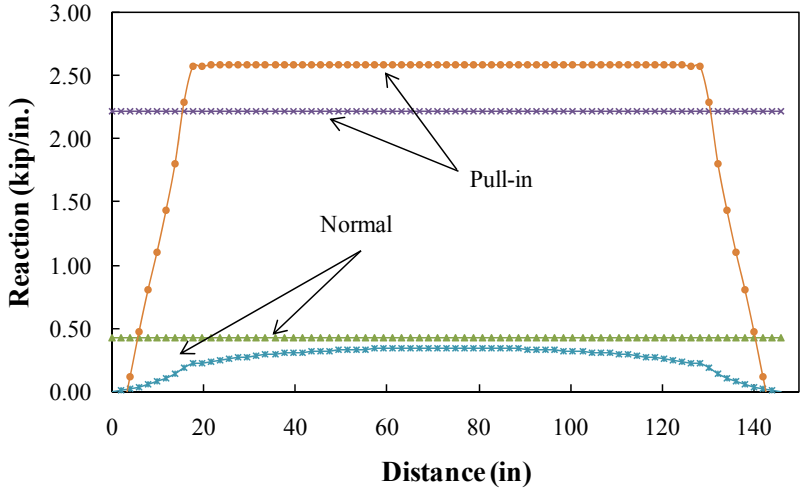

(b)

Figure E-8 Plate Edge Reactions: (a) along the Vertical Edge, and; (b) along the Horizontal Edge

E.3 Summary of Observations

When in the elastic region, the simplified method appears to predict the peak vertical and horizontal edge reactions of the longitudinal plate reasonably well. When the plate is pushed further into the inelastic range, the normal component calculated by the simplified method approximates the peak normal reactions obtained from the FE analysis well. The pull-in reaction forces, however, were found to differ from those obtained from the FE analysis.

The behavior of the transverse plate showed similar results regarding its edge reactions. For the case where the plate was loaded with 0.5 psi, the simplified method was shown to underestimate the peak distributed edge reaction obtained with FE analysis along the vertical (short) edge of the plate. Albeit small, this underestimation was seen with the horizontal (short) edge of the longitudinal plate. Along the horizontal (long) edge of the transverse plate, however, the simplified analysis method overestimated the peak reactions similar to the vertical (long) edge reactions of the longitudinal plate, which were overestimated. This trend shows that when the plates are near elastic in behavior the simplified method of analysis seems to overestimate the edge reactions along the long edges and underestimate the edge reactions along the short edges of the plate; although there are relatively small deviations for the longitudinal plate, which has an aspect ratio closer to unity than the transverse plate. This brings to question a possible impact of the aspect ratio on the effectiveness of the simplified method.

When the transverse plate was pushed further into the inelastic region, the resulting edge reactions provided by the simplified analysis compared to those from the FE analysis in the same way those from the longitudinal plate had been found to compare. The normal component from the simplified analysis predicted the peak normal edge reactions reasonably well, whereas the pull-in component of the edge reactions was underestimated by the simplified analysis. This underestimation of the pull-in edge reactions was observed with both plates and may be related back to the uniform pressure versus center displacement behavior. Figure E-2 and Figure E-6 show that with increasing pressure applied to the plates, the simplified method tends to over-predict the center displacement. This over-prediction lends itself to a greater angle of inclination at the edges of the plate. Consider the case shown in Figure E-9 and Figure E-10 that show elevations of the transverse plate deformed (with a scale factor of 10) after being subjected to 8

psi. Figure E-9 shows an elevation view of a section cut through the center of the transverse plate's short dimension with the predicted deformed shape obtained from the simplified analysis superimposed over it. The simplified analysis shows a larger deformation at the plate's center which ultimately leads to a slightly larger angle of inclination at the left and right edges. This steeper angle could result in a smaller pull-in component of the force exerted on the edge by the plate, as is seen in Figure E-8(a).

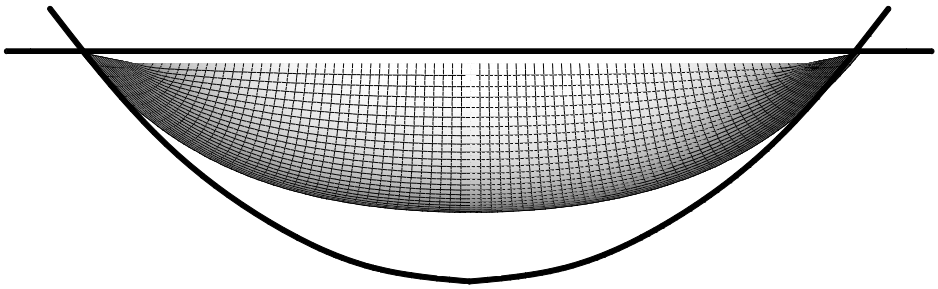

Figure E-9 Elevation of Section Cut Through the Center of the Transverse Plate's Short Dimension

The same reasoning could apply to the under-prediction of the horizontal edge pull-in reactions by the simplified method. Figure E-10 shows this case with an elevation view of a section cut through the center of the plate's long dimension. The deformed shape predicted by the simplified method over-predicts the center displacement which results in an increased angle of inclination at the horizontal edge. This results in a smaller horizontal component of force as is seen in Figure E-8(b).

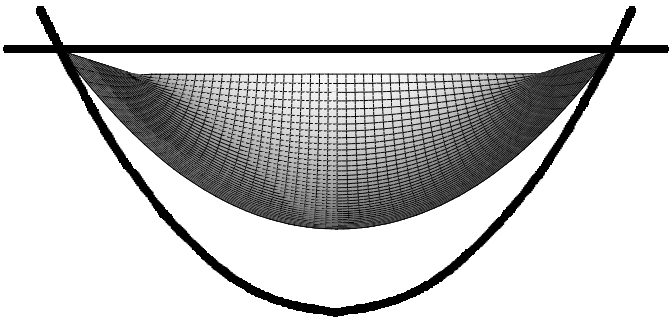

Figure E-10 Elevation of Section Cut Through the Center of the Transverse Plate's Long Dimension

This short study shows that the edge reactions provided with the simplified analysis compare reasonably with those found using FE analysis when the plate is nearly elastic and when the plate

aspect ratio is near unity. When the plates are pushed into the inelastic range, the normal components are reasonably estimated with the simplified method and the pull-in components are underestimated. Though it has some inaccuracies, the simplified analysis should provide a sufficient preliminary estimate for this research regarding the effect of out-of-plane loading on the plates and the corresponding effect on the bounding frame.

Note that this brief study was conducted only to gain a sense for how well the simplified method matched corresponding results from finite element analyses. The simplified method was never verified with experimentation, and the impact of variations in parameters such as plate thickness, and plate aspect ratio were not further studied.

APPENDIX F

CALCULATION OF LOADS AND PLATE EDGE REACTIONS FOR TSUNAMI LOAD CASES

This appendix provides the calculation of loads for the tsunami hazard. It also provides calculations for the plate edge reactions that replace the loaded plates in the analysis of the pier. The calculations presented herein are associated with the simplified plate analysis described in Section 5.5.1. Edge reactions calculated in this appendix are listed according to the numbers illustrated on the figures in Section 5.5.2.2.

The information presented in this worksheet is in reference to the figure shown below. A MATLAB program developed for the simplified plate analysis was used to determine the parameters for determining the forces imposed on the boundary elements. Such parameters include the strain, displacement of the center of the plate, and the intersection angles of the plate with the edges. When calculating the resistance of the plate, the expected yield strength was used.

Also, to calculate the force acting on the VBEs themselves, it was assumed that the pressure distributions acted over half their projected width. Therefore, the outer diameter of the VBEs was needed. $D_o := 24in$

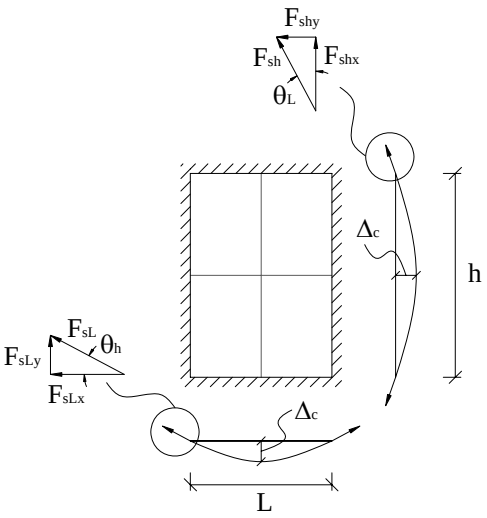

Magnitude of Pressure Distributions

$\gamma_{H2O} := 62.4 \frac{lbf}{ft^3}$

Design stillwater depth chosen for this analysis: $h := 118.1in$

Design flow velocity: $V := 2 \cdot \sqrt{g \cdot h} = 35.6 \cdot \frac{ft}{s}$

Hydrostatic pressure (P_h): $P_h := \gamma_{H2O} \cdot h = 4.3 \cdot psi$

Hydrodynamic pressure (P_D): Assume: $C_d := 2$

$P_D := \frac{1}{2} \cdot \frac{\gamma_{H2O}}{g} C_d \cdot V^2 = 17.1 \cdot psi$

Surge pressure distribution (P_s): $P_s := 3 \cdot h \cdot \gamma_{H2O} = 12.8 \cdot psi$

Impact force (F_I): Assume: $\Delta t := 0.4s$ and $W := 5000lbf$

$F_I := \frac{W}{g} \cdot \frac{V}{\Delta t} = 13.8 \cdot kip$

Plate Information and Forces Imposed on Bound. Elem. (Bottom Plate - Downstream)

Scenario when hydrostatic pressures only are acting:

$P_{eq} := 2.13psi$

$F_{y.p} := 46.8ksi$ $t_{plate} := 0.125in$ $E := 29000ksi$ $h := 92.27in$ $L\_h := 0.802$ $L := L\_h \cdot h = 74 \cdot in$

$\varepsilon_{center} := 0.000573$ $Capacity := 2.13$ $\Delta_c := 1.0823in$ $\theta_h := 0.0586rad$ $\theta_L := 0.0469rad$

Center Strip Spanning Vertically

Strip Deformed Length: $L_{def.h} := \sqrt{4 \cdot \Delta_c^{\,2} + \frac{h^2}{4}} + \frac{h^2}{8 \cdot \Delta_c} \cdot \ln\left(\frac{2 \cdot \Delta_c + \sqrt{4 \cdot \Delta_c^{\,2} + \frac{h^2}{4}}}{\frac{h}{2}} \right) = 92.304 \cdot in$

Strip Strain: $\varepsilon_h := \frac{L_{def.h}}{h} - 1 = 0.000367$

Strip Stress: $\sigma_h := \begin{cases} F_{y.p} & \text{if } \varepsilon_h \geq \frac{F_{y.p}}{E} \\ (E)(\varepsilon_h) & \text{otherwise} \end{cases} = 10.64 \cdot ksi$

Force on Half of VBE Width: $\omega_{col.DS.1} := \frac{D_o}{2} \cdot P_{eq} = 0.026 \cdot \frac{kip}{in}$

Strip Force per Edge Length: $F_{sh} := \sigma_h \cdot t_{plate} = 1.33 \cdot \frac{kip}{in}$

Components of Strip Force: $F_{shx.DS.1} := F_{sh} \cdot \cos(\theta_L) = 1.328 \cdot \frac{kip}{in}$

$F_{shy.DS.1} := F_{sh} \cdot \sin(\theta_L) = 0.062 \cdot \frac{kip}{in}$

Center Strip Spanning Horizontally

Strip Deformed Length: $L_{def.L} := \sqrt{4 \cdot \Delta_c^{\,2} + \frac{L^2}{4}} + \frac{L^2}{8 \cdot \Delta_c} \cdot \ln\left(\frac{2 \cdot \Delta_c + \sqrt{4 \cdot \Delta_c^{\,2} + \frac{L^2}{4}}}{\frac{L}{2}} \right) = 74.043 \cdot in$

Strip Strain: $\varepsilon_L := \frac{L_{def.L}}{L} - 1 = 0.00057$

Strip Stress: $\sigma_L := \begin{cases} F_{y.p} & \text{if } \varepsilon_L \geq \frac{F_{y.p}}{E} \\ (E)(\varepsilon_L) & \text{otherwise} \end{cases} = 16.53 \cdot ksi$

Strip Force per Edge Length: $F_{sL} := \sigma_L \cdot t_{plate} = 2.067 \cdot \frac{kip}{in}$

Components of Strip Force: $F_{sLx.DS.1} := F_{sL} \cdot \cos(\theta_h) = 2.063 \cdot \frac{kip}{in}$

$F_{sLy.DS.1} := F_{sL} \cdot \sin(\theta_h) = 0.121 \cdot \frac{kip}{in}$

Plate Information and Forces Imposed on Bound. Elem. (Bottom, Transverse Plates)

Scenario when hydrostatic pressures only are acting:

$P_{eq} := 2.13psi$

$F_{y.p} := 46.8ksi$ $t_{plate} := 0.0625in$ $E := 29000ksi$ $h := 92.27in$ $L\_h := 1.582$ $L := L\_h \cdot h = 146 \cdot in$

$\varepsilon_{center} := 0.001205$ $Capacity := 2.13psi$ $\Delta_c := 1.9625in$ $\theta_h := 0.0538rad$ $\theta_L := 0.0849rad$

Center Strip Spanning Vertically

Strip Deformed Length: $L_{def.h} := \sqrt{4 \cdot \Delta_c^{\,2} + \frac{h^2}{4}} + \frac{h^2}{8 \cdot \Delta_c} \cdot \ln\left(\frac{2 \cdot \Delta_c + \sqrt{4 \cdot \Delta_c^{\,2} + \frac{h^2}{4}}}{\frac{h}{2}} \right) = 92.381 \cdot in$

Strip Strain: $\varepsilon_h := \frac{L_{def.h}}{h} - 1 = 0.001205$

Force on Half of VBE Width:

$\omega_{col.Trans.1} := \frac{D_o}{2} \cdot P_{eq} = 0.026 \cdot \frac{kip}{in}$

Strip Stress: $\sigma_h := \begin{cases} F_{y.p} & \text{if } \varepsilon_h \geq \frac{F_{y.p}}{E} \\ (E)(\varepsilon_h) & \text{otherwise} \end{cases} = 34.95 \cdot ksi$

Strip Force per Edge Length: $F_{sh} := \sigma_h \cdot t_{plate} = 2.184 \cdot \frac{kip}{in}$

Components of Strip Force:

$F_{shx.Trans.1} := F_{sh} \cdot \cos(\theta_L) = 2.176 \cdot \frac{kip}{in}$

$F_{shy.Trans.1} := F_{sh} \cdot \sin(\theta_L) = 0.185 \cdot \frac{kip}{in}$

Center Strip Spanning Horizontally

Strip Deformed Length: $L_{def.L} := \sqrt{4 \cdot \Delta_c^{\,2} + \frac{L^2}{4}} + \frac{L^2}{8 \cdot \Delta_c} \cdot \ln\left(\frac{2 \cdot \Delta_c + \sqrt{4 \cdot \Delta_c^{\,2} + \frac{L^2}{4}}}{\frac{L}{2}} \right) = 146.041 \cdot in$

Strip Strain: $\varepsilon_L := \frac{L_{def.L}}{L} - 1 = 0.000482$

Strip Stress: $\sigma_L := \begin{cases} F_{y.p} & \text{if } \varepsilon_L \geq \frac{F_{y.p}}{E} \\ (E)(\varepsilon_L) & \text{otherwise} \end{cases} = 13.97 \cdot ksi$

Strip Force per Edge Length: $F_{sL} := \sigma_L \cdot t_{plate} = 0.873 \cdot \frac{kip}{in}$

Components of Strip Force:

$F_{sLx.Trans.1} := F_{sL} \cdot \cos(\theta_h) = 0.872 \cdot \frac{kip}{in}$

$F_{sLy.Trans.1} := F_{sL} \cdot \sin(\theta_h) = 0.047 \cdot \frac{kip}{in}$

Plate Information and Forces Imposed on Bound. Elem. (1st Story Plate - Upstream)

a) Scenario when surge pressure is acting alone:

$P_{eq} := 11.2psi$

$F_{y.p} := 46.8ksi$ $t_{plate} := 0.125in$ $E := 29000ksi$ $h := 92.27in$ $L\_h := 0.802$ $L := L\_h \cdot h = 74 \cdot in$

$\varepsilon_{center} := 0.00176$ $Capacity := 11.2psi$ $\Delta_c := 1.8979in$ $\theta_h := 0.1025rad$ $\theta_L := 0.0821rad$

Center Strip Spanning Vertically

Strip Deformed Length: $L_{def.h} := \sqrt{4 \cdot \Delta_c^{\,2} + \frac{h^2}{4}} + \frac{h^2}{8 \cdot \Delta_c} \cdot \ln\left(\frac{2 \cdot \Delta_c + \sqrt{4 \cdot \Delta_c^{\,2} + \frac{h^2}{4}}}{\frac{h}{2}} \right) = 92.374 \cdot in$

Strip Strain: $\varepsilon_h := \frac{L_{def.h}}{h} - 1 = 0.001127$

Force on Half of VBE Width: $\omega_{col.UpS.1a} := \frac{D_o}{2} \cdot P_{eq} = 0.134 \cdot \frac{kip}{in}$

Strip Stress: $\sigma_h := \begin{cases} F_{y.p} & \text{if } \varepsilon_h \geq \frac{F_{y.p}}{E} \\ (E)(\varepsilon_h) & \text{otherwise} \end{cases} = 32.69 \cdot ksi$

Strip Force per Edge Length: $F_{sh} := \sigma_h \cdot t_{plate} = 4.086 \cdot \frac{kip}{in}$

Components of Strip Force: $F_{shx.UpS.1a} := F_{sh} \cdot \cos(\theta_L) = 4.072 \cdot \frac{kip}{in}$

$F_{shy.UpS.1a} := F_{sh} \cdot \sin(\theta_L) = 0.335 \cdot \frac{kip}{in}$

Center Strip Spanning Horizontally

Strip Deformed Length: $L_{def.L} := \sqrt{4 \cdot \Delta_c^{\,2} + \frac{L^2}{4}} + \frac{L^2}{8 \cdot \Delta_c} \cdot \ln\left(\frac{2 \cdot \Delta_c + \sqrt{4 \cdot \Delta_c^{\,2} + \frac{L^2}{4}}}{\frac{L}{2}} \right) = 74.13 \cdot in$

Strip Strain: $\varepsilon_L := \frac{L_{def.L}}{L} - 1 = 0.001751$

Strip Stress: $\sigma_L := \begin{cases} F_{y.p} & \text{if } \varepsilon_L \geq \frac{F_{y.p}}{E} \\ (E)(\varepsilon_L) & \text{otherwise} \end{cases} = 46.8 \cdot ksi$

Strip Force per Edge Length: $F_{sL} := \sigma_L \cdot t_{plate} = 5.85 \cdot \frac{kip}{in}$

Components of Strip Force: $F_{sLx.UpS.1a} := F_{sL} \cdot \cos(\theta_h) = 5.819 \cdot \frac{kip}{in}$

$F_{sLy.UpS.1a} := F_{sL} \cdot \sin(\theta_h) = 0.599 \cdot \frac{kip}{in}$

b) Scenario when Drag and Hydrostatic pressure is acting: $P_{eq} := 19.21psi$

$F_{y.p} := 46.8ksi$ $t_{plate} := 0.125in$ $E := 29000ksi$ $h := 92.27in$ $L\_h := 0.802$ $L := L\_h \cdot h = 74 \cdot in$

$\varepsilon_{center} := 0.00302$ $Capacity := 19.21psi$ $\Delta_c := 2.4875in$ $\theta_h := 0.1340rad$ $\theta_L := 0.1074rad$

Center Strip Spanning Vertically

Strip Deformed Length: $L_{def.h} := \sqrt{4 \cdot \Delta_c^2 + \frac{h^2}{4}} + \frac{h^2}{8 \cdot \Delta_c} \cdot \ln\left(\frac{2 \cdot \Delta_c + \sqrt{4 \cdot \Delta_c^2 + \frac{h^2}{4}}}{\frac{h}{2}} \right) = 92.449 \cdot in$

Strip Strain: $\varepsilon_h := \frac{L_{def.h}}{h} - 1 = 0.001935$

Strip Stress: $\sigma_h := \begin{cases} F_{y.p} & \text{if } \varepsilon_h \geq \frac{F_{y.p}}{E} \\ (E)(\varepsilon_h) & \text{otherwise} \end{cases} = 46.8 \cdot ksi$

Force on Half of VBE Width: $\omega_{col.UpS.1b} := \frac{D_o}{2} \cdot P_{eq} = 0.231 \cdot \frac{kip}{in}$

Strip Force per Edge Length: $F_{sh} := \sigma_h \cdot t_{plate} = 5.85 \cdot \frac{kip}{in}$

Components of Strip Force: $F_{shx.UpS.1b} := F_{sh} \cdot \cos(\theta_L) = 5.816 \cdot \frac{kip}{in}$

$F_{shy.UpS.1b} := F_{sh} \cdot \sin(\theta_L) = 0.627 \cdot \frac{kip}{in}$

Center Strip Spanning Horizontally

Strip Deformed Length: $L_{def.L} := \sqrt{4 \cdot \Delta_c^2 + \frac{L^2}{4}} + \frac{L^2}{8 \cdot \Delta_c} \cdot \ln\left(\frac{2 \cdot \Delta_c + \sqrt{4 \cdot \Delta_c^2 + \frac{L^2}{4}}}{\frac{L}{2}} \right) = 74.223 \cdot in$

Strip Strain: $\varepsilon_L := \frac{L_{def.L}}{L} - 1 = 0.003005$

Strip Stress: $\sigma_L := \begin{cases} F_{y.p} & \text{if } \varepsilon_L \geq \frac{F_{y.p}}{E} \\ (E)(\varepsilon_L) & \text{otherwise} \end{cases} = 46.8 \cdot ksi$

Strip Force per Edge Length: $F_{sL} := \sigma_L \cdot t_{plate} = 5.85 \cdot \frac{kip}{in}$

Components of Strip Force: $F_{sLx.UpS.1b} := F_{sL} \cdot \cos(\theta_h) = 5.798 \cdot \frac{kip}{in}$

$F_{sLy.UpS.1b} := F_{sL} \cdot \sin(\theta_h) = 0.782 \cdot \frac{kip}{in}$

Plate Information and Forces Imposed on Bound. Elem. (2nd Story Plate - Upstream)

a) Scenario when surge pressure is alone:

$P_{eq} := 7.82psi$

$F_{y.p} := 46.8ksi$ $t_{plate} := 0.125in$ $E := 29000ksi$ $h := 92.27in$ $L\_h := 0.802$ $L := L\_h \cdot h = 74 \cdot in$

$\varepsilon_{center} := 0.001367$ $Capacity := 7.82psi$ $\Delta_c := 1.6723in$ $\theta_h := 0.0904rad$ $\theta_L := 0.0724rad$

Center Strip Spanning Vertically

Strip Deformed Length: $L_{def.h} := \sqrt{4 \cdot \Delta_c^{\,2} + \frac{h^2}{4}} + \frac{h^2}{8 \cdot \Delta_c} \cdot \ln\left(\frac{2 \cdot \Delta_c + \sqrt{4 \cdot \Delta_c^{\,2} + \frac{h^2}{4}}}{\frac{h}{2}} \right) = 92.351 \cdot in$

Strip Strain: $\varepsilon_h := \frac{L_{def.h}}{h} - 1 = 0.000875$

Force on Half of VBE Width: $\omega_{col.UpS.2} := \frac{D_o}{2} \cdot P_{eq} = 0.094 \cdot \frac{kip}{in}$

Strip Stress: $\sigma_h := \begin{cases} F_{y.p} & \text{if } \varepsilon_h \geq \frac{F_{y.p}}{E} \\ (E)(\varepsilon_h) & \text{otherwise} \end{cases} = 25.38 \cdot ksi$

Strip Force per Edge Length: $F_{sh} := \sigma_h \cdot t_{plate} = 3.173 \cdot \frac{kip}{in}$

Components of Strip Force: $F_{shx.UpS.2} := F_{sh} \cdot \cos(\theta_L) = 3.164 \cdot \frac{kip}{in}$

$F_{shy.UpS.2} := F_{sh} \cdot \sin(\theta_L) = 0.23 \cdot \frac{kip}{in}$

Center Strip Spanning Horizontally

Strip Deformed Length: $L_{def.L} := \sqrt{4 \cdot \Delta_c^{\,2} + \frac{L^2}{4}} + \frac{L^2}{8 \cdot \Delta_c} \cdot \ln\left(\frac{2 \cdot \Delta_c + \sqrt{4 \cdot \Delta_c^{\,2} + \frac{L^2}{4}}}{\frac{L}{2}} \right) = 74.101 \cdot in$

Strip Strain: $\varepsilon_L := \frac{L_{def.L}}{L} - 1 = 0.00136$

Strip Stress: $\sigma_L := \begin{cases} F_{y.p} & \text{if } \varepsilon_L \geq \frac{F_{y.p}}{E} \\ (E)(\varepsilon_L) & \text{otherwise} \end{cases} = 39.45 \cdot ksi$

Strip Force per Edge Length: $F_{sL} := \sigma_L \cdot t_{plate} = 4.931 \cdot \frac{kip}{in}$

Components of Strip Force: $F_{sLx.UpS.2} := F_{sL} \cdot \cos(\theta_h) = 4.911 \cdot \frac{kip}{in}$

$F_{sLy.UpS.2} := F_{sL} \cdot \sin(\theta_h) = 0.445 \cdot \frac{kip}{in}$

b) <u>Scenario when Drag and Hydrostatic pressure is acting:</u>

Note: The design stillwater depth is 118.11in., which is 25.84in. above the 92.27in. "story" height. For this case, there is no hydrostatic pressure acting on the plate since it is assumed all to be on the first story plate, but there is a drag pressure acting on over the 25.84in. height of the plate. Rather than transforming this pressure into an equivalent uniform pressure on the plate, it was considered as being taken completely by the HBE at that level in the form of a uniformly distributed load.

The hydrodynamic (drag) pressure was calculated as: $P_{drag} := 17.08psi$

Again, the height of the water above the HBE is: $h_{H20} := 118.11in - 92.27in = 25.84 \cdot in$

Therefore, the additional distributed load acting on the HBE is be equal to:

$$P_{dist.stiff} := P_{drag} \cdot h_{H20} = 0.441 \cdot \frac{kip}{in}$$

Plate Information and Forces Imposed on Bound. Elem. (3rd Story Plate - Upstream)

Scenario when surge pressure is acting alone:

$P_{eq} := 4.47psi$

$F_{y.p} := 46.8ksi$ $t_{plate} := 0.125in$ $E := 29000ksi$ $h := 92.27in$ $L\_h := 0.802$ $L := L\_h \cdot h = 74 \cdot in$

$\varepsilon_{center} := 0.00094$ $Capacity := 4.5psi$ $\Delta_c := 1.3865in$ $\theta_h := 0.0750rad$ $\theta_L := 0.0600rad$

Center Strip Spanning Vertically

Strip Deformed Length: $L_{def.h} := \sqrt{4 \cdot \Delta_c^2 + \frac{h^2}{4}} + \frac{h^2}{8 \cdot \Delta_c} \cdot \ln\left(\frac{2 \cdot \Delta_c + \sqrt{4 \cdot \Delta_c^2 + \frac{h^2}{4}}}{\frac{h}{2}} \right) = 92.326 \cdot in$

Strip Strain: $\varepsilon_h := \frac{L_{def.h}}{h} - 1 = 0.000602$

Force on Half of VBE Width:

$\omega_{col.UpS.3} := \frac{D_o}{2} \cdot P_{eq} = 0.054 \cdot \frac{kip}{in}$

Strip Stress: $\sigma_h := \begin{cases} F_{y.p} & \text{if } \varepsilon_h \geq \frac{F_{y.p}}{E} \\ (E)(\varepsilon_h) & \text{otherwise} \end{cases} = 17.45 \cdot ksi$

Strip Force per Edge Length: $F_{sh} := \sigma_h \cdot t_{plate} = 2.182 \cdot \frac{kip}{in}$

Components of Strip Force:

$F_{shx.UpS.3} := F_{sh} \cdot \cos(\theta_L) = 2.178 \cdot \frac{kip}{in}$

$F_{shy.UpS.3} := F_{sh} \cdot \sin(\theta_L) = 0.131 \cdot \frac{kip}{in}$

Center Strip Spanning Horizontally

Strip Deformed Length: $L_{def.L} := \sqrt{4 \cdot \Delta_c^2 + \frac{L^2}{4}} + \frac{L^2}{8 \cdot \Delta_c} \cdot \ln\left(\frac{2 \cdot \Delta_c + \sqrt{4 \cdot \Delta_c^2 + \frac{L^2}{4}}}{\frac{L}{2}} \right) = 74.07 \cdot in$

Strip Strain: $\varepsilon_L := \frac{L_{def.L}}{L} - 1 = 0.000935$

Strip Stress: $\sigma_L := \begin{cases} F_{y.p} & \text{if } \varepsilon_L \geq \frac{F_{y.p}}{E} \\ (E)(\varepsilon_L) & \text{otherwise} \end{cases} = 27.13 \cdot ksi$

Strip Force per Edge Length: $F_{sL} := \sigma_L \cdot t_{plate} = 3.391 \cdot \frac{kip}{in}$

Components of Strip Force:

$F_{sLx.UpS.3} := F_{sL} \cdot \cos(\theta_h) = 3.381 \cdot \frac{kip}{in}$

$F_{sLy.UpS.3} := F_{sL} \cdot \sin(\theta_h) = 0.254 \cdot \frac{kip}{in}$

Plate Information and Forces Imposed on Bound. Elem. (4th Story Plate - Upstream)

Scenario when surge pressure is acting alone:

$P_{eq} := 1.4psi$

$F_{y.p} := 46.8ksi$ $t_{plate} := 0.125in$ $E := 29000ksi$ $h := 92.27in$ $L\_h := 0.802$ $L := L\_h \cdot h = 74 \cdot in$

$\varepsilon_{center} := 0.00043$ $Capacity := 1.4psi$ $\Delta_c := 0.9375in$ $\theta_h := 0.0508rad$ $\theta_L := 0.0406rad$

Center Strip Spanning Vertically

Strip Deformed Length: $L_{def.h} := \sqrt{4 \cdot \Delta_c^{\,2} + \frac{h^2}{4}} + \frac{h^2}{8 \cdot \Delta_c} \cdot \ln\left(\frac{2 \cdot \Delta_c + \sqrt{4 \cdot \Delta_c^{\,2} + \frac{h^2}{4}}}{\frac{h}{2}} \right) = 92.295 \cdot in$

Strip Strain: $\varepsilon_h := \frac{L_{def.h}}{h} - 1 = 0.000275$

Strip Stress: $\sigma_h := \begin{cases} F_{y.p} & \text{if } \varepsilon_h \geq \frac{F_{y.p}}{E} \\ (E)(\varepsilon_h) & \text{otherwise} \end{cases} = 7.98 \cdot ksi$

Force on Half of VBE Width: $\omega_{col.UpS.4} := \frac{D_o}{2} \cdot P_{eq} = 0.017 \cdot \frac{kip}{in}$

Strip Force per Edge Length: $F_{sh} := \sigma_h \cdot t_{plate} = 0.998 \cdot \frac{kip}{in}$

Components of Strip Force: $F_{shx.UpS.4} := F_{sh} \cdot \cos(\theta_L) = 0.997 \cdot \frac{kip}{in}$

$F_{shy.UpS.4} := F_{sh} \cdot \sin(\theta_L) = 0.04 \cdot \frac{kip}{in}$

Center Strip Spanning Horizontally

Strip Deformed Length: $L_{def.L} := \sqrt{4 \cdot \Delta_c^{\,2} + \frac{L^2}{4}} + \frac{L^2}{8 \cdot \Delta_c} \cdot \ln\left(\frac{2 \cdot \Delta_c + \sqrt{4 \cdot \Delta_c^{\,2} + \frac{L^2}{4}}}{\frac{L}{2}} \right) = 74.032 \cdot in$

Strip Strain: $\varepsilon_L := \frac{L_{def.L}}{L} - 1 = 0.000428$

Strip Stress: $\sigma_L := \begin{cases} F_{y.p} & \text{if } \varepsilon_L \geq \frac{F_{y.p}}{E} \\ (E)(\varepsilon_L) & \text{otherwise} \end{cases} = 12.41 \cdot ksi$

Strip Force per Edge Length: $F_{sL} := \sigma_L \cdot t_{plate} = 1.551 \cdot \frac{kip}{in}$

Components of Strip Force: $F_{sLx.UpS.4} := F_{sL} \cdot \cos(\theta_h) = 1.549 \cdot \frac{kip}{in}$

$F_{sLy.UpS.4} := F_{sL} \cdot \sin(\theta_h) = 0.079 \cdot \frac{kip}{in}$

Load Magnitudes and Descriptions (Load Case 1 - Surge)

1) Pull-in from Plate (1st Story) $\omega_{ups.1a} := F_{sLx.UpS.1a} = 5.819 \cdot \frac{kip}{in}$ (Surge)

2) Pull-in from Plate (2nd Story) $\omega_{ups.2} := F_{sLx.UpS.2} = 4.911 \cdot \frac{kip}{in}$ (Surge)

3) Pull-in from Plate (3rd Story) $\omega_{ups.3} := F_{sLx.UpS.3} = 3.381 \cdot \frac{kip}{in}$ (Surge)

4) Pull-in from Plate (4th Story) $\omega_{ups.4} := F_{sLx.UpS.4} = 1.549 \cdot \frac{kip}{in}$ (Surge)

5) Normal Rxn Force (1st Plate) + VBE. Dist. Load.

$$\omega_{ups.5.a} := F_{sLy.UpS.1a} + \omega_{col.UpS.1a} = 0.733 \cdot \frac{kip}{in}$$ (Surge)

6) Normal Rxn Force (2nd Plate) + VBE. Dist. Load.

$$\omega_{ups.6a} := F_{sLy.UpS.2} + \omega_{col.UpS.2} = 0.539 \cdot \frac{kip}{in}$$ (Surge)

7) Normal Rxn Force (3rd Plate) + VBE. Dist. Load.

$$\omega_{ups.7} := F_{sLy.UpS.3} + \omega_{col.UpS.3} = 0.308 \cdot \frac{kip}{in}$$ (Surge)

8) Normal Rxn Force (4th Plate) + VBE. Dist. Load.

$$\omega_{ups.8} := F_{sLy.UpS.4} + \omega_{col.UpS.4} = 0.096 \cdot \frac{kip}{in}$$ (Surge)

9) Normal Rxn Force Along Bottom of Plate 1

$$\omega_{ups.9a} := F_{shy.UpS.1a} = 0.335 \cdot \frac{kip}{in}$$ (Surge)

10) Normal Rxn Force Summed from Plate 1 & 2

$$\omega_{ups.10a} := F_{shy.UpS.1a} + F_{shy.UpS.2} = 0.565 \cdot \frac{kip}{in}$$ (Surge)

11) Normal Rxn Force Summed from Plate 2 & 3

$$\omega_{ups.11} := F_{shy.UpS.2} + F_{shy.UpS.3} = 0.36 \cdot \frac{kip}{in}$$ (Surge)

12) Normal Rxn Force Summed from Plate 3 & 4

$$\omega_{ups.12} := F_{shy.UpS.3} + F_{shy.UpS.4} = 0.171 \cdot \frac{kip}{in}$$ (Surge)

13) Normal Rxn Force Along Top of Plate 4

$$\omega_{ups.13} := F_{shy.UpS.4} = 0.04 \cdot \frac{kip}{in}$$ (Surge)

14 & 15) Pull-in from Plate (1st Story)

$$\omega_{ups.14.15a} := F_{shx.UpS.1a} = 4.072 \cdot \frac{kip}{in} \text{ (Surge)}$$

16 & 17) Pull-in from Plate (2nd Story)

$$\omega_{ups.16.17a} := F_{shx.UpS.2} = 3.164 \cdot \frac{kip}{in} \text{ (Surge)}$$

18 & 19) Pull-in from Plate (3rd Story)

$$\omega_{ups.18.19} := F_{shx.UpS.3} = 2.178 \cdot \frac{kip}{in} \text{ (Surge)}$$

20 & 21) Pull-in from Plate (4th Story)

$$\omega_{ups.20.21} := F_{shx.UpS.4} = 0.997 \cdot \frac{kip}{in} \text{ (Surge)}$$

Load Magnitudes and Descriptions (Load Case 2 - Hydrodynamic and Hydrostatic)

1) Pull-in from Transverse Plate $\omega_{DST.1} := F_{sLx.Trans.1} = 0.872 \cdot \frac{kip}{in}$ (Hydrostatic)

2) Normal Rxn From Loaded Trans. Plate

$\omega_{DST.2} := F_{shy.Trans.1} = 0.185 \cdot \frac{kip}{in}$ (Hydrostatic)

3) Normal Rxn From Loaded Trans. Plate & VBE Load

$\omega_{DST.3} := F_{sLy.Trans.1} + \omega_{col.Trans.1} = 0.073 \cdot \frac{kip}{in}$ (Hydrostatic)

4) Normal Rxn from Trans. Plate & Pull-in & VBE Load

$\omega_{DST.4} := F_{sLy.Trans.1} + \omega_{col.Trans.1} + F_{sLx.DS.1} = 2.136 \cdot \frac{kip}{in}$ (Hydrostatic)

5) Normal Rxn from Trans. Plate & Pull-in & VBE Load

$\omega_{DST.5} := F_{sLy.DS.1} + \omega_{col.DS.1} + F_{sLx.Trans.1} = 1.019 \cdot \frac{kip}{in}$ (Hydrostatic)

6) Normal Rxn From loaded Longitudinal Plate

$\omega_{DST.6} := F_{shy.DS.1} = 0.062 \cdot \frac{kip}{in}$ (Hydrostatic)

7) Pull-in from Downstream Plate. $\omega_{DST.7} := F_{shx.DS.1} = 1.328 \cdot \frac{kip}{in}$ (Hydrostatic)

8) Pull-in from Transverse Plate $\omega_{DST.8} := F_{shx.Trans.1} = 2.176 \cdot \frac{kip}{in}$ (Hydrostatic)

9) Normal Rxn Force (1st Plate) + VBE Dist. Load.

$\omega_{ups.5.b} := F_{sLy.UpS.1b} + \omega_{col.UpS.1b} = 1.012 \cdot \frac{kip}{in}$ (Drag&Hydrostatic)

10) Pull-in from Plate (1st Story)

$\omega_{ups.1b} := F_{sLx.UpS.1b} = 5.798 \cdot \frac{kip}{in}$ (Drag&Hydrostatic)

11) Normal Rxn Force Along Bottom of Plate 1

$\omega_{ups.9b} := F_{shy.UpS.1b} = 0.627 \cdot \frac{kip}{in}$ (Drag&Hydrostatic)

12) Normal Rxn Force Summed from plate 1 & 2

$\omega_{ups.10b} := F_{shy.UpS.1b} + P_{dist.stiff} = 1.068 \cdot \frac{kip}{in}$ (Drag&Hydrostatic)

13) Pull-in from Plate (1st Story)

$F_{shx.UpS.1b} = 5.816 \cdot \frac{kip}{in}$ (Drag&Hydrostatic)

MCEER Technical Reports

MCEER publishes technical reports on a variety of subjects written by authors funded through MCEER. These reports are available from both MCEER Publications and the National Technical Information Service (NTIS). Requests for reports should be directed to MCEER Publications, MCEER, University at Buffalo, State University of New York, Red Jacket Quadrangle, Buffalo, New York 14261. Reports can also be requested through NTIS, 5285 Port Royal Road, Springfield, Virginia 22161. NTIS accession numbers are shown in parenthesis, if available.

NCEER-87-0001 "First-Year Program in Research, Education and Technology Transfer," 3/5/87, (PB88-134275, A04, MF-A01).

NCEER-87-0002 "Experimental Evaluation of Instantaneous Optimal Algorithms for Structural Control," by R.C. Lin, T.T. Soong and A.M. Reinhorn, 4/20/87, (PB88-134341, A04, MF-A01).

NCEER-87-0003 "Experimentation Using the Earthquake Simulation Facilities at University at Buffalo," by A.M. Reinhorn and R.L. Ketter, to be published.

NCEER-87-0004 "The System Characteristics and Performance of a Shaking Table," by J.S. Hwang, K.C. Chang and G.C. Lee, 6/1/87, (PB88-134259, A03, MF-A01). This report is available only through NTIS (see address given above).

NCEER-87-0005 "A Finite Element Formulation for Nonlinear Viscoplastic Material Using a Q Model," by O. Gyebi and G. Dasgupta, 11/2/87, (PB88-213764, A08, MF-A01).

NCEER-87-0006 "Symbolic Manipulation Program (SMP) - Algebraic Codes for Two and Three Dimensional Finite Element Formulations," by X. Lee and G. Dasgupta, 11/9/87, (PB88-218522, A05, MF-A01).

NCEER-87-0007 "Instantaneous Optimal Control Laws for Tall Buildings Under Seismic Excitations," by J.N. Yang, A. Akbarpour and P. Ghaemmaghami, 6/10/87, (PB88-134333, A06, MF-A01). This report is only available through NTIS (see address given above).

NCEER-87-0008 "IDARC: Inelastic Damage Analysis of Reinforced Concrete Frame - Shear-Wall Structures," by Y.J. Park, A.M. Reinhorn and S.K. Kunnath, 7/20/87, (PB88-134325, A09, MF-A01). This report is only available through NTIS (see address given above).

NCEER-87-0009 "Liquefaction Potential for New York State: A Preliminary Report on Sites in Manhattan and Buffalo," by M. Budhu, V. Vijayakumar, R.F. Giese and L. Baumgras, 8/31/87, (PB88-163704, A03, MF-A01). This report is available only through NTIS (see address given above).

NCEER-87-0010 "Vertical and Torsional Vibration of Foundations in Inhomogeneous Media," by A.S. Veletsos and K.W. Dotson, 6/1/87, (PB88-134291, A03, MF-A01). This report is only available through NTIS (see address given above).

NCEER-87-0011 "Seismic Probabilistic Risk Assessment and Seismic Margins Studies for Nuclear Power Plants," by Howard H.M. Hwang, 6/15/87, (PB88-134267, A03, MF-A01). This report is only available through NTIS (see address given above).

NCEER-87-0012 "Parametric Studies of Frequency Response of Secondary Systems Under Ground-Acceleration Excitations," by Y. Yong and Y.K. Lin, 6/10/87, (PB88-134309, A03, MF-A01). This report is only available through NTIS (see address given above).

NCEER-87-0013 "Frequency Response of Secondary Systems Under Seismic Excitation," by J.A. HoLung, J. Cai and Y.K. Lin, 7/31/87, (PB88-134317, A05, MF-A01). This report is only available through NTIS (see address given above).

NCEER-87-0014 "Modelling Earthquake Ground Motions in Seismically Active Regions Using Parametric Time Series Methods," by G.W. Ellis and A.S. Cakmak, 8/25/87, (PB88-134283, A08, MF-A01). This report is only available through NTIS (see address given above).

NCEER-87-0015 "Detection and Assessment of Seismic Structural Damage," by E. DiPasquale and A.S. Cakmak, 8/25/87, (PB88-163712, A05, MF-A01). This report is only available through NTIS (see address given above).

NCEER-87-0016 "Pipeline Experiment at Parkfield, California," by J. Isenberg and E. Richardson, 9/15/87, (PB88-163720, A03, MF-A01). This report is available only through NTIS (see address given above).

NCEER-87-0017 "Digital Simulation of Seismic Ground Motion," by M. Shinozuka, G. Deodatis and T. Harada, 8/31/87, (PB88-155197, A04, MF-A01). This report is available only through NTIS (see address given above).

NCEER-87-0018 "Practical Considerations for Structural Control: System Uncertainty, System Time Delay and Truncation of Small Control Forces," J.N. Yang and A. Akbarpour, 8/10/87, (PB88-163738, A08, MF-A01). This report is only available through NTIS (see address given above).

NCEER-87-0019 "Modal Analysis of Nonclassically Damped Structural Systems Using Canonical Transformation," by J.N. Yang, S. Sarkani and F.X. Long, 9/27/87, (PB88-187851, A04, MF-A01).

NCEER-87-0020 "A Nonstationary Solution in Random Vibration Theory," by J.R. Red-Horse and P.D. Spanos, 11/3/87, (PB88-163746, A03, MF-A01).

NCEER-87-0021 "Horizontal Impedances for Radially Inhomogeneous Viscoelastic Soil Layers," by A.S. Veletsos and K.W. Dotson, 10/15/87, (PB88-150859, A04, MF-A01).

NCEER-87-0022 "Seismic Damage Assessment of Reinforced Concrete Members," by Y.S. Chung, C. Meyer and M. Shinozuka, 10/9/87, (PB88-150867, A05, MF-A01). This report is available only through NTIS (see address given above).

NCEER-87-0023 "Active Structural Control in Civil Engineering," by T.T. Soong, 11/11/87, (PB88-187778, A03, MF-A01).

NCEER-87-0024 "Vertical and Torsional Impedances for Radially Inhomogeneous Viscoelastic Soil Layers," by K.W. Dotson and A.S. Veletsos, 12/87, (PB88-187786, A03, MF-A01).

NCEER-87-0025 "Proceedings from the Symposium on Seismic Hazards, Ground Motions, Soil-Liquefaction and Engineering Practice in Eastern North America," October 20-22, 1987, edited by K.H. Jacob, 12/87, (PB88-188115, A23, MF-A01). This report is available only through NTIS (see address given above).

NCEER-87-0026 "Report on the Whittier-Narrows, California, Earthquake of October 1, 1987," by J. Pantelic and A. Reinhorn, 11/87, (PB88-187752, A03, MF-A01). This report is available only through NTIS (see address given above).

NCEER-87-0027 "Design of a Modular Program for Transient Nonlinear Analysis of Large 3-D Building Structures," by S. Srivastav and J.F. Abel, 12/30/87, (PB88-187950, A05, MF-A01). This report is only available through NTIS (see address given above).

NCEER-87-0028 "Second-Year Program in Research, Education and Technology Transfer," 3/8/88, (PB88-219480, A04, MF-A01).

NCEER-88-0001 "Workshop on Seismic Computer Analysis and Design of Buildings With Interactive Graphics," by W. McGuire, J.F. Abel and C.H. Conley, 1/18/88, (PB88-187760, A03, MF-A01). This report is only available through NTIS (see address given above).

NCEER-88-0002 "Optimal Control of Nonlinear Flexible Structures," by J.N. Yang, F.X. Long and D. Wong, 1/22/88, (PB88-213772, A06, MF-A01).

NCEER-88-0003 "Substructuring Techniques in the Time Domain for Primary-Secondary Structural Systems," by G.D. Manolis and G. Juhn, 2/10/88, (PB88-213780, A04, MF-A01).

NCEER-88-0004 "Iterative Seismic Analysis of Primary-Secondary Systems," by A. Singhal, L.D. Lutes and P.D. Spanos, 2/23/88, (PB88-213798, A04, MF-A01).

NCEER-88-0005 "Stochastic Finite Element Expansion for Random Media," by P.D. Spanos and R. Ghanem, 3/14/88, (PB88-213806, A03, MF-A01).

NCEER-88-0006 "Combining Structural Optimization and Structural Control," by F.Y. Cheng and C.P. Pantelides, 1/10/88, (PB88-213814, A05, MF-A01).

NCEER-88-0007 "Seismic Performance Assessment of Code-Designed Structures," by H.H-M. Hwang, J-W. Jaw and H-J. Shau, 3/20/88, (PB88-219423, A04, MF-A01). This report is only available through NTIS (see address given above).

NCEER-88-0008 "Reliability Analysis of Code-Designed Structures Under Natural Hazards," by H.H-M. Hwang, H. Ushiba and M. Shinozuka, 2/29/88, (PB88-229471, A07, MF-A01). This report is only available through NTIS (see address given above).

NCEER-88-0009 "Seismic Fragility Analysis of Shear Wall Structures," by J-W Jaw and H.H-M. Hwang, 4/30/88, (PB89-102867, A04, MF-A01).

NCEER-88-0010 "Base Isolation of a Multi-Story Building Under a Harmonic Ground Motion - A Comparison of Performances of Various Systems," by F-G Fan, G. Ahmadi and I.G. Tadjbakhsh, 5/18/88, (PB89-122238, A06, MF-A01). This report is only available through NTIS (see address given above).

NCEER-88-0011 "Seismic Floor Response Spectra for a Combined System by Green's Functions," by F.M. Lavelle, L.A. Bergman and P.D. Spanos, 5/1/88, (PB89-102875, A03, MF-A01).

NCEER-88-0012 "A New Solution Technique for Randomly Excited Hysteretic Structures," by G.Q. Cai and Y.K. Lin, 5/16/88, (PB89-102883, A03, MF-A01).

NCEER-88-0013 "A Study of Radiation Damping and Soil-Structure Interaction Effects in the Centrifuge," by K. Weissman, supervised by J.H. Prevost, 5/24/88, (PB89-144703, A06, MF-A01).

NCEER-88-0014 "Parameter Identification and Implementation of a Kinematic Plasticity Model for Frictional Soils," by J.H. Prevost and D.V. Griffiths, to be published.

NCEER-88-0015 "Two- and Three- Dimensional Dynamic Finite Element Analyses of the Long Valley Dam," by D.V. Griffiths and J.H. Prevost, 6/17/88, (PB89-144711, A04, MF-A01).

NCEER-88-0016 "Damage Assessment of Reinforced Concrete Structures in Eastern United States," by A.M. Reinhorn, M.J. Seidel, S.K. Kunnath and Y.J. Park, 6/15/88, (PB89-122220, A04, MF-A01). This report is only available through NTIS (see address given above).

NCEER-88-0017 "Dynamic Compliance of Vertically Loaded Strip Foundations in Multilayered Viscoelastic Soils," by S. Ahmad and A.S.M. Israil, 6/17/88, (PB89-102891, A04, MF-A01).

NCEER-88-0018 "An Experimental Study of Seismic Structural Response With Added Viscoelastic Dampers," by R.C. Lin, Z. Liang, T.T. Soong and R.H. Zhang, 6/30/88, (PB89-122212, A05, MF-A01). This report is available only through NTIS (see address given above).

NCEER-88-0019 "Experimental Investigation of Primary - Secondary System Interaction," by G.D. Manolis, G. Juhn and A.M. Reinhorn, 5/27/88, (PB89-122204, A04, MF-A01).

NCEER-88-0020 "A Response Spectrum Approach For Analysis of Nonclassically Damped Structures," by J.N. Yang, S. Sarkani and F.X. Long, 4/22/88, (PB89-102909, A04, MF-A01).

NCEER-88-0021 "Seismic Interaction of Structures and Soils: Stochastic Approach," by A.S. Veletsos and A.M. Prasad, 7/21/88, (PB89-122196, A04, MF-A01). This report is only available through NTIS (see address given above).

NCEER-88-0022 "Identification of the Serviceability Limit State and Detection of Seismic Structural Damage," by E. DiPasquale and A.S. Cakmak, 6/15/88, (PB89-122188, A05, MF-A01). This report is available only through NTIS (see address given above).

NCEER-88-0023 "Multi-Hazard Risk Analysis: Case of a Simple Offshore Structure," by B.K. Bhartia and E.H. Vanmarcke, 7/21/88, (PB89-145213, A05, MF-A01).

NCEER-88-0024 "Automated Seismic Design of Reinforced Concrete Buildings," by Y.S. Chung, C. Meyer and M. Shinozuka, 7/5/88, (PB89-122170, A06, MF-A01). This report is available only through NTIS (see address given above).

NCEER-88-0025 "Experimental Study of Active Control of MDOF Structures Under Seismic Excitations," by L.L. Chung, R.C. Lin, T.T. Soong and A.M. Reinhorn, 7/10/88, (PB89-122600, A04, MF-A01).

NCEER-88-0026 "Earthquake Simulation Tests of a Low-Rise Metal Structure," by J.S. Hwang, K.C. Chang, G.C. Lee and R.L. Ketter, 8/1/88, (PB89-102917, A04, MF-A01).

NCEER-88-0027 "Systems Study of Urban Response and Reconstruction Due to Catastrophic Earthquakes," by F. Kozin and H.K. Zhou, 9/22/88, (PB90-162348, A04, MF-A01).

NCEER-88-0028 "Seismic Fragility Analysis of Plane Frame Structures," by H.H-M. Hwang and Y.K. Low, 7/31/88, (PB89-131445, A06, MF-A01).

NCEER-88-0029 "Response Analysis of Stochastic Structures," by A. Kardara, C. Bucher and M. Shinozuka, 9/22/88, (PB89-174429, A04, MF-A01).

NCEER-88-0030 "Nonnormal Accelerations Due to Yielding in a Primary Structure," by D.C.K. Chen and L.D. Lutes, 9/19/88, (PB89-131437, A04, MF-A01).

NCEER-88-0031 "Design Approaches for Soil-Structure Interaction," by A.S. Veletsos, A.M. Prasad and Y. Tang, 12/30/88, (PB89-174437, A03, MF-A01). This report is available only through NTIS (see address given above).

NCEER-88-0032 "A Re-evaluation of Design Spectra for Seismic Damage Control," by C.J. Turkstra and A.G. Tallin, 11/7/88, (PB89-145221, A05, MF-A01).

NCEER-88-0033 "The Behavior and Design of Noncontact Lap Splices Subjected to Repeated Inelastic Tensile Loading," by V.E. Sagan, P. Gergely and R.N. White, 12/8/88, (PB89-163737, A08, MF-A01).

NCEER-88-0034 "Seismic Response of Pile Foundations," by S.M. Mamoon, P.K. Banerjee and S. Ahmad, 11/1/88, (PB89-145239, A04, MF-A01).

NCEER-88-0035 "Modeling of R/C Building Structures With Flexible Floor Diaphragms (IDARC2)," by A.M. Reinhorn, S.K. Kunnath and N. Panahshahi, 9/7/88, (PB89-207153, A07, MF-A01).

NCEER-88-0036 "Solution of the Dam-Reservoir Interaction Problem Using a Combination of FEM, BEM with Particular Integrals, Modal Analysis, and Substructuring," by C-S. Tsai, G.C. Lee and R.L. Ketter, 12/31/88, (PB89-207146, A04, MF-A01).

NCEER-88-0037 "Optimal Placement of Actuators for Structural Control," by F.Y. Cheng and C.P. Pantelides, 8/15/88, (PB89-162846, A05, MF-A01).

NCEER-88-0038 "Teflon Bearings in Aseismic Base Isolation: Experimental Studies and Mathematical Modeling," by A. Mokha, M.C. Constantinou and A.M. Reinhorn, 12/5/88, (PB89-218457, A10, MF-A01). This report is available only through NTIS (see address given above).

NCEER-88-0039 "Seismic Behavior of Flat Slab High-Rise Buildings in the New York City Area," by P. Weidlinger and M. Ettouney, 10/15/88, (PB90-145681, A04, MF-A01).

NCEER-88-0040 "Evaluation of the Earthquake Resistance of Existing Buildings in New York City," by P. Weidlinger and M. Ettouney, 10/15/88, to be published.

NCEER-88-0041 "Small-Scale Modeling Techniques for Reinforced Concrete Structures Subjected to Seismic Loads," by W. Kim, A. El-Attar and R.N. White, 11/22/88, (PB89-189625, A05, MF-A01).

NCEER-88-0042 "Modeling Strong Ground Motion from Multiple Event Earthquakes," by G.W. Ellis and A.S. Cakmak, 10/15/88, (PB89-174445, A03, MF-A01).

NCEER-88-0043 "Nonstationary Models of Seismic Ground Acceleration," by M. Grigoriu, S.E. Ruiz and E. Rosenblueth, 7/15/88, (PB89-189617, A04, MF-A01).

NCEER-88-0044 "SARCF User's Guide: Seismic Analysis of Reinforced Concrete Frames," by Y.S. Chung, C. Meyer and M. Shinozuka, 11/9/88, (PB89-174452, A08, MF-A01).

NCEER-88-0045 "First Expert Panel Meeting on Disaster Research and Planning," edited by J. Pantelic and J. Stoyle, 9/15/88, (PB89-174460, A05, MF-A01).

NCEER-88-0046 "Preliminary Studies of the Effect of Degrading Infill Walls on the Nonlinear Seismic Response of Steel Frames," by C.Z. Chrysostomou, P. Gergely and J.F. Abel, 12/19/88, (PB89-208383, A05, MF-A01).

NCEER-88-0047 "Reinforced Concrete Frame Component Testing Facility - Design, Construction, Instrumentation and Operation," by S.P. Pessiki, C. Conley, T. Bond, P. Gergely and R.N. White, 12/16/88, (PB89-174478, A04, MF-A01).

NCEER-89-0001 "Effects of Protective Cushion and Soil Compliancy on the Response of Equipment Within a Seismically Excited Building," by J.A. HoLung, 2/16/89, (PB89-207179, A04, MF-A01).

NCEER-89-0002 "Statistical Evaluation of Response Modification Factors for Reinforced Concrete Structures," by H.H-M. Hwang and J-W. Jaw, 2/17/89, (PB89-207187, A05, MF-A01).

NCEER-89-0003 "Hysteretic Columns Under Random Excitation," by G-Q. Cai and Y.K. Lin, 1/9/89, (PB89-196513, A03, MF-A01).

NCEER-89-0004 "Experimental Study of `Elephant Foot Bulge' Instability of Thin-Walled Metal Tanks," by Z-H. Jia and R.L. Ketter, 2/22/89, (PB89-207195, A03, MF-A01).

NCEER-89-0005 "Experiment on Performance of Buried Pipelines Across San Andreas Fault," by J. Isenberg, E. Richardson and T.D. O'Rourke, 3/10/89, (PB89-218440, A04, MF-A01). This report is available only through NTIS (see address given above).

NCEER-89-0006 "A Knowledge-Based Approach to Structural Design of Earthquake-Resistant Buildings," by M. Subramani, P. Gergely, C.H. Conley, J.F. Abel and A.H. Zaghw, 1/15/89, (PB89-218465, A06, MF-A01).

NCEER-89-0007 "Liquefaction Hazards and Their Effects on Buried Pipelines," by T.D. O'Rourke and P.A. Lane, 2/1/89, (PB89-218481, A09, MF-A01).

NCEER-89-0008 "Fundamentals of System Identification in Structural Dynamics," by H. Imai, C-B. Yun, O. Maruyama and M. Shinozuka, 1/26/89, (PB89-207211, A04, MF-A01).

NCEER-89-0009 "Effects of the 1985 Michoacan Earthquake on Water Systems and Other Buried Lifelines in Mexico," by A.G. Ayala and M.J. O'Rourke, 3/8/89, (PB89-207229, A06, MF-A01).

NCEER-89-R010 "NCEER Bibliography of Earthquake Education Materials," by K.E.K. Ross, Second Revision, 9/1/89, (PB90-125352, A05, MF-A01). This report is replaced by NCEER-92-0018.

NCEER-89-0011 "Inelastic Three-Dimensional Response Analysis of Reinforced Concrete Building Structures (IDARC-3D), Part I - Modeling," by S.K. Kunnath and A.M. Reinhorn, 4/17/89, (PB90-114612, A07, MF-A01). This report is available only through NTIS (see address given above).

NCEER-89-0012 "Recommended Modifications to ATC-14," by C.D. Poland and J.O. Malley, 4/12/89, (PB90-108648, A15, MF-A01).

NCEER-89-0013 "Repair and Strengthening of Beam-to-Column Connections Subjected to Earthquake Loading," by M. Corazao and A.J. Durrani, 2/28/89, (PB90-109885, A06, MF-A01).

NCEER-89-0014 "Program EXKAL2 for Identification of Structural Dynamic Systems," by O. Maruyama, C-B. Yun, M. Hoshiya and M. Shinozuka, 5/19/89, (PB90-109877, A09, MF-A01).

NCEER-89-0015 "Response of Frames With Bolted Semi-Rigid Connections, Part I - Experimental Study and Analytical Predictions," by P.J. DiCorso, A.M. Reinhorn, J.R. Dickerson, J.B. Radziminski and W.L. Harper, 6/1/89, to be published.

NCEER-89-0016 "ARMA Monte Carlo Simulation in Probabilistic Structural Analysis," by P.D. Spanos and M.P. Mignolet, 7/10/89, (PB90-109893, A03, MF-A01).

NCEER-89-P017 "Preliminary Proceedings from the Conference on Disaster Preparedness - The Place of Earthquake Education in Our Schools," Edited by K.E.K. Ross, 6/23/89, (PB90-108606, A03, MF-A01).

NCEER-89-0017 "Proceedings from the Conference on Disaster Preparedness - The Place of Earthquake Education in Our Schools," Edited by K.E.K. Ross, 12/31/89, (PB90-207895, A012, MF-A02). This report is available only through NTIS (see address given above).

NCEER-89-0018 "Multidimensional Models of Hysteretic Material Behavior for Vibration Analysis of Shape Memory Energy Absorbing Devices, by E.J. Graesser and F.A. Cozzarelli, 6/7/89, (PB90-164146, A04, MF-A01).

NCEER-89-0019 "Nonlinear Dynamic Analysis of Three-Dimensional Base Isolated Structures (3D-BASIS)," by S. Nagarajaiah, A.M. Reinhorn and M.C. Constantinou, 8/3/89, (PB90-161936, A06, MF-A01). This report has been replaced by NCEER-93-0011.

NCEER-89-0020 "Structural Control Considering Time-Rate of Control Forces and Control Rate Constraints," by F.Y. Cheng and C.P. Pantelides, 8/3/89, (PB90-120445, A04, MF-A01).

NCEER-89-0021 "Subsurface Conditions of Memphis and Shelby County," by K.W. Ng, T-S. Chang and H-H.M. Hwang, 7/26/89, (PB90-120437, A03, MF-A01).

NCEER-89-0022 "Seismic Wave Propagation Effects on Straight Jointed Buried Pipelines," by K. Elhmadi and M.J. O'Rourke, 8/24/89, (PB90-162322, A10, MF-A02).

NCEER-89-0023 "Workshop on Serviceability Analysis of Water Delivery Systems," edited by M. Grigoriu, 3/6/89, (PB90-127424, A03, MF-A01).

NCEER-89-0024 "Shaking Table Study of a 1/5 Scale Steel Frame Composed of Tapered Members," by K.C. Chang, J.S. Hwang and G.C. Lee, 9/18/89, (PB90-160169, A04, MF-A01).

NCEER-89-0025 "DYNA1D: A Computer Program for Nonlinear Seismic Site Response Analysis - Technical Documentation," by Jean H. Prevost, 9/14/89, (PB90-161944, A07, MF-A01). This report is available only through NTIS (see address given above).

NCEER-89-0026 "1:4 Scale Model Studies of Active Tendon Systems and Active Mass Dampers for Aseismic Protection," by A.M. Reinhorn, T.T. Soong, R.C. Lin, Y.P. Yang, Y. Fukao, H. Abe and M. Nakai, 9/15/89, (PB90-173246, A10, MF-A02). This report is available only through NTIS (see address given above).

NCEER-89-0027 "Scattering of Waves by Inclusions in a Nonhomogeneous Elastic Half Space Solved by Boundary Element Methods," by P.K. Hadley, A. Askar and A.S. Cakmak, 6/15/89, (PB90-145699, A07, MF-A01).

NCEER-89-0028 "Statistical Evaluation of Deflection Amplification Factors for Reinforced Concrete Structures," by H.H.M. Hwang, J-W. Jaw and A.L. Ch'ng, 8/31/89, (PB90-164633, A05, MF-A01).

NCEER-89-0029 "Bedrock Accelerations in Memphis Area Due to Large New Madrid Earthquakes," by H.H.M. Hwang, C.H.S. Chen and G. Yu, 11/7/89, (PB90-162330, A04, MF-A01).

NCEER-89-0030 "Seismic Behavior and Response Sensitivity of Secondary Structural Systems," by Y.Q. Chen and T.T. Soong, 10/23/89, (PB90-164658, A08, MF-A01).

NCEER-89-0031 "Random Vibration and Reliability Analysis of Primary-Secondary Structural Systems," by Y. Ibrahim, M. Grigoriu and T.T. Soong, 11/10/89, (PB90-161951, A04, MF-A01).

NCEER-89-0032 "Proceedings from the Second U.S. - Japan Workshop on Liquefaction, Large Ground Deformation and Their Effects on Lifelines, September 26-29, 1989," Edited by T.D. O'Rourke and M. Hamada, 12/1/89, (PB90-209388, A22, MF-A03).

NCEER-89-0033 "Deterministic Model for Seismic Damage Evaluation of Reinforced Concrete Structures," by J.M. Bracci, A.M. Reinhorn, J.B. Mander and S.K. Kunnath, 9/27/89, (PB91-108803, A06, MF-A01).

NCEER-89-0034 "On the Relation Between Local and Global Damage Indices," by E. DiPasquale and A.S. Cakmak, 8/15/89, (PB90-173865, A05, MF-A01).

NCEER-89-0035 "Cyclic Undrained Behavior of Nonplastic and Low Plasticity Silts," by A.J. Walker and H.E. Stewart, 7/26/89, (PB90-183518, A10, MF-A01).

NCEER-89-0036 "Liquefaction Potential of Surficial Deposits in the City of Buffalo, New York," by M. Budhu, R. Giese and L. Baumgrass, 1/17/89, (PB90-208455, A04, MF-A01).

NCEER-89-0037 "A Deterministic Assessment of Effects of Ground Motion Incoherence," by A.S. Veletsos and Y. Tang, 7/15/89, (PB90-164294, A03, MF-A01).

NCEER-89-0038 "Workshop on Ground Motion Parameters for Seismic Hazard Mapping," July 17-18, 1989, edited by R.V. Whitman, 12/1/89, (PB90-173923, A04, MF-A01).

NCEER-89-0039 "Seismic Effects on Elevated Transit Lines of the New York City Transit Authority," by C.J. Costantino, C.A. Miller and E. Heymsfield, 12/26/89, (PB90-207887, A06, MF-A01).

NCEER-89-0040 "Centrifugal Modeling of Dynamic Soil-Structure Interaction," by K. Weissman, Supervised by J.H. Prevost, 5/10/89, (PB90-207879, A07, MF-A01).

NCEER-89-0041 "Linearized Identification of Buildings With Cores for Seismic Vulnerability Assessment," by I-K. Ho and A.E. Aktan, 11/1/89, (PB90-251943, A07, MF-A01).

NCEER-90-0001 "Geotechnical and Lifeline Aspects of the October 17, 1989 Loma Prieta Earthquake in San Francisco," by T.D. O'Rourke, H.E. Stewart, F.T. Blackburn and T.S. Dickerman, 1/90, (PB90-208596, A05, MF-A01).

NCEER-90-0002 "Nonnormal Secondary Response Due to Yielding in a Primary Structure," by D.C.K. Chen and L.D. Lutes, 2/28/90, (PB90-251976, A07, MF-A01).

NCEER-90-0003 "Earthquake Education Materials for Grades K-12," by K.E.K. Ross, 4/16/90, (PB91-251984, A05, MF-A05). This report has been replaced by NCEER-92-0018.

NCEER-90-0004 "Catalog of Strong Motion Stations in Eastern North America," by R.W. Busby, 4/3/90, (PB90-251984, A05, MF-A01).

NCEER-90-0005 "NCEER Strong-Motion Data Base: A User Manual for the GeoBase Release (Version 1.0 for the Sun3)," by P. Friberg and K. Jacob, 3/31/90 (PB90-258062, A04, MF-A01).

NCEER-90-0006 "Seismic Hazard Along a Crude Oil Pipeline in the Event of an 1811-1812 Type New Madrid Earthquake," by H.H.M. Hwang and C-H.S. Chen, 4/16/90, (PB90-258054, A04, MF-A01).

NCEER-90-0007 "Site-Specific Response Spectra for Memphis Sheahan Pumping Station," by H.H.M. Hwang and C.S. Lee, 5/15/90, (PB91-108811, A05, MF-A01).

NCEER-90-0008 "Pilot Study on Seismic Vulnerability of Crude Oil Transmission Systems," by T. Ariman, R. Dobry, M. Grigoriu, F. Kozin, M. O'Rourke, T. O'Rourke and M. Shinozuka, 5/25/90, (PB91-108837, A06, MF-A01).

NCEER-90-0009 "A Program to Generate Site Dependent Time Histories: EQGEN," by G.W. Ellis, M. Srinivasan and A.S. Cakmak, 1/30/90, (PB91-108829, A04, MF-A01).

NCEER-90-0010 "Active Isolation for Seismic Protection of Operating Rooms," by M.E. Talbott, Supervised by M. Shinozuka, 6/8/9, (PB91-110205, A05, MF-A01).

NCEER-90-0011 "Program LINEARID for Identification of Linear Structural Dynamic Systems," by C-B. Yun and M. Shinozuka, 6/25/90, (PB91-110312, A08, MF-A01).

NCEER-90-0012 "Two-Dimensional Two-Phase Elasto-Plastic Seismic Response of Earth Dams," by A.N. Yiagos, Supervised by J.H. Prevost, 6/20/90, (PB91-110197, A13, MF-A02).

NCEER-90-0013 "Secondary Systems in Base-Isolated Structures: Experimental Investigation, Stochastic Response and Stochastic Sensitivity," by G.D. Manolis, G. Juhn, M.C. Constantinou and A.M. Reinhorn, 7/1/90, (PB91-110320, A08, MF-A01).

NCEER-90-0014 "Seismic Behavior of Lightly-Reinforced Concrete Column and Beam-Column Joint Details," by S.P. Pessiki, C.H. Conley, P. Gergely and R.N. White, 8/22/90, (PB91-108795, A11, MF-A02).

NCEER-90-0015 "Two Hybrid Control Systems for Building Structures Under Strong Earthquakes," by J.N. Yang and A. Danielians, 6/29/90, (PB91-125393, A04, MF-A01).

NCEER-90-0016 "Instantaneous Optimal Control with Acceleration and Velocity Feedback," by J.N. Yang and Z. Li, 6/29/90, (PB91-125401, A03, MF-A01).

NCEER-90-0017 "Reconnaissance Report on the Northern Iran Earthquake of June 21, 1990," by M. Mehrain, 10/4/90, (PB91-125377, A03, MF-A01).

NCEER-90-0018 "Evaluation of Liquefaction Potential in Memphis and Shelby County," by T.S. Chang, P.S. Tang, C.S. Lee and H. Hwang, 8/10/90, (PB91-125427, A09, MF-A01).

NCEER-90-0019 "Experimental and Analytical Study of a Combined Sliding Disc Bearing and Helical Steel Spring Isolation System," by M.C. Constantinou, A.S. Mokha and A.M. Reinhorn, 10/4/90, (PB91-125385, A06, MF-A01). This report is available only through NTIS (see address given above).

NCEER-90-0020 "Experimental Study and Analytical Prediction of Earthquake Response of a Sliding Isolation System with a Spherical Surface," by A.S. Mokha, M.C. Constantinou and A.M. Reinhorn, 10/11/90, (PB91-125419, A05, MF-A01).

NCEER-90-0021 "Dynamic Interaction Factors for Floating Pile Groups," by G. Gazetas, K. Fan, A. Kaynia and E. Kausel, 9/10/90, (PB91-170381, A05, MF-A01).

NCEER-90-0022 "Evaluation of Seismic Damage Indices for Reinforced Concrete Structures," by S. Rodriguez-Gomez and A.S. Cakmak, 9/30/90, PB91-171322, A06, MF-A01).

NCEER-90-0023 "Study of Site Response at a Selected Memphis Site," by H. Desai, S. Ahmad, E.S. Gazetas and M.R. Oh, 10/11/90, (PB91-196857, A03, MF-A01).

NCEER-90-0024 "A User's Guide to Strongmo: Version 1.0 of NCEER's Strong-Motion Data Access Tool for PCs and Terminals," by P.A. Friberg and C.A.T. Susch, 11/15/90, (PB91-171272, A03, MF-A01).

NCEER-90-0025 "A Three-Dimensional Analytical Study of Spatial Variability of Seismic Ground Motions," by L-L. Hong and A.H.-S. Ang, 10/30/90, (PB91-170399, A09, MF-A01).

NCEER-90-0026 "MUMOID User's Guide - A Program for the Identification of Modal Parameters," by S. Rodriguez-Gomez and E. DiPasquale, 9/30/90, (PB91-171298, A04, MF-A01).

NCEER-90-0027 "SARCF-II User's Guide - Seismic Analysis of Reinforced Concrete Frames," by S. Rodriguez-Gomez, Y.S. Chung and C. Meyer, 9/30/90, (PB91-171280, A05, MF-A01).

NCEER-90-0028 "Viscous Dampers: Testing, Modeling and Application in Vibration and Seismic Isolation," by N. Makris and M.C. Constantinou, 12/20/90 (PB91-190561, A06, MF-A01).

NCEER-90-0029 "Soil Effects on Earthquake Ground Motions in the Memphis Area," by H. Hwang, C.S. Lee, K.W. Ng and T.S. Chang, 8/2/90, (PB91-190751, A05, MF-A01).

NCEER-91-0001 "Proceedings from the Third Japan-U.S. Workshop on Earthquake Resistant Design of Lifeline Facilities and Countermeasures for Soil Liquefaction, December 17-19, 1990," edited by T.D. O'Rourke and M. Hamada, 2/1/91, (PB91-179259, A99, MF-A04).

NCEER-91-0002 "Physical Space Solutions of Non-Proportionally Damped Systems," by M. Tong, Z. Liang and G.C. Lee, 1/15/91, (PB91-179242, A04, MF-A01).

NCEER-91-0003 "Seismic Response of Single Piles and Pile Groups," by K. Fan and G. Gazetas, 1/10/91, (PB92-174994, A04, MF-A01).

NCEER-91-0004 "Damping of Structures: Part 1 - Theory of Complex Damping," by Z. Liang and G. Lee, 10/10/91, (PB92-197235, A12, MF-A03).

NCEER-91-0005 "3D-BASIS - Nonlinear Dynamic Analysis of Three Dimensional Base Isolated Structures: Part II," by S. Nagarajaiah, A.M. Reinhorn and M.C. Constantinou, 2/28/91, (PB91-190553, A07, MF-A01). This report has been replaced by NCEER-93-0011.

NCEER-91-0006 "A Multidimensional Hysteretic Model for Plasticity Deforming Metals in Energy Absorbing Devices," by E.J. Graesser and F.A. Cozzarelli, 4/9/91, (PB92-108364, A04, MF-A01).

NCEER-91-0007 "A Framework for Customizable Knowledge-Based Expert Systems with an Application to a KBES for Evaluating the Seismic Resistance of Existing Buildings," by E.G. Ibarra-Anaya and S.J. Fenves, 4/9/91, (PB91-210930, A08, MF-A01).

NCEER-91-0008 "Nonlinear Analysis of Steel Frames with Semi-Rigid Connections Using the Capacity Spectrum Method," by G.G. Deierlein, S-H. Hsieh, Y-J. Shen and J.F. Abel, 7/2/91, (PB92-113828, A05, MF-A01).

NCEER-91-0009 "Earthquake Education Materials for Grades K-12," by K.E.K. Ross, 4/30/91, (PB91-212142, A06, MF-A01). This report has been replaced by NCEER-92-0018.

NCEER-91-0010 "Phase Wave Velocities and Displacement Phase Differences in a Harmonically Oscillating Pile," by N. Makris and G. Gazetas, 7/8/91, (PB92-108356, A04, MF-A01).

NCEER-91-0011 "Dynamic Characteristics of a Full-Size Five-Story Steel Structure and a 2/5 Scale Model," by K.C. Chang, G.C. Yao, G.C. Lee, D.S. Hao and Y.C. Yeh," 7/2/91, (PB93-116648, A06, MF-A02).

NCEER-91-0012 "Seismic Response of a 2/5 Scale Steel Structure with Added Viscoelastic Dampers," by K.C. Chang, T.T. Soong, S-T. Oh and M.L. Lai, 5/17/91, (PB92-110816, A05, MF-A01).

NCEER-91-0013 "Earthquake Response of Retaining Walls; Full-Scale Testing and Computational Modeling," by S. Alampalli and A-W.M. Elgamal, 6/20/91, to be published.

NCEER-91-0014 "3D-BASIS-M: Nonlinear Dynamic Analysis of Multiple Building Base Isolated Structures," by P.C. Tsopelas, S. Nagarajaiah, M.C. Constantinou and A.M. Reinhorn, 5/28/91, (PB92-113885, A09, MF-A02).

NCEER-91-0015 "Evaluation of SEAOC Design Requirements for Sliding Isolated Structures," by D. Theodossiou and M.C. Constantinou, 6/10/91, (PB92-114602, A11, MF-A03).

NCEER-91-0016 "Closed-Loop Modal Testing of a 27-Story Reinforced Concrete Flat Plate-Core Building," by H.R. Somaprasad, T. Toksoy, H. Yoshiyuki and A.E. Aktan, 7/15/91, (PB92-129980, A07, MF-A02).

NCEER-91-0017 "Shake Table Test of a 1/6 Scale Two-Story Lightly Reinforced Concrete Building," by A.G. El-Attar, R.N. White and P. Gergely, 2/28/91, (PB92-222447, A06, MF-A02).

NCEER-91-0018 "Shake Table Test of a 1/8 Scale Three-Story Lightly Reinforced Concrete Building," by A.G. El-Attar, R.N. White and P. Gergely, 2/28/91, (PB93-116630, A08, MF-A02).

NCEER-91-0019 "Transfer Functions for Rigid Rectangular Foundations," by A.S. Veletsos, A.M. Prasad and W.H. Wu, 7/31/91, to be published.

NCEER-91-0020 "Hybrid Control of Seismic-Excited Nonlinear and Inelastic Structural Systems," by J.N. Yang, Z. Li and A. Danielians, 8/1/91, (PB92-143171, A06, MF-A02).

NCEER-91-0021 "The NCEER-91 Earthquake Catalog: Improved Intensity-Based Magnitudes and Recurrence Relations for U.S. Earthquakes East of New Madrid," by L. Seeber and J.G. Armbruster, 8/28/91, (PB92-176742, A06, MF-A02).

NCEER-91-0022 "Proceedings from the Implementation of Earthquake Planning and Education in Schools: The Need for Change - The Roles of the Changemakers," by K.E.K. Ross and F. Winslow, 7/23/91, (PB92-129998, A12, MF-A03).

NCEER-91-0023 "A Study of Reliability-Based Criteria for Seismic Design of Reinforced Concrete Frame Buildings," by H.H.M. Hwang and H-M. Hsu, 8/10/91, (PB92-140235, A09, MF-A02).

NCEER-91-0024 "Experimental Verification of a Number of Structural System Identification Algorithms," by R.G. Ghanem, H. Gavin and M. Shinozuka, 9/18/91, (PB92-176577, A18, MF-A04).

NCEER-91-0025 "Probabilistic Evaluation of Liquefaction Potential," by H.H.M. Hwang and C.S. Lee," 11/25/91, (PB92-143429, A05, MF-A01).

NCEER-91-0026 "Instantaneous Optimal Control for Linear, Nonlinear and Hysteretic Structures - Stable Controllers," by J.N. Yang and Z. Li, 11/15/91, (PB92-163807, A04, MF-A01).

NCEER-91-0027 "Experimental and Theoretical Study of a Sliding Isolation System for Bridges," by M.C. Constantinou, A. Kartoum, A.M. Reinhorn and P. Bradford, 11/15/91, (PB92-176973, A10, MF-A03).

NCEER-92-0001 "Case Studies of Liquefaction and Lifeline Performance During Past Earthquakes, Volume 1: Japanese Case Studies," Edited by M. Hamada and T. O'Rourke, 2/17/92, (PB92-197243, A18, MF-A04).

NCEER-92-0002 "Case Studies of Liquefaction and Lifeline Performance During Past Earthquakes, Volume 2: United States Case Studies," Edited by T. O'Rourke and M. Hamada, 2/17/92, (PB92-197250, A20, MF-A04).

NCEER-92-0003 "Issues in Earthquake Education," Edited by K. Ross, 2/3/92, (PB92-222389, A07, MF-A02).

NCEER-92-0004 "Proceedings from the First U.S. - Japan Workshop on Earthquake Protective Systems for Bridges," Edited by I.G. Buckle, 2/4/92, (PB94-142239, A99, MF-A06).

NCEER-92-0005 "Seismic Ground Motion from a Haskell-Type Source in a Multiple-Layered Half-Space," A.P. Theoharis, G. Deodatis and M. Shinozuka, 1/2/92, to be published.

NCEER-92-0006 "Proceedings from the Site Effects Workshop," Edited by R. Whitman, 2/29/92, (PB92-197201, A04, MF-A01).

NCEER-92-0007 "Engineering Evaluation of Permanent Ground Deformations Due to Seismically-Induced Liquefaction," by M.H. Baziar, R. Dobry and A-W.M. Elgamal, 3/24/92, (PB92-222421, A13, MF-A03).

NCEER-92-0008 "A Procedure for the Seismic Evaluation of Buildings in the Central and Eastern United States," by C.D. Poland and J.O. Malley, 4/2/92, (PB92-222439, A20, MF-A04).

NCEER-92-0009 "Experimental and Analytical Study of a Hybrid Isolation System Using Friction Controllable Sliding Bearings," by M.Q. Feng, S. Fujii and M. Shinozuka, 5/15/92, (PB93-150282, A06, MF-A02).

NCEER-92-0010 "Seismic Resistance of Slab-Column Connections in Existing Non-Ductile Flat-Plate Buildings," by A.J. Durrani and Y. Du, 5/18/92, (PB93-116812, A06, MF-A02).

NCEER-92-0011 "The Hysteretic and Dynamic Behavior of Brick Masonry Walls Upgraded by Ferrocement Coatings Under Cyclic Loading and Strong Simulated Ground Motion," by H. Lee and S.P. Prawel, 5/11/92, to be published.

NCEER-92-0012 "Study of Wire Rope Systems for Seismic Protection of Equipment in Buildings," by G.F. Demetriades, M.C. Constantinou and A.M. Reinhorn, 5/20/92, (PB93-116655, A08, MF-A02).

NCEER-92-0013 "Shape Memory Structural Dampers: Material Properties, Design and Seismic Testing," by P.R. Witting and F.A. Cozzarelli, 5/26/92, (PB93-116663, A05, MF-A01).

NCEER-92-0014 "Longitudinal Permanent Ground Deformation Effects on Buried Continuous Pipelines," by M.J. O'Rourke, and C. Nordberg, 6/15/92, (PB93-116671, A08, MF-A02).

NCEER-92-0015 "A Simulation Method for Stationary Gaussian Random Functions Based on the Sampling Theorem," by M. Grigoriu and S. Balopoulou, 6/11/92, (PB93-127496, A05, MF-A01).

NCEER-92-0016 "Gravity-Load-Designed Reinforced Concrete Buildings: Seismic Evaluation of Existing Construction and Detailing Strategies for Improved Seismic Resistance," by G.W. Hoffmann, S.K. Kunnath, A.M. Reinhorn and J.B. Mander, 7/15/92, (PB94-142007, A08, MF-A02).

NCEER-92-0017 "Observations on Water System and Pipeline Performance in the Limón Area of Costa Rica Due to the April 22, 1991 Earthquake," by M. O'Rourke and D. Ballantyne, 6/30/92, (PB93-126811, A06, MF-A02).

NCEER-92-0018 "Fourth Edition of Earthquake Education Materials for Grades K-12," Edited by K.E.K. Ross, 8/10/92, (PB93-114023, A07, MF-A02).

NCEER-92-0019 "Proceedings from the Fourth Japan-U.S. Workshop on Earthquake Resistant Design of Lifeline Facilities and Countermeasures for Soil Liquefaction," Edited by M. Hamada and T.D. O'Rourke, 8/12/92, (PB93-163939, A99, MF-E11).

NCEER-92-0020 "Active Bracing System: A Full Scale Implementation of Active Control," by A.M. Reinhorn, T.T. Soong, R.C. Lin, M.A. Riley, Y.P. Wang, S. Aizawa and M. Higashino, 8/14/92, (PB93-127512, A06, MF-A02).

NCEER-92-0021 "Empirical Analysis of Horizontal Ground Displacement Generated by Liquefaction-Induced Lateral Spreads," by S.F. Bartlett and T.L. Youd, 8/17/92, (PB93-188241, A06, MF-A02).

NCEER-92-0022 "IDARC Version 3.0: Inelastic Damage Analysis of Reinforced Concrete Structures," by S.K. Kunnath, A.M. Reinhorn and R.F. Lobo, 8/31/92, (PB93-227502, A07, MF-A02).

NCEER-92-0023 "A Semi-Empirical Analysis of Strong-Motion Peaks in Terms of Seismic Source, Propagation Path and Local Site Conditions, by M. Kamiyama, M.J. O'Rourke and R. Flores-Berrones, 9/9/92, (PB93-150266, A08, MF-A02).

NCEER-92-0024 "Seismic Behavior of Reinforced Concrete Frame Structures with Nonductile Details, Part I: Summary of Experimental Findings of Full Scale Beam-Column Joint Tests," by A. Beres, R.N. White and P. Gergely, 9/30/92, (PB93-227783, A05, MF-A01).

NCEER-92-0025 "Experimental Results of Repaired and Retrofitted Beam-Column Joint Tests in Lightly Reinforced Concrete Frame Buildings," by A. Beres, S. El-Borgi, R.N. White and P. Gergely, 10/29/92, (PB93-227791, A05, MF-A01).

NCEER-92-0026 "A Generalization of Optimal Control Theory: Linear and Nonlinear Structures," by J.N. Yang, Z. Li and S. Vongchavalitkul, 11/2/92, (PB93-188621, A05, MF-A01).

NCEER-92-0027 "Seismic Resistance of Reinforced Concrete Frame Structures Designed Only for Gravity Loads: Part I - Design and Properties of a One-Third Scale Model Structure," by J.M. Bracci, A.M. Reinhorn and J.B. Mander, 12/1/92, (PB94-104502, A08, MF-A02).

NCEER-92-0028 "Seismic Resistance of Reinforced Concrete Frame Structures Designed Only for Gravity Loads: Part II - Experimental Performance of Subassemblages," by L.E. Aycardi, J.B. Mander and A.M. Reinhorn, 12/1/92, (PB94-104510, A08, MF-A02).

NCEER-92-0029 "Seismic Resistance of Reinforced Concrete Frame Structures Designed Only for Gravity Loads: Part III - Experimental Performance and Analytical Study of a Structural Model," by J.M. Bracci, A.M. Reinhorn and J.B. Mander, 12/1/92, (PB93-227528, A09, MF-A01).

NCEER-92-0030 "Evaluation of Seismic Retrofit of Reinforced Concrete Frame Structures: Part I - Experimental Performance of Retrofitted Subassemblages," by D. Choudhuri, J.B. Mander and A.M. Reinhorn, 12/8/92, (PB93-198307, A07, MF-A02).

NCEER-92-0031 "Evaluation of Seismic Retrofit of Reinforced Concrete Frame Structures: Part II - Experimental Performance and Analytical Study of a Retrofitted Structural Model," by J.M. Bracci, A.M. Reinhorn and J.B. Mander, 12/8/92, (PB93-198315, A09, MF-A03).

NCEER-92-0032 "Experimental and Analytical Investigation of Seismic Response of Structures with Supplemental Fluid Viscous Dampers," by M.C. Constantinou and M.D. Symans, 12/21/92, (PB93-191435, A10, MF-A03). This report is available only through NTIS (see address given above).

NCEER-92-0033 "Reconnaissance Report on the Cairo, Egypt Earthquake of October 12, 1992," by M. Khater, 12/23/92, (PB93-188621, A03, MF-A01).

NCEER-92-0034 "Low-Level Dynamic Characteristics of Four Tall Flat-Plate Buildings in New York City," by H. Gavin, S. Yuan, J. Grossman, E. Pekelis and K. Jacob, 12/28/92, (PB93-188217, A07, MF-A02).

NCEER-93-0001 "An Experimental Study on the Seismic Performance of Brick-Infilled Steel Frames With and Without Retrofit," by J.B. Mander, B. Nair, K. Wojtkowski and J. Ma, 1/29/93, (PB93-227510, A07, MF-A02).

NCEER-93-0002 "Social Accounting for Disaster Preparedness and Recovery Planning," by S. Cole, E. Pantoja and V. Razak, 2/22/93, (PB94-142114, A12, MF-A03).

NCEER-93-0003 "Assessment of 1991 NEHRP Provisions for Nonstructural Components and Recommended Revisions," by T.T. Soong, G. Chen, Z. Wu, R-H. Zhang and M. Grigoriu, 3/1/93, (PB93-188639, A06, MF-A02).

NCEER-93-0004 "Evaluation of Static and Response Spectrum Analysis Procedures of SEAOC/UBC for Seismic Isolated Structures," by C.W. Winters and M.C. Constantinou, 3/23/93, (PB93-198299, A10, MF-A03).

NCEER-93-0005 "Earthquakes in the Northeast - Are We Ignoring the Hazard? A Workshop on Earthquake Science and Safety for Educators," edited by K.E.K. Ross, 4/2/93, (PB94-103066, A09, MF-A02).

NCEER-93-0006 "Inelastic Response of Reinforced Concrete Structures with Viscoelastic Braces," by R.F. Lobo, J.M. Bracci, K.L. Shen, A.M. Reinhorn and T.T. Soong, 4/5/93, (PB93-227486, A05, MF-A02).

NCEER-93-0007 "Seismic Testing of Installation Methods for Computers and Data Processing Equipment," by K. Kosar, T.T. Soong, K.L. Shen, J.A. HoLung and Y.K. Lin, 4/12/93, (PB93-198299, A07, MF-A02).

NCEER-93-0008 "Retrofit of Reinforced Concrete Frames Using Added Dampers," by A. Reinhorn, M. Constantinou and C. Li, to be published.

NCEER-93-0009 "Seismic Behavior and Design Guidelines for Steel Frame Structures with Added Viscoelastic Dampers," by K.C. Chang, M.L. Lai, T.T. Soong, D.S. Hao and Y.C. Yeh, 5/1/93, (PB94-141959, A07, MF-A02).

NCEER-93-0010 "Seismic Performance of Shear-Critical Reinforced Concrete Bridge Piers," by J.B. Mander, S.M. Waheed, M.T.A. Chaudhary and S.S. Chen, 5/12/93, (PB93-227494, A08, MF-A02).

NCEER-93-0011 "3D-BASIS-TABS: Computer Program for Nonlinear Dynamic Analysis of Three Dimensional Base Isolated Structures," by S. Nagarajaiah, C. Li, A.M. Reinhorn and M.C. Constantinou, 8/2/93, (PB94-141819, A09, MF-A02).

NCEER-93-0012 "Effects of Hydrocarbon Spills from an Oil Pipeline Break on Ground Water," by O.J. Helweg and H.H.M. Hwang, 8/3/93, (PB94-141942, A06, MF-A02).

NCEER-93-0013 "Simplified Procedures for Seismic Design of Nonstructural Components and Assessment of Current Code Provisions," by M.P. Singh, L.E. Suarez, E.E. Matheu and G.O. Maldonado, 8/4/93, (PB94-141827, A09, MF-A02).

NCEER-93-0014 "An Energy Approach to Seismic Analysis and Design of Secondary Systems," by G. Chen and T.T. Soong, 8/6/93, (PB94-142767, A11, MF-A03).

NCEER-93-0015 "Proceedings from School Sites: Becoming Prepared for Earthquakes - Commemorating the Third Anniversary of the Loma Prieta Earthquake," Edited by F.E. Winslow and K.E.K. Ross, 8/16/93, (PB94-154275, A16, MF-A02).

NCEER-93-0016 "Reconnaissance Report of Damage to Historic Monuments in Cairo, Egypt Following the October 12, 1992 Dahshur Earthquake," by D. Sykora, D. Look, G. Croci, E. Karaesmen and E. Karaesmen, 8/19/93, (PB94-142221, A08, MF-A02).

NCEER-93-0017 "The Island of Guam Earthquake of August 8, 1993," by S.W. Swan and S.K. Harris, 9/30/93, (PB94-141843, A04, MF-A01).

NCEER-93-0018 "Engineering Aspects of the October 12, 1992 Egyptian Earthquake," by A.W. Elgamal, M. Amer, K. Adalier and A. Abul-Fadl, 10/7/93, (PB94-141983, A05, MF-A01).

NCEER-93-0019 "Development of an Earthquake Motion Simulator and its Application in Dynamic Centrifuge Testing," by I. Krstelj, Supervised by J.H. Prevost, 10/23/93, (PB94-181773, A-10, MF-A03).

NCEER-93-0020 "NCEER-Taisei Corporation Research Program on Sliding Seismic Isolation Systems for Bridges: Experimental and Analytical Study of a Friction Pendulum System (FPS)," by M.C. Constantinou, P. Tsopelas, Y-S. Kim and S. Okamoto, 11/1/93, (PB94-142775, A08, MF-A02).

NCEER-93-0021 "Finite Element Modeling of Elastomeric Seismic Isolation Bearings," by L.J. Billings, Supervised by R. Shepherd, 11/8/93, to be published.

NCEER-93-0022 "Seismic Vulnerability of Equipment in Critical Facilities: Life-Safety and Operational Consequences," by K. Porter, G.S. Johnson, M.M. Zadeh, C. Scawthorn and S. Eder, 11/24/93, (PB94-181765, A16, MF-A03).

NCEER-93-0023 "Hokkaido Nansei-oki, Japan Earthquake of July 12, 1993, by P.I. Yanev and C.R. Scawthorn, 12/23/93, (PB94-181500, A07, MF-A01).

NCEER-94-0001 "An Evaluation of Seismic Serviceability of Water Supply Networks with Application to the San Francisco Auxiliary Water Supply System," by I. Markov, Supervised by M. Grigoriu and T. O'Rourke, 1/21/94, (PB94-204013, A07, MF-A02).

NCEER-94-0002 "NCEER-Taisei Corporation Research Program on Sliding Seismic Isolation Systems for Bridges: Experimental and Analytical Study of Systems Consisting of Sliding Bearings, Rubber Restoring Force Devices and Fluid Dampers," Volumes I and II, by P. Tsopelas, S. Okamoto, M.C. Constantinou, D. Ozaki and S. Fujii, 2/4/94, (PB94-181740, A09, MF-A02 and PB94-181757, A12, MF-A03).

NCEER-94-0003 "A Markov Model for Local and Global Damage Indices in Seismic Analysis," by S. Rahman and M. Grigoriu, 2/18/94, (PB94-206000, A12, MF-A03).

NCEER-94-0004 "Proceedings from the NCEER Workshop on Seismic Response of Masonry Infills," edited by D.P. Abrams, 3/1/94, (PB94-180783, A07, MF-A02).

NCEER-94-0005 "The Northridge, California Earthquake of January 17, 1994: General Reconnaissance Report," edited by J.D. Goltz, 3/11/94, (PB94-193943, A10, MF-A03).

NCEER-94-0006 "Seismic Energy Based Fatigue Damage Analysis of Bridge Columns: Part I - Evaluation of Seismic Capacity," by G.A. Chang and J.B. Mander, 3/14/94, (PB94-219185, A11, MF-A03).

NCEER-94-0007 "Seismic Isolation of Multi-Story Frame Structures Using Spherical Sliding Isolation Systems," by T.M. Al-Hussaini, V.A. Zayas and M.C. Constantinou, 3/17/94, (PB94-193745, A09, MF-A02).

NCEER-94-0008 "The Northridge, California Earthquake of January 17, 1994: Performance of Highway Bridges," edited by I.G. Buckle, 3/24/94, (PB94-193851, A06, MF-A02).

NCEER-94-0009 "Proceedings of the Third U.S.-Japan Workshop on Earthquake Protective Systems for Bridges," edited by I.G. Buckle and I. Friedland, 3/31/94, (PB94-195815, A99, MF-A06).

NCEER-94-0010 "3D-BASIS-ME: Computer Program for Nonlinear Dynamic Analysis of Seismically Isolated Single and Multiple Structures and Liquid Storage Tanks," by P.C. Tsopelas, M.C. Constantinou and A.M. Reinhorn, 4/12/94, (PB94-204922, A09, MF-A02).

NCEER-94-0011 "The Northridge, California Earthquake of January 17, 1994: Performance of Gas Transmission Pipelines," by T.D. O'Rourke and M.C. Palmer, 5/16/94, (PB94-204989, A05, MF-A01).

NCEER-94-0012 "Feasibility Study of Replacement Procedures and Earthquake Performance Related to Gas Transmission Pipelines," by T.D. O'Rourke and M.C. Palmer, 5/25/94, (PB94-206638, A09, MF-A02).

NCEER-94-0013 "Seismic Energy Based Fatigue Damage Analysis of Bridge Columns: Part II - Evaluation of Seismic Demand," by G.A. Chang and J.B. Mander, 6/1/94, (PB95-18106, A08, MF-A02).

NCEER-94-0014 "NCEER-Taisei Corporation Research Program on Sliding Seismic Isolation Systems for Bridges: Experimental and Analytical Study of a System Consisting of Sliding Bearings and Fluid Restoring Force/Damping Devices," by P. Tsopelas and M.C. Constantinou, 6/13/94, (PB94-219144, A10, MF-A03).

NCEER-94-0015 "Generation of Hazard-Consistent Fragility Curves for Seismic Loss Estimation Studies," by H. Hwang and J-R. Huo, 6/14/94, (PB95-181996, A09, MF-A02).

NCEER-94-0016 "Seismic Study of Building Frames with Added Energy-Absorbing Devices," by W.S. Pong, C.S. Tsai and G.C. Lee, 6/20/94, (PB94-219136, A10, A03).

NCEER-94-0017 "Sliding Mode Control for Seismic-Excited Linear and Nonlinear Civil Engineering Structures," by J. Yang, J. Wu, A. Agrawal and Z. Li, 6/21/94, (PB95-138483, A06, MF-A02).

NCEER-94-0018 "3D-BASIS-TABS Version 2.0: Computer Program for Nonlinear Dynamic Analysis of Three Dimensional Base Isolated Structures," by A.M. Reinhorn, S. Nagarajaiah, M.C. Constantinou, P. Tsopelas and R. Li, 6/22/94, (PB95-182176, A08, MF-A02).

NCEER-94-0019 "Proceedings of the International Workshop on Civil Infrastructure Systems: Application of Intelligent Systems and Advanced Materials on Bridge Systems," Edited by G.C. Lee and K.C. Chang, 7/18/94, (PB95-252474, A20, MF-A04).

NCEER-94-0020 "Study of Seismic Isolation Systems for Computer Floors," by V. Lambrou and M.C. Constantinou, 7/19/94, (PB95-138533, A10, MF-A03).

NCEER-94-0021 "Proceedings of the U.S.-Italian Workshop on Guidelines for Seismic Evaluation and Rehabilitation of Unreinforced Masonry Buildings," Edited by D.P. Abrams and G.M. Calvi, 7/20/94, (PB95-138749, A13, MF-A03).

NCEER-94-0022 "NCEER-Taisei Corporation Research Program on Sliding Seismic Isolation Systems for Bridges: Experimental and Analytical Study of a System Consisting of Lubricated PTFE Sliding Bearings and Mild Steel Dampers," by P. Tsopelas and M.C. Constantinou, 7/22/94, (PB95-182184, A08, MF-A02).

NCEER-94-0023 “Development of Reliability-Based Design Criteria for Buildings Under Seismic Load,” by Y.K. Wen, H. Hwang and M. Shinozuka, 8/1/94, (PB95-211934, A08, MF-A02).

NCEER-94-0024 “Experimental Verification of Acceleration Feedback Control Strategies for an Active Tendon System,” by S.J. Dyke, B.F. Spencer, Jr., P. Quast, M.K. Sain, D.C. Kaspari, Jr. and T.T. Soong, 8/29/94, (PB95-212320, A05, MF-A01).

NCEER-94-0025 “Seismic Retrofitting Manual for Highway Bridges,” Edited by I.G. Buckle and I.F. Friedland, published by the Federal Highway Administration (PB95-212676, A15, MF-A03).

NCEER-94-0026 “Proceedings from the Fifth U.S.-Japan Workshop on Earthquake Resistant Design of Lifeline Facilities and Countermeasures Against Soil Liquefaction,” Edited by T.D. O’Rourke and M. Hamada, 11/7/94, (PB95-220802, A99, MF-E08).

NCEER-95-0001 "Experimental and Analytical Investigation of Seismic Retrofit of Structures with Supplemental Damping: Part 1 - Fluid Viscous Damping Devices," by A.M. Reinhorn, C. Li and M.C. Constantinou, 1/3/95, (PB95-266599, A09, MF-A02).

NCEER-95-0002 "Experimental and Analytical Study of Low-Cycle Fatigue Behavior of Semi-Rigid Top-And-Seat Angle Connections," by G. Pekcan, J.B. Mander and S.S. Chen, 1/5/95, (PB95-220042, A07, MF-A02).

NCEER-95-0003 "NCEER-ATC Joint Study on Fragility of Buildings," by T. Anagnos, C. Rojahn and A.S. Kiremidjian, 1/20/95, (PB95-220026, A06, MF-A02).

NCEER-95-0004 "Nonlinear Control Algorithms for Peak Response Reduction," by Z. Wu, T.T. Soong, V. Gattulli and R.C. Lin, 2/16/95, (PB95-220349, A05, MF-A01).

NCEER-95-0005 "Pipeline Replacement Feasibility Study: A Methodology for Minimizing Seismic and Corrosion Risks to Underground Natural Gas Pipelines," by R.T. Eguchi, H.A. Seligson and D.G. Honegger, 3/2/95, (PB95-252326, A06, MF-A02).

NCEER-95-0006 "Evaluation of Seismic Performance of an 11-Story Frame Building During the 1994 Northridge Earthquake," by F. Naeim, R. DiSulio, K. Benuska, A. Reinhorn and C. Li, to be published.

NCEER-95-0007 "Prioritization of Bridges for Seismic Retrofitting," by N. Basöz and A.S. Kiremidjian, 4/24/95, (PB95-252300, A08, MF-A02).

NCEER-95-0008 "Method for Developing Motion Damage Relationships for Reinforced Concrete Frames," by A. Singhal and A.S. Kiremidjian, 5/11/95, (PB95-266607, A06, MF-A02).

NCEER-95-0009 "Experimental and Analytical Investigation of Seismic Retrofit of Structures with Supplemental Damping: Part II - Friction Devices," by C. Li and A.M. Reinhorn, 7/6/95, (PB96-128087, A11, MF-A03).

NCEER-95-0010 "Experimental Performance and Analytical Study of a Non-Ductile Reinforced Concrete Frame Structure Retrofitted with Elastomeric Spring Dampers," by G. Pekcan, J.B. Mander and S.S. Chen, 7/14/95, (PB96-137161, A08, MF-A02).

NCEER-95-0011 "Development and Experimental Study of Semi-Active Fluid Damping Devices for Seismic Protection of Structures," by M.D. Symans and M.C. Constantinou, 8/3/95, (PB96-136940, A23, MF-A04).

NCEER-95-0012 "Real-Time Structural Parameter Modification (RSPM): Development of Innervated Structures," by Z. Liang, M. Tong and G.C. Lee, 4/11/95, (PB96-137153, A06, MF-A01).

NCEER-95-0013 "Experimental and Analytical Investigation of Seismic Retrofit of Structures with Supplemental Damping: Part III - Viscous Damping Walls," by A.M. Reinhorn and C. Li, 10/1/95, (PB96-176409, A11, MF-A03).

NCEER-95-0014 "Seismic Fragility Analysis of Equipment and Structures in a Memphis Electric Substation," by J-R. Huo and H.H.M. Hwang, 8/10/95, (PB96-128087, A09, MF-A02).

NCEER-95-0015 "The Hanshin-Awaji Earthquake of January 17, 1995: Performance of Lifelines," Edited by M. Shinozuka, 11/3/95, (PB96-176383, A15, MF-A03).

NCEER-95-0016 "Highway Culvert Performance During Earthquakes," by T.L. Youd and C.J. Beckman, available as NCEER-96-0015.

NCEER-95-0017 "The Hanshin-Awaji Earthquake of January 17, 1995: Performance of Highway Bridges," Edited by I.G. Buckle, 12/1/95, to be published.

NCEER-95-0018 "Modeling of Masonry Infill Panels for Structural Analysis," by A.M. Reinhorn, A. Madan, R.E. Valles, Y. Reichmann and J.B. Mander, 12/8/95, (PB97-110886, MF-A01, A06).

NCEER-95-0019 "Optimal Polynomial Control for Linear and Nonlinear Structures," by A.K. Agrawal and J.N. Yang, 12/11/95, (PB96-168737, A07, MF-A02).

NCEER-95-0020 "Retrofit of Non-Ductile Reinforced Concrete Frames Using Friction Dampers," by R.S. Rao, P. Gergely and R.N. White, 12/22/95, (PB97-133508, A10, MF-A02).

NCEER-95-0021 "Parametric Results for Seismic Response of Pile-Supported Bridge Bents," by G. Mylonakis, A. Nikolaou and G. Gazetas, 12/22/95, (PB97-100242, A12, MF-A03).

NCEER-95-0022 "Kinematic Bending Moments in Seismically Stressed Piles," by A. Nikolaou, G. Mylonakis and G. Gazetas, 12/23/95, (PB97-113914, MF-A03, A13).

NCEER-96-0001 "Dynamic Response of Unreinforced Masonry Buildings with Flexible Diaphragms," by A.C. Costley and D.P. Abrams," 10/10/96, (PB97-133573, MF-A03, A15).

NCEER-96-0002 "State of the Art Review: Foundations and Retaining Structures," by I. Po Lam, to be published.

NCEER-96-0003 "Ductility of Rectangular Reinforced Concrete Bridge Columns with Moderate Confinement," by N. Wehbe, M. Saiidi, D. Sanders and B. Douglas, 11/7/96, (PB97-133557, A06, MF-A02).

NCEER-96-0004 "Proceedings of the Long-Span Bridge Seismic Research Workshop," edited by I.G. Buckle and I.M. Friedland, to be published.

NCEER-96-0005 "Establish Representative Pier Types for Comprehensive Study: Eastern United States," by J. Kulicki and Z. Prucz, 5/28/96, (PB98-119217, A07, MF-A02).

NCEER-96-0006 "Establish Representative Pier Types for Comprehensive Study: Western United States," by R. Imbsen, R.A. Schamber and T.A. Osterkamp, 5/28/96, (PB98-118607, A07, MF-A02).

NCEER-96-0007 "Nonlinear Control Techniques for Dynamical Systems with Uncertain Parameters," by R.G. Ghanem and M.I. Bujakov, 5/27/96, (PB97-100259, A17, MF-A03).

NCEER-96-0008 "Seismic Evaluation of a 30-Year Old Non-Ductile Highway Bridge Pier and Its Retrofit," by J.B. Mander, B. Mahmoodzadegan, S. Bhadra and S.S. Chen, 5/31/96, (PB97-110902, MF-A03, A10).

NCEER-96-0009 "Seismic Performance of a Model Reinforced Concrete Bridge Pier Before and After Retrofit," by J.B. Mander, J.H. Kim and C.A. Ligozio, 5/31/96, (PB97-110910, MF-A02, A10).

NCEER-96-0010 "IDARC2D Version 4.0: A Computer Program for the Inelastic Damage Analysis of Buildings," by R.E. Valles, A.M. Reinhorn, S.K. Kunnath, C. Li and A. Madan, 6/3/96, (PB97-100234, A17, MF-A03).

NCEER-96-0011 "Estimation of the Economic Impact of Multiple Lifeline Disruption: Memphis Light, Gas and Water Division Case Study," by S.E. Chang, H.A. Seligson and R.T. Eguchi, 8/16/96, (PB97-133490, A11, MF-A03).

NCEER-96-0012 "Proceedings from the Sixth Japan-U.S. Workshop on Earthquake Resistant Design of Lifeline Facilities and Countermeasures Against Soil Liquefaction, Edited by M. Hamada and T. O'Rourke, 9/11/96, (PB97-133581, A99, MF-A06).

NCEER-96-0013 "Chemical Hazards, Mitigation and Preparedness in Areas of High Seismic Risk: A Methodology for Estimating the Risk of Post-Earthquake Hazardous Materials Release," by H.A. Seligson, R.T. Eguchi, K.J. Tierney and K. Richmond, 11/7/96, (PB97-133565, MF-A02, A08).

NCEER-96-0014 "Response of Steel Bridge Bearings to Reversed Cyclic Loading," by J.B. Mander, D-K. Kim, S.S. Chen and G.J. Premus, 11/13/96, (PB97-140735, A12, MF-A03).

NCEER-96-0015 "Highway Culvert Performance During Past Earthquakes," by T.L. Youd and C.J. Beckman, 11/25/96, (PB97-133532, A06, MF-A01).

NCEER-97-0001 "Evaluation, Prevention and Mitigation of Pounding Effects in Building Structures," by R.E. Valles and A.M. Reinhorn, 2/20/97, (PB97-159552, A14, MF-A03).

NCEER-97-0002 "Seismic Design Criteria for Bridges and Other Highway Structures," by C. Rojahn, R. Mayes, D.G. Anderson, J. Clark, J.H. Hom, R.V. Nutt and M.J. O'Rourke, 4/30/97, (PB97-194658, A06, MF-A03).

NCEER-97-0003 “Proceedings of the U.S.-Italian Workshop on Seismic Evaluation and Retrofit,” Edited by D.P. Abrams and G.M. Calvi, 3/19/97, (PB97-194666, A13, MF-A03).

NCEER-97-0004 "Investigation of Seismic Response of Buildings with Linear and Nonlinear Fluid Viscous Dampers," by A.A. Seleemah and M.C. Constantinou, 5/21/97, (PB98-109002, A15, MF-A03).

NCEER-97-0005 "Proceedings of the Workshop on Earthquake Engineering Frontiers in Transportation Facilities," edited by G.C. Lee and I.M. Friedland, 8/29/97, (PB98-128911, A25, MR-A04).

NCEER-97-0006 "Cumulative Seismic Damage of Reinforced Concrete Bridge Piers," by S.K. Kunnath, A. El-Bahy, A. Taylor and W. Stone, 9/2/97, (PB98-108814, A11, MF-A03).

NCEER-97-0007 "Structural Details to Accommodate Seismic Movements of Highway Bridges and Retaining Walls," by R.A. Imbsen, R.A. Schamber, E. Thorkildsen, A. Kartoum, B.T. Martin, T.N. Rosser and J.M. Kulicki, 9/3/97, (PB98-108996, A09, MF-A02).

NCEER-97-0008 "A Method for Earthquake Motion-Damage Relationships with Application to Reinforced Concrete Frames," by A. Singhal and A.S. Kiremidjian, 9/10/97, (PB98-108988, A13, MF-A03).

NCEER-97-0009 "Seismic Analysis and Design of Bridge Abutments Considering Sliding and Rotation," by K. Fishman and R. Richards, Jr., 9/15/97, (PB98-108897, A06, MF-A02).

NCEER-97-0010 "Proceedings of the FHWA/NCEER Workshop on the National Representation of Seismic Ground Motion for New and Existing Highway Facilities," edited by I.M. Friedland, M.S. Power and R.L. Mayes, 9/22/97, (PB98-128903, A21, MF-A04).

NCEER-97-0011 "Seismic Analysis for Design or Retrofit of Gravity Bridge Abutments," by K.L. Fishman, R. Richards, Jr. and R.C. Divito, 10/2/97, (PB98-128937, A08, MF-A02).

NCEER-97-0012 "Evaluation of Simplified Methods of Analysis for Yielding Structures," by P. Tsopelas, M.C. Constantinou, C.A. Kircher and A.S. Whittaker, 10/31/97, (PB98-128929, A10, MF-A03).

NCEER-97-0013 "Seismic Design of Bridge Columns Based on Control and Repairability of Damage," by C-T. Cheng and J.B. Mander, 12/8/97, (PB98-144249, A11, MF-A03).

NCEER-97-0014 "Seismic Resistance of Bridge Piers Based on Damage Avoidance Design," by J.B. Mander and C-T. Cheng, 12/10/97, (PB98-144223, A09, MF-A02).

NCEER-97-0015 “Seismic Response of Nominally Symmetric Systems with Strength Uncertainty,” by S. Balopoulou and M. Grigoriu, 12/23/97, (PB98-153422, A11, MF-A03).

NCEER-97-0016 “Evaluation of Seismic Retrofit Methods for Reinforced Concrete Bridge Columns,” by T.J. Wipf, F.W. Klaiber and F.M. Russo, 12/28/97, (PB98-144215, A12, MF-A03).

NCEER-97-0017 “Seismic Fragility of Existing Conventional Reinforced Concrete Highway Bridges,” by C.L. Mullen and A.S. Cakmak, 12/30/97, (PB98-153406, A08, MF-A02).

NCEER-97-0018 “Loss Asssessment of Memphis Buildings,” edited by D.P. Abrams and M. Shinozuka, 12/31/97, (PB98-144231, A13, MF-A03).

NCEER-97-0019 “Seismic Evaluation of Frames with Infill Walls Using Quasi-static Experiments,” by K.M. Mosalam, R.N. White and P. Gergely, 12/31/97, (PB98-153455, A07, MF-A02).

NCEER-97-0020 “Seismic Evaluation of Frames with Infill Walls Using Pseudo-dynamic Experiments,” by K.M. Mosalam, R.N. White and P. Gergely, 12/31/97, (PB98-153430, A07, MF-A02).

NCEER-97-0021 “Computational Strategies for Frames with Infill Walls: Discrete and Smeared Crack Analyses and Seismic Fragility,” by K.M. Mosalam, R.N. White and P. Gergely, 12/31/97, (PB98-153414, A10, MF-A02).

NCEER-97-0022 "Proceedings of the NCEER Workshop on Evaluation of Liquefaction Resistance of Soils," edited by T.L. Youd and I.M. Idriss, 12/31/97, (PB98-155617, A15, MF-A03).

MCEER-98-0001 "Extraction of Nonlinear Hysteretic Properties of Seismically Isolated Bridges from Quick-Release Field Tests," by Q. Chen, B.M. Douglas, E.M. Maragakis and I.G. Buckle, 5/26/98, (PB99-118838, A06, MF-A01).

MCEER-98-0002 "Methodologies for Evaluating the Importance of Highway Bridges," by A. Thomas, S. Eshenaur and J. Kulicki, 5/29/98, (PB99-118846, A10, MF-A02).

MCEER-98-0003 "Capacity Design of Bridge Piers and the Analysis of Overstrength," by J.B. Mander, A. Dutta and P. Goel, 6/1/98, (PB99-118853, A09, MF-A02).

MCEER-98-0004 "Evaluation of Bridge Damage Data from the Loma Prieta and Northridge, California Earthquakes," by N. Basoz and A. Kiremidjian, 6/2/98, (PB99-118861, A15, MF-A03).

MCEER-98-0005 "Screening Guide for Rapid Assessment of Liquefaction Hazard at Highway Bridge Sites," by T. L. Youd, 6/16/98, (PB99-118879, A06, not available on microfiche).

MCEER-98-0006 "Structural Steel and Steel/Concrete Interface Details for Bridges," by P. Ritchie, N. Kauhl and J. Kulicki, 7/13/98, (PB99-118945, A06, MF-A01).

MCEER-98-0007 "Capacity Design and Fatigue Analysis of Confined Concrete Columns," by A. Dutta and J.B. Mander, 7/14/98, (PB99-118960, A14, MF-A03).

MCEER-98-0008 "Proceedings of the Workshop on Performance Criteria for Telecommunication Services Under Earthquake Conditions," edited by A.J. Schiff, 7/15/98, (PB99-118952, A08, MF-A02).

MCEER-98-0009 "Fatigue Analysis of Unconfined Concrete Columns," by J.B. Mander, A. Dutta and J.H. Kim, 9/12/98, (PB99-123655, A10, MF-A02).

MCEER-98-0010 "Centrifuge Modeling of Cyclic Lateral Response of Pile-Cap Systems and Seat-Type Abutments in Dry Sands," by A.D. Gadre and R. Dobry, 10/2/98, (PB99-123606, A13, MF-A03).

MCEER-98-0011 "IDARC-BRIDGE: A Computational Platform for Seismic Damage Assessment of Bridge Structures," by A.M. Reinhorn, V. Simeonov, G. Mylonakis and Y. Reichman, 10/2/98, (PB99-162919, A15, MF-A03).

MCEER-98-0012 "Experimental Investigation of the Dynamic Response of Two Bridges Before and After Retrofitting with Elastomeric Bearings," by D.A. Wendichansky, S.S. Chen and J.B. Mander, 10/2/98, (PB99-162927, A15, MF-A03).

MCEER-98-0013 "Design Procedures for Hinge Restrainers and Hinge Sear Width for Multiple-Frame Bridges," by R. Des Roches and G.L. Fenves, 11/3/98, (PB99-140477, A13, MF-A03).

MCEER-98-0014 "Response Modification Factors for Seismically Isolated Bridges," by M.C. Constantinou and J.K. Quarshie, 11/3/98, (PB99-140485, A14, MF-A03).

MCEER-98-0015 "Proceedings of the U.S.-Italy Workshop on Seismic Protective Systems for Bridges," edited by I.M. Friedland and M.C. Constantinou, 11/3/98, (PB2000-101711, A22, MF-A04).

MCEER-98-0016 "Appropriate Seismic Reliability for Critical Equipment Systems: Recommendations Based on Regional Analysis of Financial and Life Loss," by K. Porter, C. Scawthorn, C. Taylor and N. Blais, 11/10/98, (PB99-157265, A08, MF-A02).

MCEER-98-0017 "Proceedings of the U.S. Japan Joint Seminar on Civil Infrastructure Systems Research," edited by M. Shinozuka and A. Rose, 11/12/98, (PB99-156713, A16, MF-A03).

MCEER-98-0018 "Modeling of Pile Footings and Drilled Shafts for Seismic Design," by I. PoLam, M. Kapuskar and D. Chaudhuri, 12/21/98, (PB99-157257, A09, MF-A02).

MCEER-99-0001 "Seismic Evaluation of a Masonry Infilled Reinforced Concrete Frame by Pseudodynamic Testing," by S.G. Buonopane and R.N. White, 2/16/99, (PB99-162851, A09, MF-A02).

MCEER-99-0002 "Response History Analysis of Structures with Seismic Isolation and Energy Dissipation Systems: Verification Examples for Program SAP2000," by J. Scheller and M.C. Constantinou, 2/22/99, (PB99-162869, A08, MF-A02).

MCEER-99-0003 "Experimental Study on the Seismic Design and Retrofit of Bridge Columns Including Axial Load Effects," by A. Dutta, T. Kokorina and J.B. Mander, 2/22/99, (PB99-162877, A09, MF-A02).

MCEER-99-0004 "Experimental Study of Bridge Elastomeric and Other Isolation and Energy Dissipation Systems with Emphasis on Uplift Prevention and High Velocity Near-source Seismic Excitation," by A. Kasalanati and M. C. Constantinou, 2/26/99, (PB99-162885, A12, MF-A03).

MCEER-99-0005 "Truss Modeling of Reinforced Concrete Shear-flexure Behavior," by J.H. Kim and J.B. Mander, 3/8/99, (PB99-163693, A12, MF-A03).

MCEER-99-0006 "Experimental Investigation and Computational Modeling of Seismic Response of a 1:4 Scale Model Steel Structure with a Load Balancing Supplemental Damping System," by G. Pekcan, J.B. Mander and S.S. Chen, 4/2/99, (PB99-162893, A11, MF-A03).

MCEER-99-0007 "Effect of Vertical Ground Motions on the Structural Response of Highway Bridges," by M.R. Button, C.J. Cronin and R.L. Mayes, 4/10/99, (PB2000-101411, A10, MF-A03).

MCEER-99-0008 "Seismic Reliability Assessment of Critical Facilities: A Handbook, Supporting Documentation, and Model Code Provisions," by G.S. Johnson, R.E. Sheppard, M.D. Quilici, S.J. Eder and C.R. Scawthorn, 4/12/99, (PB2000-101701, A18, MF-A04).

MCEER-99-0009 "Impact Assessment of Selected MCEER Highway Project Research on the Seismic Design of Highway Structures," by C. Rojahn, R. Mayes, D.G. Anderson, J.H. Clark, D'Appolonia Engineering, S. Gloyd and R.V. Nutt, 4/14/99, (PB99-162901, A10, MF-A02).

MCEER-99-0010 "Site Factors and Site Categories in Seismic Codes," by R. Dobry, R. Ramos and M.S. Power, 7/19/99, (PB2000-101705, A08, MF-A02).

MCEER-99-0011 "Restrainer Design Procedures for Multi-Span Simply-Supported Bridges," by M.J. Randall, M. Saiidi, E. Maragakis and T. Isakovic, 7/20/99, (PB2000-101702, A10, MF-A02).

MCEER-99-0012 "Property Modification Factors for Seismic Isolation Bearings," by M.C. Constantinou, P. Tsopelas, A. Kasalanati and E. Wolff, 7/20/99, (PB2000-103387, A11, MF-A03).

MCEER-99-0013 "Critical Seismic Issues for Existing Steel Bridges," by P. Ritchie, N. Kauhl and J. Kulicki, 7/20/99, (PB2000-101697, A09, MF-A02).

MCEER-99-0014 "Nonstructural Damage Database," by A. Kao, T.T. Soong and A. Vender, 7/24/99, (PB2000-101407, A06, MF-A01).

MCEER-99-0015 "Guide to Remedial Measures for Liquefaction Mitigation at Existing Highway Bridge Sites," by H.G. Cooke and J. K. Mitchell, 7/26/99, (PB2000-101703, A11, MF-A03).

MCEER-99-0016 "Proceedings of the MCEER Workshop on Ground Motion Methodologies for the Eastern United States," edited by N. Abrahamson and A. Becker, 8/11/99, (PB2000-103385, A07, MF-A02).

MCEER-99-0017 "Quindío, Colombia Earthquake of January 25, 1999: Reconnaissance Report," by A.P. Asfura and P.J. Flores, 10/4/99, (PB2000-106893, A06, MF-A01).

MCEER-99-0018 "Hysteretic Models for Cyclic Behavior of Deteriorating Inelastic Structures," by M.V. Sivaselvan and A.M. Reinhorn, 11/5/99, (PB2000-103386, A08, MF-A02).

MCEER-99-0019 "Proceedings of the 7th U.S.- Japan Workshop on Earthquake Resistant Design of Lifeline Facilities and Countermeasures Against Soil Liquefaction," edited by T.D. O'Rourke, J.P. Bardet and M. Hamada, 11/19/99, (PB2000-103354, A99, MF-A06).

MCEER-99-0020 "Development of Measurement Capability for Micro-Vibration Evaluations with Application to Chip Fabrication Facilities," by G.C. Lee, Z. Liang, J.W. Song, J.D. Shen and W.C. Liu, 12/1/99, (PB2000-105993, A08, MF-A02).

MCEER-99-0021 "Design and Retrofit Methodology for Building Structures with Supplemental Energy Dissipating Systems," by G. Pekcan, J.B. Mander and S.S. Chen, 12/31/99, (PB2000-105994, A11, MF-A03).

MCEER-00-0001 "The Marmara, Turkey Earthquake of August 17, 1999: Reconnaissance Report," edited by C. Scawthorn; with major contributions by M. Bruneau, R. Eguchi, T. Holzer, G. Johnson, J. Mander, J. Mitchell, W. Mitchell, A. Papageorgiou, C. Scaethorn, and G. Webb, 3/23/00, (PB2000-106200, A11, MF-A03).

MCEER-00-0002 "Proceedings of the MCEER Workshop for Seismic Hazard Mitigation of Health Care Facilities," edited by G.C. Lee, M. Ettouney, M. Grigoriu, J. Hauer and J. Nigg, 3/29/00, (PB2000-106892, A08, MF-A02).

MCEER-00-0003 "The Chi-Chi, Taiwan Earthquake of September 21, 1999: Reconnaissance Report," edited by G.C. Lee and C.H. Loh, with major contributions by G.C. Lee, M. Bruneau, I.G. Buckle, S.E. Chang, P.J. Flores, T.D. O'Rourke, M. Shinozuka, T.T. Soong, C-H. Loh, K-C. Chang, Z-J. Chen, J-S. Hwang, M-L. Lin, G-Y. Liu, K-C. Tsai, G.C. Yao and C-L. Yen, 4/30/00, (PB2001-100980, A10, MF-A02).

MCEER-00-0004 "Seismic Retrofit of End-Sway Frames of Steel Deck-Truss Bridges with a Supplemental Tendon System: Experimental and Analytical Investigation," by G. Pekcan, J.B. Mander and S.S. Chen, 7/1/00, (PB2001-100982, A10, MF-A02).

MCEER-00-0005 "Sliding Fragility of Unrestrained Equipment in Critical Facilities," by W.H. Chong and T.T. Soong, 7/5/00, (PB2001-100983, A08, MF-A02).

MCEER-00-0006 "Seismic Response of Reinforced Concrete Bridge Pier Walls in the Weak Direction," by N. Abo-Shadi, M. Saiidi and D. Sanders, 7/17/00, (PB2001-100981, A17, MF-A03).

MCEER-00-0007 "Low-Cycle Fatigue Behavior of Longitudinal Reinforcement in Reinforced Concrete Bridge Columns," by J. Brown and S.K. Kunnath, 7/23/00, (PB2001-104392, A08, MF-A02).

MCEER-00-0008 "Soil Structure Interaction of Bridges for Seismic Analysis," I. PoLam and H. Law, 9/25/00, (PB2001-105397, A08, MF-A02).

MCEER-00-0009 "Proceedings of the First MCEER Workshop on Mitigation of Earthquake Disaster by Advanced Technologies (MEDAT-1), edited by M. Shinozuka, D.J. Inman and T.D. O'Rourke, 11/10/00, (PB2001-105399, A14, MF-A03).

MCEER-00-0010 "Development and Evaluation of Simplified Procedures for Analysis and Design of Buildings with Passive Energy Dissipation Systems, Revision 01," by O.M. Ramirez, M.C. Constantinou, C.A. Kircher, A.S. Whittaker, M.W. Johnson, J.D. Gomez and C. Chrysostomou, 11/16/01, (PB2001-105523, A23, MF-A04).

MCEER-00-0011 "Dynamic Soil-Foundation-Structure Interaction Analyses of Large Caissons," by C-Y. Chang, C-M. Mok, Z-L. Wang, R. Settgast, F. Waggoner, M.A. Ketchum, H.M. Gonnermann and C-C. Chin, 12/30/00, (PB2001-104373, A07, MF-A02).

MCEER-00-0012 "Experimental Evaluation of Seismic Performance of Bridge Restrainers," by A.G. Vlassis, E.M. Maragakis and M. Saiid Saiidi, 12/30/00, (PB2001-104354, A09, MF-A02).

MCEER-00-0013 "Effect of Spatial Variation of Ground Motion on Highway Structures," by M. Shinozuka, V. Saxena and G. Deodatis, 12/31/00, (PB2001-108755, A13, MF-A03).

MCEER-00-0014 "A Risk-Based Methodology for Assessing the Seismic Performance of Highway Systems," by S.D. Werner, C.E. Taylor, J.E. Moore, II, J.S. Walton and S. Cho, 12/31/00, (PB2001-108756, A14, MF-A03).

MCEER-01-0001 "Experimental Investigation of P-Delta Effects to Collapse During Earthquakes," by D. Vian and M. Bruneau, 6/25/01, (PB2002-100534, A17, MF-A03).

MCEER-01-0002 "Proceedings of the Second MCEER Workshop on Mitigation of Earthquake Disaster by Advanced Technologies (MEDAT-2)," edited by M. Bruneau and D.J. Inman, 7/23/01, (PB2002-100434, A16, MF-A03).

MCEER-01-0003 "Sensitivity Analysis of Dynamic Systems Subjected to Seismic Loads," by C. Roth and M. Grigoriu, 9/18/01, (PB2003-100884, A12, MF-A03).

MCEER-01-0004 "Overcoming Obstacles to Implementing Earthquake Hazard Mitigation Policies: Stage 1 Report," by D.J. Alesch and W.J. Petak, 12/17/01, (PB2002-107949, A07, MF-A02).

MCEER-01-0005 "Updating Real-Time Earthquake Loss Estimates: Methods, Problems and Insights," by C.E. Taylor, S.E. Chang and R.T. Eguchi, 12/17/01, (PB2002-107948, A05, MF-A01).

MCEER-01-0006 "Experimental Investigation and Retrofit of Steel Pile Foundations and Pile Bents Under Cyclic Lateral Loadings," by A. Shama, J. Mander, B. Blabac and S. Chen, 12/31/01, (PB2002-107950, A13, MF-A03).

MCEER-02-0001 "Assessment of Performance of Bolu Viaduct in the 1999 Duzce Earthquake in Turkey" by P.C. Roussis, M.C. Constantinou, M. Erdik, E. Durukal and M. Dicleli, 5/8/02, (PB2003-100883, A08, MF-A02).

MCEER-02-0002 "Seismic Behavior of Rail Counterweight Systems of Elevators in Buildings," by M.P. Singh, Rildova and L.E. Suarez, 5/27/02. (PB2003-100882, A11, MF-A03).

MCEER-02-0003 "Development of Analysis and Design Procedures for Spread Footings," by G. Mylonakis, G. Gazetas, S. Nikolaou and A. Chauncey, 10/02/02, (PB2004-101636, A13, MF-A03, CD-A13).

MCEER-02-0004 "Bare-Earth Algorithms for Use with SAR and LIDAR Digital Elevation Models," by C.K. Huyck, R.T. Eguchi and B. Houshmand, 10/16/02, (PB2004-101637, A07, CD-A07).

MCEER-02-0005 "Review of Energy Dissipation of Compression Members in Concentrically Braced Frames," by K.Lee and M. Bruneau, 10/18/02, (PB2004-101638, A10, CD-A10).

MCEER-03-0001 "Experimental Investigation of Light-Gauge Steel Plate Shear Walls for the Seismic Retrofit of Buildings" by J. Berman and M. Bruneau, 5/2/03, (PB2004-101622, A10, MF-A03, CD-A10).

MCEER-03-0002 "Statistical Analysis of Fragility Curves," by M. Shinozuka, M.Q. Feng, H. Kim, T. Uzawa and T. Ueda, 6/16/03, (PB2004-101849, A09, CD-A09).

MCEER-03-0003 "Proceedings of the Eighth U.S.-Japan Workshop on Earthquake Resistant Design f Lifeline Facilities and Countermeasures Against Liquefaction," edited by M. Hamada, J.P. Bardet and T.D. O'Rourke, 6/30/03, (PB2004-104386, A99, CD-A99).

MCEER-03-0004 "Proceedings of the PRC-US Workshop on Seismic Analysis and Design of Special Bridges," edited by L.C. Fan and G.C. Lee, 7/15/03, (PB2004-104387, A14, CD-A14).

MCEER-03-0005 "Urban Disaster Recovery: A Framework and Simulation Model," by S.B. Miles and S.E. Chang, 7/25/03, (PB2004-104388, A07, CD-A07).

MCEER-03-0006 "Behavior of Underground Piping Joints Due to Static and Dynamic Loading," by R.D. Meis, M. Maragakis and R. Siddharthan, 11/17/03, (PB2005-102194, A13, MF-A03, CD-A00).

MCEER-04-0001 "Experimental Study of Seismic Isolation Systems with Emphasis on Secondary System Response and Verification of Accuracy of Dynamic Response History Analysis Methods," by E. Wolff and M. Constantinou, 1/16/04 (PB2005-102195, A99, MF-E08, CD-A00).

MCEER-04-0002 "Tension, Compression and Cyclic Testing of Engineered Cementitious Composite Materials," by K. Kesner and S.L. Billington, 3/1/04, (PB2005-102196, A08, CD-A08).

MCEER-04-0003 "Cyclic Testing of Braces Laterally Restrained by Steel Studs to Enhance Performance During Earthquakes," by O.C. Celik, J.W. Berman and M. Bruneau, 3/16/04, (PB2005-102197, A13, MF-A03, CD-A00).

MCEER-04-0004 "Methodologies for Post Earthquake Building Damage Detection Using SAR and Optical Remote Sensing: Application to the August 17, 1999 Marmara, Turkey Earthquake," by C.K. Huyck, B.J. Adams, S. Cho, R.T. Eguchi, B. Mansouri and B. Houshmand, 6/15/04, (PB2005-104888, A10, CD-A00).

MCEER-04-0005 "Nonlinear Structural Analysis Towards Collapse Simulation: A Dynamical Systems Approach," by M.V. Sivaselvan and A.M. Reinhorn, 6/16/04, (PB2005-104889, A11, MF-A03, CD-A00).

MCEER-04-0006 "Proceedings of the Second PRC-US Workshop on Seismic Analysis and Design of Special Bridges," edited by G.C. Lee and L.C. Fan, 6/25/04, (PB2005-104890, A16, CD-A00).

MCEER-04-0007 "Seismic Vulnerability Evaluation of Axially Loaded Steel Built-up Laced Members," by K. Lee and M. Bruneau, 6/30/04, (PB2005-104891, A16, CD-A00).

MCEER-04-0008 "Evaluation of Accuracy of Simplified Methods of Analysis and Design of Buildings with Damping Systems for Near-Fault and for Soft-Soil Seismic Motions," by E.A. Pavlou and M.C. Constantinou, 8/16/04, (PB2005-104892, A08, MF-A02, CD-A00).

MCEER-04-0009 "Assessment of Geotechnical Issues in Acute Care Facilities in California," by M. Lew, T.D. O'Rourke, R. Dobry and M. Koch, 9/15/04, (PB2005-104893, A08, CD-A00).

MCEER-04-0010 "Scissor-Jack-Damper Energy Dissipation System," by A.N. Sigaher-Boyle and M.C. Constantinou, 12/1/04 (PB2005-108221).

MCEER-04-0011 "Seismic Retrofit of Bridge Steel Truss Piers Using a Controlled Rocking Approach," by M. Pollino and M. Bruneau, 12/20/04 (PB2006-105795).

MCEER-05-0001 "Experimental and Analytical Studies of Structures Seismically Isolated with an Uplift-Restraint Isolation System," by P.C. Roussis and M.C. Constantinou, 1/10/05 (PB2005-108222).

MCEER-05-0002 "A Versatile Experimentation Model for Study of Structures Near Collapse Applied to Seismic Evaluation of Irregular Structures," by D. Kusumastuti, A.M. Reinhorn and A. Rutenberg, 3/31/05 (PB2006-101523).

MCEER-05-0003 "Proceedings of the Third PRC-US Workshop on Seismic Analysis and Design of Special Bridges," edited by L.C. Fan and G.C. Lee, 4/20/05, (PB2006-105796).

MCEER-05-0004 "Approaches for the Seismic Retrofit of Braced Steel Bridge Piers and Proof-of-Concept Testing of an Eccentrically Braced Frame with Tubular Link," by J.W. Berman and M. Bruneau, 4/21/05 (PB2006-101524).

MCEER-05-0005 "Simulation of Strong Ground Motions for Seismic Fragility Evaluation of Nonstructural Components in Hospitals," by A. Wanitkorkul and A. Filiatrault, 5/26/05 (PB2006-500027).

MCEER-05-0006 "Seismic Safety in California Hospitals: Assessing an Attempt to Accelerate the Replacement or Seismic Retrofit of Older Hospital Facilities," by D.J. Alesch, L.A. Arendt and W.J. Petak, 6/6/05 (PB2006-105794).

MCEER-05-0007 "Development of Seismic Strengthening and Retrofit Strategies for Critical Facilities Using Engineered Cementitious Composite Materials," by K. Kesner and S.L. Billington, 8/29/05 (PB2006-111701).

MCEER-05-0008 "Experimental and Analytical Studies of Base Isolation Systems for Seismic Protection of Power Transformers," by N. Murota, M.Q. Feng and G-Y. Liu, 9/30/05 (PB2006-111702).

MCEER-05-0009 "3D-BASIS-ME-MB: Computer Program for Nonlinear Dynamic Analysis of Seismically Isolated Structures," by P.C. Tsopelas, P.C. Roussis, M.C. Constantinou, R. Buchanan and A.M. Reinhorn, 10/3/05 (PB2006-111703).

MCEER-05-0010 "Steel Plate Shear Walls for Seismic Design and Retrofit of Building Structures," by D. Vian and M. Bruneau, 12/15/05 (PB2006-111704).

MCEER-05-0011 "The Performance-Based Design Paradigm," by M.J. Astrella and A. Whittaker, 12/15/05 (PB2006-111705).

MCEER-06-0001 "Seismic Fragility of Suspended Ceiling Systems," H. Badillo-Almaraz, A.S. Whittaker, A.M. Reinhorn and G.P. Cimellaro, 2/4/06 (PB2006-111706).

MCEER-06-0002 "Multi-Dimensional Fragility of Structures," by G.P. Cimellaro, A.M. Reinhorn and M. Bruneau, 3/1/06 (PB2007-106974, A09, MF-A02, CD A00).

MCEER-06-0003 "Built-Up Shear Links as Energy Dissipators for Seismic Protection of Bridges," by P. Dusicka, A.M. Itani and I.G. Buckle, 3/15/06 (PB2006-111708).

MCEER-06-0004 "Analytical Investigation of the Structural Fuse Concept," by R.E. Vargas and M. Bruneau, 3/16/06 (PB2006-111709).

MCEER-06-0005 "Experimental Investigation of the Structural Fuse Concept," by R.E. Vargas and M. Bruneau, 3/17/06 (PB2006-111710).

MCEER-06-0006 "Further Development of Tubular Eccentrically Braced Frame Links for the Seismic Retrofit of Braced Steel Truss Bridge Piers," by J.W. Berman and M. Bruneau, 3/27/06 (PB2007-105147).

MCEER-06-0007 "REDARS Validation Report," by S. Cho, C.K. Huyck, S. Ghosh and R.T. Eguchi, 8/8/06 (PB2007-106983).

MCEER-06-0008 "Review of Current NDE Technologies for Post-Earthquake Assessment of Retrofitted Bridge Columns," by J.W. Song, Z. Liang and G.C. Lee, 8/21/06 (PB2007-106984).

MCEER-06-0009 "Liquefaction Remediation in Silty Soils Using Dynamic Compaction and Stone Columns," by S. Thevanayagam, G.R. Martin, R. Nashed, T. Shenthan, T. Kanagalingam and N. Ecemis, 8/28/06 (PB2007-106985).

MCEER-06-0010 "Conceptual Design and Experimental Investigation of Polymer Matrix Composite Infill Panels for Seismic Retrofitting," by W. Jung, M. Chiewanichakorn and A.J. Aref, 9/21/06 (PB2007-106986).

MCEER-06-0011 "A Study of the Coupled Horizontal-Vertical Behavior of Elastomeric and Lead-Rubber Seismic Isolation Bearings," by G.P. Warn and A.S. Whittaker, 9/22/06 (PB2007-108679).

MCEER-06-0012 "Proceedings of the Fourth PRC-US Workshop on Seismic Analysis and Design of Special Bridges: Advancing Bridge Technologies in Research, Design, Construction and Preservation," Edited by L.C. Fan, G.C. Lee and L. Ziang, 10/12/06 (PB2007-109042).

MCEER-06-0013 "Cyclic Response and Low Cycle Fatigue Characteristics of Plate Steels," by P. Dusicka, A.M. Itani and I.G. Buckle, 11/1/06 06 (PB2007-106987).

MCEER-06-0014 "Proceedings of the Second US-Taiwan Bridge Engineering Workshop," edited by W.P. Yen, J. Shen, J-Y. Chen and M. Wang, 11/15/06 (PB2008-500041).

MCEER-06-0015 "User Manual and Technical Documentation for the REDARS^{TM} Import Wizard," by S. Cho, S. Ghosh, C.K. Huyck and S.D. Werner, 11/30/06 (PB2007-114766).

MCEER-06-0016 "Hazard Mitigation Strategy and Monitoring Technologies for Urban and Infrastructure Public Buildings: Proceedings of the China-US Workshops," edited by X.Y. Zhou, A.L. Zhang, G.C. Lee and M. Tong, 12/12/06 (PB2008-500018).

MCEER-07-0001 "Static and Kinetic Coefficients of Friction for Rigid Blocks," by C. Kafali, S. Fathali, M. Grigoriu and A.S. Whittaker, 3/20/07 (PB2007-114767).

MCEER-07-0002 "Hazard Mitigation Investment Decision Making: Organizational Response to Legislative Mandate," by L.A. Arendt, D.J. Alesch and W.J. Petak, 4/9/07 (PB2007-114768).

MCEER-07-0003 "Seismic Behavior of Bidirectional-Resistant Ductile End Diaphragms with Unbonded Braces in Straight or Skewed Steel Bridges," by O. Celik and M. Bruneau, 4/11/07 (PB2008-105141).

MCEER-07-0004 "Modeling Pile Behavior in Large Pile Groups Under Lateral Loading," by A.M. Dodds and G.R. Martin, 4/16/07(PB2008-105142).

MCEER-07-0005 "Experimental Investigation of Blast Performance of Seismically Resistant Concrete-Filled Steel Tube Bridge Piers," by S. Fujikura, M. Bruneau and D. Lopez-Garcia, 4/20/07 (PB2008-105143).

MCEER-07-0006 "Seismic Analysis of Conventional and Isolated Liquefied Natural Gas Tanks Using Mechanical Analogs," by I.P. Christovasilis and A.S. Whittaker, 5/1/07.

MCEER-07-0007 "Experimental Seismic Performance Evaluation of Isolation/Restraint Systems for Mechanical Equipment – Part 1: Heavy Equipment Study," by S. Fathali and A. Filiatrault, 6/6/07 (PB2008-105144).

MCEER-07-0008 "Seismic Vulnerability of Timber Bridges and Timber Substructures," by A.A. Sharma, J.B. Mander, I.M. Friedland and D.R. Allicock, 6/7/07 (PB2008-105145).

MCEER-07-0009 "Experimental and Analytical Study of the XY-Friction Pendulum (XY-FP) Bearing for Bridge Applications," by C.C. Marin-Artieda, A.S. Whittaker and M.C. Constantinou, 6/7/07 (PB2008-105191).

MCEER-07-0010 "Proceedings of the PRC-US Earthquake Engineering Forum for Young Researchers," Edited by G.C. Lee and X.Z. Qi, 6/8/07 (PB2008-500058).

MCEER-07-0011 "Design Recommendations for Perforated Steel Plate Shear Walls," by R. Purba and M. Bruneau, 6/18/07, (PB2008-105192).

MCEER-07-0012 "Performance of Seismic Isolation Hardware Under Service and Seismic Loading," by M.C. Constantinou, A.S. Whittaker, Y. Kalpakidis, D.M. Fenz and G.P. Warn, 8/27/07, (PB2008-105193).

MCEER-07-0013 "Experimental Evaluation of the Seismic Performance of Hospital Piping Subassemblies," by E.R. Goodwin, E. Maragakis and A.M. Itani, 9/4/07, (PB2008-105194).

MCEER-07-0014 "A Simulation Model of Urban Disaster Recovery and Resilience: Implementation for the 1994 Northridge Earthquake," by S. Miles and S.E. Chang, 9/7/07, (PB2008-106426).

MCEER-07-0015 "Statistical and Mechanistic Fragility Analysis of Concrete Bridges," by M. Shinozuka, S. Banerjee and S-H. Kim, 9/10/07, (PB2008-106427).

MCEER-07-0016 "Three-Dimensional Modeling of Inelastic Buckling in Frame Structures," by M. Schachter and AM. Reinhorn, 9/13/07, (PB2008-108125).

MCEER-07-0017 "Modeling of Seismic Wave Scattering on Pile Groups and Caissons," by I. Po Lam, H. Law and C.T. Yang, 9/17/07 (PB2008-108150).

MCEER-07-0018 "Bridge Foundations: Modeling Large Pile Groups and Caissons for Seismic Design," by I. Po Lam, H. Law and G.R. Martin (Coordinating Author), 12/1/07 (PB2008-111190).

MCEER-07-0019 "Principles and Performance of Roller Seismic Isolation Bearings for Highway Bridges," by G.C. Lee, Y.C. Ou, Z. Liang, T.C. Niu and J. Song, 12/10/07 (PB2009-110466).

MCEER-07-0020 "Centrifuge Modeling of Permeability and Pinning Reinforcement Effects on Pile Response to Lateral Spreading," by L.L Gonzalez-Lagos, T. Abdoun and R. Dobry, 12/10/07 (PB2008-111191).

MCEER-07-0021 "Damage to the Highway System from the Pisco, Perú Earthquake of August 15, 2007," by J.S. O'Connor, L. Mesa and M. Nykamp, 12/10/07, (PB2008-108126).

MCEER-07-0022 "Experimental Seismic Performance Evaluation of Isolation/Restraint Systems for Mechanical Equipment – Part 2: Light Equipment Study," by S. Fathali and A. Filiatrault, 12/13/07 (PB2008-111192).

MCEER-07-0023 "Fragility Considerations in Highway Bridge Design," by M. Shinozuka, S. Banerjee and S.H. Kim, 12/14/07 (PB2008-111193).

MCEER-07-0024 "Performance Estimates for Seismically Isolated Bridges," by G.P. Warn and A.S. Whittaker, 12/30/07 (PB2008-112230).

MCEER-08-0001 "Seismic Performance of Steel Girder Bridge Superstructures with Conventional Cross Frames," by L.P. Carden, A.M. Itani and I.G. Buckle, 1/7/08, (PB2008-112231).

MCEER-08-0002 "Seismic Performance of Steel Girder Bridge Superstructures with Ductile End Cross Frames with Seismic Isolators," by L.P. Carden, A.M. Itani and I.G. Buckle, 1/7/08 (PB2008-112232).

MCEER-08-0003 "Analytical and Experimental Investigation of a Controlled Rocking Approach for Seismic Protection of Bridge Steel Truss Piers," by M. Pollino and M. Bruneau, 1/21/08 (PB2008-112233).

MCEER-08-0004 "Linking Lifeline Infrastructure Performance and Community Disaster Resilience: Models and Multi-Stakeholder Processes," by S.E. Chang, C. Pasion, K. Tatebe and R. Ahmad, 3/3/08 (PB2008-112234).

MCEER-08-0005 "Modal Analysis of Generally Damped Linear Structures Subjected to Seismic Excitations," by J. Song, Y-L. Chu, Z. Liang and G.C. Lee, 3/4/08 (PB2009-102311).

MCEER-08-0006 "System Performance Under Multi-Hazard Environments," by C. Kafali and M. Grigoriu, 3/4/08 (PB2008-112235).

MCEER-08-0007 "Mechanical Behavior of Multi-Spherical Sliding Bearings," by D.M. Fenz and M.C. Constantinou, 3/6/08 (PB2008-112236).

MCEER-08-0008 "Post-Earthquake Restoration of the Los Angeles Water Supply System," by T.H.P. Tabucchi and R.A. Davidson, 3/7/08 (PB2008-112237).

MCEER-08-0009 "Fragility Analysis of Water Supply Systems," by A. Jacobson and M. Grigoriu, 3/10/08 (PB2009-105545).

MCEER-08-0010 "Experimental Investigation of Full-Scale Two-Story Steel Plate Shear Walls with Reduced Beam Section Connections," by B. Qu, M. Bruneau, C-H. Lin and K-C. Tsai, 3/17/08 (PB2009-106368).

MCEER-08-0011 "Seismic Evaluation and Rehabilitation of Critical Components of Electrical Power Systems," S. Ersoy, B. Feizi, A. Ashrafi and M. Ala Saadeghvaziri, 3/17/08 (PB2009-105546).

MCEER-08-0012 "Seismic Behavior and Design of Boundary Frame Members of Steel Plate Shear Walls," by B. Qu and M. Bruneau, 4/26/08 . (PB2009-106744).

MCEER-08-0013 "Development and Appraisal of a Numerical Cyclic Loading Protocol for Quantifying Building System Performance," by A. Filiatrault, A. Wanitkorkul and M. Constantinou, 4/27/08 (PB2009-107906).

MCEER-08-0014 "Structural and Nonstructural Earthquake Design: The Challenge of Integrating Specialty Areas in Designing Complex, Critical Facilities," by W.J. Petak and D.J. Alesch, 4/30/08 (PB2009-107907).

MCEER-08-0015 "Seismic Performance Evaluation of Water Systems," by Y. Wang and T.D. O'Rourke, 5/5/08 (PB2009-107908).

MCEER-08-0016 "Seismic Response Modeling of Water Supply Systems," by P. Shi and T.D. O'Rourke, 5/5/08 (PB2009-107910).

MCEER-08-0017 "Numerical and Experimental Studies of Self-Centering Post-Tensioned Steel Frames," by D. Wang and A. Filiatrault, 5/12/08 (PB2009-110479).

MCEER-08-0018 "Development, Implementation and Verification of Dynamic Analysis Models for Multi-Spherical Sliding Bearings," by D.M. Fenz and M.C. Constantinou, 8/15/08 (PB2009-107911).

MCEER-08-0019 "Performance Assessment of Conventional and Base Isolated Nuclear Power Plants for Earthquake Blast Loadings," by Y.N. Huang, A.S. Whittaker and N. Luco, 10/28/08 (PB2009-107912).

MCEER-08-0020 "Remote Sensing for Resilient Multi-Hazard Disaster Response – Volume I: Introduction to Damage Assessment Methodologies," by B.J. Adams and R.T. Eguchi, 11/17/08.

MCEER-08-0021 "Remote Sensing for Resilient Multi-Hazard Disaster Response – Volume II: Counting the Number of Collapsed Buildings Using an Object-Oriented Analysis: Case Study of the 2003 Bam Earthquake," by L. Gusella, C.K. Huyck and B.J. Adams, 11/17/08.

MCEER-08-0022 "Remote Sensing for Resilient Multi-Hazard Disaster Response – Volume III: Multi-Sensor Image Fusion Techniques for Robust Neighborhood-Scale Urban Damage Assessment," by B.J. Adams and A. McMillan, 11/17/08.

MCEER-08-0023 "Remote Sensing for Resilient Multi-Hazard Disaster Response – Volume IV: A Study of Multi-Temporal and Multi-Resolution SAR Imagery for Post-Katrina Flood Monitoring in New Orleans," by A. McMillan, J.G. Morley, B.J. Adams and S. Chesworth, 11/17/08.

MCEER-08-0024 "Remote Sensing for Resilient Multi-Hazard Disaster Response – Volume V: Integration of Remote Sensing Imagery and VIEWS^{TM} Field Data for Post-Hurricane Charley Building Damage Assessment," by J.A. Womble, K. Mehta and B.J. Adams, 11/17/08.

MCEER-08-0025 "Building Inventory Compilation for Disaster Management: Application of Remote Sensing and Statistical Modeling," by P. Sarabandi, A.S. Kiremidjian, R.T. Eguchi and B. J. Adams, 11/20/08 (PB2009-110484).

MCEER-08-0026 "New Experimental Capabilities and Loading Protocols for Seismic Qualification and Fragility Assessment of Nonstructural Systems," by R. Retamales, G. Mosqueda, A. Filiatrault and A. Reinhorn, 11/24/08 (PB2009-110485).

MCEER-08-0027 "Effects of Heating and Load History on the Behavior of Lead-Rubber Bearings," by I.V. Kalpakidis and M.C. Constantinou, 12/1/08.

MCEER-08-0028 "Experimental and Analytical Investigation of Blast Performance of Seismically Resistant Bridge Piers," by S.Fujikura and M. Bruneau, 12/8/08.

MCEER-08-0029 "Evolutionary Methodology for Aseismic Decision Support," by Y. Hu and G. Dargush, 12/15/08.

MCEER-08-0030 "Development of a Steel Plate Shear Wall Bridge Pier System Conceived from a Multi-Hazard Perspective," by D. Keller and M. Bruneau, 12/19/08.

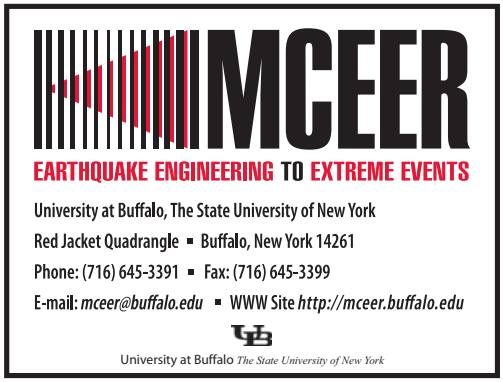

ISSN 1520-295X